8-9-2022

# Behavioral and histological inflammatory analysis of a single, mild traumatic brain injury and repeated subconcussive brain injury using a rodent model.

Anna Marie Clay
amd406@msstate.edu

# Behavioral and histological inflammatory analysis of a single, mild traumatic brain injury and repeated subconcussive brain injury using a rodent model.

By

Anna Marie Clay

Approved by:

Filip S. D. To (Major Professor)
Russell Carr
Janice DuBien
Lauren Priddy

Steven H. Elder (Graduate Coordinator)
Jason M. Keith (Dean, Bagley College of Engineering)

A Dissertation
Submitted to the Faculty of
Mississippi State University
in Partial Fulfillment of the Requirements
for the Degree of Doctor of Philosophy
in Biomedical Engineering
in the Department of Agricultural and Biological Engineering.

Mississippi State, Mississippi

August 2022

Name: Anna Marie Clay

Date of Degree: August 9, 2022

Institution: Mississippi State University

Major Field: Biomedical Engineering

Major Professor: Filip S. D. To

Title of Study: Behavioral and histological inflammatory analysis of a single, mild traumatic brain injury and repeated subconcussive brain injury using a rodent model.

Pages in Study: 196

Candidate for Degree of Doctor of Philosophy

Subconcussive (SC) impacts have become a growing concern within the neuroscience community regarding the immediate and long-lasting effects of sports-related injuries. While a single low-level impact, i.e., a subconcussion, may not cause cerebral perturbations, it has been increasingly recognized that repeated SC exposure can induce deleterious effects. Therefore, determining the lower limits of systematic perturbation resulting from multiple SC impacts is of critical importance in expanding our understanding of cerebral vulnerability and recovery. Currently, there is a lack of correlation between a mild traumatic brain injury (mTBI) and repeated SC impacts with respect to injury biomechanics. Moreover, the cumulative threshold for repetitive low-level impacts is currently undefined. Thus, this research was designed to determine the pathophysiological differences between a single impact of an mTBI and repeated SC impacts with a subdivided cumulative kinetic energy of the single mTBI impact.

In order to address this gap in knowledge, the present investigation employed a surgery-free, closed-head, weight drop injury device capable of producing repeatable, head impacts within a rat model. General locomotion and anxiety-like behavior were assessed using an Open Field Test and motor coordination dysfunction was measured using the rotarod assay.

Neuroinflammation was measured using immunohistochemical assessment of astrogliosis (GFAP) and microgliosis (Iba-1) within the hippocampus. Additionally, immunohistochemical assessment of neuronal loss (NeuN) was measured within the hippocampus. To investigate the tolerance and the persistence of cerebral vulnerability following a single mTBI and repeated subconcussive impacts, measurement outcomes were assessed over two-time points (3- and 7-days) post final impact.

Although injury groups were not statistically different from their associated sham groups with respect to behavioral outcomes; on average, RSC injury rats displayed a significant increase in anxious-like behavior after 7-days of recovery compared to the single mTBI group. From an inflammatory perspective, both mTBI and RSC injury groups led to extensive microgliosis in the gray matter following 3-days post-impact. Overall, this work's findings do not provide evidence in support of the notion that repeated subconcussive impacts do result in behavioral disturbances and neuroinflammation, that do not manifest following a single mTBI of the same energy input.

# DEDICATION

To my parents, Bill and Cheryl Dulaney, for creating a path for me to achieve my dreams. Your words of encouragement and push for tenacity ring in my ears. Both of you have been my best cheerleaders. To my husband, Richard Clay, for providing support, patience, and love.

ACKNOWLEDGEMENTS

I would like to acknowledge the many individuals who had a hand in contributing to the completion of this work. I would like to acknowledge Dr. Bridget Williford and Dr. Anmbriel Schwirian for their veterinary assistance. I would like to acknowledge Dr. Alicia Olivier, Stephany Mays, and Samantha Buxton for their time and assistance with histology. I would like to express gratitude to Darby Stanford and Dr. Folly Patterson for their guidance in image analysis and multiplex assays, respectively. I would like to acknowledge Dr. Raj Prabhu for informing the experimental design of this project. A special thanks to Dr. David van den Heever for his valuable comments and suggestions, which helped to improve the quality of the manuscript. I would like to thank the undergraduate students, Luke Johnson, Andrea Turnbow, Mia Pensa, and Macy Moore, for their research assistance during the experimentation. A special thanks is due to Dr. Sonja Virkus for her support, advice, and friendship. Furthermore, I would like to acknowledge all the members of my dissertation committee. Special thanks to Dr. Russel Carr for his assistance during experimentation and expert guidance in experimental neuroscience that helped inform our investigation. I wish to acknowledge Dr. Lauren Priddy for her guidance and support throughout the investigation. I also wish to thank Dr. Janice Dubien for informing my statistical analysis. I wish to acknowledge and extend my deepest gratitude to my major professor, Dr. Filip To, not only for his professional mentorship and generosity in the aid of the project but also for his personal and spiritual guidance throughout my graduate career. Lastly, I would like to extend my sincere gratitude to the Mississippi Space Grant Fellowship Program for

awarding me the NASA fellowship for the past three years and making the completion of this project a reality.

TABLE OF CONTENTS

LIST OF TABLES

LIST OF FIGURES

# CHAPTER I

# INTRODUCTION

## 1.1 Definition of Traumatic Brain Injury

Traumatic brain injury (TBI) is best defined as a neurological event causing a “complex pathophysiological process affecting the brain, induced by biomechanical forces” (Budson et al., 2017, pg. 11). Biomechanical forces can include any of the following: the head being struck by an object, the head striking an object, the brain undergoing rapid acceleration/deceleration movement without any external trauma applied to the head (i.e., whiplash), an object penetrating the brain, or a force to the head applied from a blast or explosion. When there is a mechanical insult, force, acceleration/deceleration, or rotational stress conveyed on the brain that causes modified brain function leading to symptoms and signs, it is recognized as a concussion (Budson et al., 2017, pg. 6). Symptoms and signs include temporary loss of consciousness, headaches, dizziness, fatigue, irritability, memory loss, inability to concentrate, and emotional lability such as depression and anxiety (Arciniegas et al., 1999; Kibby and Long, 1996; Levin et al., 1987). It is important to note, the mechanical force needed to impart some of these symptoms is not as great as the forces needed to cause a loss of consciousness. Thus, while loss of consciousness is a clinical hallmark of concussion, it is not required to make the diagnosis. For most patients, rest over time helps alleviate symptoms of a brain injury within an hour or days. However, others may have symptoms lasting much longer.

Diagnosis of TBI is made clinically and relies on several clinical criteria (Blyth & Bazarian, 2010), one of which is the Glasgow Coma Scale (GCS). The Glasgow Coma Scale is a neurological scale based on motor responsiveness, verbal performance, and eye-opening analysis to appropriate stimuli to assess the level of impaired consciousness among individuals (Teasdale et al., 2014) and is a widely used and accepted prognosis indicator for head injuries. Traditionally, the GCS classifies head injuries according to their injury severity, mild (GCS 14-15), moderate (GCS 9-13), or severe (GCS 3-8) (Mena et al., 2011). However, the Canadian Computed Tomography (CT) Head Rule Study, Advanced Trauma Life Support (ATLS) reports a modification to the GCS classifications so that a GCS score of 13 falls under a mild TBI category (GCS 13-15) (Kortbeek et al., 2008; Smits et al., 2005; Stiell et al., 2005). Other criteria used to identify the severity of head injury includes structural imaging of the head, duration of unconsciousness, post-traumatic amnesia, and any alteration of mental state (see Table 1.1) (Blyth & Bazarian, 2010).

Table 1.1 Clinical criteria for classifying the severity of injury for traumatic brain injury.

| Criteria | Mild TBI | Moderate TBI | Severe TBI |
|---|---|---|---|
| Structural imaging of the head | Normal | Normal or abnormal | Normal or abnormal |
| Duration of unconsciousness | 0-30 min | > 30 minutes and < 24 hrs | > 24 hrs |
| Post-traumatic amnesia | A moment up to 24 hrs | > 24 hrs Severity based on other criteria | |
| Alteration of mental state | 0-1 day | > 1 and < 7 days | > 7 days |
| Glasgow Coma Scale score (within first 24 hours) | 13-15 | 9-12 | < 9 |

Notes: This table was adapted from Blyth, B. J., & Bazarian, J. J. (2010), Traumatic alterations in consciousness: traumatic brain injury, Emergency Medicine Clinics, 28(3), 571-594.

Mild TBI (mTBI), interchanged with concussion throughout this dissertation, is clinically characterized as an individual with normal structural imaging i.e., no hemorrhaging or bleeding or skull fracture (Blyth & Bazarian, 2010). However, in conjunction, individuals may have a loss of consciousness up to 30 minutes or any period of altered amnesia within 24 hours post-injury and have a GCS score of 14-15 (Blyth & Bazarian, 2010). Moderate TBI is defined as loss of consciousness of 30 minutes to 24 hours, amnesia lasting more than 24 hours, normal to abnormal structural imaging, or a period of 1-7 days of amnesia with a lower GCS score of 9-12 (Blyth & Bazarian, 2010). Finally, a severe TBI is classified to patients who show normal to abnormal structural imaging, a loss of consciousness greater than 24 hours, any period of altered amnesia greater than 24 hours post-injury, or any alteration of mental state greater than 7-days and have a GCS score of 3-8 (Blyth & Bazarian, 2010). The vast majority of head traumas are categorized as mild, up to 90% of all cases, and occur during sports-related activities (Gardner & Zafonte, 2016; Leo & McCrea, 2016; Langlois, Rutland-Brown, and Wald 2006, Centers for Disease Control and Prevention (CDC) 2003).

## 1.2 Incidence, prevalence, and cost estimates of TBI

According to the Centers for Disease and Control (CDC), each year the number of new cases of TBI in the United States is over 2.8 million (Peterson, et. al, 2019). These incidence rates include approximately 2.5 million TBI-related emergency room visits, around 288,000 TBI-related hospitalizations, and over 57,000 deaths related to TBI. Mounting evidence suggests that the number of incidences is much larger than that reported because many cases are unreported or undiagnosed due to the mild nature of the initial injury (Faul et al., 2010). According to the National Center for Injury Prevention and Control, an estimated 5.3 million individuals are living with a disability due to a traumatic brain jury in the United States (Centers for Disease Control

and Prevention, 2003). This represents a prevalence of about 2% of the U.S. population (Peterson, et. al, 2019). These disabilities can range from symptoms that have a minimal effect on everyday life to those that cause physical, emotional, and mental alterations that may interfere with daily activities. Not only can there be acute and chronic outcomes following a TBI, but there is also the economic burden that patients pose to their families, careers, and society. According to van Dijck et al. (2019), estimations of the in-hospital cost for patients with severe TBI were between $2,130 to $401,808. Variations in cost were primarily due to the heterogeneity in patient and treatment characteristics including the length of stay and surgical (van Dijck et al., 2019). Although in-hospital costs are an important part of the overall costs for patients, this study did not include other major contributors to the total cost post-injury including post-discharge rehabilitation, disability, or long-term care costs (van Dijck et al., 2019).

### 1.3 Anatomy of the Human Head

The brain and spinal cord form what is known as the central nervous system (CNS). The CNS is responsible for integrating sensory information and responding accordingly. The brain is responsible for coordinating sensory and motor systems, both voluntary and involuntary, of the body as well as facilitating our ability to perceive and interact with the environment. Although the brain only represents 2% of the body weight, it also consumes 15% of the cardiac output, 20% of total body oxygen, and 20% of the body's energy supply at rest (Maldonado & Alsayouri, 2020). The functional complexity of the brain is intricate in itself due to the large magnitude of neuronal (up to 86 billion) and non-neuronal (up to 86 billion) cells which results in a substantial metabolic demand (Azevedo et al., 2009). The brain's structural complexity is multi-layered and includes various gross anatomical components, cellular organization, and morphology.

### 1.3.1 Gross Components

The human head is a complex anatomical structure comprised of hard (bone) and soft tissues. It contains important parts of the body's sensory nervous system such as the nose, ears, eyes, and brain. The brain is the most essential organ that integrates and coordinates all information and activity of all the body parts. To protect this vital and delicate organ, a multi-layered structure encompasses the brain comprised of scalp, skull, and meninges (see Figure 1.1).

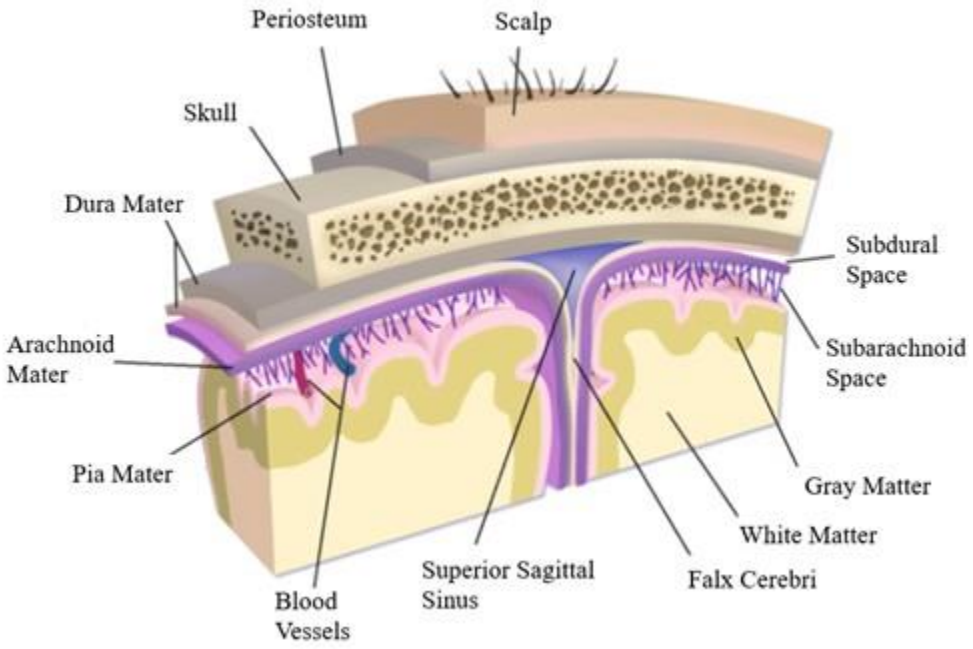


Figure 1.1 Illustration of the structural layers of the human head ("Medical Gallery of Blausen Medical 2014," 2014).

Notes: Illustration was obtained and adapted courtesy of © Blausen Medical (https://en.wikiversity.org); Illustrator: N/A.

The skull or cranium is separated from the scalp by the periosteum, as seen in Figure 1.1, a fibrous layer that is connected to the skull at the skull sutures (Ellis & Mahadevan, 2014). The

skull is comprised of three layers, the cortical outer layer, the cancellous, or diploe, the inner layer, and the cortical inner layer. Inside the cranial cavity, enclosing the brain, is the meninges (consisting of three distinct membrane layers) (Weller, 2005). These membranes, the dura mater, arachnoid mater, and pia mater, envelop the brain and spinal cord (Weller, 2005). The outermost layer, the dura mater, is a thick fibrous tissue that lines the inner layer of the skull. It deviates from the contours of the skull by forming the double fold, known as the falx cerebri, as seen in Figure 1.1 (Abrahams, 2016). The middle membrane, the arachnoid mater, is an impermeable membrane comprised of web-like, fibrous tissue (Abrahams, 2016; Weller, 2005). This second layer is separated from the dura mater by a small gap called the subdural space, as seen in Figure 1.1. The pia mater, the innermost meninx layer, adheres to the brain following its unique contours. The space between the arachnoid and pia (subarachnoid space) is filled with cerebrospinal fluid (CSF) (Weller, 2005). This fluid is a clear and colorless body fluid, that circulates and surrounds the brain, ventricles (lateral, third, and fourth ventricles), and spinal cord (Kegel, 2018), as seen in Figure 1.2. Not only is this fluid an essential component for nutrient delivery, waste clearance, and pressure regulation of the brain, but it also cushions the brain against mechanical impacts (Linninger et al., 2016).

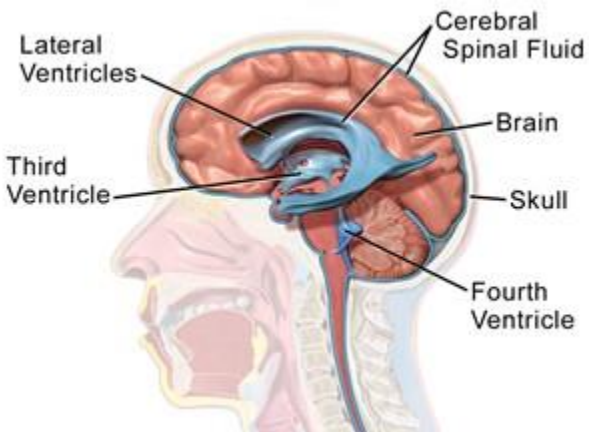


Figure 1.2 Illustration of the ventricular system (shown in blue) ("Medical gallery of Blausen Medical 2014," 2014).

Notes: Illustration was obtained courtesy of © Blausen Medical (https://en.wikiversity.org); Illustrator: N/A.

The brain can be separated into two parts, the cerebrum and cerebellum. The cerebrum is the largest component of the brain and is characterized by two symmetrical hemispheres separated by the falx cerebri. Within these convoluted hemispheres are four lobes – the frontal, parietal, temporal, and occipital lobe (Figure 1.3). The cerebrum consists of an outer cerebral cortex, composed of gray matter, and an underlying white matter, as seen in Figure 1.1. Although macroscopically different in color characteristics, microscopically the two differ in functionality based on the cellular structures present (Maldonado & Alsayouri, 2020). The gray matter primarily consists of neuronal cell bodies, dendrites, unmyelinated axons, glial cells, synapsis, and capillaries (Bayly et al., 2014; Maldonado & Alsayouri, 2020). Alternatively, the subcortical (beneath the cortex) area is mostly white matter, where its major component is myelinated axons (Bayly et al., 2014; Maldonado & Alsayouri, 2020). The cerebellum is a much smaller structure lies between the cerebrum and the spinal cord (Figure 1.3).

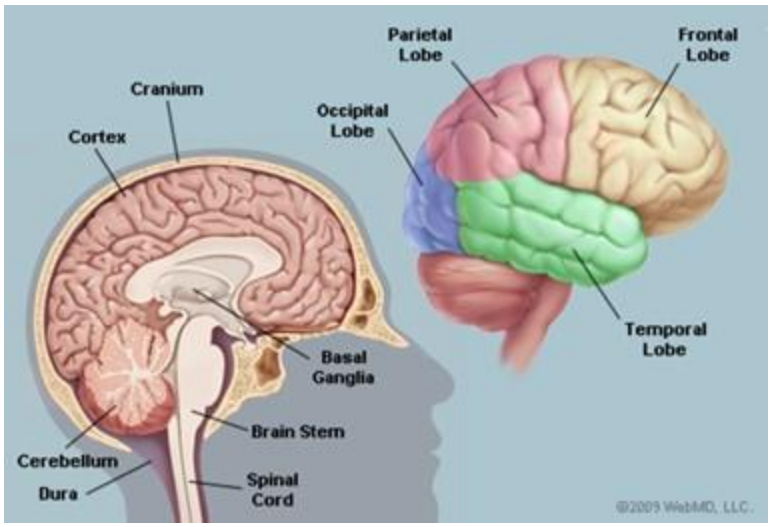


Figure 1.3 Illustration of external and internal cortical structures.

Notes: Central internal structures of the cortical and spinal cord (sagittal view; bottom left) and external cortical structure (lateral view; top right). The illustration was obtained courtesy of © WebMD, LLC (www.webmd.com); Illustrator: N/A.

### 1.3.2 Cellular Components

Brain tissue is comprised of two major cellular populations – neuron and glial cells. Both the gray and white matter are comprised of glial cells. Neurons are the basic and functional units of the nervous system, that convey information both electrically and chemically. Within the neuron itself, information is passed along through the movement of an electrical charge (i.e., an impulse or action potential) ("The Principles of Nerve Cell Communication," 1997). The neuron has three main components – the dendrites, cell body, and axon (Figure 1.4). Dendrites are short, thin fibers that extend from the cell in branched tendrils to receive electrical impulses from other surrounding neurons ("The Principles of Nerve Cell Communication," 1997). The cell body is the enlarged portion of the neuron that contains the nucleus and carries out most of the neuron's basic cellular functioning. The axon is a thin, long extension that is responsible for signal transmission. For the axon to maintain its signal strength as action potentials travel down

towards the axon terminals to reach the synapse, a segmented insulation casing called myelin surrounds the axonal membrane. (Figure 1.4) (Maldonado & Alsayouri, 2020).

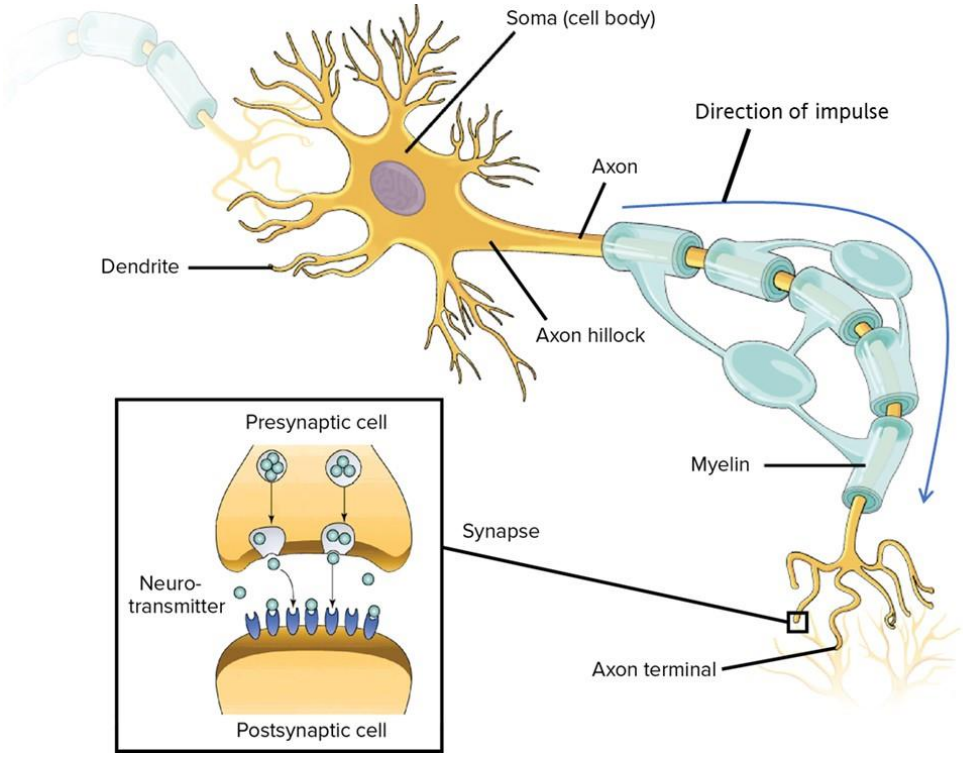


Figure 1.4 Illustration of a neuron and synapse.

The image was obtained and modified from "Overview of neuron structure and function" by Khan Academy, (www.khanacademy.org); Illustrator: N/A.

The segments of myelin are separated by unmyelinated regions called the Nodes of Ranvier. Nodes of Ranvier are highly enriched in ion channels, allowing them to participate in the exchange of ions required to regenerate the action potential. This results in faster conduction of the action potential along the axon (Nelson & Jenkins, 2017). Both the axonal and dendritic processes allow neuron cells to create a dense network of communication across the nervous system.

At rest, a neuron maintains a polarized membrane potential utilizing specialized ionic pumps. The main function of these pumps is to keep the outside of the cell positively charged relative to the inside of the cell (Fox, 2009, pg.171-173). Neurons propagate information to one another via electrochemical impulses, called action potentials (Fox, 2009, pg.170-172). Upon sufficient stimulation of ions, the cellular membrane begins depolarizing and an action potential is fired (Fox, 2009, pg.72-173). When an action potential is triggered, the membrane depolarization spreads down the length of the axon to the axon terminal (Fox, 2009, pg.172-173). Here, the action potential then triggers the presynaptic neuron to release a cluster of chemical regulators called neurotransmitters from the axon endings into a space called the synaptic gap, or cleft (Fox, 2009, pg.177-180). Neurotransmitters then begin to diffuse rapidly across the synaptic cleft to bind to receptor sites of the postsynaptic neuron (see Figure 1.4) (Fox, 2009, p.178-182).

Glial cells, consisting of oligodendrocytes, astrocytes, and microglia, constitute a large fraction of the brain. Glial cells are anything but a small cellular fraction, as they constitute between 33 and 66% of the total brain volume, depending on the mammalian species (Azevedo et al., 2009; Herculano-Houzel, 2014). Primarily, glial cells provide support for the neurons. Structurally, glial cells are smaller than neurons and lack axons and dendrites (Purves et al., 2001). Oligodendrocytes are responsible for forming myelin sheaths around adjacent neuronal axons in the CNS. Again, these myelin sheaths enwrap axons to allow fast conduction of action potentials. One single oligodendrocyte is capable of ensheathing as many as 40-50 axons (Popovich et al., 2009). Oligodendrocytes are most abundant in the white matter region of the cerebral tissue; however, some are found in gray matter (Hofmann et al., 2017).

Astrocytes are the most abundant cell type in the CNS. Astrocytes appear to have a star-shaped morphology with a multitude of processes extending from their cell body (Argente-

Arizón et al., 2015). Using their expanded processes called “end-feet,” astrocytes are involved in the formation and maintenance of some of the blood-brain barrier (BBB) properties (Janzer & Raff, 1987) and can regulate vasodilatation, thus controlling the flow of blood-borne substances (Macvicar & Newman, 2015; Zonta et al., 2003). The BBB is a critical protective border that prevents toxins or pathogens from entering the brain through the bloodstream (Freire-Regatillo et al., 2017). In addition to their maintenance role of the BBB, astrocytes also play a critical role in maintaining the homeostasis of ions, transmitters, and blood flow that are critical for neural circuit functions (Burda et al., 2016). Among neurons, astrocytes participate in the reuptake and recycling of glutamate and gamma-aminobutyric acid (GABA) neurotransmitters from the extracellular space after neuronal activity (Mederos et al., 2018). This process of reuptake is essential to prevent glutamate-derived excitotoxicity during neuronal synaptic transmission (Danbolt, 2001). In response to all forms of CNS insults, astrocytes become activated, a process called astrogliosis, where they take on a hypertrophic morphology with their processes increasing in length and size (Burda et al., 2016).

Microglial cells account for 5–12% of the total cell numbers and are mainly responsible for immune defense in the brain. (Alekseeva et al., 2019; Hanisch, 2013). Under normal physiological conditions, microglia have long radial processes and are highly motile as they constantly survey their microenvironment for harmful agents and injurious processes (Sominsky et al., 2018). Functionally, microglia are involved in brain development, have phagocytosis properties, and respond rapidly to any immune challenge, pathogen, or injury in the CNS in order to maintain normal cellular homeostasis (Alekseeva et al., 2019; Loane & Kumar, 2016; Sominsky et al., 2018). In non-pathological environments, a major function of microglia in the intact brain is to monitor and maintain the balance between pro- and anti-inflammatory factors

(Alekseeva, Kirik, Gilerovich, & Korzhevskii, 2019). In response to trauma, microglia enter into an inflammatory response mode where their morphology is changed to short and thick projections and assume an ameboid shape extending their processes towards the site of injury (Alekseeva et al., 2019; Sominsky et al., 2018). In this microglia phenotype form, microglia are characterized by a predominance of the phagocytic function (phagocytosis of cell debris) and reception and secretion of various factors, including cytokines (Alekseeva, Kirik, Gilerovich, & Korzhevskii, 2019).

## 1.4 Biomechanics of Traumatic Brain Injury

The biomechanics of head injuries has been investigated in a variety of labs over several decades (Meaney et al., 2014). When a force or load is applied to a system, it may cause initial damage or lead to delayed damage, however, the point at which the system, in this case, tissue damage, reaches its tolerance level, is determined by the type and duration of force or load (LaPlaca et al., 2007).

The most common cause of head injuries is due to dynamic loadings, or high-speed impact loadings, which occur in rapid durations (under 1 sec) (LaPlaca et al., 2007). These high-speed impact loadings can be further broken down as direct and indirect loading. As the name suggests, direct loading occurs when there is physical contact between an external object and the head. Depending on the rate of impact, magnitude of force, and size of the impact area, direct loading can cause focal or diffuse axonal injury (DAI) (LaPlaca et al., 2007). Indirect loading occurs when there is motion of the head without an external object encountering the head. This type of loading is due to inertial forces alone which leads to diffuse axonal injuries (Su & Bell, 2016).

Magnetic resonance imaging (MRI) findings showed that the concurrence of both injury types is commonly seen in patients who have suffered from moderate to severe TBI, however, DAI is one of the most common across all severities of closed head injury (CHI) (Skandsen et al., 2010; Su & Bell, 2016). Focal brain damage is visibly seen by the naked eye at the site of impact and is generally associated with an impact that exerts lacerations of the cerebral tissue due to compressive and concussive forces with evidence of skull fracture and localized contusion at the site of impact (coup injury; (Schmidt et al., 2004)). At the coup site, the occurrence of hematoma, epidural, subdural and intracerebral hemorrhages may transpire along with the accumulation of neuronal and glial cells (LaPlaca et al., 2007; Ng & Lee, 2019) As the brain tissue rebounds and strikes the opposite site of the skull, a secondary impact, called contrecoup, may cause a secondary contusion (Schmidt et al., 2004). In contrast to focal injury, the main mechanism of DAI is indirect loading of rapid acceleration and deceleration which cause shearing and stretching injury in the cerebral tissue (Koliatsos et al., 2020). More specifically, diffuse TBI is immense damage of axons throughout the white matter which involves degradation of axonal cytoskeleton and impairment of axonal transport (Meaney et al., 2014). Additionally, as one can assume, the degree of axonal injury and neuronal degeneration determines the severity of TBI.

Understanding the relationship between loading conditions and cellular responses in the context of injury biomechanics is a deeply complex problem. As a result, many researchers are characterizing these loading events from the perspective of injury biomechanics in order to better understand this intricate relationship (Meaney et al., 2014). Furthermore, because concussion and mTBI are categorized as predominately, if not purely, diffuse injuries (Zacko et al., 2011), the following pathophysiology described will mainly focus on a diffuse axonal injury.

## 1.5 Pathophysiology of Traumatic Brain Injury

There are two aspects to injury caused by a traumatic brain injury: primary and secondary injury. The primary stage is characterized by the moment and duration of impact involving the initial tear, neuronal injury and hemorrhage of the cerebral tissue caused by the mechanical insult (Mustafa & Al-Shboul, 2013). The secondary stage, also referred to as secondary injury, occurs at the moment of primary injury and subsequently evolves over hours to days and even months (Kumar & Brain, 2012). The secondary phase of injury may be characterized by metabolic dysfunction, neurovascular damage, altered cerebral blood flow, neuronal apoptosis, excitotoxicity, oxidative stress, and inflammation (Pavlova et al., 2018).

Diffuse axonal injury entails both structural and functional alterations. From a structural standpoint, DAI is a primary axonal perturbation that is featured by fracture of the stiffest part of the axon cytoskeletal structure, the microtubules (Blennow et al., 2012; Koliatsos et al., 2020). Mainly caused by ultra-rapid shearing or tensile deformation, the breakdown of microtubules causes a halt in vesicular transport along the axon (Blennow et al., 2012; Koliatsos et al., 2020). Once microtubules are fractured, this leads to microtubular undulations, impairment of axonal transport with an ensuing accumulation of axonal transport cargos, axonal swelling called axonal retraction balls, followed by eventual disconnection and axotomy (Blennow et al., 2012; Koliatsos et al., 2020). Additional primary structural effects include mechanoporation of the axolemma (the cell membrane of an axon) and neurofilament breakdown (Koliatsos et al., 2020). Furthermore, if the axon is unable to recover, the damage eventually spreads throughout the cell causing further functional impairments and may lead to neuronal cell death in addition to network disconnection (Greve & Zink, 2009; Meythaler et al., 2001).

Even in instances where the axon's structure is not directly damaged, the forces imparted to the cerebral tissue typically result in the stretching and tearing of axons causing axonal disruption to neurons (Greve & Zink, 2009). As a result, dysregulation of protein channels within the neuronal plasmalemma then ensues, resulting in uncontrolled ion flux and neurotransmitter effects (Hovda et al., 2014, pg. 209). Specifically, liberation of potassium (K+) ions with a large influx of sodium (Na+) and calcium (Ca2+) ions (Hovda et al., 2014, pg. 209). The influx of Na+ and Ca2+ elicits rapid neuronal depolarization thus triggering the release of glutamate (Hovda et al., 2014, pg. 209). Glutamate then acts on several receptors causing further depolarization and calcium influx into the neuron which can lead to excitotoxicity (Greve & Zink, 2009).

While excess intracellular calcium can lead to axonal swelling, it also promotes oxygen radical reactions causing a further unstable environment (Greve & Zink, 2009). Due to the imbalance of normal ionic concentrations, the neuron must rely on the sodium-potassium pumps to restore ionic homeostasis (Hovda et al., 2014, pg. 209). However, since sodium-potassium pumps are not passive and are adenosine triphosphate (ATP)–dependent pumps, this leads to the rapid, acute depletion of ATP and consequently to an immediate period of hyperglycolysis (Hovda et al., 2014, pg. 210). Moreover, in an attempt to avert the glutamate-mediated accumulation of intracellular Ca2+ ions, the mitochondria begin sequestering the Ca2+, which in turn, causes the mitochondria to become less efficient at converting glucose to ATP, creating an energy crisis, and producing less ATP to drive the sodium-potassium pumps (Hovda et al., 2014, pg. 210). Consequently, this energy crisis, in turn, exacerbates the cellular conditions to a state in which, if not corrected, may lead to cell death (Greve & Zink, 2009).

Thus, as the name may lead readers to believe, there is nothing "mild" about an mTBI at the cellular level. Similarly, repetitive subconcussive (SC) head impacts can also trigger

neurochemical and neurometabolic reactions, although to a reduced degree which may lead to chronic neurological syndromes (Bailes et al., 2013). Consequently, in response to the disruption of homeostasis and the ensuing metabolic crisis, the immune system response is initiated and neuroinflammation begins.

### 1.5.1 Neuroinflammation

Neuroinflammation is an important secondary injury mechanism in TBI that involves a complex process of cumulative changes within the cerebral tissue. Post-traumatic cerebral inflammation is characterized by the combination of glial cell activation, such as microglia, and astrocytes, as well as macrophage and leukocyte recruitment, all modulated by complex pro-and anti-inflammatory mediators, such as cytokine and chemokines (Simon et al., 2017).

Increased neuronal permeability, caused by the shearing and stretching of axons due to mechanical tissue deformation, is thought to be the initiation of the inflammatory process (Wofford et al., 2019). As previously described, following mechanoporation to neuronal membranes, the excessive extracellular levels of glutamate from leaky neuronal membranes are claimed to be powerful drivers of inflammation (Wofford et al., 2019). Commonly observed features of neuronal permeability have been seen in the cortex, sub-cortical white matter, and in the hippocampus of the brain parenchyma (Wofford et al., 2019). In a healthy environment, astrocytes aid in the reuptake of glutamate from the synapses and recycle it back to neurons, however, following cerebral injury, excessive glutamate released from neurons and impaired astrocytic clearance of glutamate further aid the initiation of the inflammatory process (Sofroniew & Vinters, 2010; Yi & Hazell, 2006). Additionally, microglia, monocyte, and macrophage immune cells possess glutamatergic receptors; thus, it is further supported that this

rise of glutamate within the cerebral tissue, as monitored by microglia and astrocytes, is a key contributor to the immune response process (Kumar & Brain, 2012).

As pathological sensors of TBI, microglia rapidly enter into a state of activation, called microgliosis, by taking on an amoeboid shape resembling peripheral macrophages, and scavenge the CNS producing and releasing cytotoxic molecules (i.e., oxygen-free radicals and inflammatory cytokines) in order to protect and repair the damaged cells (Kumar & Brain, 2012; Chiu et al., 2016; Aihara et al., 2009). Simultaneously, microglia play a role in clearing cellular debris (i.e., broken myelin or cellular membranes) and toxic substances by phagocytosis (Chiu et al., 2016). However, if the damage is too severe or the impact is ongoing, microglia will remain in a state of continual defense which leads to persistent inflammation and has been shown to result in neurodegeneration and functional deficits in preclinical (Fehily & Fitzgerald, 2017) and clinical studies (Faden et al., 2016).

Like microglia, astrocytes are also involved in neuroinflammation, undergoing a morphological change known as reactive astrogliosis that involves cellular hypertrophy, lengthened processes, increased expression of intermediate filaments (vimentin and glial fibrillary acidic protein (GFAP)), and the production/release of pro-inflammatory mediators (Sofroniew & Vinters, 2010; Zhang et al., 2010). Following injury, hypertrophic astrocytes are recruited to surround the lesion site not only to protect damaged cells but also to restrict inflammation and preserve cellular domains and tissue structure through scar formation (Sofroniew & Vinters, 2010). Additionally, astrocytes play a vital role in regulating extracellular glutamate levels, which can reduce glutamate excitotoxicity to neurons and surrounding cells (Schousboe & Waagepetersen, 2005)

Furthermore, similarly to microglia, reactive astrocytes can have detrimental and/or beneficial roles following CNS injury (Yuan & Wu, 2022). While astrocytes have been shown to provide neurotrophic support and guidance for axonal growth following CNS injury (Chung et al., 2015; Zhou et al., 2020), prolonged astrogliosis can also inhibit axon regeneration and hinder functional recovery (Furman et al., 2016; Perez et al., 2017).

Bidirectional communication between glial cells is crucial for functions, homeostasis, and recovery from injury. Studies have shown that activated microglia directly impact the activation state of astrocytes via the generation and release of inflammatory mediators, such as cytokines, that, in turn, act on surrounding glia and neurons (Liu et al., 2011; Jha et al., 2019). Concurrently, activated astrocytes can secrete both pro- and anti-inflammatory cytokines on microglia (Jha et al., 2019; Sofroniew & Vinters, 2010). Among various cytokines, pivotal mediators associated with post-traumatic neuropathological damage include tumor necrosis factor (TNF) and the interleukin (IL) family of peptides and have been shown to markedly increase in the acute period following both experimental (Holmin et al., 1997; Jha et al., 2019; Robinson et al., 2017; Zhao et al., 2014) and clinical (Ziebell & Morganti-Kossmann, 2010) brain trauma.

However, depending on the type of impact, its intensity, and the time of exposure, this crosstalk of inflammatory mediators does have the capacity to create a neurotoxic environment thus augmenting the initial injury (Clark et al., 2019; Kreutzberg, 1996; Liddelow et al., 2017). In synopsis, neuroinflammation is considered to have both beneficial and detrimental roles. Significant benefits can be achieved when the inflammation is controlled in a regulated manner and for an acute period. However, when excessive, it can become a major cause of several neuropathologies and, thereby, drive neurodegenerative processes (Bao et al., 2012; Block et al.,

2007; Sheng et al., 2013; Shultz et al., 2013; Webster et al., 2015). Thus, understanding the initiation of immune cell reactivity in addition to its consequences on neuronal health is essential for preserving the beneficial effects of acute inflammation while minimizing the destructive consequences of sustained inflammation (Wofford et al., 2019).

### 1.6 Repeated Head Trauma

Recurrent traumatic brain injury, especially mTBI, has become a popular interest within the research realm of neurotrauma due to the concern that repeated mTBI increases the risk of cognitive impairment later in life or possible neurodegenerative diseases such as Chronic Traumatic Encephalopathy (CTE) and/or Alzheimer's Disease (Galgano et al., 2016; Prins et al., 2013; Safinia et al., 2016; Shurley & Todd, 2016; Witcher et al., 2015). CTE is a tau protein neurodegenerative disorder that, thus far, can only be diagnosed post-mortem (Baugh et al., 2012). In the past, mounting clinical and preclinical evidence suggested that the pathology contributing to CTE was caused by repetitive exposure to concussive impacts (Baugh et al., 2012; Fujita et al., 2012; Hoogenboom et al., 2019; McAteer et al., 2016; A. L. Petraglia et al., 2014; Prins et al., 2010; Shitaka et al., 2011a; Smith et al., 2013; Stein et al., 2014; Stern et al., 2011; Thomsen et al., 2017; VanItallie, 2019). However, recent post-mortem neuropathology has confirmed CTE in football players with no history of diagnosed or reported concussions (but played in positions, such as lineman, with the greatest exposure to repetitive hits to the head (Greenwald et al., 2008)), suggesting that repetitive SC impacts may also lead to the development of this neurodegenerative disease (Bailes et al., 2013; Dashnaw et al., 2012; Gavett et al., 2011; A. L. Petraglia et al., 2014; Spiotta et al., 2012; Talavage et al., 2014).

Although SC events do not result in observable symptoms and apparent behavioral modifications (Miller et al., 2007), exposure to repetitive SC blows to the head may result in

equivalent, if not greater damage than a single concussive event (Bazarian et al., 2012) and may have cumulative effects (Breedlove et al., 2012). Even though SC impacts are not medically diagnosed, clinical data has shown that these repetitive low-load impacts can result in neuropsychological changes (Bazarian et al., 2012; Killam et al., 2005; McAllister et al., 2012; Talavage et al., 2014). However, what is not known is the number of head impacts and their intensity that might lead to similar pathophysiological concussive effects (i.e. a concussion cumulative threshold) (King et al., 2015). The injury threshold is likely to be different for each person given the multifactorial nature of head injuries, such as age at exposure of impact, type and magnitude of exposure, location of impact, recovery periods, individual vulnerability, and others (Bailes et al., 2013). Though, if a threshold could be determined, players could be monitored to reduce their potential risk for a serious and irreversible cerebral injury.

The increased incidence of repeated head trauma has generated new topics of discussion about the existence of cerebral vulnerability, its duration, and its relationship to subsequent injuries. Evidence suggests that repeated head injuries may lead to a state of enhanced vulnerability in which a secondary insult may exacerbate the initial damage (Gennarelli, 1993; Jenkins et al., 1989; Yoshino, Hovda, Kawamata, Katayama, & Becker, 1991; Mayumi L. Prins, Alexander, Giza, & Hovda, 2013a). Recent studies of TBI have shown that while repeat trauma can exacerbate structural, functional, metabolic, and behavioral responses, these responses only occur when the injury is repeated within a certain period post-injury (Bolton & Saatman, 2014; Fehily et al., 2019; Meehan III et al., 2012; Prins et al., 2013). Using rodent models to model repeated mTBI, this window of vulnerability to the brain is greatest when the interval between head injuries, also called an inter-injury interval, is short, between hours to days (Bolton & Saatman, 2014; Fehily et al., 2019; Meehan III et al., 2012; Mayumi L. Prins et al., 2013a), while

any risk of enhanced damage due to a secondary insult is averted when the inter-injury interval is elongated, days to weeks (Meehan III, Zhang, Mannix, & Whalen, 2012; Mayumi L. Prins et al., 2013a). According to Bolton and Saatman (2014), a longer inter-injury interval allows the brain to recover and reduces the potential for exacerbation of the secondary injury cascade.

Unfortunately, there is not a universal window of vulnerability for repeated head impacts. Not only does the inter-injury interval between impacts influence the brain's window of vulnerability, but also the severity of the initial injury, subconcussive, mild, or severe, can influence this variable. As such, investigators are forced to rethink the issue of repeated injury to frame discussions to consider both of these influencers, inter-injury interval and severity of injuries, as predictors of increased neuroinflammation and neurodegeneration.

## 1.7 Motivation for Study

While the term concussion is frequently used synonymously with mTBI, some distinguish mTBI as a post-mortem head injury diagnosis evident through pathophysiology and concussion as a pre-mortem diagnosis related to functional disturbance symptoms (for example, fatigue, headache, dizziness, irritability, memory impairment, etc.) (Anderson et al., 2006). Regardless of the ambiguity of terminology, there is universal agreement that a concussion can lead to significant impairment and reduced quality of life (Anderson et al., 2006). As such, concussion has become a widely studied field in neurotrauma. Increased awareness of this epidemic has led to research efforts focused on determining the threshold of head impact that will result in cerebral damage and loss of function (Hsieh et al., 2017; Ma et al., 2019; McNamara et al., 2020). However, these much lighter forms of head impacts, so-called subconcussive, are currently understudied and their underlying mechanisms and potentially detrimental effects are unknown (Rawlings et al., 2020).

While this low-level impact may not induce symptoms that are immediate or necessarily delayed in onset, it has been increasingly recognized that repeated SC exposure has long-term consequences (Bailes et al., 2013). Numerous studies have demonstrated that repetitive concussive and even SC impacts strongly correlate with the development of the neurodegenerative disease, CTE (Bailes et al., 2013; Galgano et al., 2016; Prins et al., 2013; Safinia et al., 2016; Shurley & Todd, 2016; Witcher et al., 2015). As such, many preclinical studies have been conducted to investigate the sequelae of repetitive mTBI impacts in relation to the pathological presentation of CTE (Fujita et al., 2012; Hoogenboom et al., 2019; McAteer et al., 2016; Petraglia et al., 2014; Prins et al., 2010; Shitaka et al., 2011b; Thomsen et al., 2017). Alternatively, limited preclinical studies have been conducted to investigate the pathophysiological effects of repetitive SC impacts (Bree, Stratton, et al., 2020; Rawlings et al., 2020; Sagarkar et al., 2017).

Determining the lower limits of systematic perturbation resulting from repeated SC impacts is of critical importance in expanding our understanding of cerebral vulnerability and recovery. However, the impact loads utilized in preclinical SC impact studies implement impact load magnitudes falling within the range of those used to model mTBI (Bree, Stratton, et al., 2020; Sagarkar et al., 2017). This choice in methodology largely stems from the absence of well-defined guidelines and mechanical parameters for modeling head injury of graded severities (Siebold, Obenaus, & Goyal, 2018). Furthermore, because of the undefined cumulative threshold for the repetitive occurrence of low-level impacts, there is a lack of correlation between an mTBI and repetitive SC impacts with respect to injury biomechanics. Such data would lay the foundation for a kinetic and kinematically defined threshold of repeated low-level impact

tolerance and expand upon the current understanding of cerebral vulnerability resulting from SC head impacts.

## 1.8 Objectives

The following investigation aimed to address these gaps in knowledge through the utilization of an in-house built weight drop injury device using a rat model. In order to investigate the pathophysiological differences between a single mTBI and repeated subconcussive (RSC) impacts with subdivided cumulative kinetic energy (KE) equal to the single mTBI impact, a pilot study was performed in order to determine the appropriate impact load suitable for an mTBI using the in-house built impact device. Results obtained from the pilot study were used to inform the appropriate impact load to model an mTBI necessary for use in the full study design. Both study designs evaluated evidence of behavioral alterations, inflammation, and cerebral vulnerability using behavioral assays and immunohistochemistry. Measurement outcomes were assessed at two recovery time points, 3- and 7-days, following the final impact.

The primary objective for this investigation was to develop a rodent model of a single closed head mTBI and repeated SC impacts with subdivided cumulative kinetic energies equal to the single mTBI impact utilizing an in-house developed weight drop injury device capable of producing a wide range of repeatable impact loads, including below those reported in the literature. This not only establishes the foundation for subsequent analyses but addresses the absence of knowledge surrounding the comparative effects between a concussive and repeated SC impact. Based on a thorough review of available literature, no study has utilized impact loads below a KE of 0.146 J for a closed head impact using a rat model. Kinetic energy (J) is the measure of energy of a moving object (for this study, the impactor to the rat's head). Furthermore, the majority of the few laboratories that have utilized impact loads below the range

associated with an mTBI have done so in the context of open-scalp or craniectomy techniques. The present investigation aims to achieve an impact load of similar intensity without surgical procedures directly addressing this knowledge gap.

This is addressed in the second and third objectives for the investigation which aimed to investigate indications of system perturbation and/or inflammation and cerebral vulnerability over two-time points (3- and 7-days) post-impact between impact loads (single mTBI vs. repeated SC). System perturbation investigation includes behavioral tests of anxiety and general locomotive activity (Open Field Test), as well as neuromotor deficits (Rotarod). The final and third aim of this study was to assess and compare evidence of inflammation and cerebral vulnerability using immunohistochemical assessment of astrogliosis (GFAP), microgliosis (Iba-1), neuronal loss (NeuN), as well as inflammatory cytokine proteins (IL-6, TNF-α, and IL-10) within the hippocampus and motor cortex of the treatment groups (mTBI vs RSC). By bridging investigative measurements from objectives two and three, this study was able to expand the current understanding and body of knowledge surrounding the cumulative effects between a single mTBI and RSC impacts.

# CHAPTER II

# LITERATURE REVIEW

## 2.1 Rodent Models of Traumatic Brain Injury

As mentioned earlier, there is a vast array of injury combinations (whiplash, blunt, and blast) that can induce a traumatic brain injury (TBI) with various injury severities that may result in acute and chronic symptoms. It is therefore critical to have a wide range of robust, reproducible preclinical animal models that capture these variations in injury models and severities to investigate the underlying pathology and functional deficits associated with TBI. Animal models are typically designed to produce homogeneous injuries, with demographic features (age and sex) and injury parameters tightly controlled.

Preclinical rodent models of TBI typically employ one of three popular blunt impact models, Fluid Percussion Impact (FPI), Controlled Cortical Impact (CCI), or Weight Drop Injury (WDI), to induce brain injury replicating features and outcomes that are seen clinically (Bondi et al., 2015). Each can be used to produce mild to severe injury and has been subject to variation due to investigator customization (Bondi et al., 2015). The FPI model is an open head model (exposed cortical surface) that requires a craniotomy (a surgical opening into the skull) to expose the dura mater, a thick membrane of connective tissue that surrounds the cerebral tissue, for injury (Bolouri & Zetterberg, 2015). A major limitation to this choice of head injury model is its inability to be modified for closed head impacts due to its mechanism of injury. It has been suggested that the craniotomy procedure itself has been associated with inflammation that can

exacerbate TBI symptoms and neuropathology (Cole et al., 2011). As such, investigators that employ an open head model must consider the procedure as a confounding influencer in their neuroinflammatory analysis. Alternatively, both the CCI and WDI models can be performed as open head, closed-skull (open-scalp), and closed head (closed-scalp) models (Bondi et al., 2015; Bree, Mackenzie, et al., 2020; H. Chen et al., 2017; Clark, Schiding, et al. 1994; Flierl et al., 2009; Fujita et al., 2012; Igarashi et al., 2007; Jamnia et al., 2017; Osier & Dixon, 2016; Yates et al., 2017). The fluid percussion device induces an injury through a craniectomy by applying a brief pressurized pulse through a fluidic medium onto the exposed dura resulting in a brief compression of the neural tissue (Alder et al., 2011). Alterations of severity intensities can be achieved by adjusting the pressure pulse through the modification of fluid volume and loading rate (Kabadi et al., 2010). Alternatively, the CCI model employs a pneumatic piston or electrical actuator to achieve rapid speeds of the impact rod to induce injury (Dixon et al., 1991). In rodent models, the CCI's impactor rod tip diameter ranges from 1-6 mm in size in order to localize the impact at specified stereotaxis coordinates on the rodent's cortical surface (Osier & Dixon, 2016). Generally, 3 mm tips are commonly used for mice and 5-6 mm tips for rats (Osier & Dixon, 2016). Alternatively, the WDI model involves exposing the rodent's head to a free-falling, guided weight. As the name suggests, the technique uses a specified weight to be dropped through a tube from a precise distance from the rodent head to impact the cranial surface (Bolouri & Zetterberg, 2015; Fujita et al., 2012; Hoogenboom et al., 2019).

Because there is no defined threshold for modeling a mild traumatic brain injury (mTBI), there is wide variation in the literature with respect to appropriate input parameters using a rat model. The injury severity level induced by the CCI device is often tuned through adjustments of the following input parameters: depth of impact (displacement of cortical tissue), velocity, and

dwell time (Osier & Dixon, 2016). The WDI model typically uses a specified weight dropped from a particular height to induce an mTBI (Bodnar et al., 2019; Hoogenboom et al., 2019; Marmarou et al., 1994). Both the CCI and WDI models typically accept the absence of skull fracture and 0% mortality as an affirmation of successful modeling of an mTBI/concussion (Abd-Elfattah Foda & Marmarou, 1994; Bodnar et al., 2019; Hoogenboom et al., 2019; Marmarou et al., 1994). Alternatively, an FPI model confirms an mTBI when a righting reflex time occurs between 2-4 minutes along with a 0-5% mortality rate (Alder et al., 2011). A description of each model is summarized in Table 2.1 in addition to typical parameters, limitations, and outcomes commonly used to verify successful modeling of an mTBI.

Table 2.1 Typical Impact Parameters and Limitations for Rodent Head Injury Models of an mTBI.

| **Head Injury Model** (*Abbr.*) | **Parameters** (*Range*) | **Limitations** (*Injury Type*) | **References** |
|---|---|---|---|
| Fluid Percussion Injury (*FPI*) | Fluid pressure (*0.9-2.2 atm*) | Craniotomy required (*open head*)<br><br>Focal Injury | (Brooks et al., 2017; Chitturi et al., 2019; Kabadi et al., 2010; Selwyn et al., 2016; Shultz et al., 2011; Wright et al., 2019; Zhang et al., 2018) |
| Controlled Cortical Impact (*CCI*) | Depth (*1-3 mm*)<br>Velocity (*3-6 $ms^{-1}$*)<br>Dwell time (*50-250 ms*) | Typically open head (open-skull or open-scalp)<br><br>Focal Injury | (Bondi et al., 2015; Hoogenboom et al., 2019; Osier & Dixon, 2016) |
| Weight Drop Injury (*WDI*) | Weight mass (*450 g*)<br>Drop Height (*1.0 m*) | Possible rebound impact | (Bodnar et al., 2019; Hoogenboom et al., 2019; Marmarou et al., 1994) |

As each model has multiple variations including whether the animal's skull or scalp is open or closed during injury, whether the head is fixed in place (using a stereotaxic instrument) or allowed to move freely for a rotational impact, or whether the impact is given laterally or centrally to the animal's head, this introduces a wide array of heterogeneous methods and

outcome metrics (Bondi et al., 2015). As such, it is difficult to compare the majority of preclinical investigations due to the diversity of methodologies.

## 2.2 Rat Models of Closed-Head Subconcussive Impacts

Based on an extensive literature search, a finite number of studies have been conducted investigating the cumulative effects of repeated impacts loads below the range used to model an mTBI. According to the limited reports available, the majority of literature indicates that a single SC impact is not expected to produce detectable pathology or functional alterations (Bree, Stratton, et al., 2020; Gavett et al., 2011; McKee et al., 2009; Spiotta et al., 2012; Stern et al., 2011; Talavage et al., 2014). However, according to an extensive review from Bailes et al. (2013), a single SC head injury can create an environment of cerebral vulnerability that increases the determinantal effects of subsequent impacts.

Further, the few studies that explore impact loads labeled as "subconcussive" typically do so in the context of a repetitive impact model. As previously mentioned, while there are a few studies employing rodent models of single SC impact loads in the literature, for the sake of brevity, these studies will not be included in this review. Additionally, attention was focused on rat models, rather than murine. It should be noted that three additional studies utilizing repeated low-level impact loads were identified in the literature, however, these employed a murine animal model (Gangolli et al., 2019; Honig et al., 2020; Namjoshi et al., 2014).

In a 2017 study, Sagarkar et al. used a Wistar rat model to study the effects of a repeated SC head injury (n=5) with a 48 hr recovery period between impacts using a WDI apparatus. Rather than labeling the CHI as subconcussive, the authors used the terminology "minimal traumatic brain injury." Each head impact generated an impact energy load of 0.588 J and an impact velocity of 2.425 $ms^{-1}$ using a cylindrical metal weight of 200 g from a 30 cm height onto

the exposed skull of the rat (Sagarkar et al., 2017). Thus, the total kinetic energy (KE) transfer to the skull of each treatment animal for 5 impacts was 2.94 J. The purpose of this study was to detect possible dysregulation of the amygdaloid brain-derived neurotrophic factor (BDNF) expression as a consequence of injury-induced DNA methylation at 48 hrs and 30 days after repetitive minimal TBIs (Sagarkar et al., 2017). Amygdaloid BDNF has been widely accepted as a contributor to abnormalities caused in synaptic plasticity and dendritic maintenance making it a useful target for detecting low-level disturbances (Bennett & Lagopoulos, 2014). Using a Light-Dark Box exploration test, investigators measured anxiety in conjunction with genomic testing related to their objective (Sagarkar et al., 2017). Results indicated that, after a single impact, minimal TBI animals showed a significant increase in anxiety at 48 hrs and 30 days post-injury compared to sham animals. Furthermore, significantly increased levels of cytosine methylation (5-mc) were found in minimal TBI-induced rats at 48 hrs and 30 days post-trauma indicating the persistent effects of trauma on BDNF promoter DNA methylation in comparison to sham levels. These findings indicate that the accumulation of repeated low-level impacts results in acute and chronic systemic perturbations (Sagarkar et al., 2017).

Christie et al. used a juvenile rat model to establish a new rapid neurological assessment protocol (NAP) for reliably and repeatedly inducing a mild awake closed head injury (ACHI) with 0% mortality or clinical indications of persistent pain using a CCI apparatus (Christie et al., 2019). The authors aimed to provide a standardized set of procedures allowing the ACHI and NAP protocol to be used reliably and repeatedly in various laboratories (Christie et al., 2019). To immobilize the awake animals during impact, a restraining cone was utilized. A 3D-printed helmet was affixed to the rodent's head to better distribute the force of impact across the head. Before impact, the animal was placed on a foam pad where the impactor tip was positioned on

the target site of the helmet. A CCI (7 mm diameter tip, 10 mm depth, 6.0 $ms^{-1}$ speed, 10 ms dwell) was then delivered to the helmet surface generating a KE of 0.146 J. Depending on group assignments, rats received 8 ACHI procedures over 1, 2, or 4 days. Immediately after impact, NAP scores were obtained for both sham and treatment groups following the first, second, fourth, and eighth ACHI procedure. The NAP consisted of a set of rapid assessment regimes focused on different tasks (state of consciousness, startle reflex, limb extension, flat beam walk, rotating beam walk) that are sensitive to mTBI measurements (Christie et al., 2019). Results revealed no significant indications of pain exhibited by animals. These findings indicated that according to the neurological assessment protocol, repeated impacts at this low-level load results in negligible pain (Christie et al., 2019). Furthermore, to the best of our knowledge, the impact load investigated in this study (~ 0.15 J) is the lowest explorative impact load for a rat model using a closed head injury (CHI) encountered in the literature.

In a 2020 study, Bree, Stratton, et al. utilized a Sprague-Dawley rat model to investigate the development of posttraumatic headache-like (PTH) pain and anxiogenic behavior following three different CHI paradigms, employed in separate cohorts of rats. Using a WDI model, the first paradigm involved a single, moderate to severe impact, using a 450 g weight from a height of 80 cm to induce an impact velocity of approximately 3.959 $ms^{-1}$ inducing an impact KE load of 3.528 J. The second paradigm involved a single 150 g weight drop from the same height to induce an impact velocity of 1.176 $ms^{-1}$ and an energy of 1.176 J. Lastly, the third paradigm involved three successive 150 g weight drop events, conducted 72 hrs apart, imparting a cumulative KE of 3.528 J (Bree, Stratton, et al., 2020). The authors labeled the impact load of 1.176 J as subconcussive. However, according to a different laboratory, using a WDI system on a rat model, investigators label a similar energy load (1.103 J) as an mTBI impact (Singh et al.,

2016). As such, the appropriate labeling of this impact load is in question. Bree, Stratton, et al. (2020) employed two behavioral assays, an Open Field Test (locomotion and anxiety-like behavior) and von Frey Test (tactile pain hypersensitivity). No neuroinflammatory analysis was investigated in this study. According to group assignments, the open field test (OFT) was conducted at 3-, 7-, and 14-days post-injury and the Von Frey testing was similarly conducted with additional investigations at 4- and 6-weeks post-injury. As expected, rats subjected to a single, moderate to severe CHI displayed an acute decrease in locomotion and increased anxiety-like behavior together with headache-like pain that resolved by 6 weeks post-injury. Animals subjected to a single SC head impact did not lead to any changes in locomotion or indicate evidence of anxiety or PTH pain behavior compared to shams. However, repeating these SC impacts in rats did give rise to persistently decreased locomotion in the OFT, which likely suggests brain injury. In addition, rats receiving repetitive 150 g weight drop injuries displayed persistent PTH pain behavior resembling that encountered in animals subjected to the single 450 g weight drop injury. These findings indicated that the repeated low-level impacts with subdivided cumulative kinetic energies of the single, moderate to severe injury resulted in similar behavioral responses compared to shams (Bree, Stratton, et al., 2020).

### 2.3 Assessments of Behavioral Deficits Following Traumatic Brain Injury

Individuals sustaining an mTBI often complain of several physical, cognitive, and emotional/behavioral symptoms generally referred to as post-concussion syndrome (PCS) (Ryan & Warden, 2003). Commonly self-reported symptoms can include headache, nausea, dizziness, irritability, balance or motor disturbances, decreased concentration, memory problems, depression, anxiety, deficits of executive function, and sleep disturbances (Iverson & Lange, 2011; Ryan & Warden, 2003). The majority of these symptoms are often reported between days

and weeks but can also prolong from months to years following injury (Ryan & Warden, 2003). It is understood now that individuals diagnosed with a concussion are not always characterized by diagnosable objective structural brain alterations in congruence with functional disturbances (Nauman et al., 2020). Interestingly, though, within the last decade, we have begun to see evidence of the physical and/or behavioral disturbances commonly observed in a diagnosed symptomatic concussive setting, in both clinical and preclinical SC injuries which are characteristically asymptomatic (Bailes et al., 2013; Broglio et al., 2012; Talavage et al., 2014; Gysland et al., 2012; Breedlove et al., 2014; Bree et al., 2020; Christie et al., 2019; Lavender et al., 2020; Sagarkar et al., 2017).

As previously mentioned, anxiety and sensorimotor impairments are among the commonly reported post-concussive symptoms (Armstrong & Morrow, 2019). Subsequently, rodent models of concussion and subconcussion frequently employ a variety of behavioral assays aiming to understand the physiological basis for these symptoms (Bodnar et al., 2019; Almeida-Suhett et al., 2014; Beitchman et al., 2020; Bree, Mackenzie, et al., 2020; Kosari-Nasab et al., 2019; Meyer et al., 2012; Namjoshi et al., 2017; Sagarkar et al., 2017). Two widely used assays are the Open Field Test (OFT) and rotarod test (Bodnar et al., 2019; Bondi et al., 2015). The OFT can be used to assess general locomotor activity as well as anxiety-like behaviors (Seibenhener & Wooten, 2015). Rodents are placed in an open arena and allowed to freely explore the arena or field in an uninterrupted room for a set duration (typically, <1 hr) (Seibenhener & Wooten, 2015). To evaluate locomotive activity, the animal's total distance traveled and time spent mobile/immobile are typically measured (Seibenhener & Wooten, 2015). Rodents are naturally curious and explorative creatures. However, in cases where rodents remain close to the walls of the arena while they explore the arena, commonly referred to as "wall-

hugging" tendency, investigators frequently relate this behavior to anxiety (Seibenhener & Wooten, 2015). Typically, a non-anxious rodent will cross through the center of the arena during exploration, while an anxious-like rodent will avoid leaving the wall boundary (Seibenhener & Wooten, 2015). Thus, common variables to measure for anxious-like behavior during an OFT is the time spent near the walls of the arena versus the time spent in the center area, thigmotaxis (the tendency of a subject to remain close to walls), and the number of center area crossings (Seibenhener & Wooten, 2015).

Similarly, the rotarod test has been utilized in many TBI models as an indicative measure of motor deficits such as coordination and balance (Bondi et al., 2015; Y. C. Chen et al., 2014; Hamm et al., 1994; Kim & Han, 2017; Lavender et al., 2020; Mouzon et al., 2012; Onyszchuk et al., 2007; Thomsen et al., 2017; S. H. Yang et al., 2013). For the rotarod test, rodents are placed on a rotating spindle for a limited time. Recorded measurements include the time of fall for each subject, the reason for fall (jump, passive rotation, or actual fall), and all experimental setup parameters. Typically, rats are trained for this behavior assay prior to surgery and/or injury and consist of multiple trial runs of both fixed-rate and accelerating protocols, which may vary from laboratory to laboratory, to establish their baseline performance (Bondi et al., 2015). After surgery or injury has occurred, measurements of alterations in motor coordination are then conducted at prescribed time points. Finally, the two outcome variables used to evaluate the assessment of motor function are the total time (seconds) and/or speed of revolutions (revolutions per minute, rpm) before the animal loses its balance and falls off the accelerating rotating rod (Bondi et al., 2015).

## 2.4 Assessments of Neuroinflammation and Cytokine Expression Following Traumatic Brain Injury

Neuroinflammation is a primary consequence of neuronal injury following a traumatic brain injury (Chiu et al., 2016). It has also been suggested as a potential contributor to the cumulative neurodegenerative effects of repeated SC injuries (Shultz et al., 2012). Following an injury to the cerebral tissue, multiple types of dormant glial cells, including microglia and astrocytes, will undergo a morphological change to become rapidly activated in a process called "reactive gliosis" (Chiu et al., 2016). During this state of reactive gliosis, activated microglia begin to initiate and sustain astrocytic activation via the generation and release of inflammatory mediators such as cytokines and chemokines that, in turn, act on surrounding glia and neurons to facilitate tissue repair (Chiu et al., 2016). Microglia are considered to protect neurons by migrating to the site of injury to clear debris (Chiu et al., 2016). Astrocytes play a role in inflammation signaling, blood-brain barrier maintenance, lesion isolation, debris clearing, and axonal scar formation (Burda et al., 2016). Detection of glial reactivity is commonly employed in neurotrauma research and can be accomplished by targeting and measuring the expression of various biomarkers. Ionized calcium binding adaptor molecule 1 (Iba-1) and glial fibrillary acidic protein (GFAP) are two popular biomarkers used to identify and measure microgliosis and astrogliosis (Chiu et al., 2016; Lafrenaye et al., 2020; Z. Yang & Wang, 2015). Cytokine detection methods include protein analyses methods such as an enzyme-linked immunosorbent assay (ELISA) as well as multiplex technologies (Chiu et al., 2016).

While neuroinflammatory measures of astrocytic and microglial activity following injury has been investigated in a large quantity of mTBI/concussive preclinical studies (Bodnar et al., 2019; Karve et al., 2016; Velayudhan et al., 2021), knowledge of these glial reactivities is limited for SC impacts employing rodent models (Shultz et al., 2012; Singh et al., 2016). Further, the

majority of what is known about the temporal expression of cytokines has been explored as a consequence of mild to severe traumatic brain injury (Kamm et al., 2006; Robinson et al., 2017; Ziebell & Morganti-Kossmann, 2010) and/or in an open head injury model (Briones et al., 2014; Holmin et al., 1997; Lagraoui et al., 2012; Lee et al., 2012; Zhao et al., 2014).

Lagaoui et al. employed a murine model to investigate behavioral changes and cytokine protein responses following a single mTBI using a CCI apparatus (Lagraoui et al., 2012). Although this study discusses data from a murine model, work from Natalie et al. reveals the inflammatory response to TBI in mice and rats is highly similar (Natale et al., 2003). A CCI was performed immediately after a craniotomy using a 3 mm flat tip at an impact velocity of 5 $ms^{-1}$, a depth of 2 mm, and a duration of 200 ms, to deliver a KE of 0.086 J (Lagraoui et al., 2012). A second animal cohort was only subjected to a craniotomy and underwent the same procedures as the CCI group; they were labeled as "mild brain injury." Because the impact injury was performed directly over the motor cortex, post-injury motor function was assessed via rotarod and balance beam assays. In the rotarod task, CCI mice (labeled as "severe brain injury") showed a significant deficit in performance in both the maximum speed attained and latency to fall from an accelerating rotarod compared to the craniotomy mice (labelled as "mild brain injury") at 1- and 3-days following impact. Although not statistically significant after 3-days post-impact, CCI mice continued to reveal a consistent deficit compared to craniotomy animals persisting up to 3 weeks post-injury. After one week of recovery, CCI mice returned to the baseline level of performance in rotarod tasks. In the balance beam task, both CCI and craniotomy mice were significantly affected during the first-week post-injury. Notably, during the first-week post-injury, motor performance was more severely impaired by CCI than by craniotomy. These data were significant for the beam crossing time on day 7 and for foot slips on days 3 and 7 after

injury. By recovery day 10, both animal groups showed a significant improvement in their performance on the balance beam. In summary, motor function was most pronounced during the first-week post-TBI, with deficits in function observed in both CCI and craniotomy animals.

In congruence with motor function deficits, Lagaoui et al. (2012) performed histological analysis of astrogliosis near the site of injury in CCI, craniotomy, and naive animals. Results showed high astrocyte density and enlarged astrocyte bodies at 3-days post-injury in CCI and craniotomy animals, relative to naïve controls. Furthermore, a small collection of cytokine protein levels was assessed at 1-, 3-, and 7-days post-injury, again, comparing tissues of CCI, craniotomy, and naïve animals (Lagraoui et al., 2012). Cytokines of interest for this study included the following: chemokine (C-X-C motif) ligand 1 (CXCL1), interleukin (IL)-1 beta (IL-1β), IL-6, interleukin-12p70 (IL-12), interferon-gamma (IFNγ), and IL-10. Results showed all six cytokines significantly increasing following the controlled cortical impact compared to the naïve controls. Of these six cytokines, peak expression was observed on recovery day 1 for three cytokines (CXCL1, IL-1β, and IL-6) in the CCI and craniotomy groups, while the other three cytokines (IL-12p70, IFN-γ, and IL-10) exhibited peak expression on recovery day 3 for CCI mice and day 7 for craniotomy mice. The only statistically significant difference between CCI and craniotomy mice was for IL-6 at 1-day post-injury, where CCI mice expressed significantly higher levels. In general, protein expression data were consistent with the behavior data: significant behavioral deficits correlated with the peaks of the inflammatory response. These data suggest that major differences in the extent of brain tissue injury (craniotomy vs. CCI) are reflected by modest differences in behavioral deficits and inflammatory cytokine production (Lagraoui et al., 2012).

Zhao et. al. carried out an inflammatory analysis of TBI using an open head (craniotomy required) WDI rat model (Zhao et al., 2014). Before impact, a helmet-like disc was placed on the dura of the rat. Using a 20 g steel rod, dropped from a height of 25 cm, an impact velocity of approximately 2.214 $ms^{-1}$ with approximately 0.049 J of kinetic energy was achieved. Sham-operated rats were anesthetized and only received the right parietal craniotomy operation. The levels of TNF-α, IL-1β, IL-6, and IL-10 were examined from six rats in each group 72 hrs after injury. Subsequently, an additional six were euthanized on days 5 or 14 following injury for determination of astrocyte (GFAP) and microglial (Iba-1) cell markers in the cortex and hippocampal cornu ammonis 3 (CA3) area (Zhao et al., 2014). Results indicated in the TBI groups, the levels of IL-1β, IL-6, and tumor necrosis factor-alpha (TNF-α) in the brain tissue ipsilateral to impact were significantly increased 3-days after injury compared to sham. In contrast, the level of IL-10 was significantly decreased in the brain tissue ipsilateral to injury 3-days post-injury compared to sham. In congruence with these findings, the number of microglia and astrocytes were also significantly increased in the TBI groups compared to sham (Zhao et al., 2014). Overall, these data are evidence of the inflammatory response to low-level impacts and their role in the initiation and progression of the secondary phase of TBI.

Singh et al. (2016) carried out an inflammatory analysis of mTBI using a closed-head WDI rat model. Dropping a 450 g brass rod weight from a height of 25 cm, an impact velocity of approximately 2.21 $ms^{-1}$ and a KE of 1.10 J was achieved. Diffuse tensor imaging was used to investigate morphological changes associated with inflammatory evaluation (serum cytokine levels (TNF-α and IL-10) and astrocytic (GFAP) expressions) at 4 hrs, 1-, 3- and 5-days post-impact for sham comparison (0 hr PI) (Singh et al., 2016). A significant elevation in serum levels of pro-inflammatory cytokine TNF-α was observed at 4 hrs and anti-inflammatory cytokine, IL-

10, at day 1 post-impact compared to sham (0 hr) (Singh et al., 2016). Additionally, GFAP immunoreactivity in the cerebral cortex was significantly increased at day 3 and day 5 as compared to sham (Singh et al., 2016). Notably, there was no substantial changes of GFAP expression observed in the hippocampal or corpus collosum regions (Singh et al., 2016). Concurrently, a significant decrease in cortical mean diffusivity (MD) was observed 3- and 5-days post-impact (Singh et al., 2016). Additionally, a significant decrease in cortical radial diffusivity was observed at 1-, 3-, and 5-days post-impact (Singh et al., 2016). However, the hippocampus and corpus collosum did not show signs of significant alteration in diffuse tensor imaging measurements (Singh et al., 2016). Overall, these results suggest that an mTBI can initiate microstructural alterations and an inflammatory cascade at an acute timeline, when no injury is visible on conventional MRI.

Collectively, these studies all provide evidence of a significant biological response to mild TBIs. Additionally, evidence has shown this response can lead to neuroinflammatory events that may or may not recover (Singh et al., 2016). Furthermore, while there is limited data regarding the investigation of cytokine expressions due to low-level impacts using rodent models, they are all open head investigated injuries (Lagraoui et al., 2012; Zhao et al., 2014). As such, the investigation of cytokine analysis has yet to be employed in low-level, closed head, impact studies.

# CHAPTER III

# A NEW WEIGHT DROP INJURY DEVICE SUITABLE FOR MILD AND SUBCONCUSSIVE CLOSED HEAD INJURIES USING A RODENT MODEL

## 3.1 Introduction

Numerous animal models have been developed over several decades to address the heterogeneous nature of the clinical conditions following a traumatic brain injury (TBI). Still, most models are unable to simulate the entire spectrum of human TBI or reproduce common mechanisms of injury due to biomechanical forces and pathophysiological complexity of the injury process (Shultz et al., 2017). Further, as seen in extensive literature reviews, it has been shown that all models are confounded by the variability of injury severity and neurological outcomes due to TBI (Hoogenboom et al., 2019; Xiong et al., 2014). Thus, these limitations make biomechanical, cellular, molecular, and translational studies challenging.

Weight drop models have been gaining attention in the field of neuroscience given their similarities to clinical TBI (Albert-Weissenberger & Sirén, 2010) and their ability to simulate the full spectrum of TBI, ranging from subconcussive (SC) to severe TBI (Lavender et al., 2020; Bodnar et al., 2019; Ma et al., 2019). Other commonly employed TBI models, such as the fluid percussion injury and controlled cortical impact induce a focal brain contusion with little axonal injury (Johnson et al., 2015; Marklund, 2016). Conversely, weight drop injury models aim to reproduce diffuse brain injury (Marmarou et al., 1994). The basis for a WDI model is an impact

from a free-falling guided weight onto the head (open (with or without craniotomy) or closed) of a lightly anesthetized animal. In WDI models, injury severity is related to gravity force, thus the severity of impact can be controlled via modifications to the weight mass or release height. Additionally, the nature of injury and affiliated neurological deficits are dependent upon impact location (central or lateral), biomechanics (i.e., the weight's geometry (Pleasant et al., 2011) and degree of head movement (Mychasiuk et al., 2016)), and sex differences (Mychasiuk et al., 2016).

The vast majority of experimental investigations that employ a WDI model relate to exploring the pathophysiological consequences and functional deficits following a mild traumatic brain injury (mTBI) (Ma et al., 2019; Bodnar et al., 2019; Bree, Stratton, et al., 2020; B Fehily et al., 2019; Henninger et al., 2007; Hsieh et al., 2017; Kim & Han, 2017; K Singh et al., 2016). A finite number of studies using a WDI model have focused on the sequalae of events following a single (Bree, Mackenzie, et al., 2020; Bree & Levy, 2018) and repeated occurrence of a SC impact (Bree, Stratton, et al., 2020; Lavender et al., 2020; Sagarkar et al., 2017). Currently, there is a dearth of knowledge regarding a threshold of multiple SC injuries and their frequency before permanent cerebral damage occurs (Bailes et al., 2013; King et al., 2015). As such, given the current lack of understanding between concussive and SC impacts in clinical cases, there is a need for the development of an in-house built, weight drop injury device suitable for a mild and SC closed head impact (CHI) using a rodent model.

This chapter describes the development of a non-surgical rodent model for a diffuse closed head injury (CHI) to utilize as a model of a mild and SC TBI. The in-house built weight drop model was developed to reproduce key aspects of head injuries so that a mechanistic

understanding of how behavioral deficits and neuroinflammation might be developed in a rodent model.

## 3.2 Materials and Methods

A weight drop apparatus suitable for a CHI was designed and implemented to model a wide range of brain injuries in rats. The CHI design intended to meet two sets of criteria for TBI: improve the controllability of weight drop release and provide repeatability. One major goal in the development of this in-house CHI device was to be able to achieve a range of thresholds for brain injury, from mild to SC, to compare single versus repeated injuries.

### 3.2.1 System Overview

The in-house CHI model design used a polyvinyl chloride (PVC) tube to guide an impactor to fall from a predetermined height, an impactor weight of a predetermined mass, an electromagnetic solenoid to hold/release the impactor from a predetermined height, a 12-voltage direct current (DC) switching power supply to power the solenoid, a switch to turn on/off the supply power to the solenoid, a chronograph system to provide a change in time (i.e., velocity) data as the impactor passed through the tube, and an Arduino to control the chronograph system. A photograph of the system, seen in Figure 3.1, shows all the parts of the novel device: (1) 12-Volt switching power supply, (2) Arduino, (3) hold/release switch, (4) impactor weights, (5) chronograph system, (6) PVC tube, and (7) electromagnetic solenoid.

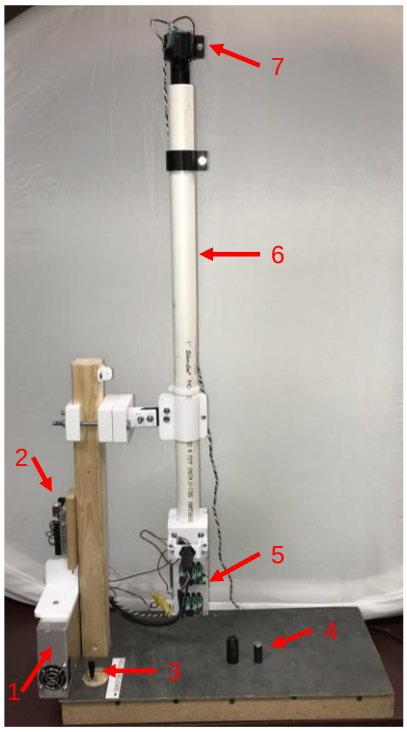


Figure 3.1 Weight Drop Injury apparatus used for experimental procedures.

Illustrative image of the novel, in-house, weight drop injury apparatus. Photograph of functional elements of the apparatus labeled as follows: 1) 12-Volt power supply, 2) Arduino, 3) release switch, 4) projectile weights, 5) chronograph system, 6) PVC tube, 7) electromagnetic solenoid.

The controllability of the weight drop system was achieved using an electromagnetic solenoid powered by a 12-voltage direct current (DC) power switching supply. Finally, the following electrical hardware arrangement was used to facilitate repeatability: an Arduino and computer to operate the system using a LabVIEW program (National Instruments).

### 3.2.2 Mechanical Hardware and Linkages

The framework of the system to hold the 0.654 m PVC tube (0.033 m outer diameter (OD)) consisted of a wooden board (0.038 x 0.038 x 0.445 m) mounted to a wooden framework base to allow for a rigid, but portable structure. The base of the framework, called the bedding,

was also made of wood and covered with a vinyl tile (0.451 x 0.197 x 0.038 m) to serve as an area for the anesthetized rodent to lay on. A foam bedding (mass 32.60 g, thickness 0.025 m, density 16.30 kg/$m^3$) was placed on top of vinyl tile (under animal) to support the head to allow some linear anterior-posterior motion with minimal angular rotational movement at the moment of impact. To ensure linear anterior-posterior motion of the rat head, the impactor weight was positioned to impact the animal's head 90 degrees from the horizontal plane (bedding). This was ensured by the PVC tube which was also square to the bedding. The foam was chosen and tested in the lab using a static weight equal to the maximum planned impact force with compression less than 50% of the initial thickness of the foam.

The design used an electromagnetic solenoid (White Rodgers Part # 70-111224), mounted on the top of the PVC tube using a 3D-printed polylactic acid (PLA) holder (see Figure 3.2A), to provide control of the hold and release of the impactor. To alter the severity of impact by modifying the impact height, the PLA holder was specifically designed to allow the solenoid to be moved vertically above the top of the tube. Furthermore, the use of the solenoid ensured repeatability of the impactor's velocity. To control the power stage of the solenoid connected to the 12-Volt power switching supply, a toggle switch, located on the base of the wooden framework, was added to the system (Figure 3.2B).

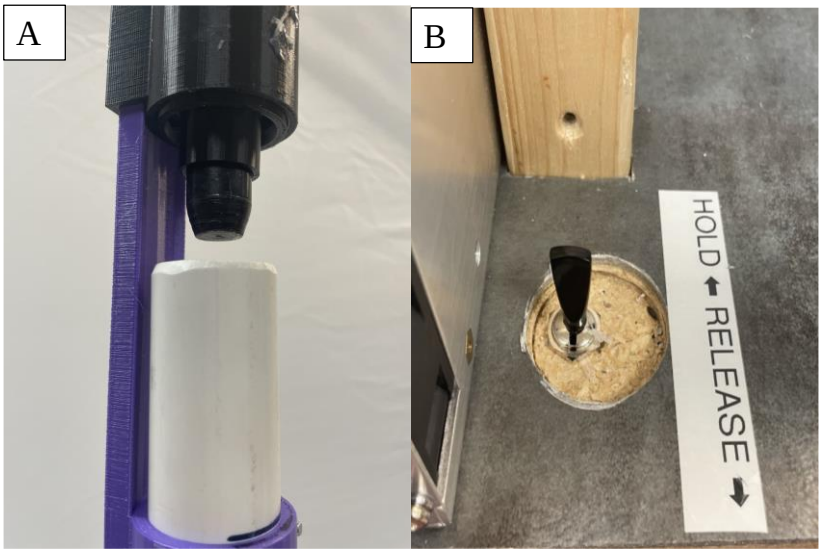


Figure 3.2 Close-up view of the electromagnetic solenoid and release switch for the weight drop injury apparatus.

(4) Picture of the 'hold' state of the electromagnetic solenoid in the PLA (black) holder holding the impactor at the top of the PVC tube. (B) Photo of the toggle switch used to control power to the solenoid using a 12-Volt power supply.

### 3.2.3 Electronics

To measure the velocity of impact, a chronograph system (Figure 3.3) was incorporated to validate the impactor's speed. The chronograph system consisted of two light gate (LG) sensor boards, each with four infrared (IR) transmitter photodiodes (Vishay Semiconductors Part # TSUS5400), on one side of a 3D-printed PLA holder (Figure 3.3A), and 8 IR emitter photodiodes mounted on the opposite side to create a light-sensing area. On the inside of the chronograph PLA holder, slits were made for each IR transmitter to direct light to its receiver (Figure 3.3B). The distal spacing between photodiodes slits on LG sensor boards 1 and 2 was 51 mm. The LG sensors, connected directly to an Arduino, operated on transmission mode to detect an interruption of light path (in time) between photodiodes when the impactor mass passed through. Time (microseconds) of light path interruption for each LG sensor board was collected

by the Arduino and used to calculate the impact velocity. This electrical enhancement of the chronograph system gave our weight drop impact design the capability to have a high degree of consistency measuring impact timing and velocity needed to verify the repeatability of impact.

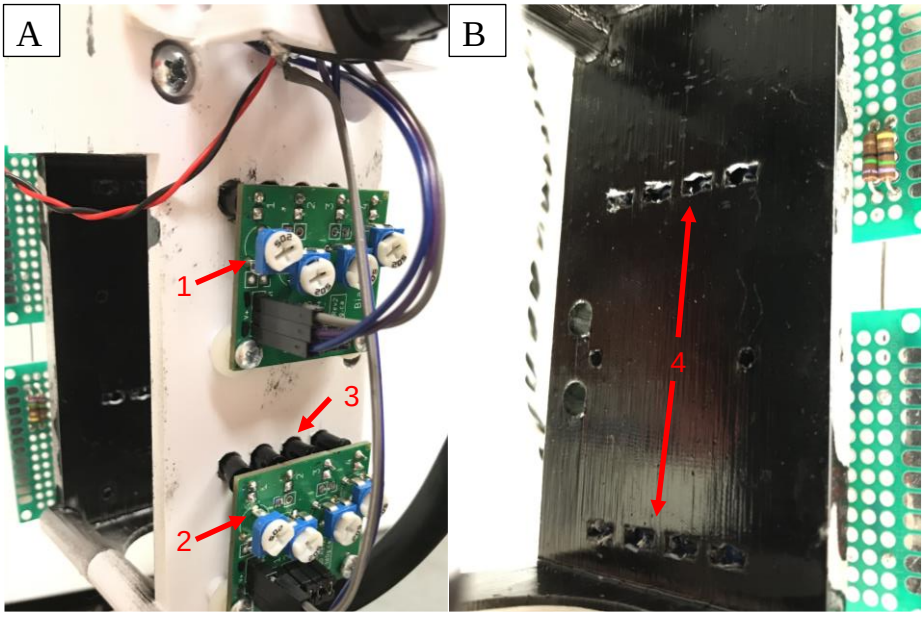


Figure 3.3 Chronograph system.

Illustrative images of the chronograph system of the weight drop injury apparatus. (A) Outside view of light gate sensor boards (numerically labeled 1 and 2) using photodiodes (labeled as 3) mounted on a 3D-printed PLA holder. (B) Inside view of the chronograph system showing slits (labeled 4) used for directing light of one light gate sensor board to the parallel light gate sensor board.

### 3.2.4 Software

The main controller for the WDI system was the 12-Volt DC switching power supply. The sequence of data calculation was automatically handled with a custom Arduino code and data collection by a custom-designed LabVIEW program using a Windows-10 computer. The user interface of the LabVIEW program consisted of three input parameters for the operation including a file path for data recording into a file, a drop-down box for selecting the impactor's

weight, and a user note section (Figure 3.4). As part of the custom-designed LabVIEW program, each time the toggle switch moves from the hold to release state, the user note, velocity, and kinetic energy (KE) of impact are collected and stored to the file path. Figure 3.5 illustrates the order of events for the weight drop injury design.

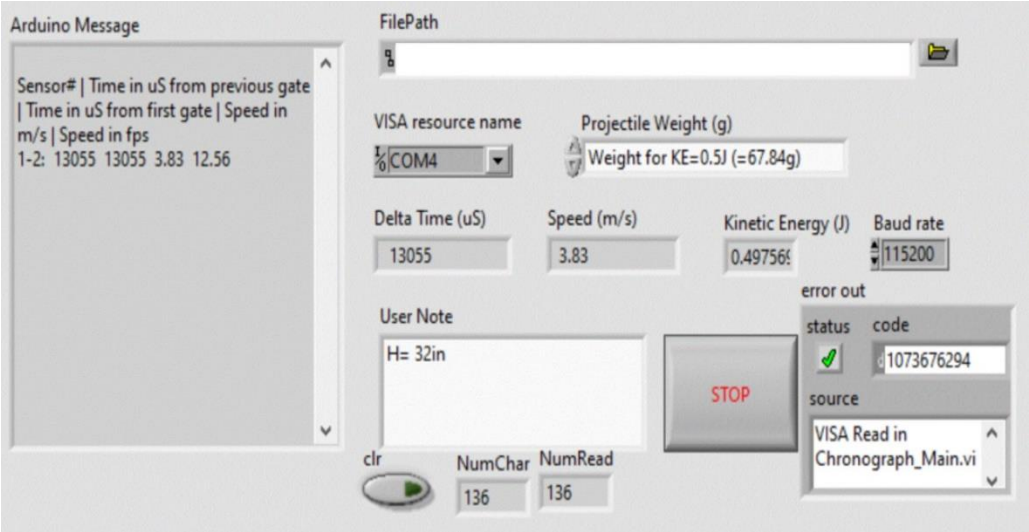


Figure 3.4 Screenshot of the custom-designed LabVIEW program for the weight drop apparatus.

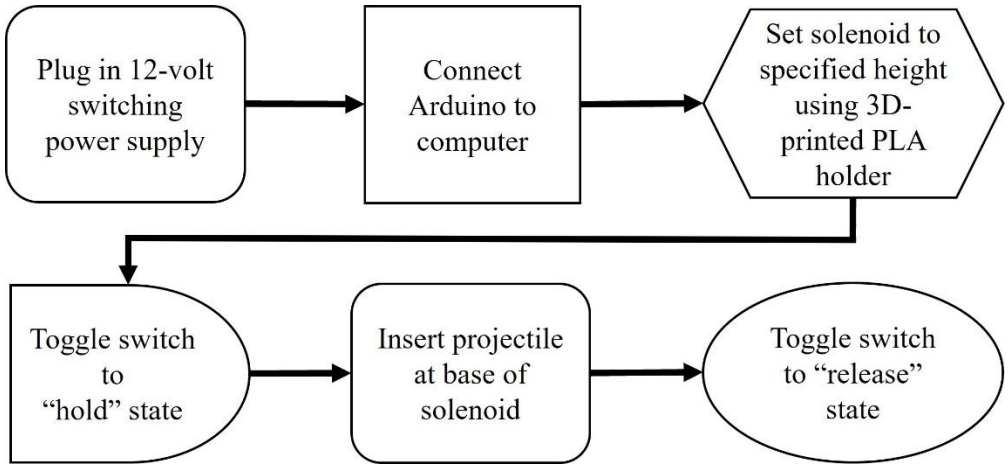


Figure 3.5 Schematic of the order of events for the in-house built weight drop injury device.

### 3.2.5 Impact Data Analysis

In post-processing, the data from the chronograph (i.e., the time difference of the impactor passing through the LG sensor boards) and data calculated in the Arduino code (velocity and KE) were collected and stored after each impact. The velocity ($ms^{-1}$) for each impact was calculated as the distance between light gate sensors (~51 mm) divided by the time (μs) of light path interruption between the two sensors. The formula for this calculation is shown in Equation 3.1 where *v* is the velocity, *d* is the distance between photodiodes on LG sensor boards 1 and 2, and *t* is the time of light path interruption between photodiodes LG sensor boards. Further, the kinetic energy was calculated from velocity (*v*) using Equation 3.2 where $E_K$ is the kinetic energy (J) and *m* is the mass (kg) of the impactor.

$$v = \frac{d}{t} \tag{3.1}$$

$$E_K = \frac{1}{2}mv^2 \tag{3.2}$$

## 3.3 Statistical Analysis

To gather the dynamics of impact for our weight drop injury device, two impactor weights (27.17 and 67.84 g) were dropped from a height of 0.81 m upon the head of rat cadavers. Twelve drop measurements were collected for each weight and used to represent the device's reproducible performance. Measurements included velocity and KE. A univariate analysis was conducted using the PROC UNIVARIATE in SAS (SAS Institute, Cary NC) for the maximum and minimum velocity and kinetic energy (KE) values obtained for all impacts. Although normal distribution could be assumed due to the large sample size, the assumption of normality was confirmed using a Shapiro-Wilk test ($p>0.05$). All statistical analyses were assessed at the

α=0.05 level of significance. The null hypothesis was rejected when $p<0.05$. The mean ± standard deviation (STD) obtained for each group can be found in Table 3.1.

## 3.4 Results

Dropping the 67.84 g weight from a height of 0.81 m yielded an average impact velocity of 3.83 ± 0.01 $ms^{-1}$ and an average KE of 0.50 ± 0.00 J. Alternatively, the lower impactor weight (27.17 gms) yielded an average impact velocity of 3.84 ± 0.01 $ms^{-1}$ with a mean KE of 0.20 ± 0.00 J. Descriptive Statistics obtained from the univariate analysis performed on the impact data can be found in Table 3.1. The impact dynamic results for each variable from the Shapiro-Wilk test of normality are as follows: velocity for the 27.17 g weight (p=0.0003), KE for the 27.17 g weight (p=0.0003), velocity for the 67.84 g weight (p=0.0171), and KE for the 67.84 g weight (p=0.0181). With an alpha level of 0.05, these results rejected normality of variables. Lastly, no skull fractures were present during experimental testing of the impactors.

Table 3.1 Impact dynamics of in-house built weight drop device.

| Projectile Weight (gms) | Variable | Mean | Standard Deviation | Minimum | Maximum |
|---|---|---|---|---|---|
| 27.17 | Velocity ($ms^{-1}$) | 3.838 | 0.009 | 3.820 | 3.850 |
| | Kinetic Energy (J) | 0.200 | 0.001 | 0.198 | 0.201 |
| 67.84 | Velocity ($ms^{-1}$) | 3.825 | 0.010 | 3.800 | 3.840 |
| | Kinetic Energy (J) | 0.496 | 0.003 | 0.490 | 0.500 |

The projectile weight (gms), mean, standard deviation, minimum and maximum values for velocity ($ms^{-1}$) and kinetic energy (J) calculated impact data.

## 3.5 Discussion

This chapter describes the construction and operation of the in-house developed weight drop injury device which was designed to simulate any severity of TBI. Among the design's strengths is its high repeatability and controllability of injury dynamics including impact velocity

and KE. These two impact parameters are essential for monitoring and recording when designing and using a mechanical means to induce brain trauma.

There is no definable impact threshold for the spectrum of mild injury severities; however, based on an extensive literature search, rat CHI models that employed WDI devices ranged in investigative KE impact loads of 0.25 (Lavender et al., 2020) – 4.42 J (Fujita et al., 2012; Hsieh et al., 2017). Our weight drop injury device is capable of inducing impact loads within these mTBI ranges and below. Impact dynamics of the in-house built device, described in Table 3.1, indicate high repeatability and controllability of injury mechanics. Thus, the goal to develop a device that can range in injury metrics suitable for mTBI and SC impact loads was achieved.

Each impactor's tip was specifically designed according to size (12.7 mm) and shape (flat tip). To compare, CCI impactor tips (diameters) range from 1-6 mm in size depending on the rodent. Generally, 3 mm tips are commonly used for mice and 5-6 mm tips for rats (Osier & Dixon, 2016). Again, most CCI designs are confined to one area of the brain (focal) due to their tip size. When a force is applied perpendicular to the top of the rodent's head, it exerts pressure on the head's surface equal to the ratio of force ($F$) to surface area ($A$). Recall the formula for pressure ($p$) in Equation 3.3.

$$p = \frac{F}{A} \tag{3.3}$$

An interesting consequence of this ratio is that the force will not change regardless of pressure increase or decrease. However, as surface area reduces, net pressure increases. In the tip design for the in-house weight drop injury apparatus, a greater tip diameter was preferred to produce a more diffuse injury rather than a focal impact injury. Tip geometry shape was influenced by

Pleasant et. al. (2011) who used finite element modeling to demonstrate that tip geometry was a significant determinant of cell death in cortical tissues (Pleasant et al., 2011). Using a CCI device on a murine model, their findings report that injury with a flat tip resulted in greater acute cortical hemorrhage and neuron loss in mice compared to a rounded tip (Pleasant et al., 2011). The flat tip impactor showed more regional hippocampal neurodegeneration at earlier time points in mice compared to the rounded tip impactor (Pleasant et al., 2011). Even though the CCI brain injury with a flat tip impactor resulted in greater maximal tissue strains than impacts with a rounded tip, behavioral responses, such as motor and cognitive functions, of brain-injured mice were not grossly influenced by impactor tip geometry (Pleasant et al., 2011). These results suggest that slowing the progression of cortical cell death through the use of a rounded tip did not compromise the fidelity of the behavioral response (Pleasant et al., 2011).

## 3.6 Conclusion

The development and characterization of an in-house built WDI apparatus for CHIs was achieved for producing experimental and repeatable brain injury for rodent models. The injury model produced impact ranges of those reported in literature and below using a rat model. In publishing the characterization and results of the in-house built design, it is hoped this device will lay the groundwork for research investigations exploring the relationship between concussive and SC injuries in the context of single and repeated impacts.

# CHAPTER IV

# BEHAVIORAL AND HISTOLOGICAL INFLAMMATORY ANALYSIS FOLLOWING A MILD TRAUMATIC BRAIN INJURY USING A RODENT MODEL: A PILOT STUDY

## 4.1 Introduction

It has been historically proven that animal models are instrumental in increasing our understanding of the pathophysiological and behavioral consequences of traumatic brain injury. While mTBI has been the subject of numerous clinical and preclinical research efforts, there remains a lack of identifying the threshold for an mTBI. Several preclinical studies utilize impact magnitudes that overlap in severity of impact (concussive and subconcussive) among different labs. For instance, preclinical investigations aiming to model SC impacts in rat models (Bree, Stratton, et al., 2020; Lavender et al., 2020; Sagarkar et al., 2017) are seen overlapping with impact magnitudes reported from research modeling mTBI in rats (Christie et al., 2019; Henninger et al., 2007; Kim & Han, 2017; Singh et al., 2016). For this reason, the present pilot study was designed to determine the lowest impact magnitude suitable for an mTBI using the previously discussed in-house built impact device. As previously mentioned in Chapter II (see section 2.2), according to literature, the lowest explorative closed head impact load labeled as an mTBI for a rat model was approximately 0.15 J. Thus, the present investigation aimed to explore two impact magnitudes slightly higher than the lowest reported mTBI impact load. The criteria for determining the appropriate mTBI load for a rat model included the absence of skull fracture,

the presence of acute behavioral measures, and/or evidence of neuroinflammation following impact.

The amount of time required for recovery from a single mTBI, or if full recovery occurs, has been a leading focus of preclinical investigations of head trauma (Bree, Mackenzie, et al., 2020; Fraunberger et al., 2020; Hsieh et al., 2017; Shapira et al., 1988; Singh et al., 2016). In terms of concussion, it is fundamentally important to determine the lower limits of system perturbation and establish the time frame of recovery. This would not only expand our understanding of secondary brain injury but may also provide insight for identifying a threshold for injury tolerance. The majority of preclinical investigations aiming to model a single closed head concussive head impact in rats concentrate on acute (0-24 hours) and subacute (1-14 days) sequalae to determine secondary injury phenomena (Brian R. Christie et al., 2019; Jamnia et al., 2017; Kim & Han, 2017; Li et al., 2015; Yates et al., 2017; Motoki Fujita et al., 2012; Bree, Mackenzie, et al., 2020; Dara Bree & Levy, 2018; Fraunberger et al., 2020; T.-H. Hsieh et al., 2017; Shapira et al., 1988; Singh et al., 2016). However, literature reports peak changes in inflammation at 3- and 7-days post-injury (Ekmark-Lewén et al., 2013; Fraunberger et al., 2020; Hsieh et al., 2017; Lagraoui et al., 2012; Marschner et al., 2019; Singh et al., 2016; Zhao et al., 2014). As such, we investigated evidence of secondary injury phenomena following a single blunt impact with a kinetic energy of either 0.2 or 0.5 J at two recovery time points, 3- and 7-days, following impact. Animal groups consisting of 6 animals each were labeled as follows: High3, Low3, High7, Low7, Sham3, and Sham7.

## 4.2 Methods

The following sections outline the experimental design and methods utilized for each procedure. In addition, this section provides animal number details along with impact,

behavioral, euthanasia, cytokine multiplex, and histological procedures. Analytical and statistical methods have been outlined as appropriate for each experimental procedure.

### 4.2.1 Experimental Design

An overview of the experimental elements and design for the pilot study can be seen in Figure 4.1. All procedures for the experimental pilot study were approved by the Mississippi State University Institutional Animal Care and Use Committee (IACUC) under protocol number 20-456 (see Appendix A).

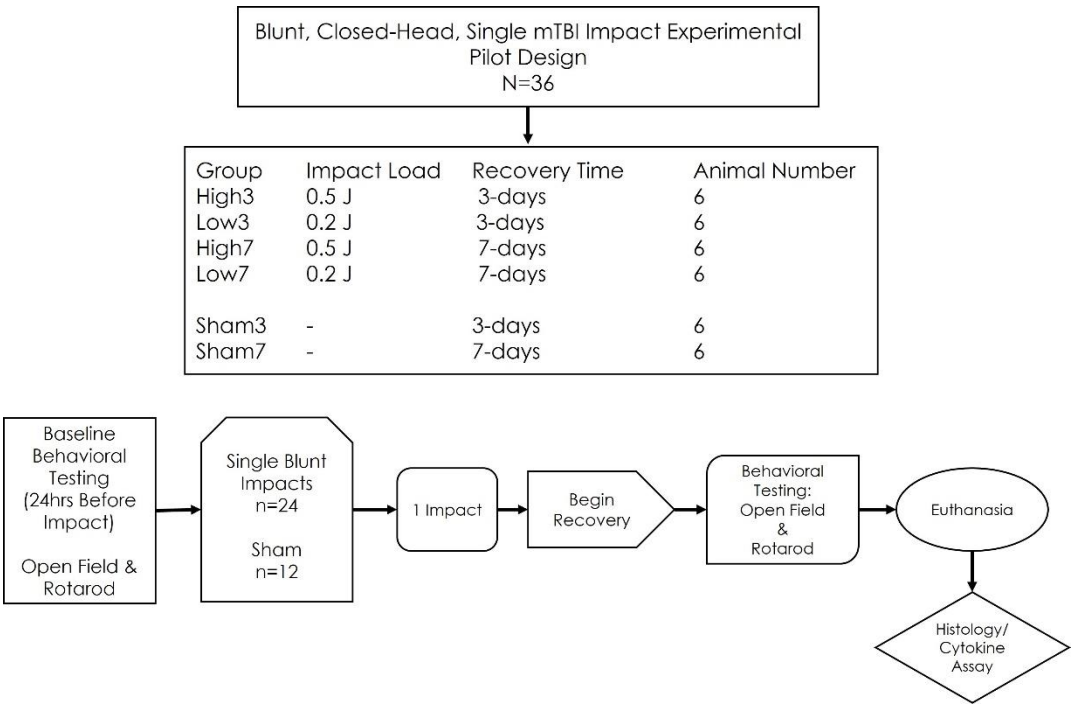


Figure 4.1 An overview of the experimental elements and design for the pilot study.

### 4.2.2 Animals

Thirty-six male Sprague-Dawley rats (250-300 g; Envigo, Indianapolis, IN) were housed three per cage in an Association for Assessment and Accreditation of Laboratory Animal Care

(AAALAC) accredited facility on a 12-hour light/dark cycle and provided free access to food and water in accordance with an Institutional Animal Care and Use Committee (IACUC)-approved protocol. Upon arrival, rats were randomly assigned to one of four injury (impact) or sham groups. Animal groups (n=6) were divided by assigned recovery time (3- or 7-days post-impact (DPI)) and labeled as follows: High3 (0.5 J impact load with 3-day recovery period), Low3 (0.2 J impact load with 3-day recovery period), High7 (0.5 J impact load with 7-day recovery period), Low7 (0.2 J impact load with 7-day recovery period), Sham3 (no impact with 3-day recovery period), and Sham7 (no impact with 7-day recovery period). To control for environmental variation due to cage placement, rats remained in their original cage placement after random assignment. Sham rats underwent all procedures as the impact rats (n=36) excluding the blunt impact. All animals were sacrificed on the final day of recovery (3- or 7-DPI).

Prior to the impact procedure, rats were administered ketamine (100-200 mg/kg intraperitoneal injection (IP)) and xylazine (5-10 mg/kg IP) for analgesia. Loss of righting reflex was used to indicate the depth of anesthesia. Upon completion of head impact, atipamezole (0.05-0.06 mg/kg intramuscular injection (IM)) was administered to reverse the effects of xylazine. In addition to this reversal agent, rats were administered a single dose of Buprenorphine IR (0.05 mg/kg subcutaneous injection) for analgesia.

To control pica behavior, a common side effect of buprenorphine, rats were housed individually on cage paper with two to three food pellets to encourage food intake for approximately 24 hours as opposed to standard rodent bedding when returned to the colony post-impact. After 24 hours following analgesic administration, animals were returned to group

housing and placed on standard bedding with food and water provided ad libitum. Pica behavior was monitored for 3-days following the duration of analgesia.

### 4.2.3 Impact Device and Procedures

A novel, in-house-built weight drop injury device (WDI) was used to deliver a single, closed head, blunt impact to the external head surface of each impact-assigned rat (n=24). Here, we tested two different closed head impact paradigms, employed in separate cohorts of rats. The first paradigm involved a single impact, using a 67.97 g weight drop. The second paradigm employed a single 27.17 g weight drop. All head injury paradigms were conducted on animals after the loss of tail-pinch reflex and righting reflex following anesthesia. While anesthetized, all animals (n=36) were placed chest down directly under the weight-drop head trauma device on the foam-covered (density 16.30 kg/m3) horizontal platform. The device consisted of a hollow cylindrical tube (81 cm) placed vertically over the center of the rat's head. At the end of the tube was an attachment with a target circle cut out that marks the location where the projectile mass would impact the head of the rat. To ensure consistency of the hit location, each rat head was flushed against the target circle of the attachment at the end of the tube (see Figure 4.2) so that the projectile weight struck the scalp slightly anterior to the center point between the ears. No physical constraints were applied to the anesthetized rats.

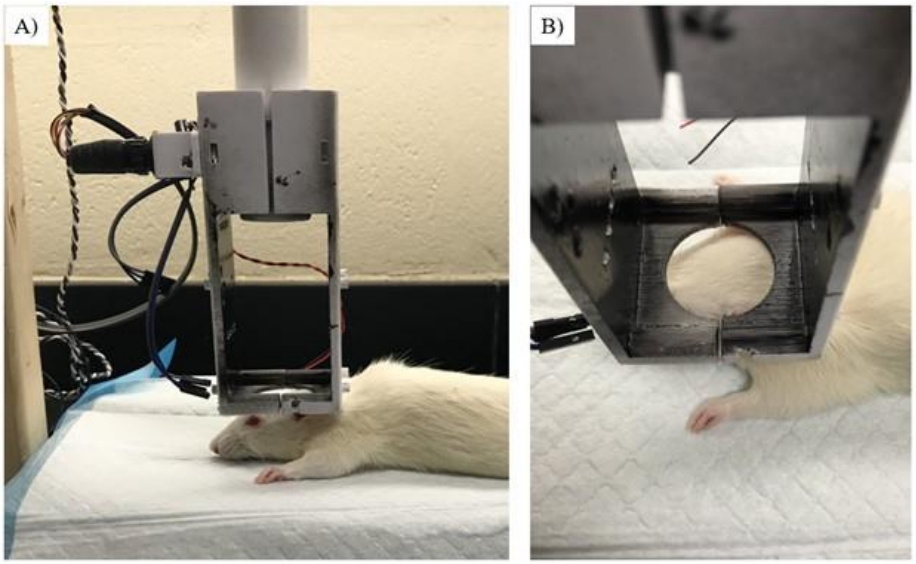


Figure 4.2 Weight drop injury device.

Notes: Sagittal viewpoint of a rat placed on the platform under the novel, in-house, weight drop injury apparatus. B) Aerial perspective of a rat placed on the platform under the chronograph system of the weigh drop injury apparatus.

After animals regained their righting reflex upon administration of the reversal agent, rats were returned immediately to individual cages for recovery. For all paradigms, sham animals were administered the same drugs as impact animals, but not subjected to the weight drop. Finally, biomechanics, e.g., impact velocity ($ms^{-1}$) and kinetic energy (J), of all injury paradigms were recorded.

#### 4.2.3.1 Statistical Analysis of Impact Data Analysis

A univariate analysis was conducted using the PROC UNIVARIATE in SAS (SAS Institute, Cary NC) for the maximum and minimum velocity and kinetic energy (KE) values obtained for all impacts. All statistical analyses were assessed at the $\alpha=0.05$ level of significance. The null hypothesis was rejected when $p<0.05$.

### 4.2.4 Behavioral Analysis

Behavioral testing was performed for all animals 24 hours before impact and on the final day of recovery post-impact (3-days and 7-days, respectively). Each experimental run included two impact animals (a high-load and low-load impact) and one sham animal. The Open Field Test (OFT) was conducted in a 1.02 m (length) x 1.02 m (width) x 0.36 m (height) apparatus divided into four equal quadrants allowing three animals to be run simultaneously (a high-load impact animal, low-load impact animal, and sham). Low illumination was achieved using red-LED light strips mounted to the inner top edges of the apparatus via an adhesive backing. Light pollution from other areas near the experimental room was minimized by blacking out the window on the door with an impenetrable material. All open field tests were video recorded using a Canon EOS Rebel digital camera mounted above the testing apparatus. Videos were uploaded and scored using ANY-maze behavioral tracking software (ANY-maze, Stoelting Co., USA). Raw scores were collected from ANY-maze and analyzed.

The rotarod assay was conducted in an automated 4-lane rotarod unit (Dual Species Economic Rotarod, Columbus Instruments, USA), again, allowing three animals to be run simultaneously (a high-load impact animal, low-load impact animal, and sham). The rotarod unit consisted of a rotating spindle (diameter 7.3025 cm) and individual compartments (‘lanes’) for each rat. A personal Windows-10 computer using a custom-designed LabVIEW program was connected to the rotarod unit for data collection. Recorded data included the time of fall for each subject, the reason for fall (jump, passive rotation, or actual fall), and all experimental setup parameters. The attained speed (rpm) and latency to fall (sec) for each subject were used for analysis. An overview of the behavioral timeline can be seen in Figure 4.3.

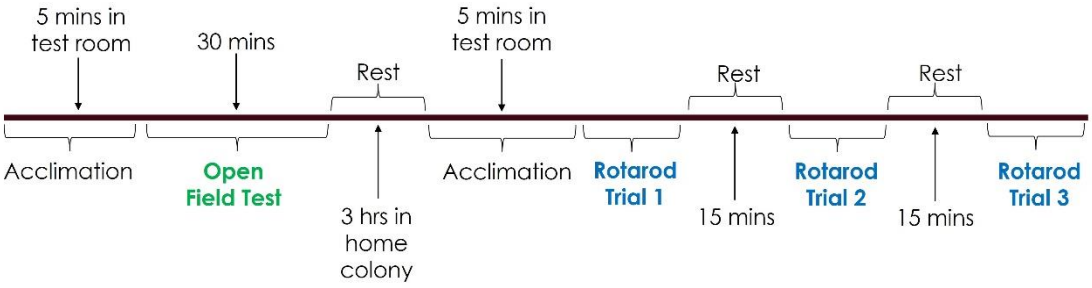


Figure 4.3 Behavioral timeline for the Open Field Test (green font) and rotarod (blue font) assays.

#### 4.2.4.1 Open Field Test Procedures and Data Acquisition

An acclimation period of 5-minutes was provided for each rat prior to testing. During acclimation, rats were placed alone in the testing room (in their home cages) with the overhead lights turned off. Following acclimation, video recording began, and three animals were simultaneously placed into their respective quadrant of the open field. For each experimental run, two impact animals were accompanied by one sham animal (a high-load impact, low-load impact, and sham). The duration of the OFT assay was 30 minutes. Upon completion of the test, the video recording was stopped, the animals were removed and returned to their colony as the apparatus was cleaned. Each test group remained in their colony for 3 hours before beginning the rotarod assay.

Video files were uploaded into ANY-maze for post-test tracking analysis. Using the apparatus tools within ANY-maze, the outer and center zones were defined as represented in Figure 4.4. The outer zone was defined as the outer-most border and extended far enough to accommodate the width of the rats. For the software to detect entry into the defined center zone, the animal had to completely exit the outer zone.

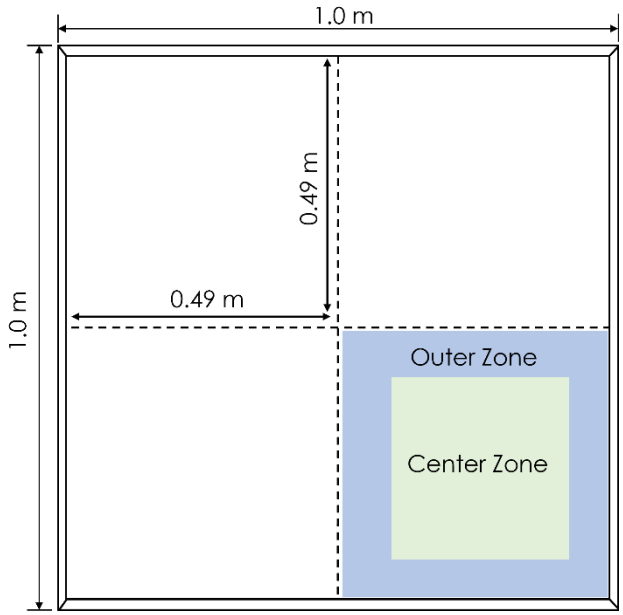


Figure 4.4 Representation of the Open Field Test apparatus.

The diagram represents the top perspective of the OFT apparatus and indicates the separation of the outer zone (blue) and center zone (green) in the bottom-right quadrant.

Locomotor activity was measured by the following eleven variables: 1) total distance traveled (m), 2) average speed ($ms^{-1}$), 3) maximum speed (m/s), 4) total time mobile overall (mins), 5) total time immobile overall (mins), 6) total time mobile in the outer zone (mins), 7) total time immobile in the outer zone (mins), 8) total distance traveled in the outer zone (m), 9) total time mobile in the center zone (mins), 10) total time immobile in the center zone (mins), and 11) total distance traveled in the center zone (m).

Metrics of anxiety-like behavior were measured by the total time spent in the outer zone (mins), the total time in the center zone (mins), and the number of entries into the center zone. The Thigmotaxis Index (TI) was calculated using Equation 4.1 where $OZ$ represents the time spent in the outer zone and $CZ$ represents the time spent in the center zone.

$$TI = \frac{OZ - CZ}{OZ + CZ} \tag{5.1}$$

#### 4.2.4.2 Rotarod Procedures and Data Acquisition

Three hours following the completion of the OFT, rats were removed from the colony, returned to the behavior testing room, and allowed a 5-minute acclimation period in their home cage before testing. During acclimation, rats remained in their cages while the rotarod unit ran from 4 to 40 rpm in 300 sec. Following acclimation, each experimental group (high-load impact, low-load impact, and sham animal) underwent three test trials separated by 15-minute inter-trial intervals. Before each trial began, rodents were placed in individual lanes (see Fig. 4.5) and allowed to walk at 4 rpm. Once all animals began walking without aid, the acceleration mode of the unit was turned on and set to begin accelerating from 4 to 40 rpm in 300 sec (5 minutes). Upon completion of the third and final trial, the LabVIEW recording was stopped, the animals were removed, and returned to their colony as the apparatus was cleaned for the next group.

Figure 4.5 Image of an experimental group (includes a high-load impact, low-load impact, and sham rat) walking on the rotating rod of rotarod assay.

The determination of maximal performance capacity and motor learning were measured by recording the attained speed (rpm) and latency to fall (sec) of each subject.

#### 4.2.4.3 Statistical Analysis of Behavioral Assays

Data analysis for behavioral tests were analyzed using two different statistical computations. For the analysis of treatment groups where repeated measures occurred (baseline vs. recovery day performance), a linear mixed model analysis with treatment, day, and their interaction as fixed effects and animal within treatment as the random effect was performed using PROC MIXED in SAS. Main effects and interactions were assessed at the $\alpha=0.05$ level of significance. The null hypothesis was rejected when $p<0.05$. The mean ± standard error of the mean (SEM) obtained for each group was used to describe the center and spread of group data. All plots were obtained using GraphPad Prism® 8 (GraphPad Software, Inc., La Jolla, CA, USA).

### 4.2.5 Brain Collection Process

After completion of all behavioral testing on recovery days (3- and 7-DPI), animals were euthanized using carbon dioxide in a chamber. Subsequently, rats were decapitated using a guillotine as a confirmation of euthanasia. Following this, the brain samples were extracted and submerged in phosphate-buffered saline (PBS; pH 7.4, Sigma-Aldrich, St. Louis, MO) for approximately 10 minutes. Brain tissues were then trimmed using a 1 mm coronal acrylic brain matrix (Ted Pella, Inc., Redding, CA, USA) to improve consistency. Using a Rat Brain Atlas (Paxinos, Watson: The Rat Brain in Stereotaxic Coordinates, 7$^{th}$ Edition) as a guide, the first trim was made 2 mm directly in front of the optic chiasm (2.48 bregma; see blade 1 in Figure 4.6). The second trim was made at the optic chiasm (0.48 bregma; see blade 2 in Figure 4.6) with each subsequent cut made 2 mm caudal to the preceding trim for a total of five tissue sections (each section was 2 mm thick). For the first three trims, the motor cortex was cut out from each side of the cerebral hemisphere and immediately stored in microcentrifuge tubes placed in dry ice (−20 °C) and then stored at −80 °C until further analysis. On the fourth trimmed tissue section (-2.56 bregma; tissue between blades 4 and 5 in Figure 4.6), where both the hippocampus and motor cortex were present in the tissue, this section was placed in a cassette and submerged in 10% neutral buffered formalin (NBF) solution for 72 hours for the preparation of histological analysis. The fifth and final trimmed tissue section (-3.56 bregma; tissue between blades 5 and 6 in Figure 4.6) was used to cut out the hippocampus of each cerebral hemisphere, placed in dry ice, and then stored at −80 °C until further analysis. Brain samples were typically extracted and properly stored within 20 minutes.

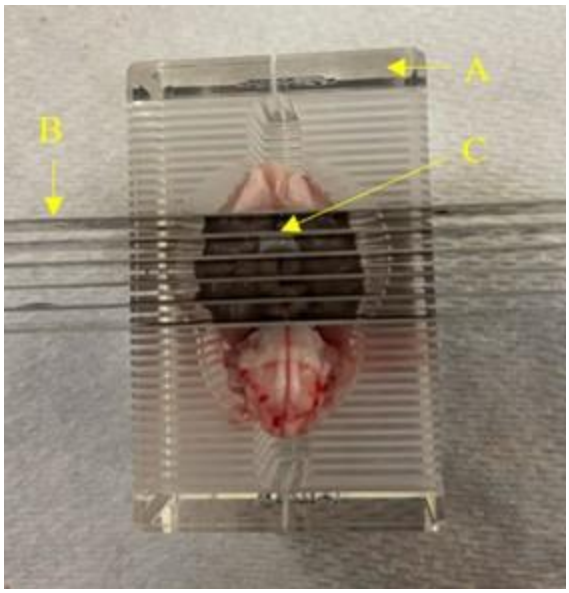


Figure 4.6 Representative image of brain tissue trimming protocol.

Shown are the A) acrylic brain trimming matrix, B) blades used for trimming, and C) optic chiasm (the location of the second trim). The distance between each razor was 2 mm.

### 4.2.6 Cytokine Analysis and Data Acquisition

To measure cytokine concentrations in brain lysates, a custom Procartaplex multiplex immunoassay (catalog no. PPX-03; Thermo Fisher Scientific, Carlsbad, CA) was used. The multiplex immunoassay was used to measure IL-6, TNF-α, and IL-10 concentrations in the hippocampus and motor cortex regions of animals. Upon analysis, tissue samples of each region (~20 mg) were thawed on ice and homogenized with a rotor-stator in 100 µL of ProcartaPlex cell lysis buffer (catalog no. EPX-99999-000; Life Technologies, Carlsbad, CA) for 30 sec each at 4°C. Brain tissue lysates were then centrifuged at 10,000 G for 10 minutes at 4°C and lysate supernatants were collected and prepared for analysis in a multiplex assay reader (Luminex 200). Finally, each brain lysate and standard concentrations were determined using Bio-Plex manager software (Bio-Rad).

### 4.2.7 Histology

Using a Leica RM2255 rotary microtome (Leica Microsystems Inc., Buffalo Grove, IL), 5 µm sections were obtained from paraffin embedded tissues and prepared for hematoxylin and eosin (H&E), ionized calcium binding adaptor molecule 1 (Iba-1), and glial fibrillary acidic protein (GFAP) staining.

#### 4.2.7.1 H&E

Paraffin embedded tissues were sectioned at 5 µm onto charged slides and stained with hematoxylin and eosin (H&E). Upon analysis of the 36 H&E tissue sections, only one group assignment, High7, showed all six tissue blocks confirmed with an appropriate tissue depth for immunohistochemistry. The remaining group assignment blocks (High3, Low3, Sham3, Low7, and Sham7) were cut too deep, anatomically, in the tissue for the study's regions of interest. A table of the original and final number of tissue blocks can be seen in Table 4.1.

Table 4.1 Initial and Final Tissue Block Numbers

| **Recovery Group** | **Initial Number of Blocks** *(High / Low / Sham)* | **Final Number of Blocks Chosen for Immunohistochemical Staining** *(High / Low / Sham)* |
|---|---|---|
| 3-Days | (n=6) / (n=6) / (n=6) | (n=4) / (n=2) / (n=4) |
| 7-Days | (n=6) / (n=6) / (n=6) | (n=6) / (n=3) / (n=5) |

Tissue block numbers within each experimental group prior to H&E staining and after visual analysis of H&E staining under the Olympus BX60 microscope. From the 3-day recovery assigned groups, 4, 3, and 4 tissue blocks from High, Low, and Sham groups, respectively, were confirmed with an appropriate tissue depth for immunohistochemical staining. Of the 7-day recovery group assignments, 6, 3, and 5 tissue blocks of groups High, Low, and Sham, respectively, were approved for immunohistochemistry staining.

#### 4.2.7.2 Immunohistochemistry

In order to investigate evidence of inflammation (microgliosis and astrogliosis) due to injury, each tissue section underwent Iba-1 and GFAP immunostaining. Paraffin embedded

tissues were sectioned at 5 μm onto charged slides. Unstained slides were deparaffinized and pretreated as follows: endogenous peroxidase activity was blocked with 3% hydrogen peroxide (Biocare ipb5000) for 5 minutes. The primary antibodies were applied as follows: GFAP (Agilent z0334, 1:2000, 30min) and IBA-1 (Biocare cp290, 1:100, 30 min). All immunostaining was performed on an IntelliPATH autostainer. A negative control without primary was included for each. Detection was performed using Rabbit-on-Canine HRP polymer (Biocare rc542) according to insert directions mixed in with DaVinci green diluent (Biocare pd900). The tissues were developed with DAB chromogen substrate (Biocare) for 5 minutes. The slides were then counterstained with hematoxylin (Biocare) for 5 minutes. The slides were then washed, dehydrated and coverslipped.

Due to unknown error, both GFAP and Iba-1 slides were unevenly stained. Possibilities for unevenness could be due to inadequate fixation, air drying of tissue samples, or staining issues. It is not likely that the error might be due to inadequate fixation because we submerged all the cassettes in approximately half a liter of 10% NBF. It is also unlikely that the error may be due to air drying of samples because, after extraction, tissues were immediately dropped in PBS for ~10 minutes before being removed and placed in the acrylic matrix for slicing. Slicing of tissue for appropriate sections took approximately 5-10 minutes. Finally, the error for uneven staining might be due to the staining process itself. However, the positive control slides used by the histology lab had no issues (no evidence of irregularity) and controls were run at the same time as research slides. To attempt to get the full section stained on the slides, the stained slides were re-run through the immunostaining protocol. The resulting GFAP and Iba-1 slides resulted in weak/irregular staining of the same areas (see Appendix B) necessitating a criterion to be met for determining which tissue section and hemisphere of the section was appropriately stained.

The criteria for selecting the appropriate section and hemisphere of the cerebral tissues were based on the stained areas that have a correctly stained internal control (cells around blood vessels). Depending on which hemisphere of the cerebral tissue met the criteria for appropriate GFAP and Iba-1 staining for each tissue section, either the left or right cingulum was imaged. Whichever section and hemisphere met this criterion was marked to move forward with image analysis. Lastly, because there were not enough slides to rerun the stain, image analysis via threshold was no longer an appropriate method to measure immunoreactivity of astrocytes (GFAP) and microglia (Iba-1) due to unevenness of staining through sections. Thus, positively stained cell count was used to measure the immunoreactivity of astrocytes and microglia.

#### 4.2.7.3 Microscopy and Image Analysis

The anatomical regions of interest selected for this study were comprised in the hippocampal area of the cerebral tissue: cornu ammonia 1 (CA1), cornu ammonis 3 (CA3), and the dentate gyrus (DG). It was originally planned to explore evidence of Iba-1 and GFAP immunoreactivity within the motor cortex (MC) region of the cerebral cortex, however, because this region encompasses a larger area of the cerebral tissue than the DG, CA1, and CA3 regions, the Olympus BX60 (Olympus Optical Co Ltd, Tokyo Japan) microscope was unable to capture the entire region at 20x magnification. Consequently, there was an increase in the possibility of image overlapping caused by human error. Thus, it was decided not to move forward with the image analysis of the MC region.

As mentioned before, due to an undetermined error, GFAP and Iba-1 slides were unevenly stained. Thus, the tissue section chosen for image analysis of stained slides depended on which hemisphere of the tissue met the criteria for appropriate GFAP and Iba-1 staining. Again, the criteria for selecting the appropriate hemisphere(s) of the cerebral tissue section were

based on the stained areas that had a correctly stained internal control (positively stained cells around blood vessels). Whichever section and hemisphere(s) met this criterion were then marked to move forward with the cell count image analysis. Micrographs for each hippocampal region of interest that were appropriately stained were taken at 20x magnification using an Olympus BX60 microscope equipped with an Infinity3 Lumenera (Lumenera Corporation, ON, CA) camera and the Infinity Analyze (Lumenera) imaging software. Representative micrographs were captured at 4x magnification for illustration only and were not analyzed. See Appendix C for selected representative micrographs (4x and 20x magnification) of GFAP and Iba-1 immunostained tissue sections based on sections with a measurement most representative of the mean positive cell count for each group.

Micrographs captured at 20x magnification were analyzed in QuPath (v.0.2.0) software (Bankhead et al., 2017). The micrograph scale bar (100μm) was used to set the scale in QuPath to ensure accurate measurements (1.465 pixels per micron). The general processing and analysis workflow in QuPath for each image consisted of several steps: selecting the image type and region of interest, applying the positive pixel count, and data collection. The image type of each image was selected as Brightfield (H-DAB). By selecting Brightfield (H-DAB), QuPath then sets default stain vectors to characterize hematoxylin and DAB.

Following the selection of image type, the area of interest of each image was manually outlined by use of the Rectangle tool. Once the region was defined, the positive cell detection tool was used to detect positive pixels. During this process, QuPath detects every cell in the selected region by using a built-in cell segmentation algorithm. Immunoreactivity in the tissues was shown by positive DAB staining within the tissue. QuPath's default DAB threshold for GFAP and Iba-1 stained images was 0.1. Finally, the number of positive cell counts was

computed, and the numbers of astrocytes (both positively and negatively stained) were automatically counted. The resultant image from QuPath contained both blue and red pixels. The red pixels contained the areas that the program determined as positive stains and the blue pixels were classified as negative stains. Representative examples of a non-processed and processed GFAP-stained cerebral section are shown in Figure 4.7. All data were extracted from QuPath and further calculations were performed in Microsoft Excel. The density of positive astrocytes was defined as the number of positively stained astrocytes/$mm^2$. In excel, the density of positive astrocytes was calculated by dividing the number of positive cells by the total number of pixels in the defined region of interest (1 $px^2$ = 4.66e-7 $mm^2$). The number of positively stained astrocytes/$mm^2$ was then used for statistical analysis as a measure of immunoreactivity.

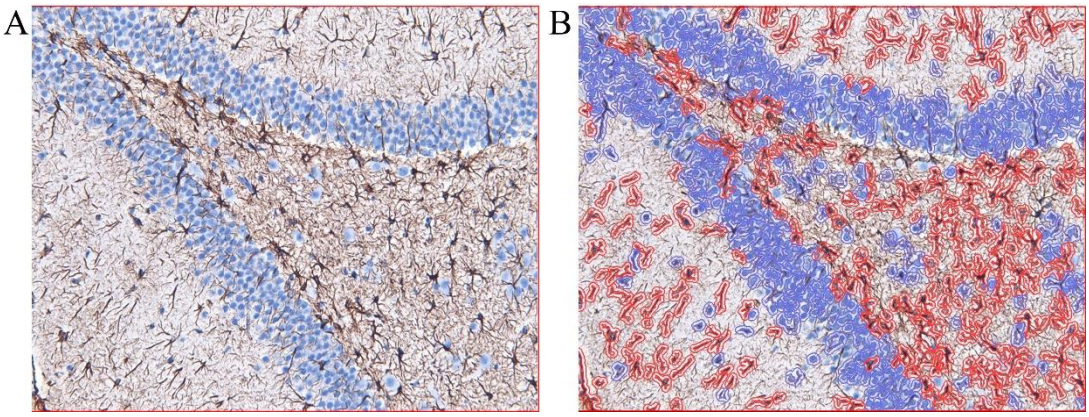


Figure 4.7 Representative example of a non-processed and processed cell count analysis using QuPath.

Representative pictures of an unanalyzed (A) and QuPath-analyzed (B) GFAP-stained section of the dentate gyrus, the latter with coloring of the positively stained astrocyte cells (red) and negatively stained astrocyte cells (blue).

#### 4.2.7.4 Statistical Analysis of Immunostaining

The number of positive cell counts/$mm^2$ of the generalized hippocampal region of interest (DG, CA1, and CA3) was calculated from all sections obtained from all 20x microscopic images collected. Of the slides that had appropriate staining over the left and right hemispheres, the left and right hemisphere 20x images were not analyzed separately due to the wide surface area of the head impact. The mean ± SEM number of positive cell counts/$mm^2$ for each group was used to describe the center and spread of the positive cell counts/$mm^2$ results per group per brain region of interest (DG, CA1, and CA3). Additionally, the difference in group mean number of positive cells per $mm^2$ vs. sham mean number of positive cell counts/$mm^2$ was also calculated. Data analysis and statistical computations were carried out using a one-way ANOVA model, with treatment as the explanatory variable, in SAS (SAS Institute, Cary NC). Pairwise comparisons were conducted using a post hoc LSMeans Difference test. Normality was determined using a Shapiro-Wilk test and the homogeneity of variances was determined using

Levene's test. If the assumption of normality was not met, nonparametric methods were employed. In incidences where the assumption of equal variance was not met, a Welch's test was used in lieu of the ANOVA p-value. All statistical analyses were conducted using SAS with a significant level of $p<0.05$. Furthermore, all plots were obtained using GraphPad Prism® 8.

## 4.3 Results

### 4.3.1 Impact Data

A weight drop injury device was employed to induce a head injury from two projectile weights (27.17 and 67.84 gms) at an impact height of 0.81 m. Animals that were impacted with the higher projectile weight were considered "high" impact groups. Alternately, those who received an impact with the lower weight (27.17 g) were labeled as "low" impact groups. According to the data, high impact groups received an average impact velocity of $3.83 \pm 0.01$ $ms^{-1}$ and average kinetic energy of $0.50 \pm 0.00$ J. Alternatively, low impact groups had an average impact velocity of $3.86 \pm 0.00$ $ms^{-1}$ and kinetic energy of $0.20 \pm 0.00$ J. Descriptive Statistics obtained from the univariate analysis performed on the impact data can be found in Table 4.2.

Impact dynamics results from the Shapiro-Wilk test of normality for each variable are as follows: velocity for high impact groups ($p=0.018$), KE for high impact groups ($p=0.018$), velocity for low impact groups ($p=0.160$), and KE for low impact groups ($p<0.0001$).

Table 4.2 Impact dynamics according to projectile weights.

| Projectile Weight (gms) | Variable | Mean | Standard Deviation | Minimum | Maximum |
|---|---|---|---|---|---|
| 27.17 | Velocity ($ms^{-1}$) | 3.863 | 0.009 | 3.850 | 3.880 |
| | Kinetic Energy (J) | 0.203 | 0.001 | 0.201 | 0.205 |
| 67.84 | Velocity ($ms^{-1}$) | 3.832 | 0.013 | 3.820 | 3.860 |
| | Kinetic Energy (J) | 0.498 | 0.003 | 0.495 | 0.505 |

The projectile weight (gms), mean, standard deviation, minimum and maximum values for velocity ($ms^{-1}$) and kinetic energy (J) calculated impact data.

### 4.3.2 Behavior

#### 4.3.2.1 Open Field Test

An Open Field Test (OFT) was employed to investigate indications of altered general locomotor activity or anxiety-like behavior due to impact and throughout recovery (3- and 7-days). In Tables 4.3-4.4, the overall significance of the effects is presented beside the variable's name. Results from the ANOVA test for the repeated measures design indicated only two variables, from the 3-day recovery groups, showed a significant interaction effect between treatment and day. As such, a separate table with the specific groups and day of testing showing significant differences was reported (Table 4.5). Plots represent the mean with error bars representing the SEM. For all plots, significant differences ($p<0.05$) between group pairs are denoted with one asterisk (*).

Table 4.3 Open Field Test ANOVA summary for the repeated measures design of the 3-day recovery groups.

| Open Field Test Variables | ANOVA For Repeated Measures Design of 3-Day Recovery Groups | | |
|---|---|---|---|
| | Treatment x Day | Treatment | Day |
| Total Distance Traveled (m) | 0.054 | 0.277 | 0.001 * |
| Average Speed (m/s) | 0.046 * | - | - |
| Maximum Speed (m/s) | 0.291 | 0.675 | 0.269 |

Table 4.3 (continued)

| | | | |
|---|---|---|---|
| Total Time Mobile (mins) | 0.878 | 0.402 | 0.000 * |
| Total Time Immobile (mins) | 0.879 | 0.402 | 0.000 * |
| Total Time in Outer Zone (mins) | 0.702 | 0.670 | 0.991 |
| Distance Traveled Outer Zone (m) | 0.037 * | - | - |
| Time Mobile Outer Zone (mins) | 0.681 | 0.056 | 0.000 * |
| Time Immobile Outer Zone (mins) | 0.929 | 0.534 | 0.002 * |
| Number of Entries into Center Zone | 0.113 | 0.553 | 0.022 * |
| Distance Traveled Center Zone (m) | 0.562 | 0.806 | 0.396 |
| Total Time in Center Zone (mins) | 0.699 | 0.667 | 0.986 |
| Time Mobile Center Zone (mins) | 0.897 | 0.777 | 0.632 |
| Time Immobile Center Zone (mins) | 0.381 | 0.537 | 0.410 |
| Thigmotaxis Index | 0.699 | 0.668 | 0.986 |

The p-values obtained from the mixed model ANOVA tests for each OFT variable is presented. Significant differences of the effect are indicated by an asterisk (*).

Table 4.4 Open Field Test ANOVA summary for the repeated measures design of the 7-day recovery groups.

| **Open Field Test Variables** | **ANOVA For Repeated Measures Design of 7-Day Recovery Groups** | | |
|---|---|---|---|
| | **Treatment x Day** | **Treatment** | **Day** |
| Total Distance Traveled (m) | 0.376 | 0.262 | 0.025 * |
| Average Speed (m/s) | 0.293 | 0.254 | 0.030 * |
| Maximum Speed (m/s) | 0.156 | 0.619 | 0.863 |
| Total Time Mobile (mins) | 0.923 | 0.055 | 0.005 * |
| Total Time Immobile (mins) | 0.923 | 0.055 | 0.005 * |
| Total Time in Outer Zone (mins) | 0.642 | 0.042 * | 0.593 |
| Distance Traveled Outer Zone (m) | 0.467 | 0.412 | 0.008 * |
| Time Mobile Outer Zone (mins) | 0.617 | 0.847 | 0.005 * |
| Time Immobile Outer Zone (mins) | 0.980 | 0.028 * | 0.008 * |
| Number of Entries into Center Zone | 0.090 | 0.101 | 0.713 |
| Distance Traveled Center Zone (m) | 0.618 | 0.270 | 0.472 |
| Total Time in Center Zone (mins) | 0.642 | 0.042 * | 0.599 |
| Time Mobile Center Zone (mins) | 0.505 | 0.029 * | 0.362 |

Table 4.4 (continued)

| | | | |
|---|---|---|---|
| Time Immobile Center Zone (mins) | 0.287 | 0.189 | 0.417 |
| Thigmotaxis Index | 0.642 | 0.042 * | 0.598 |

The p-values obtained from the mixed model ANOVA tests for each OFT variable is presented. Significant differences of the effects are indicated by an asterisk (*).

Table 4.5 Open field test result summary of Fisher's least significant difference test for day 3 recovery groups where significant differences were observed for the interaction effect.

| **Open Field Test Variables** | **Differences of Least Square Means for Day 3 Recovery Groups** | | | | |
|---|---|---|---|---|---|
| | **Effect** | **Group** | **Day** | **Group** | **Day** |
| Average Speed (m/s) | Treatment*Day ANOVA (p=0.001) * | High | BL | High | TD |
| | Treatment*Day ANOVA (p=0.007) * | Sham | BL | Sham | TD |
| Distance Traveled in Outer Zone (m) | Treatment*Day ANOVA (p=0.0003) * | High | BL | High | TD |
| | Treatment*Day ANOVA (p=0.021) * | Low | TD | Sham | TD |
| | Treatment*Day ANOVA (p=0.003) * | Sham | BL | Sham | TD |

Significant differences between group pairs by day of behavioral testing (baseline vs. recovery day) are identified from the Fisher's LSD test procedure next to each group's statistic.

For the sake of brevity, the remainder of this research will focus only on the following general locomotive activity variables: total distance traveled and total time immobile (mins). Furthermore, the following variables associated with measuring anxious-like behavior, total time in outer zone (mins), and total time in center zone (mins), thigmotaxis index, and number of center zone entries, will be further discussed from this point forward.

With respect to measurements related to general locomotor activity, no significant differences were seen between injury and sham groups, regardless of recovery (Figure 4.8A).; however, on average, the animals traveled significantly more total distance at baseline compared to recovery days (Table 4.3-4.4). In the context of the total time animals spent immobile during

the OFT, data indicated on average, regardless of recovery time, the animals spent significantly more time immobile on the day of recovery compared to baseline (Tables 4.3-4.4) (Figure 4.8B).

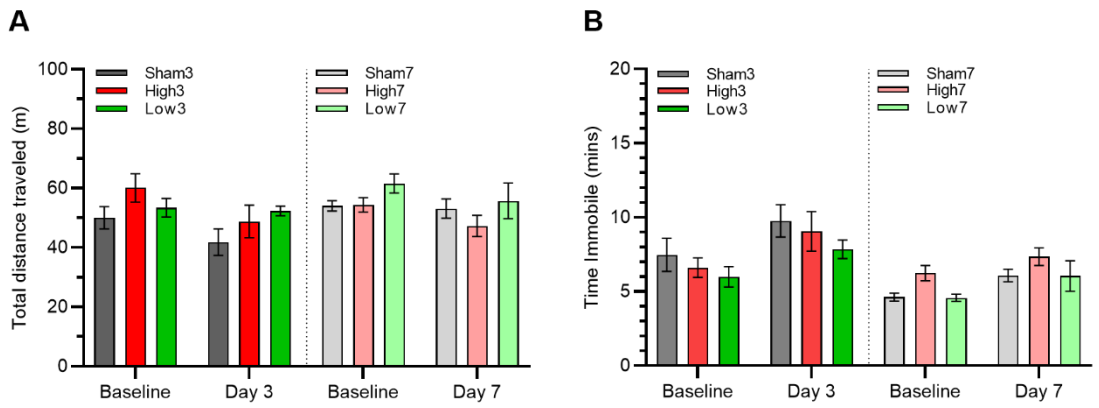


Figure 4.8 Total distance traveled (m) and total time immobile (mins).

Comparison plots of the (A) total distance traveled in meters and the (B) total time immobile in minutes among impact recovery groups High3, Low3, High7, Low7, and sham groups, Sham3 and Sham7, during the 30 minute OFT assay. The ANOVA results indicated no significant differences among groups with respect to the total distance traveled and total time immobile of OFT. On average, recovery groups travelled significant less distance and were immobile for a greater amount of time than baseline groups. Plots show the mean and the standard error of the mean (error bars).

Significant differences between injury and shams were evident between 7-day recovery groups with respect to the total time spent in the outer zone and total time spent in the center zone (Table 4.4). Post hoc LSMeans Difference test revealed that, on average, the High7 impact group spent significantly less time in the center zone (Figure 4.9A) and more time in the outer zone (Figure 4.9B) than sham ($p=0.017$ and $p=0.017$, respectively) group (Table 4.4). This phenomenon is further reflected in the analysis of the thigmotaxis index analysis (Figure 4.9C), which indicates, on average, the High7 impact group spent a significantly greater test duration in the outer zone (higher thigmotaxis index) compared to Sham7 ($p=0.017$) (Table 4.4). Overall,

these results support the indication that the higher-impact load injury group shows increased anxiety-like behaviors, as indicated by a significant increase in the thigmotaxis index after 7-days of recovery. Finally, post hoc LSMeans Difference test results showed no significant differences concerning the number of center zone entries between injury and sham groups, regardless of recovery day (Figure 4.9D). However, on average, the 3-day recovery assigned animals did enter the center zone significantly fewer times upon recovery compared to their baseline measurements (Table 4.3).

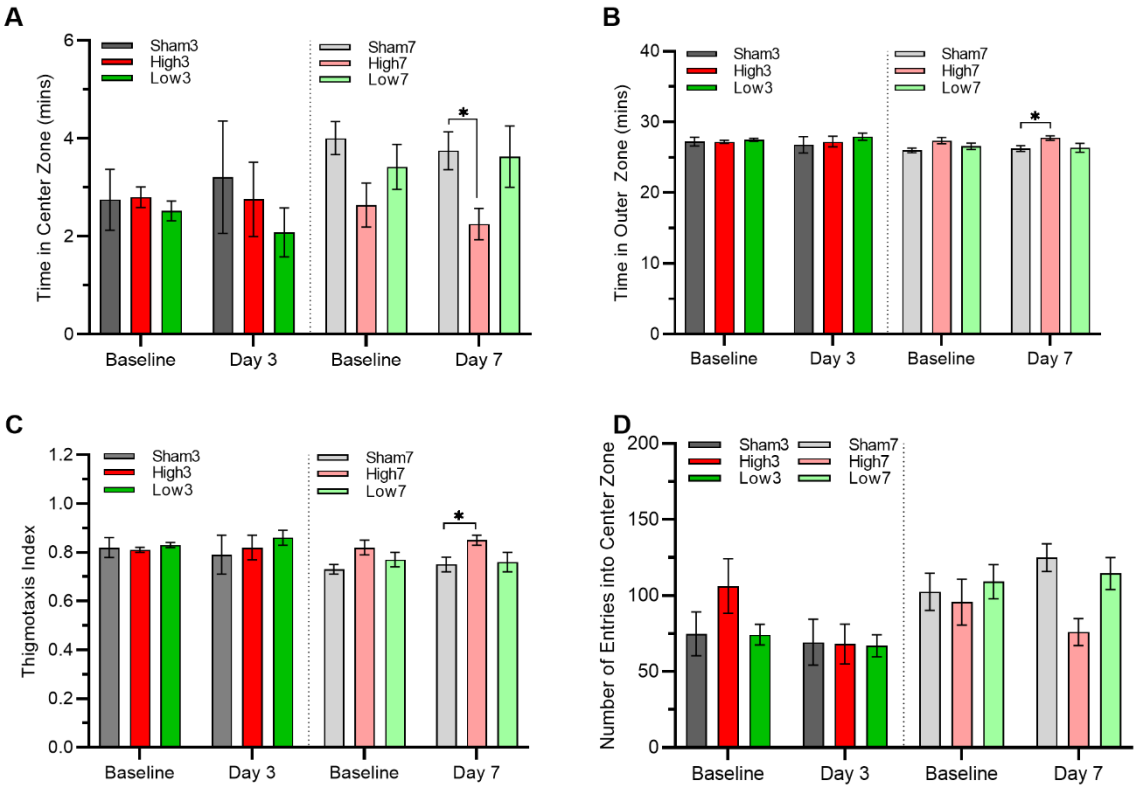


Figure 4.9 Plots for (a) time in center zone (mins), (b) time in outer zone (mins), (c) the index of thigmotaxis, and (d) the number of entries into the center zone.

Comparison plots of the OFT group results for (A) time in center zone (mins), (B) time in outer zone (mins), (C) the index of thigmotaxis, and (D) the number of entries into the center zone among impact recovery groups High3, Low3, High7, Low7, and sham groups, Sham3 and

Sham7, during the 30 minute OFT assay. Post hoc LSMeans Difference test results indicated, on average, significant differences between High7 and Sham7 groups for (A) time in outer zone (mins), (B) time in center zone (mins) and (C) the index of thigmotaxis. An asterisk (*) denotes a significant difference ($p<0.05$). Plots show the mean and the standard error of the mean (error bars).

#### 4.3.2.2 Rotarod Test

Somewhat surprisingly, injury groups did not show impairment of motor coordination on the rotarod compared to their sham groups, regardless of recovery day. However, when comparing the differences of latency performance for all animals, regardless of group assignment, by recovery groups, significant differences were present. The differences in latency performance between 3- and 7-day recovery groups have been summarized as the mean ± SEM in Tables 4.6 and 4.7, respectively.

When comparing the differences of latency time for all animals, regardless of group assignment, by recovery groups, significant differences among groups were present between day of rotarod testing ($p<0.0001$) and trials ($p<0.0001$) (Tables 4.5 and 4.6). According to Tables 4.6 and 4.7, on average, all animals, across trials and treatment, performed significantly better on the day of recovery compared to baseline (3DPI: $p<0.0001$, and 7DPI: $p=0.0006$). Additionally, data showed that on average, all animals, across treatment and recovery days, performed significantly better on trials 2 and 3 compared to trial 1 (see Tables 4.6 and 4.7), most likely due to a learning effect.

Table 4.6 Differences in latency (s) summary for 3-day recovery groups across all animals, regardless of group assignment.

| **Differences in Latency (s) of Day 3 Recovery Groups** | | | |
|---|---|---|---|
| **Effect** | **Trials by Day of Testing** | | **Mean ± SEM** |
| Day<br>ANOVA ($p<0.0001$) * | Baseline | Recovery | -97.19 ± 13.75 |
| Trial<br>ANOVA ($p=0.0002$) * | Trial 1 | Trial 2 | -49.40 ± 12.16 |
| Trial<br>ANOVA ($p<0.0001$) * | Trial 1 | Trial 3 | -63.22 ± 11.89 |
| Trial<br>ANOVA ($p=0.2116$) | Trial 2 | Trial 3 | -13.83 ± 10.93 |

The mean ± standard error of the mean (SEM) of latency (s) for the differences between test day (baseline vs. recovery) and trials (1, 2, and 3) of all animals within the 3-day recovery groups, High3 (n=6), Low3 (n=6), and sham3 (n=6), during the rotarod test. The p-values obtained from the ANVOA suggest that on average, all animals, across trials and treatment, performed significantly better on the day of recovery compared to baseline. Furthermore, on average, all animals, across treatment and recovery days, performed significantly better on trials 2 and 3 compared to trial 1. Significant differences ($p<0.05$) between effects are denoted with one asterisk (*).

Table 4.7 Differences in latency (s) summary for 7-day recovery groups across all animals, regardless of group assignment.

| **Differences in Latency (s) of Day 7 Recovery Groups** | | | |
|---|---|---|---|
| **Effect** | **Trials by Day of Testing** | | **Mean ± SEM** |
| Day<br>ANOVA ($p=0.0006$) * | Baseline | Recovery | -61.41 ± 14.30 |
| Trial<br>ANOVA ($p<0.0001$) * | Trial 1 | Trial 2 | -40.34 ± 8.59 |
| Trial<br>ANOVA ($p=0.0005$) * | Trial 1 | Trial 3 | -32.23 ± 8.69 |
| Trial<br>ANOVA ($p=0.3489$) | Trial 2 | Trial 3 | 8.12 ± 8.59 |

The mean ± standard error of the mean (SEM) of latency (s) for the differences between day (baseline vs. recovery) and trials (1, 2, and 3) of all animals within the 7-day recovery groups, High7 (n=6), Low7 (n=6), and sham7 (n=6), during the rotarod test. The p-values obtained from the ANVOA suggest that on average, all animals, across trials and treatment, performed significantly better on the day of recovery compared to baseline. Furthermore, on average, all animals, across treatment and recovery days, performed significantly better on trials 2 and 3 compared to trial 1. Significant differences ($p<0.05$) between effects are denoted with one asterisk (*).

### 4.3.3 Histology

To investigate histological evidence of neuroinflammation, positive cell count analysis was performed for brain tissue sections to assess microgliosis and astrogliosis using immunohistochemical markers Iba-1 and GFAP, respectively. Histological analysis was performed for the dentate gyrus (DG), cornu ammonis 1 (CA1), and cornu ammonis 3 (CA3) subregions of the hippocampus. Histochemical assessment of H&E tissue sections revealed no macroscopic lesions due to impact. Representative micrographs of GFAP and Iba-1 tissue sections for each region of interest can be seen in Appendix C.2.1 and Appendix C.2.2, respectively. Plots for GFAP (Figure 4.10) and Iba-1 (Figure 4.11) analysis present the mean positive cell counts/mm$^2$. Error bars represent the SEM. For all plots, significance is denoted with one asterisk (*) indicative as p-value smaller than 0.05 ($p<0.05$).

#### 4.3.3.1 GFAP

Glial fibrillary acidic protein (GFAP) was used as an immunohistochemical marker for astrocytes. The number of positive cell counts/mm$^2$ was used to analyze the proportion of GFAP immunoreactivity within each brain region of interest (DG, CA1, and CA3) for each group as a measure of astrogliosis. Summary statistics for the GFAP positive cell counts/mm$^2$ measurements obtained for each region analyzed can be seen in Table 4.7. Descriptive statistics of animal groups for each region (DG, CA1, and CA3) are displayed by region of interest in Table 4.7.

Table 4.8 GFAP positive cell count/mm$^2$ summary.

| Brain Region | Group | Day of Recovery | Mean ± SEM | 95% CI | | Impact vs. Sham Mean Diff ± SEM |
|---|---|---|---|---|---|---|
| | | | | Lower | Upper | |
| DG *ANOVA (p=0.579)* | High | 3 | 332.32 ± 93.27 | -69.00 | 733.63 | 90.78 ± 111.324 |
| | Low | | 230.98 ± 8.73 | 120.01 | 341.95 | -10.56 ± 115.032 |
| | Sham | | 241.54 ± 68.52 | 51.30 | 431.78 | |
| | High | 7 | 394.67 ± 68.65 | 204.08 | 585.27 | 28.01 ± 92.785 |
| | Low | | 331.14 ± 93.78 | -860.48 | 1522.77 | -35.52 ± 106.951 |
| | Sham | | 366.66 ± 68.37 | 176.82 | 556.5 | |
| CA1 *ANOVA (p=0.760)* | High | 3 | 278.51 ± 87.48 | 0.11 | 556.91 | -9.15 ± 122.915 |
| | Low | | 157.22 ± 6.2 | 78.45 | 236.00 | -130.43 ± 129.573 |
| | Sham | | 287.65 ± 77.23 | 73.22 | 502.07 | |
| | High | 7 | 361.9 ± 87.89 | 117.87 | 605.92 | 21.13 ± 107.504 |
| | Low | | 324.5 ± 79.3 | -683.07 | 1332.06 | -16.27 ± 101.414 |
| | Sham | | 340.77 ± 67.29 | 153.94 | 527.59 | |
| CA3 *ANOVA (p=0.742)* | High | 3 | 190.75 ± 43.37 | 0.11 | 556.91 | 37.17 ± 80.305 |
| | Low | | 130.31 ± 22.29 | 78.45 | 236.00 | -23.27 ± 87.308 |
| | Sham | | 153.58 ± 51.42 | 73.22 | 502.07 | |
| | High | 7 | 281.89 ± 94.62 | 117.87 | 605.92 | 67.75 ± 119.433 |
| | Low | | 219.54 ± 26.41 | -683.07 | 1332.06 | 5.40 ± 87.3 |
| | Sham | | 214.14 ± 63.86 | 153.94 | 527.59 | |

Summary of cell count of positive GFAP immunoreactivity within the DG, CA1, and CA3 for impact recovery and sham groups. For the mean differences ± SEM between injury and sham groups, comparisons were based on recovery time (e.g., High3 vs. Sham3, Low3 vs. Sham3, High7 vs. Sham7, and Low7 vs. Sham7). The p-value obtained from ANOVA procedures is listed beneath each brain region title.

Results from GFAP immunostaining indicated no significant differences between groups with respect to the number of GFAP positive cells/mm$^2$ (Figure 4.10). Moreover, positive cell count analysis of GFAP immunoreactivity did not indicate any injury group, regardless of recovery, to be statistically significant from sham (Figure 4.10). Although group Low3 visually seems statistically different from High3 and Sham3 groups within the CA1 region, according to our statistical analysis, they were not (p=0.411 and p=0.361, respectfully) (Figure 4.10B). Furthermore, the trends observed for GFAP positive cells/mm$^2$ analysis were mimicked for all three regions of interest with respect to recovery days between animal groups (Figure 4.10A-C).

In short, the GFAP positive cell count analysis showed no evidence of increased astrogliosis in the hippocampus for DG, CA1, or CA3 (Figure 4.10A-C).

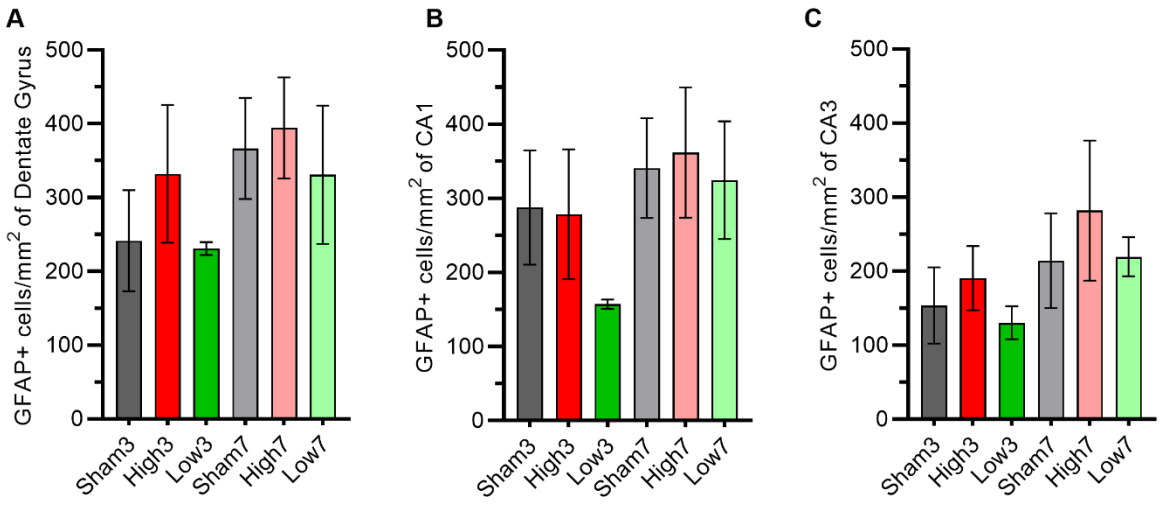


Figure 4.10 The number of positive GFAP cell counts/mm$^2$ for (A) DG, (B) CA1, and (C) CA3.

Comparison plots of the cell count of positive GFAP immunoreactivity (number of GFAP+ cells/mm$^2$). Data are presented as mean ± SEM for impact recovery groups High3, High7, Low3, Low7, Sham3, and Sham7 in the (A) DG, (B) CA1, and (C) CA3.

#### 4.3.3.2 Iba-1

Ionized calcium-binding adaptor molecule-1 (Iba-1) was used as an immunohistochemical marker for microglia. The number of positive cell counts/mm$^2$ was used to analyze the proportion of Iba-1 immunoreactivity within the DG, CA1, and CA3 regions for each group as a measure of microgliosis. Summary statistics for the Iba-1 manual positive cell counts/mm$^2$ measurements obtained for each region can be seen in Table 4.8. Results of the one-way ANOVA analysis are displayed by region of interest in Table 4.8.

Table 4.9 Iba-1 positive cell count summary.

| Brain Region | Group | Day of Recovery | Mean ± SEM | 95% CI | | Impact vs. Sham Mean Diff ± SEM |
|---|---|---|---|---|---|---|
| | | | | Lower | Upper | |
| DG *ANOVA (p=0.580)* | High | 3 | 42.54 ± 4.97 | 21.17 | 63.91 | -6.15 ± 8.612 |
| | Low | | 57.74 ± 30.79 | -333.49 | 448.98 | 9.05 ± 19.016 |
| | Sham | | 48.69 ± 5.86 | 32.43 | 64.96 | |
| | High | 7 | 81.82 ± 29.35 | 0.33 | 163.31 | -8.24 ± 35.625 |
| | Low | | 67 ± 21.55 | -25.72 | 159.71 | -23.06 ± 18.087 |
| | Sham | | 90.06 ± 21.92 | 29.18 | 150.93 | |
| CA1 *ANOVA (p=0.719)* | High | 3 | 33.32 ± 3.69 | 17.42 | 49.22 | -5.34 ± 9.594 |
| | Low | | 37.31 ± 13.92 | -139.6 | 214.21 | -1.35 ± 13.703 |
| | Sham | | 38.66 ± 6.9 | 19.49 | 57.83 | |
| | High | 7 | 44.34 ± 21.18 | -14.46 | 103.14 | -30.46 ± 37.614 |
| | Low | | 30.64 ± 7.17 | -0.23 | 61.51 | -44.16 ± 39.26 |
| | Sham | | 74.8 ± 34.29 | -20.39 | 170 | |
| CA3 *ANOVA (p=0.096)* | High | 3 | 24.51 ± 3.81 | 8.11 | 40.92 | -2.86 ± 5.189 |
| | Low | | 23.38 ± 8.75 | -87.75 | 134.52 | -3.99 ± 7.183 |
| | Sham | | 27.37 ± 3.28 | 18.25 | 36.49 | |
| | High | 7 | 97.52 ± 37.02 | -5.27 | 200.31 | 42.82 ± 38.301 |
| | Low | | 41.26 ± 7.5 | 17.41 | 65.11 | -13.44 ± 12.446 |
| | Sham | | 54.7 ± 9.31 | 28.84 | 80.56 | |

Summary of positive cells (number of positive cell counts/$mm^2$) of Iba-1immunoreactivity within the DG, CA1, and CA3 for impact recovery and sham groups. For the mean differences ± SEM between impact groups and sham, comparisons were based on recovery time (e.g., High3 vs. Sham3, Low3 vs. Sham3, High7 vs. Sham7, and Low7 vs. Sham7). The p-value obtained from ANOVA procedures is listed beneath each brain region title.

Similar to the positive cell counts/$mm^2$ for GFAP, analysis of the Iba-1 positive cell counts/$mm^2$ revealed no significant differences between injury and sham groups, regardless of recovery, within the DG, CA1, and CA3 regions (Figure 4.11A-C). Although not significant, on average, the low impact group exhibited the highest hippocampal expression of Iba-1 immunoreactivity after a 3-day recovery in the DG region (Figure 4.11A). However, in the CA1 and CA3 regions, on average, the sham group exhibited the highest hippocampal Iba-1 positive cell count/$mm^2$ expression after a 3-day recovery (Figure 4.11B-C). For the 7-day recovery

groups, although insignificant, the sham group exhibited the highest hippocampal expression, apart from the CA3 region, which was most apparent within DG (Figure 4.11A).

Mean positive cells/mm$^2$ of Iba-1 immunoreactivity for the low impact group showed the greatest deviation from sham with a larger mean positive cells/mm$^2$ at 3-DPI within the DG region (9.05 ± 19.016) compared to the higher impact group (-6.15 ± 8.612) (Table 4.8). Alternatively, the high impact group expressed a greater mean deviation of Iba-1 positive cells/mm$^2$ from sham within the CA3 region after 7-day of recovery (42.82 ± 38.301) (Table 4.8).

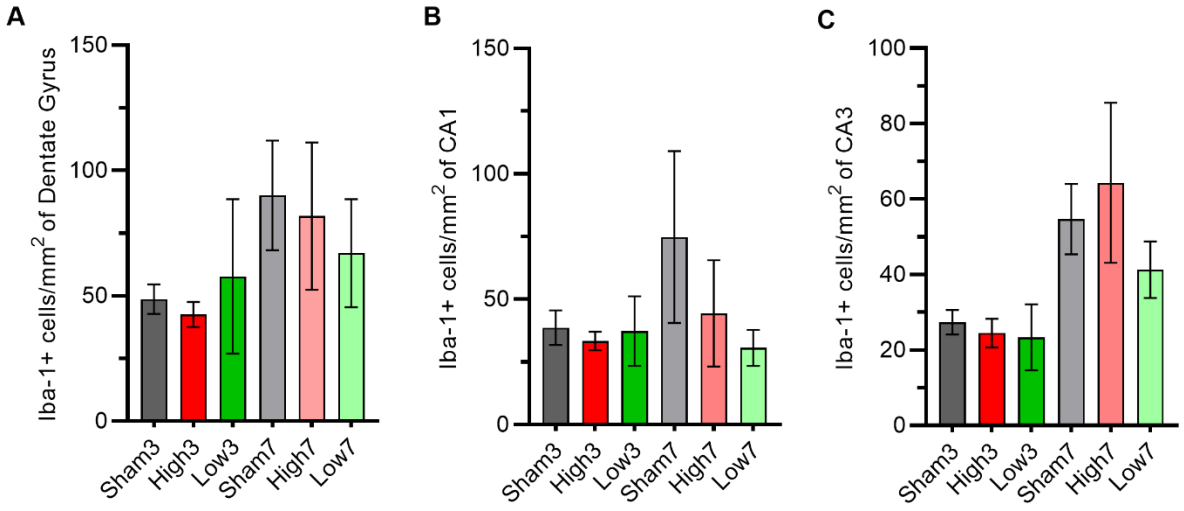


Figure 4.11 The number of positive Iba-1 cell counts/mm$^2$ for (a) DG, (b) CA1, and (c) CA3.

Comparison plots of the cell count of positive Iba-1 immunoreactivity (Number of Iba-1 + cells/mm$^2$). Data are presented as mean ± SEM for impact recovery groups High3, High7, Low3, Low7, sham3, and sham7 in the (a) DG, (b) CA1, and (c) CA3. Within the CA1 hippocampal region (B), pairwise comparison results indicated a significant decrease in the number of positive Iba-1 cell counts/mm$^2$ for each experimental group after 7-days of recovery compared to 3-days of recovery.

### 4.3.4 Cytokines

In the 36 brain sections that were used to detect the presence of IL-6, TNF-α, and IL-10, in the motor cortex and hippocampus regions, levels were below the threshold of detection. To review plate setup and the detection signal of each analyte for each region of interest see Tables D.1 and D.2 in Appendix D.

## 4.4 Discussion

Using a novel weight drop injury device capable of producing repeatable, closed head impact loads, the present study first aimed to develop a rodent model of a single, surgery-free, blunt impact to determine the appropriate impact magnitude suitable for an mTBI. Secondly, this study was designed to establish the foundation for the subsequent analysis thereby addressing the absence of knowledge surrounding the comparative effects between a single concussive impact and repeated SC impacts.

### 4.4.1 Behavioral Alterations Due to Impact

A substantial amount of evidence has classified mTBI as a functional disruptive injury (Bodnar et al., 2019; Eme, 2017; Emery et al., 2016; Hartlage et al., 2001). However, a fair number of preclinical observations have reported subtle behavioral deficits resulting from a concussion (Bodnar et al., 2019; Henninger et al., 2007; T. H. Hsieh et al., 2017). In the present study, we explored evidence of altered behavioral function in groups High3, Low3, High7, and Low7 using commonly utilized behavioral tests of general locomotor activity (OFT), anxiety-like behavior (OFT), and motor coordination (rotarod).

#### 4.4.1.1 General Locomotor Activity

Here we utilized an Open Field Test (OFT) to assess changes in general locomotor activity throughout a 30-minute test (Figure 4.7). Results showed that, following a 3- and 7-day recovery period from impact, the general locomotor activities of injury groups did not significantly differ from shams, pointing to the possibility of the low form of mTBI. Similarly, several other rodent models of mTBI have also reported unaffected general locomotor activity in an open field assay (D Bree, Mackenzie, et al., 2020; Dara Bree & Levy, 2018; Broussard et al., 2018; Taib et al., 2017; Tweedie et al., 2016; Wirth et al., 2017; Wilson, 2019) Thus, our discovery of an absence of alteration due to a lower range magnitude of mTBI severity in locomotor activity was consequently expected.

#### 4.4.1.2 Anxiety-like Behavior

A commonly affected behavior due to mild traumatic brain injury includes elevated anxiety and is frequently investigated in other models of mTBI (Bodnar et al., 2019; Malkesman et al., 2013) and clinical concussion (Armstrong & Morrow, 2019; Wood et al., 2014). As a measurement of anxiety-related behavior in rodents, activity in the center region of an open field apparatus is commonly focused upon. In the context of an OFT, wall-hugging behavior, or thigmotaxis, is observed in rodents and is linked to anxiety-like behavior (Gould et al., 2009; Seibenhener & Wooten, 2015). Thigmotaxis is determined as a ratio of the difference in the time spent in the outer and center zone relative to the total time spent in both zones (Equation 4.1). Increased thigmotaxis is interpreted as elevated anxiety and is commonly reported in rodent models of head trauma (Bodnar et al., 2019; Bree, Stratton, et al., 2020; Jamnia et al., 2017). Animals that are considered less anxious are viewed as more willing to explore the open and brightly lit center zone of the arena (Prut & Belzung, 2003).

In the present study, after 7-days of recovery, the high impact recovery group displayed a significant increase in anxious-like behavior as seen in the thigmotaxis index analysis (Figure 4.9C). These findings align with other previous studies exploring anxiogenic-like behavior in OFT which identify elevated thigmotaxis in rodents following a single concussion. A murine mTBI study conducted by Tucker et al. (2017) observed an increase in thigmotaxis following a 1- and 10-day recovery from a controlled cortical impact (CCI) with an impact velocity of 5 $ms^{-1}$ (KE = 0.09 J). Another study performed by Namjoshi et al. (2017) observed an increase in thigmotactic behavior of mice in mTBI groups (0.6 and 0.7 J) compared to sham at 1- and 7-days post-TBI using a Closed Head Impact Model of Engineered Rotational Acceleration (CHIMERA) piston design. Furthermore, according to a widely cited review article by Bodnar et al. (2019), the majority of preclinical mTBI investigations identify an elevation of the thigmotaxic index in rodents following head impact. Thus, our finding of anxiety-like behavior due to a concussion, albeit a low-grade concussion, was consequently expected.

Furthermore, a previous study exploring center zone entries using an OFT, after a 5-day recovery period, also reports an insignificant decrease in the number of center zone entries after a single mTBI, using a controlled cortical impact model, compared to shams (Broussard et al., 2018). Additionally, to the best of the investigator's knowledge, only one other study has also reported an insignificant difference, after 7-days of recovery, in rats exposed to a single concussive impact using a fluid percussion impact model (2.19 atm) (Beitchman et al., 2020).

In summary, results from the present behavioral investigation revealed no significant changes in general locomotor activity from a low-level mTBI. However, we observed that the higher mTBI impact load led to a significant increase in thigmotaxis, after 7-days of recovery, compared to shams, suggesting anxiogenic-like behavior due to the 0.5 J mTBI impact load.

#### 4.4.1.3 Motor Coordination

In order to explore alterations in motor coordination due to impact, we utilized a rotarod test. Results showed that while the performance of rats improved over time, there were no differences found between injury and sham groups for the latency to fall, suggesting that our investigative impact magnitudes of mTBI do not affect gross motor function. These results agree with one other study that employed a WDI apparatus to model a blunt, closed-scalp head injury (0.5 J) in rats to measure neurologic functions using a rotarod test (Kim & Han, 2017). Results indicated that there were no significant differences in latency to fall for injured rats compared to sham (Kim & Han, 2017).

In contrast to these findings, a murine study conducted by Namjoshi et al. (2017) reported the minimum injury level required with a single impact, using the CHIMERA platform (a piston-based model), to result in rotarod deficits up to 14-days following injury was observed at impact energies of 0.6 and 0.7 J. Interestingly, in another previously investigative murine study using a modified version of the CHIMERA model, no motor impairments on the rotarod was found after 1-, 3-, or 5-days following a single impact with energies of 1.7 J or 2.1 J (Sauerbeck et al., 2018). Furthermore, several studies that report significant differences of motor deficits between mTBI and sham groups typically employ a murine model with an impact magnitude range distinguishably lower (0.00075 – 0.06 J) than the present study's investigative range (Y. C. Chen et al., 2014; G Onyszchuk et al., 2007; S. H. Yang et al., 2013). Thus, it has been noted that data and conclusions regarding the effects of mTBI on motor coordination in rodents are inconsistent and that additional research is warranted.

### 4.4.2 Neuroinflammation Due to Impact

In the present study, we evaluated the response of reactive astrocytes between the two investigative injury groups through the analysis of the positive cell counts of GFAP immunoreactivity. Similarly, we performed a positive cell count analysis of Iba -1 immunoreactivity to assess the microglial response. Both positive cell counts of Iba-1 and GFAP immunoreactivity were assessed within the DG, CA1, and CA3 subregions of the hippocampus.

Results indicated that the number GFAP and Iba-1 positive cells/$mm^2$ for both injury groups, High and Low, following a 3- and 7-day recovery, was approximately equal to sham for all three brain regions indicating no evidence of astrogliosis or microgliosis (Figure 4.10-4.11). However, although insignificant, on average, high impact groups exhibited the highest hippocampal expression of GFAP immunoreactivity in all three hippocampal regions of interest, regardless of recovery time, except within the CA1 region after 3-DPI (Figure 4.10), which was most apparent within the DG (Figure 4.10A). Moreover, although insignificant, GFAP immunoreactivity appeared to be consistently upregulated for all experimental groups as recovery time increased within all three regions of interest (Figure 4.10).

Overall, these results indicate that again, although insignificant from shams, the high impact load groups exhibited slightly more GFAP positive cells/$mm^2$ signaling a potential increase in astrocytic reactivity. Therefore, our results suggest a minimal presence of neuroinflammation within the hippocampus after 3-days of recovery, apart from the CA1 region, which increases 7-days after injury for injury groups who received the higher impact load. More conservatively, these results signal a degree of cellular perturbation due to the higher impact load injury compared to low impact and sham groups. These results were expected as nearly all preclinical models and clinical observations of head injury report an increase in GFAP

expression (Abdelhak et al., 2022; Bogoslovsky et al., 2017; Fehily et al., 2019; Fraunberger et al., 2020; Kim & Han, 2017; Marschner et al., 2019; Singh et al., 2016).

As with the GFAP analysis results, injury groups, regardless of recovery assignments, did not reveal a significant difference from sham with respect to Iba-1 immunoreactivity indicating no evidence of microgliosis (Figure 4.11A-C). Overall, although insignificant, Iba-1 immunoreactivity appeared to be consistently upregulated for all experimental groups as recovery time increased, except for the lower impact group in the CA1 region (Figure 4.11B). This subtle reduction in GFAP immunoreactivity over time within the CA1 region is most likely because of the low number of samples available for groups Low3 (n=2) and Low7 (n=3) compared to the other experimental groups (High3 (n=4), Sham3 (n=5), High7 (n=6), and Sham7 (n=5)). As such, our results suggest that a minimal presence of microgliosis was seen for all groups within each hippocampal region as recovery time increased. From a conservative point of view, the histological findings signal a subtle degree of cellular perturbation due to injury.

### 4.4.3 Cytokine Expression Due to Impact

An unexpected limitation of this work is the lack of cytokine detection in experimental rats. Surprisingly, the procarta multiplex assay for IL-6, TNF-α, and IL-10 cytokines was not successful using the brain tissues from this study. Possible reasons for low signal levels or negligible expression of cytokines could be due to targets falling below detection limits of the assay or a human error (i.e., the appropriate detection timeline of these specific cytokines was missed, not enough detector antibody used, or the standards may not have been reconstituted or diluted correctly).

Several rodent models investigating cytokines produced following low-level mTBIs report an increase in IL-6 and TNF-$\alpha$ levels as well as a decrease in IL-10 concentrations in

brain tissue within the acute and subacute phases of secondary injury (Lee et al., 2012; Wang et al., 2011; Xia et al., 2012; Lagraoui et al., 2012; Dalgard et al., 2012; Zhao et al., 2014). Thus, these data are evidence of the inflammatory response of TBI at low-level impacts. It is important to note that compared to our investigative model of an mTBI, these are more severe models requiring the generation of craniotomies, with the subsequent disruption of the blood brain barrier, which has been shown to influence the pathology of inflammation (Cole et al., 2011).

Works of others in the field of TBI have shown that with more severe levels of head injuries the greater are the inflammatory markers of pathology. This has been shown in injury models including FPI (Mukherjee et al., 2011), CCI (Harting et al., 2008), and WDI (Holmin et al., 1997; Sarkaki et al., 2013). In the present study, it is not possible to say to what extent the evidence of cytokine expression is due to the absence of results. However, according to literature and with the present study's histological findings, it is conjectured that a minimal elevation of pro-inflammatory cytokine (TNF-$\alpha$ and IL-6) concentration levels in animal groups would be present as recovery increased as seen in the subtle increase of microgliosis in the histological findings. It is widely accepted that microglia are potent producers of TNF-$\alpha$ and IL-6 when they assume a pro-inflammatory phenotype (Bell-Temin et al., 2015; Madathil et al., 2018). However, because Iba-1 does not differentiate between pro- and anti-inflammatory microglial phenotypes, it is not possible to confirm the above hypothesis unless future analysis exploring this avenue is performed.

## 4.5 Conclusion

In brief, our data showed no evidence of disruption of motor coordination in injured animals compared to shams. There was, however, evidence of elevated anxiety-like behavior in the high impact group compared to sham. Additionally, there was minimal evidence of

neuroinflammation between the high impact and sham groups. Notably, although not significant, overall, animals who received the higher impact load expressed the highest (50%) number of GFAP and Iba-1 positive cells/mm$^2$ followed by low impact (42%) and sham groups (8%). Therefore, our pilot study exploring the comparative pathophysiology between single low-level impacts (0.2 J vs. 0.5 J) showed that animals receiving the higher impact load led to a significant increase in anxiety-like behavior compared to sham.

The present work has laid the foundation for a biomechanically informed model of the lower end ranges of mTBI, according to literature, that manifests pathology unlike that currently seen in models of concussion. Despite the insignificant results of alterations in motor coordination and inflammatory analysis, it revealed important aspects of lower-level impact loads. First, this work provides evidence in support of the notion that not every closed head impact has the capacity to result in system perturbations. Although a theoretical injury threshold may not exist for rats using a WDI model, based on the present study's findings, we hypothesize a biomechanical threshold level of impact associated with a lack of functional impairment and neuroinflammation due to a single closed head injury is likely around an energy level of 0.2 J. However, targeted investigations would be necessary to explore this hypothesis. Investigations may include expanding the recovery timeline between 12 hours and 2 weeks post-injury, involving additional behavior tests to test cognitive impairment, and/or analyzing brain tissues for the presence of cytokines, just to name a few. Not only could this data inform investigators of injury relief strategies, but it would directly affect treatment targets and the development of therapeutic interventions.

# CHAPTER V

# BEHAVIORAL AND HISTOLOGICAL INFLAMMATORY ANALYSIS FOLLOWING A SINGLE MILD TRAUMATIC BRAIN INJURY AND REPEATED SUBCONCUSSIVE INJURY USING A RODENT MODEL

## 5.1 Introduction

Previous work aimed to explore two impact magnitudes slightly higher than the lowest reported mTBI for a closed head impact found in literature. However, since the results did not present significant evidence of neuroinflammation due to a single impact of 0.2 or 0.5 J, it was decided to use the energy intensity of 0.5 J as the impact load for the repetitive SC impact group in the present study. Using a rodent model, the present study aimed to investigate the pathophysiological differences between the two injury paradigms, a single mTBI, with a kinetic energy (KE) of 1.5 J, and repeated subconcussive (RSC) impacts, KE = 0.5 J, with subdivided cumulative KEs equal to the single mTBI impact (i.e., 0.5 J x 3 = 1.5 J). However, upon the first day of impacts for rodents receiving a single mTBI impact (1.5 J), two of the four rodents died within 5 minutes following head trauma. After necropsy was performed on the two rodents, the final diagnosis concluded both rats sustained subdural hemorrhage with one rat showing evidence of a fractured parietal bone. As such, it was decided to decrease the severity of impact load for mTBI from 1.5 to 1.0 J. Subsequently, the impact load for the RSC impacts was also decreased to a kinetic energy of 0.33 J. The following criteria were used to determine the appropriate mTBI impact load for a rat model: 0% mortality due to impact, the absence of skull

fracture, the presence of behavioral measures, and/or neuroinflammation via immunohistochemistry.

To understand the analysis of the sequelae following the two injury paradigms, impact animals were divided into four groups and subjected to either a single mTBI load of 1 J or three SC impact loads of 0.33 J with an assigned recovery time of either 3- or 7-days post-final impact and compared to sham. Similar to the previous study's design (see Chapter 4), the present study evaluated evidence of behavioral alterations, inflammation, and cerebral vulnerability using behavioral assays and immunohistochemistry. Measurement outcomes were assessed at two recovery time points, 3- and 7-days, following the final closed head injury (CHI).

## 5.2 Methods

The following sections outline the experimental design and methods utilized for each procedure. In addition, this section provides animal number details along with impact, behavioral, euthanasia, and histological procedures for the full study. Analytical and statistical methods have been outlined as appropriate for each experimental procedure.

### 5.2.1 Experimental Design

An overview of the experimental elements and design for the full study can be viewed in Figure 5.1. All procedures for the experimental full study have been approved by the Mississippi State University Institutional Animal Care and Use Committee (IACUC) under protocol number 20-456 (see Appendix A).

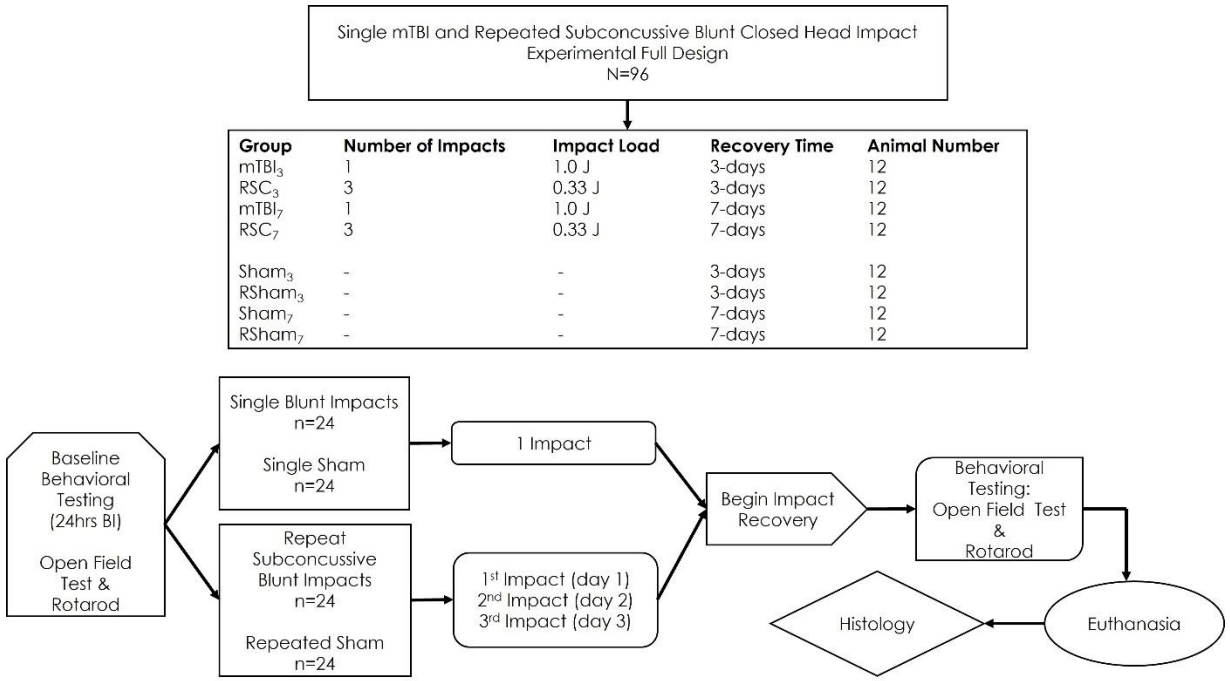


Figure 5.1 An overview of the experimental elements and design for the full study.

### 5.2.2 Animals

Ninety-six male Sprague-Dawley rats (250-300 g; Envigo, Indianapolis, IN) were housed in a 12-hour light/dark cycle facility accredited by the Association for Assessment and Accreditation of Laboratory Animal Care (AAALAC). Upon arrival, animals were kept in quarantine for 3-days before experimentation to ensure the quality of health and adequate acclimation to the environment. Rats were housed in groups of two in transparent cages on standard bedding with unlimited access to food pellets and water ad libitum prior to testing and again after 24 hours following the final administration of analgesia.

Rats were randomly assigned to one of 4 injury groups (n=48) or sham groups (n=48). Groups were then divided by assigned recovery time (3- or 7-days post-impact (DPI)). Each impact-recovery group (n=4) consisted of twelve rats and was accompanied by twelve sham rats.

Sham rats underwent all procedures as the impact rats excluding the blunt impact. For each cage, one rat was assigned as an impact rat while the other was assigned as a sham.

Prior to each impact procedure, rats were administered ketamine (100-200 mg/kg IP) and xylazine (5-10 mg/kg IP). Loss of righting reflex was used to indicate the depth of anesthesia. Upon completion of head impact, atipamezole (5-10 mg/ml IM) was administered to reverse the effects of xylazine. In addition to this reversal agent, rats were administered a single dose of Buprenorphine SR (1 mg/ml SC) for analgesia. Following the impact procedure (or post-final impact for repeated SC recovery groups), each rat begins their assigned recovery time (3- or 7-days). On the final day of recovery, animals were sacrificed.

To control pica behavior, a common side effect of buprenorphine, rats were housed individually on cage paper for approximately 24 hours as opposed to standard rodent bedding when returned to the colony post-impact. After 24 hours following analgesic administration, animals were returned to group housing and placed on standard bedding with food and water provided ad libitum. Pica behavior was monitored throughout the 3-day effective duration of analgesia.

Eleven animals died before the completion of the study due to an adverse reaction to anesthesia. According to the veterinary doctor on staff, the rats most likely aspirated saliva due to hypersalivation from ketamine. Using all the precautionary extra rodents on hand, only six of the eleven animals were replaced. A table of original animal numbers and final animal numbers can be seen in Table 5.1.

Table 5.1 Initial and Final Animal Numbers

| **Recovery Group** | **Starting Number of Rats** *(mTBI / RSC / Sham / RSham)* | **Final Number of Rats** *(mTBI / RSC / Sham / RSham)* |
|---|---|---|
| 3-Days | (n=12) / (n=12) / (n=12) / (n= 12) | (n=12) / (n=10) / (n=12) / (n= 9) |
| 7-Days | (n=12) / (n=12) / (n=12) / (n= 12) | (n=12) / (n=12) / (n=12) / (n= 12) |

Animal numbers within each experimental group at the beginning and end of the study reflecting animals lost. From the 3-day recovery assigned groups, two rats within the repeated SC impact group and three rats from the repeated sham group died shortly after impact due to anesthesia. Note: mTBI=mild Traumatic Brain Injury; RSC = repeated subconcussive injury; RSham = repeated Sham.

### 5.2.3 Impact Device and Procedures

The impact device, procedures, and statistical analysis of the impact data used in the present study have been previously described (see Chapters 4.2.3). The only modifications made to the present study's impact device were the projectile weights. Animals assigned to receive a single mTBI impact (n=24) were hit to the top side of the head with a 136.03 g weight. Those assigned to receive a repeated SC impact within an inter-injury interval of 24 hours for 3 consecutive days (n=24) were impacted with a 44.72 g weight.

### 5.2.4 Behavioral Analysis

All behavior and statistical analysis used in the present study have been previously described (see Chapters 4.2.4). The only modification made to the present study's setup was for each experimental run of the open field and rotarod tests a total of four rodents were employed, two injury (a single mTBI and RSC) and two sham animals (a sham and repeated sham).

### 5.2.5 Brain Collection Process

After completion of all behavioral testing on recovery days (3- and 7-DPI), animals were euthanized using carbon dioxide in a chamber. Subsequently, rats were decapitated using a guillotine as a confirmation of euthanasia. Following this, the brain samples were dissected and

hemisected by a midline sagittal cut. One-half of each brain was placed in dry ice and stored at −80 °C until further analysis. The other half was trimmed using a 1 mm coronal acrylic brain matrix (Ted Pella, Inc., Redding, CA, USA). Using a Rat Brain Atlas (Paxinos, Watson: The Rat Brain in Stereotaxic Coordinates, 7th Edition) as a guide, the first trim was made 2 mm directly in front of the optic chiasm (2.48 bregma; see blade 1 in Figure 5.2) with each subsequent cut made 2 mm caudal to the preceding trim for a total of three 2 mm tissue sections. Trimmed sections were placed in cassettes (2-3 trims from the same brain per cassette) and submerged in 10% neutral buffered formalin (NBF) solution for at least 3 weeks in preparation for processing and paraffin embedding.

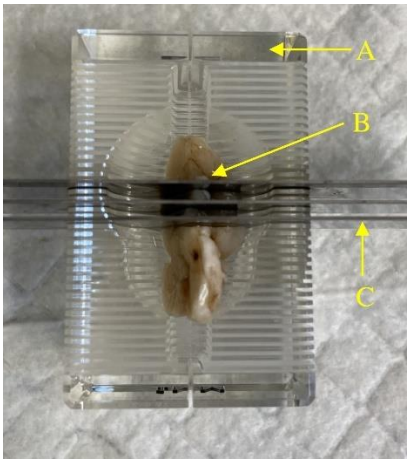


Figure 5.2 Representative image of left cerebral hemisphere tissue trimming protocol. Shown are the A) acrylic brain trimming matrix, B) optic chiasm (the location of the first trim), and C) blades used for trimming. The distance between each razor was 2 mm.

### 5.2.6 Histology

All histological and statistical analyses used in the present study have been previously described (see Chapters 4.2.7). The only modification made to the present study's immunohistochemical investigation was adding an immunohistochemical stain for the

assessment of neuronal loss due to injury. To investigate evidence of neuronal loss, each tissue section underwent NeuN (neuronal nuclei) immunostaining.

Prior to NeuN staining, paraffin-embedded tissues were sectioned at 5 μm onto charged slides. Unstained slides were deparaffinized and pretreated with Reveal Decloaker (Biocare rv1000m) in a Decloaking Chamber (Biocare) for 15 minutes at 110°C. Immunostaining was performed on an IntelliPATH autostainer. Endogenous peroxidase activity was blocked with 3% hydrogen peroxide (Biocare ipb5000) for 5 minutes. The primary antibody for NeuN (Abcam ab177487, 1:800, 1hr) was then applied. A negative control without primary was included. Detection was performed using Rabbit-on-Canine HRP polymer (Biocare rc542) according to insert directions mixed in with DaVinci green diluent (Biocare pd900). The tissues were then developed with DAB chromogen substrate (Biocare) for 5 minutes. Following that, slides were counterstained with hematoxylin (Biocare) for 5 minutes. Finally, slides were washed, dehydrated and coverslipped.

## 5.3 Results

### 5.3.1 Impact Data

A weight drop injury device was employed to induce either mTBI or subconcussive injury using two projectile weights (136.03 and 44.72 g) at an impact height of 0.81 m. Animals that were impacted with the greater projectile weight were considered mTBI impact groups. Alternately, those who received an impact with the lower weight (44.72 g) were labeled as RSC impact groups. Descriptive Statistics obtained from the univariate analysis performed on the impact data can be found in Table 5.2. According to the data, mTBI impact groups received an average impact velocity of $3.87 \pm 0.01$ $ms^{-1}$ and average kinetic energy of $1.02 \pm 0.00$ J.

Alternatively, RSC impact groups had an average impact velocity of 3.89 ± 0.14 $ms^{-1}$ and kinetic energy of 0.34 ± 0.03 J.

Impact dynamics results from the Shapiro-Wilk test of normality for each variable are as follows: velocity for mTBI impact groups ($p<0.001$), KE for mTBI impact groups ($p=0.0002$), velocity for RSC impact groups ($p<0.001$), and KE for RSC impact groups ($p<0.0001$).

Table 5.2 Impact dynamics according to projectile weight.

| Projectile Weight (gms) | Variable | Mean | Standard Deviation | Minimum | Maximum |
|---|---|---|---|---|---|
| 44.72 | Velocity ($ms^{-1}$) | 3.891 | 0.140 | 3.190 | 4.680 |
| | Kinetic Energy (J) | 0.339 | 0.025 | 0.228 | 0.490 |
| 136.03 | Velocity ($ms^{-1}$) | 3.866 | 0.006 | 3.860 | 3.880 |
| | Kinetic Energy (J) | 1.016 | 0.003 | 1.013 | 1.024 |

The projectile weight (gms), mean, standard deviation, minimum and maximum values for velocity ($ms^{-1}$) and kinetic energy (J) calculated impact data.

### 5.3.2 Behavior

#### 5.3.2.1 Open Field Test

An Open Field Test (OFT) was employed to investigate indications of altered general locomotor activity or anxiety-like behavior due to impact and throughout recovery (3- and 7-days). In Tables 5.3-5.4, overall significance of three main effects are presented beside the variable's name. Results from the ANOVA test for the repeated measures design did indicate four variables showing a significant interaction effect between treatment and day, but only following 3 days of recovery (Table 5.3). As such, a separate table with the specific groups and day of testing showing significant differences was reported for the 3-day recovery groups (Table 5.5). Moreover, there were several variables, within both recovery groups, that showed a significant effect for either treatment, day of testing, or both (Tables 5.3-5.4). Plots represent the

mean with error bars representing the SEM. For all plots, significant differences ($p<0.05$) between group pairs are denoted with one asterisk (*).

Table 5.3 Open Field Test ANOVA summary for the repeated measures design of the 3-day recovery groups.

| Open Field Test Variables | ANOVA For Repeated Measures Design of 3-Day Recovery Groups | | |
|---|---|---|---|
| | **Treatment x Day** | **Treatment** | **Day** |
| Total Distance Traveled (m) | 0.176 | 0.262 | 0.001 * |
| Average Speed (m/s) | 0.801 | 0.145 | <0.0001 * |
| Maximum Speed (m/s) | 0.179 | 0.373 | 0.418 |
| Total Time Mobile (mins) | 0.016 * | - | - |
| Total Time Immobile (mins) | 0.562 | 0.633 | <0.0001 * |
| Total Time in Outer Zone (mins) | 0.019 * | - | - |
| Distance Traveled Outer Zone (m) | 0.262 | 0.036 * | 0.002 * |
| Time Mobile Outer Zone (mins) | 0.039 * | - | - |
| Time Immobile Outer Zone (mins) | 0.745 | 0.752 | <0.0001 * |
| Number of Entries into Center Zone | 0.106 | 0.047 * | 0.033 * |
| Distance Traveled Center Zone (m) | 0.1501 | 0.878 | 0.006 * |
| Total Time in Center Zone (mins) | 0.0443 * | - | - |
| Time Mobile Center Zone (mins) | 0.0836 | 0.002 * | 0.000 * |
| Time Immobile Center Zone (mins) | 0.0986 | 0.137 | 0.203 |
| Thigmotaxis Index | 0.1961 | 0.006 * | <0.0001 * |

The p-values obtained from the mixed model ANOVA tests for each OFT variable is presented. Significant differences of the effect are indicated by an asterisk (*).

Table 5.4 Open Field Test ANOVA summary for the repeated measures design of the 7-day recovery groups.

| Open Field Test Variables | ANOVA For Repeated Measures Design of 7-Day Recovery Groups | | |
|---|---|---|---|
| | **Treatment x Day** | **Treatment** | **Day** |
| Total Distance Traveled (m) | 0.523 | 0.051 | 0.053 |
| Average Speed (m/s) | 0.711 | 0.195 | 0.300 |
| Maximum Speed (m/s) | 0.688 | 0.401 | 0.265 |
| Total Time Mobile (mins) | 0.208 | 0.000 * | 0.005 * |

Table 5.4 (continued)

| | | | |
|---|---|---|---|
| Total Time Immobile (mins) | 0.870 | 0.110 | 0.275 |
| Total Time in Outer Zone (mins) | 0.064 | 0.006 * | 0.001 * |
| Distance Traveled Outer Zone (m) | 0.459 | 0.064 | 0.176 |
| Time Mobile Outer Zone (mins) | 0.192 | 0.003 * | 0.007 * |
| Time Immobile Outer Zone (mins) | 0.854 | 0.135 * | 0.283 |
| Number of Entries into Center Zone | 0.989 | 0.037 * | 0.003 * |
| Distance Traveled Center Zone (m) | 0.912 | 0.248 | 0.002 * |
| Total Time in Center Zone (mins) | 0.816 | 0.504 | 0.248 |
| Time Mobile Center Zone (mins) | 0.893 | 0.249 | 0.232 |
| Time Immobile Center Zone (mins) | 0.839 | 0.382 | 0.869 |
| Thigmotaxis Index | 0.810 | 0.767 | 0.750 |

The p-values obtained from the mixed model ANOVA tests for each OFT variable is presented. Significant differences of the effects are indicated by an asterisk (*).

Table 5.5 Open field test result summary of Fisher's least significant difference test for day 3 recovery groups where significant differences were observed for the interaction effect.

| **Open Field Test Variables** | **Differences of Least Square Means for Day 3 Recovery Groups** | | | | |
|---|---|---|---|---|---|
| | **Effect** | **Group** | **Day** | **Group** | **Day** |
| Total Time Mobile (mins) | Treatment*Day ANOVA (p=0.008) * | mTBI | BL | mTBI | TD |
| Total Time in Outer Zone (mins) | Treatment*Day ANOVA (p=0.005) * | RSC | BL | RSC | TD |
| | Treatment*Day ANOVA (p=0.002) * | RSham | BL | RSham | TD |
| Time Mobile Outer Zone (mins) | Treatment*Day ANOVA (p=0.003) * | Sham | BL | Sham | TD |
| Total Time in Center Zone (mins) | Treatment*Day ANOVA (p<0.0001) * | mTBI | BL | mTBI | TD |

Significant differences between group pairs by day of behavioral testing (baseline vs. recovery day) are identified from the Fisher's LSD test procedure next to each group's statistic.

As previously mentioned in section 4.3.2, the following variables will be further discussed in detail: total distance traveled and total time mobile (mins), total time in outer zone

(mins), and total time in center zone (mins), thigmotaxis index, and number of center zone entries.

With respect to measurements related to general locomotor activity, no significant differences were seen between injury and sham groups, regardless of recovery (Figure 5.3A); however, on average, the 3-day recovery group animals traveled significantly more total distance at baseline compared to recovery days (Table 5.3). In the context of the total time animals spent mobile during the OFT, data indicated, group $mTBI_3$ spent a significantly reduced amount of time mobile following 3-days of recovery compared to baseline measurements (p=0.008) (Table 5.3) (Figure 5.3B). Furthermore, on average, the 7-day recovery group animals spent significantly more time mobile on the day of recovery compared to baseline (Tables 5.4).

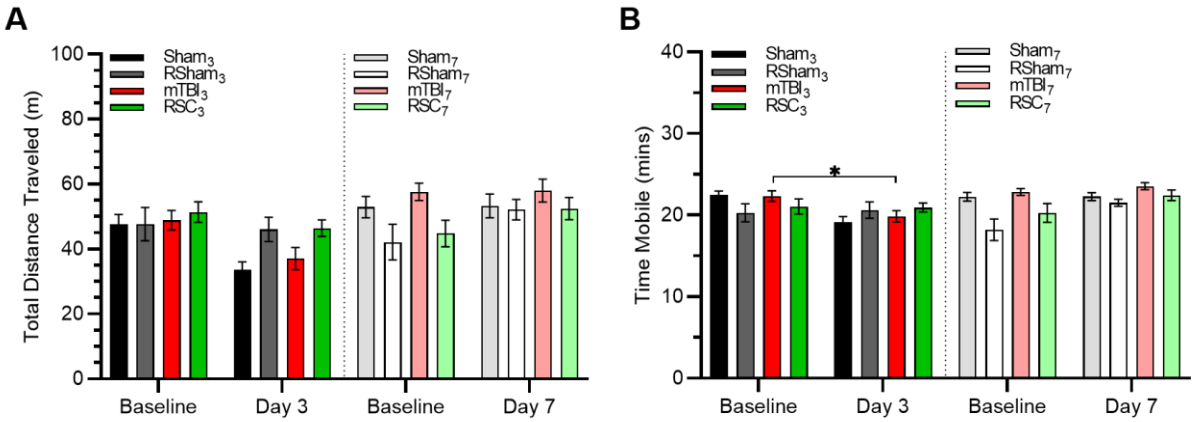


Figure 5.3 Total distance traveled (m) and total time immobile (sec).

Comparison plots of the (A) total distance traveled in meters and the (B) total time immobile in minutes among impact recovery groups $mTBI_3$ (n=12) and $RSC_3$ (n=10), $mTBI_7$ (n=11), and $RSC_7$ (n=11), and control groups, $Sham_3$ (n=12), $RSham_3$ (n=9), $Sham_7$ (n=12), $RSham_7$ (n=12), during the 30 minute OFT assay. Fisher's LSD method indicated that group $mTBI_3$ spent a significantly reduced amount of time mobile following 3-days of recovery compared to baseline measurements (p=0.008) (B). The asterisk located above the bracket indicates significance ($p<0.05$) between groups. Plots show the mean and the standard error of the mean (error bars).

In terms of time spent in the outer zone, data revealed that $RSham_3$ ($p=0.0002$) and $RSC_3$ ($p=0.005$) injury groups spent a significantly greater amount of time in the outer zone upon recovery time compared to baseline measurements (Table 5.5) (Figure 5.4A). Moreover, on average, the 7-day recovery group animals spent significantly more time in the outer zone upon recovery compared to baseline (Table 5.4). Additionally, on average, $RSC_7$ animals spent significantly more time in the outer zone compared to $mTBI_7$ animals (Table 5.4). Alternatively, Fisher's LSD method test results revealed that group $mTBI_3$ spent a significantly reduced amount of time in the center zone upon recovery time compared to baseline ($p<0.0001$) (Figure 5.4B). According to the thigmotaxis index analysis, no differences were seen between injury and sham groups, regardless of recovery (Figure 5.4C); however, on average, the 3-day recovery group animals traveled significantly more total distance upon recovery compared to baseline (Table 5.3). Furthermore, on average, groups $RSC_3$ and $Sham_3$ showed significantly greater thigmotaxis indexes compared to group $mTBI_3$ (0.007 and 0.003, respectively) (Table 5.3). Overall, these results further support the indication that injury groups showed no evidence of anxiety-like behaviors, as indicated by similarity in the thigmotaxis index measurements with their associated shams upon recovery days.

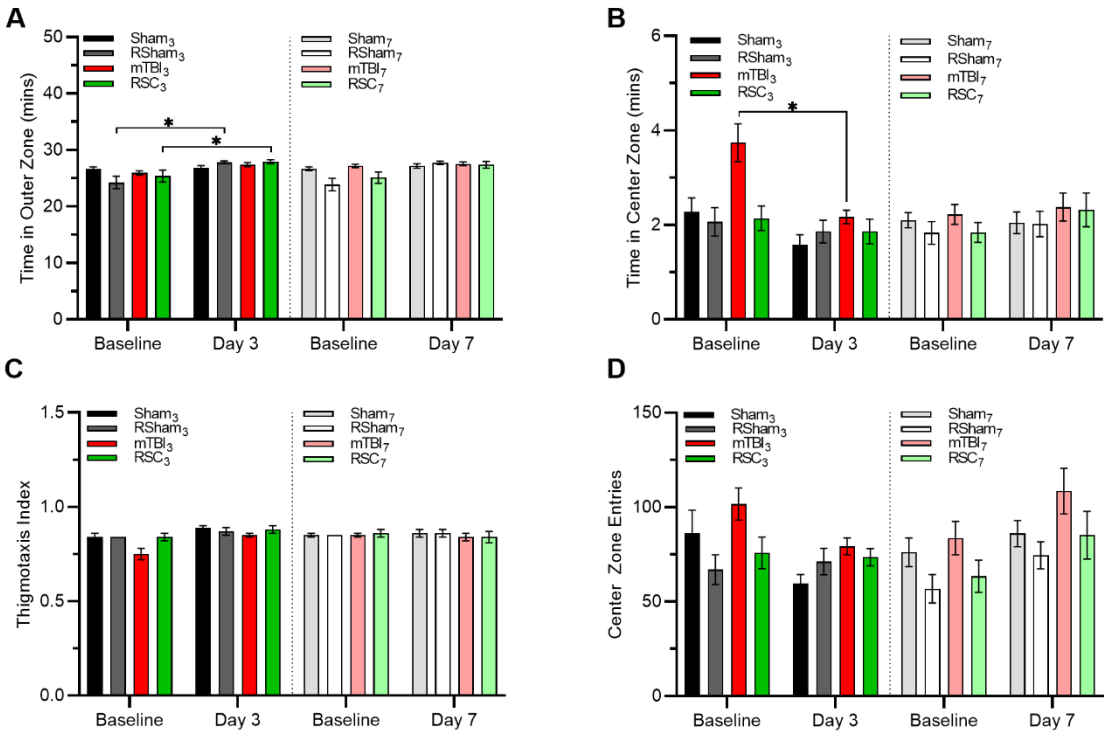


Figure 5.4 Plots for (A) time in the outer zone (mins), (B) time in the center zone (mins), (C) the index of thigmotaxis, and (D) the number of center zone entries.

Comparison plots of the OFT group results for (A) time in outer zone (mins), (B) time in center zone (mins), (C) the index of thigmotaxis, and (D) the number of center zone entries among impact recovery groups $mTBI_3$ (n=12) and $RSC_3$ (n=10), $mTBI_7$ (n=11), and $RSC_7$ (n=11), and control groups, $Sham_3$ (n=12), $RSham_3$ (n=9), $Sham_7$ (n=12), $RSham_7$ (n=12) was used to assess anxiety-like behavior. Fisher's LSD method indicated groups $RSham_3$ and $RSC_3$ spending a significantly greater amount of time in the outer zone upon recovery time compared to baseline measurements. Alternatively, group $mTBI_3$ spent a significantly reduced amount of time in the center zone upon recovery time compared to baseline. No differences were seen between injury and sham groups with respect to thigmotaxis index and number of center zone entries. An asterisk (*) denotes a significant difference ($p<0.05$). Plots show the mean (symbols) and the standard error of the mean (error bars).

Lastly, no significant differences were observed between injury and their associated sham groups, regardless of recovery time, with respect to the number of center zone entries (Figure 5.4D). However, within the 3-day recovery animal groups, on average, group $mTBI_3$ entered the

center zone a significantly greater amount of time than $Sham_3$ rats (p=0.042) (Table 5.3). Moreover, on average, group $mTBI_7$ entered the center zone a significantly greater amount of time than $RSC_7$ injury rats (p=0.030) (Table 5.4). Fisher's LSD test also indicated, on average, the 3-day recovery group animals entered the center zone a significantly greater amount at baseline compared to their 3-day recovery day (p=0.025) (Table 5.3). Alternatively, the 7-day recovery animal groups, on average, transversed the center zone a significantly greater number of times upon their recovery test day compared to their baseline test day (p=0.004) (Table 5.4). Overall, these open field test results indicate that impact animals, regardless of recovery, were not significantly different from sham in terms of general locomotive activity. Additionally, these data indicate that injury groups result in negligible expression of anxiety-like behavior, regardless of recovery time, as indicated by similarities in the thigmotaxis index and the number of center zone entries when compared to shams.

#### 5.3.2.2 Rotarod Test

A rotarod test was employed to investigate indications of altered sensory/locomotive coordination due to injury and throughout recovery (3- and 7-days). According to the ANOVA model, when comparing the differences in latency performance between animal groups, none showed a significant interaction effect between treatment and day (Table 5.6). Interestingly, when comparing the differences in latency time between treatment groups within the 3-day recovery assigned animals, significant differences were present (Table 5.6). However, because the two treatment groups showing significant differences in latency performance ($mTBI_3$ vs $RSham_3$) were not between appropriate injury and sham groups, this finding was not discussed further.

When comparing the differences in latency time for all animals, regardless of group assignment, by recovery groups, data showed a significant effect on the day of testing ($p<0.0001$) and of trials ($p<0.0001$) (Table 5.6). The differences in latency performance between 3- and 7- day recovery groups have been summarized as the mean ± the standard error of the mean in Tables 5.7 and 5.8, respectively.

Table 5.6 Rotarod ANOVA summary for the repeated measures design of all recovery groups.

| **Recovery Animal Groups** | **ANOVA For Repeated Measures Design** | | | |
|---|---|---|---|---|
| | **Treatment x Day** | **Treatment** | **Day** | **Trial** |
| 3-Day Groups | 0.316 | 0.041 * | <.0001 * | <.0001 * |
| 7-Day Groups | 0.328 | 0.431 | <.0001 * | <.0001 * |

The p-values obtained from the mixed model ANOVA tests is presented. Significant differences of the effect are indicated by an asterisk (*).

Table 5.7 Differences in latency (s) summary for 3-day recovery groups across all animals, regardless of group assignment.

| **Differences in Latency (s) of Day 3 Recovery Groups** | | | |
|---|---|---|---|
| **Effect** | **Trials by Day of Testing** | | **Mean ± SEM** |
| Day ANOVA ($p<0.0001$) * | Baseline | Recovery | -39.88 ± 6.16 |
| Trial ANOVA ($p=0.0007$) * | Trial 1 | Trial 2 | -23.60 ± 6.79 |
| Trial ANOVA ($p<0.0001$) * | Trial 1 | Trial 3 | -31.18 ± 6.79 |
| Trial ANOVA ($p=0.2565$) | Trial 2 | Trial 3 | -7.58 ± 6.66 |

The mean ± standard error of the mean (SEM) of latency (s) for the differences between day (baseline vs. recovery) and trials (1, 2, and 3) of all animals within the 3-day recovery groups, $mTBI_3$ (n=12), $RSC_3$ (n=10), $Sham_3$ (n=12), and $RSham_3$ (n=9), during the rotarod test. The p-value obtained from the ANVOA performed on each day of testing is presented. Significant differences ($p<0.05$) between effects are denoted with one asterisk (*).

Table 5.8 Differences in latency (s) summary for 7-day recovery groups across all animals, regardless of group assignment.

| Differences in Latency (s) of Day 7 Recovery Groups | | | |
|---|---|---|---|
| **Effect** | **Trials by Day of Testing** | | **Mean ± SEM** |
| Day<br>ANOVA ($p<0.0001$) * | Baseline | Recovery | -44.51 ± 6.12 |
| Trial<br>ANOVA ($p<0.0001$) * | Trial 1 | Trial 2 | -26.63 ± 5.39 |
| Trial<br>ANOVA ($p<0.0001$) * | Trial 1 | Trial 3 | -36.76 ± 5.45 |
| Trial<br>ANOVA ($p=0.0627$) | Trial 2 | Trial 3 | -10.13 ± 5.41 |

The mean ± standard error of the mean (SEM) of latency (s) for the differences between day (baseline vs. recovery) and trials (1, 2, and 3) of all animals within the 7-day recovery groups, $mTBI_7$ (n=11), $RSC_7$ (n=11), $Sham_7$ (n=12), and $RSham_7$ (n=12), during the rotarod test. The p-value obtained from the ANVOA performed on each day of testing is presented. Significant differences ($p<0.05$) between effects are denoted with one asterisk (*).

According to Tables 5.7 and 5.8, on average, all animals, across trials and treatment, performed significantly better on the day of recovery compared to baseline. Additionally, data showed that on average, all rats, across treatment and recovery days, performed significantly better on trials 2 and 3 compared to trial 1 (see Tables 5.7 and 5.8).

### 5.3.3 Histology

To investigate histological evidence of neuronal loss and neuroinflammation, positive cell count analysis was performed for brain tissue sections to assess mature neurons, microglia, and astrocytes using immunohistochemical markers NeuN, Iba-1, and GFAP, respectively. Histological analysis was performed for the dentate gyrus (DG), cornu ammonis 1 (CA1), and cornu ammonis 3 (CA3) subregions of the hippocampus. Histochemical assessment of H&E tissue sections revealed no macroscopic lesions due to impact. Representative micrographs of NeuN, GFAP, and Iba-1 tissue sections can be seen in Appendix E.2.1, E.2.2, and E.2.3, respectively. Plots for NeuN (Figure 5.6), GFAP (Figure 5.7), and Iba-1 (Figure 5.8) analysis

present the mean positive cell counts/mm$^2$. Error bars represent the SEM. For all plots, significance is denoted with one asterisk (*) indicative of a p-value smaller than 0.05 ($p<0.05$).

#### 5.3.3.1 NeuN

Neuronal Nuclei (NeuN) was used as an immunohistochemical marker for mature neurons. The number of positive cell counts/mm$^2$ was used to analyze the proportion of mature neuronal immunoreactivity within each brain hippocampal region of interest (DG, CA1, and CA3) for each group as a measure of neuronal loss due to injury. Summary statistics for the NeuN positive cell counts/mm$^2$ measurements obtained for each region analyzed can be seen in Table 5.7. Descriptive statistics of animal groups for each hippocampal region are displayed by region of interest in Table 5.7. Representative micrographs for each region can be found in Appendix E.2.1.

Table 5.9 NeuN positive cell count/mm$^2$ summary.

| Brain Region | Group | Day of Recovery | Mean ± SEM | 95% CI | | Impact vs. Control Mean Diff ± SEM |
|---|---|---|---|---|---|---|
| | | | | Lower | Upper | |
| DG ANOVA (p=0.690) | mTBI | 3 | 420.38 ± 8.33 | 401.82 | 438.95 | -2.48 ± 13.07 |
| | RSC | | 423.63 ± 11.47 | 397.67 | 449.58 | -8.04 ± 13.03 |
| | Sham | | 422.86 ± 10.35 | 400.08 | 445.63 | |
| | RSham | | 431.67 ± 5.02 | 420.09 | 443.25 | |
| | mTBI | 7 | 426.70 ± 5.76 | 414.02 | 439.39 | -17.67 ± 15.09 |
| | RSC | | 421.18 ± 10.54 | 397.98 | 444.37 | 1.97 ± 16.02 |
| | Sham | | 444.37 ± 13.95 | 413.68 | 475.06 | |
| | RSham | | 419.21 ± 12.16 | 392.11 | 446.30 | |
| CA1 *ANOVA* (p=0.831) | mTBI | 3 | 135.73 ± 5.91 | 122.72 | 148.74 | -0.79 ± 6.33 |
| | RSC | | 130.63 ± 5.79 | 117.52 | 143.73 | 0.34 ± 7.34 |
| | Sham | | 136.52 ± 2.28 | 131.50 | 141.54 | |
| | RSham | | 130.29 ± 4.28 | 120.43 | 140.15 | |
| | mTBI | 7 | 135.8 ± 3.95 | 127.11 | 144.49 | 4.13 ± 5.29 |
| | RSC | | 136.02 ± 3.74 | 127.79 | 144.26 | -6.85 ± 11.53 |
| | Sham | | 131.67 ± 3.51 | 123.94 | 139.41 | |
| | RSham | | 142.87 ± 11.36 | 117.56 | 168.17 | |
| CA3 ANOVA (p=0.810) | mTBI | 3 | 301.67 ± 10.44 | 278.69 | 324.65 | 6.31 ± 14.35 |
| | RSC | | 282.62 ± 16 | 246.42 | 318.81 | 0.79 ± 19.42 |
| | Sham | | 295.36 ± 9.85 | 273.69 | 317.04 | |
| | RSham | | 281.83 ± 10.09 | 258.57 | 305.09 | |
| | mTBI | 7 | 285.81 ± 11.97 | 259.47 | 312.14 | -6.99 ± 17.65 |
| | RSC | | 310.3 ± 16.32 | 274.39 | 346.21 | 24.96 ± 25.55 |
| | Sham | | 292.8 ± 12.98 | 264.24 | 321.36 | |
| | RSham | | 285.34 ± 19.89 | 241.03 | 329.65 | |

Summary of cell count of positive NeuN immunoreactivity within the DG, CA1, and CA3 for impact recovery and their associated sham groups. For the mean differences ± SEM between injury and their associated sham groups, comparisons were based on recovery time (e.g., mTBI3 vs. $Sham_3$, $RSC_3$ vs. $RSham_3$, $mTBI_7$ vs. $Sham_7$, and $RSC_7$ vs. $RSham_7$). The p-value obtained from ANOVA procedures is listed beneath each brain region title

Results from NeuN immunostaining indicated no significant differences between groups, regardless of recovery time and region of interest, with respect to the number of NeuN positive cells/mm$^2$ (Figure 5.6). As a result, the NeuN positive cell count analysis showed no evidence of neuronal loss in the hippocampus for DG, CA1, or CA3 (Figure 5.6A-C). Interestingly, though, mean NeuN positive cells/mm$^2$ analysis for the three hippocampal regions of interest yielded

lower levels of positive NeuN immunoreactivity in the CA1 region (Figure 5.6B) than in the DG (Figure 5.6A) and CA3 (Figure 5.6C) regions.

Finally, the number of NeuN positive cells/mm$^2$ of NeuN immunoreactivity for the mTBI group shows the greatest deviation from Sham with a larger mean number of NeuN positive cells/mm$^2$ with respect to the CA3 region at 3-DPI (Table 5.7). In that same region of interest, the repeated SC injury group also shows a greater mean count of NeuN positive cells/mm$^2$ than RSham after 7-DPI (Table 5.7).

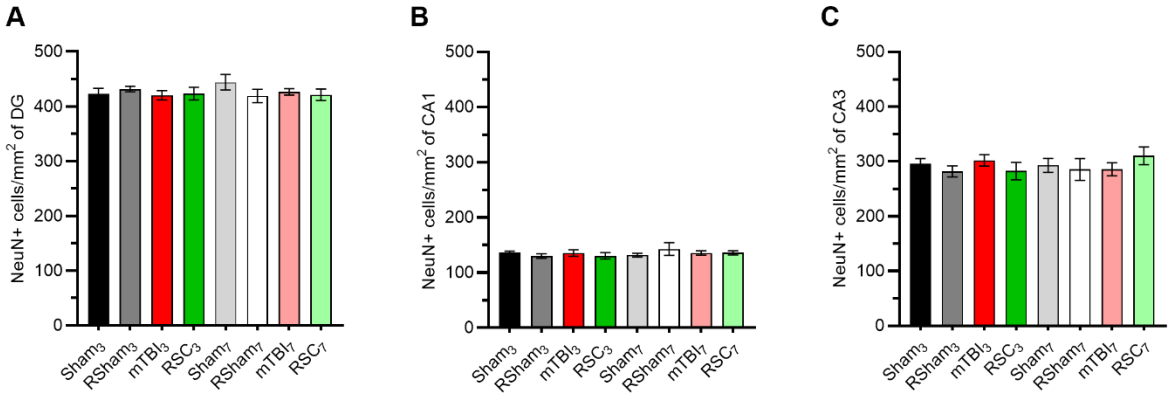


Figure 5.5 The number of positive NeuN cell counts/mm$^2$ for(A) DG, (B) CA1, and (C) CA3. Comparison plots of the cell count of positive NeuN immunoreactivity (number of NeuN+ cells/mm$^2$). Data are presented as mean ± SEM for recovery groups Sham$_3$, RSham$_3$, mTBI$_3$, RSC$_3$, Sham$_7$, RSham$_7$, mTBI$_7$, and RSC$_7$ in the (A) DG, (B) CA1, and (C) CA3.

#### 5.3.3.2 GFAP

Glial fibrillary acidic protein (GFAP) was used as an immunohistochemical marker for astrocytes. The number of positive cell counts/mm$^2$ was used to analyze the proportion of GFAP immunoreactivity within each brain region of interest for each group as a measure of astrogliosis. Summary statistics for the GFAP positive cell counts/mm$^2$ measurements obtained for each

region of interest by animal groups were analyzed and can be seen in Table 5.8. Representative micrographs for each region can be found in Appendix E.2.2.

Table 5.10 GFAP positive cell count/mm$^2$ summary.

| Brain Region | Group | Day of Recovery | Mean ± SEM | 95% CI | | Impact vs. Control Mean Diff ± SEM |
|---|---|---|---|---|---|---|
| | | | | Lower | Upper | |
| DG ANOVA (p=0.343) | mTBI | 3 | 109.91 ± 10.81 | 86.11 | 133.71 | 17.49 ± 16.21 |
| | RSC | | 107.91 ± 11.88 | 81.02 | 134.79 | -20.00 ± 19.66 |
| | Sham | | 92.42 ± 12.08 | 65.83 | 119.00 | |
| | RSham | | 127.91 ± 15.99 | 91.03 | 164.78 | |
| | mTBI | 7 | 85.27 ± 11.00 | 61.05 | 109.48 | -17.57 ± 15.66 |
| | RSC | | 88.34 ± 15.4 | 54.44 | 122.23 | -25.12 ± 21.93 |
| | Sham | | 102.84 ± 11.15 | 78.30 | 127.38 | |
| | RSham | | 113.46 ± 15.58 | 78.75 | 148.16 | |
| CA1 *ANOVA* (p=0.292) | mTBI | 3 | 116.36 ± 13.32 | 87.04 | 145.68 | 30.91 ± 19.05 |
| | RSC | | 101.12 ± 17.11 | 62.41 | 139.83 | -23.40 ± 26.91 |
| | Sham | | 85.45 ± 13.62 | 55.47 | 115.42 | |
| | RSham | | 124.52 ± 21.07 | 75.94 | 173.10 | |
| | mTBI | 7 | 78.86 ± 11.83 | 52.83 | 104.90 | -27.37 ± 19.34 |
| | RSC | | 87.32 ± 15.81 | 52.52 | 122.12 | -32.60 ± 22.85 |
| | Sham | | 87.32 ± 15.81 | 72.55 | 139.92 | |
| | RSham | | 119.92 ± 16.5 | 83.16 | 156.68 | |
| CA3 ANOVA (p=0.734) | mTBI | 3 | 81.91 ± 10.97 | 57.76 | 106.06 | 15.47 ± 15.39 |
| | RSC | | 88.2 ± 18.72 | 45.02 | 131.37 | 3.22 ± 22.91 |
| | Sham | | 66.44 ± 10.79 | 42.69 | 90.20 | |
| | RSham | | 84.98 ± 13.88 | 52.97 | 116.99 | |
| | mTBI | 7 | 65.34 ± 11.53 | 39.97 | 90.71 | 4.32 ± 14.64 |
| | RSC | | 70.05 ± 14.61 | 37.89 | 102.20 | -9.94 ± 19.62 |
| | Sham | | 61.02 ± 9.02 | 41.17 | 80.88 | |
| | RSham | | 79.99 ± 12.87 | 51.30 | 108.68 | |

Summary of cell count of positive GFAP immunoreactivity within the DG, CA1, and CA3 for impact recovery and their associated sham groups. For the mean differences ± SEM between injury and their associated sham groups, comparisons were based on recovery time (e.g., $mTBI_3$ vs. $Sham_3$, $RSC_3$ vs. $RSham_3$, $mTBI_7$ vs. $Sham_7$, and $RSC_7$ vs. $RSham_7$). The p-value obtained from ANOVA procedures is listed beneath each brain region title.

Results from GFAP immunostaining also indicated no significant differences between groups with respect to the number of GFAP positive cells/mm$^2$ (Figure 5.7). Moreover, positive cell count analysis of GFAP immunoreactivity did not indicate any injury group, regardless of recovery, to be statistically significant from sham (Figure 5.7). Therefore, the GFAP positive cell

count analysis showed no evidence of increased astrogliosis in the hippocampus for DG, CA1, or CA3 (Figure 5.7A-C).

The trends observed for GFAP positive cells/mm$^2$ analysis in CA1 were mimicked in results obtained for the DG and CA1 region with respect to recovery days between animal groups (Figure 5.7A-B). In the CA3 region, all 7-day recovery groups showed a decreasing trend in GFAP immunoreactivity compared to 3-day recovery groups (Figure 5.7C). Overall, the post hoc LSMeans Difference test indicated that, although insignificant, injury groups did not consistently show increased expression of astrogliosis compared to their associated shams (Table 5.8 and Figure 5.7).

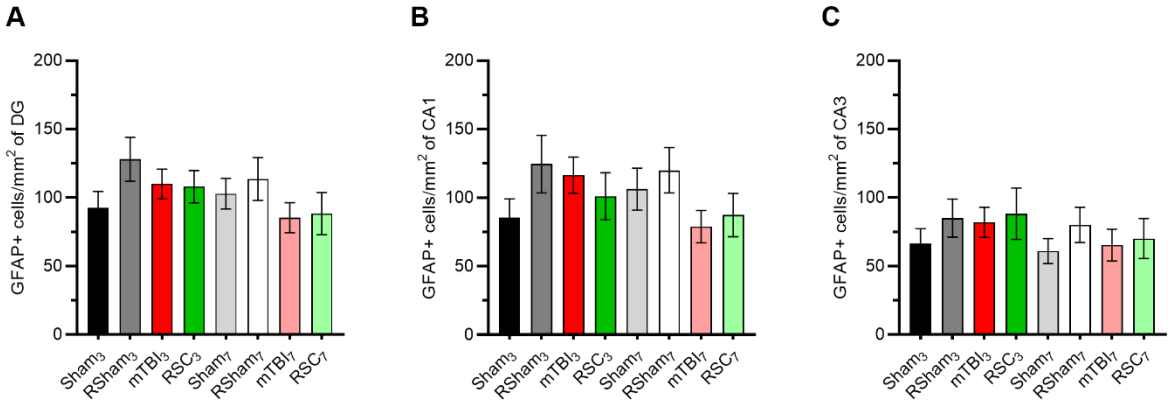


Figure 5.6 The number of positive GFAP cell counts/mm$^2$ for (A) DG, (B) CA1, and (C) CA3.

Comparison plots of the cell count of positive GFAP immunoreactivity (number of GFAP+ cells/mm2). Data are presented as mean ± SEM for recovery groups Sham$_3$, RSham$_3$, mTBI$_3$, RSC$_3$, Sham$_7$, RSham$_7$, mTBI$_7$, and RSC$_7$ in the (A) DG, (B) CA1, and (C) CA3.

Notably, the mean positive cells/mm$^2$ of GFAP immunoreactivity for mTBI groups show the greatest deviation from sham with a larger mean positive cells/mm$^2$ with respect to the CA1 and CA3 hippocampal regions after 3-days of recovery (Table 5.8). Conversely, RSC injury

groups show the greatest deviation from RSham with a smaller mean GFAP positive cells/$mm^2$ for the DG regions after a 3-day recovery and all hippocampal regions analyzed after 7-days of recovery (Table 5.8). Finally, mean GFAP positive cells/$mm^2$ analysis for the three hippocampal regions of interest yielded lower levels of positive GFAP immunoreactivity in the CA3 region (Figure 5.7C) than in the DG (Figure 5.7A) and CA1 (Figure 5.7B) regions.

Lastly, the trends observed for the GFAP positive cells/$mm^2$ analysis in all three hippocampal regions of interest were in agreeance with respect to recovery days between injury and sham, except within the CA3 region where $Sham_7$ showed a subtle decrease in GFAP immunoreactivity but not within the DG and CA1 regions(Figure 5.7A-C).

#### 5.3.3.3 Iba-1

Ionized calcium-binding adaptor molecule-1 (Iba-1) was used as an immunohistochemical marker for microglia. The number of positive cell counts/$mm^2$ was used to analyze the proportion of Iba-1 immunoreactivity within the DG, CA1, and CA3 regions for each group as a measure of microgliosis. Summary statistics for the Iba-1 positive cell counts/$mm^2$ measurements obtained for each region can be seen in Table 5.9. Representative micrographs for each region can be found in Appendix E.2.3.

Table 5.11 Iba-1 positive cell count/mm$^2$ summary.

| Brain Region | Group | Day of Recovery | Mean ± SEM | 95% CI | | Impact vs. Control Mean Diff ± SEM |
|---|---|---|---|---|---|---|
| | | | | Lower | Upper | |
| DG ANOVA (p=0.151) | mTBI | 3 | 186.66 ± 26.77 | 127.74 | 245.57 | 67.90 ± 38.90 |
| | RSC | | 194.60 ± 32.18 | 121.81 | 267.39 | 54.22 ± 46.99 |
| | Sham | | 118.76 ± 28.23 | 56.63 | 180.88 | |
| | RSham | | 140.38 ± 34.29 | 61.30 | 219.45 | |
| | mTBI | 7 | 145.43 ± 26.85 | 86.34 | 204.53 | -15.05 ± 39.13 |
| | RSC | | 96.60 ± 13.24 | 67.46 | 125.73 | -66.95 ± 22.02 |
| | Sham | | 160.48 ± 28.46 | 97.84 | 223.13 | |
| | RSham | | 163.55 ± 17.92 | 123.63 | 203.48 | |
| CA1 *Welch's ANOVA* (p=0.022) | mTBI | 3 | 164.83 ± 25.6 | 108.48 | 221.17 | 85.84 ± 29.06 |
| | RSC | | 187.2 ± 29.35 | 120.80 | 253.59 | 72.80 ± 32.84 |
| | Sham | | 78.99 ± 13.75 | 48.72 | 109.26 | |
| | RSham | | 114.40 ± 11.37 | 88.17 | 140.63 | |
| | mTBI | 7 | 115.75 ± 22.5 | 66.22 | 165.28 | -18.12 ± 34.17 |
| | RSC | | 100.79 ± 14.99 | 67.80 | 133.79 | -48.20 ± 23.45 |
| | Sham | | 133.87 ± 25.71 | 77.27 | 190.46 | |
| | RSham | | 148.99 ± 18.24 | 108.34 | 189.64 | |
| CA3 ANOVA (p=0.351) | mTBI | 3 | 162.42 ± 22.36 | 113.21 | 211.62 | 68.05 ± 31.73 |
| | RSC | | 160.59 ± 25.94 | 101.91 | 219.26 | 30.17 ± 39.89 |
| | Sham | | 94.37 ± 22.52 | 44.80 | 143.94 | |
| | RSham | | 130.42 ± 30.64 | 59.78 | 201.07 | |
| | mTBI | 7 | 108.70 ± 25.44 | 52.70 | 164.71 | -43.43 ± 42.203 |
| | RSC | | 114.59 ± 27.09 | 54.96 | 174.23 | -48.87 ± 33.852 |
| | Sham | | 152.13 ± 33.67 | 78.02 | 226.24 | |
| | RSham | | 163.46 ± 19.35 | 120.34 | 206.58 | |

Summary of cell count of positive Iba-1 immunoreactivity within the DG, CA1, and CA3 for impact recovery and their associated sham groups. For the mean differences ± SEM between injury and their associated sham groups, comparisons were based on recovery time (e.g., $mTBI_3$ vs. $Sham_3$, $RSC_3$ vs. $RSham_3$, $mTBI_7$ vs. $Sham_7$, and $RSC_7$ vs. $RSham_7$). The p-value obtained from ANOVA procedures is listed beneath each brain region title.

In contrast to the positive cell counts/mm$^2$ for GFAP (Table 5.8), analysis of the Iba-1 positive cell counts/mm$^2$ showed significant differences between recovery day groups for the DG and CA1 brain regions (Figure 5.8A-B) but not CA3 region (Figure 5.8C). Within the CA1 hippocampal regions, Fisher's LSD test results indicated a significant reduction in the number of Iba-1 positive cell counts/mm$^2$ for the repeated subconcussive injury group after 7-days of recovery compared to 3-days of recovery (p=0.006) (Figure 5.8B). Although insignificant,

similar trends are expressed for the RSC group after 7-DPI within the DG and CA3 regions (Figure 5.8A,C). Furthermore, results within the CA1 region also showed both injury groups expressing significantly more positive Iba-1 cell counts/$mm^2$ compared to their associated sham groups ($mTBI_3$ vs $Sham_3$: p=0.004; $RSC_3$ vs $RSham_3$: p=0.0294) (Figure 5.8B). However, it should be noted that the two injury groups were not statistically different from each other (p=0.467).

Results indicated that after 3-days of recovery, peak expression of positive Iba-1 cell counts/$mm^2$ was achieved for both injury groups in all three hippocampal regions of interest (Figure 5.8A-C). These results were unsurprising and agreed with other reports of increased inflammation of microglial marker expression 3-DPI (Sandhir et al., 2008; G. Wang et al., 2013). Within the 3-day recovery groups, the repeated SC impact group showed the highest hippocampal expression of positive Iba-1 cells/$mm^2$ within the DG (194.6 ± 32.18) and CA1 (187.2 ± 29.35) brain regions. Alternatively, the mTBI group displayed the greatest number of positive Iba-1 cells/$mm^2$ within the CA3 (162.42 ± 22.36) region after 3-DPI (Table 5.11). Mean positive cells/$mm^2$ of Iba-1 immunoreactivity at 7-DPI showed that the RSham group exhibited the highest hippocampal expression that was most apparent within DG (163.55 ± 17.92, Table 5.11).

Mean positive cells/$mm^2$ of Iba-1 immunoreactivity for the mTBI group showed the greatest deviation from Sham, with a larger mean positive cells/$mm^2$ with respect to all hippocampal regions after 3-days of recovery (Table 5.11). Alternatively, the RSC injury group shows the greatest deviation from RSham with a smaller mean Iba-1 positive cells/$mm^2$ for all hippocampal regions analyzed after 7-days of recovery (Table 5.11).

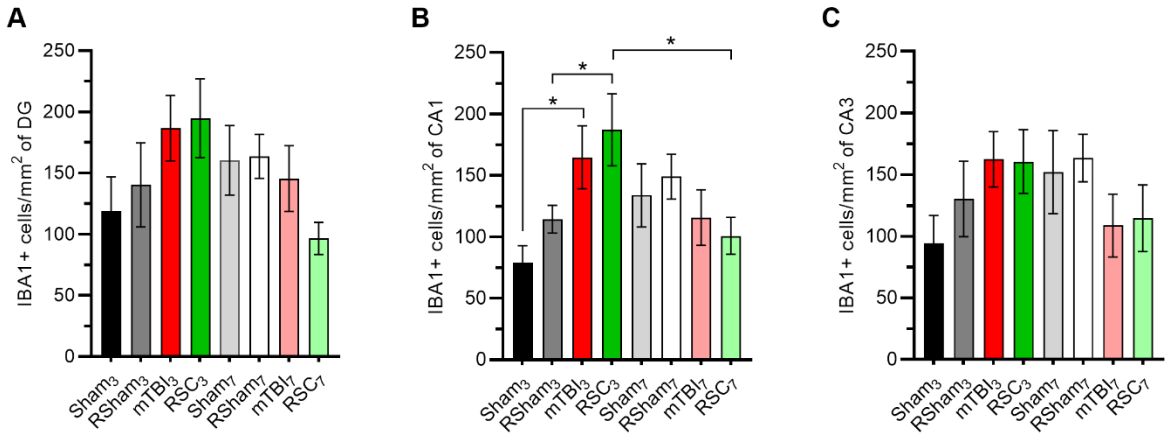


Figure 5.7 The number of positive Iba-1 cell counts/mm$^2$ for (A) DG, (B) CA1, and (C) CA3. Comparison plots of the cell count of positive Iba-1 immunoreactivity (number of Iba-1+ cells/mm2). Data are presented as mean ± SEM for recovery groups Sham$_3$, RSham$_3$, mTBI$_3$, RSC$_3$, Sham$_7$, RSham$_7$, mTBI$_7$, and RSC$_7$ in the (A) DG, (B) CA1, and (C) CA3.

Finally, the trends observed for the Iba-1 positive cells/mm$^2$ analysis in all three hippocampal regions of interest were in agreeance with respect to recovery days between experimental groups (Figure 5.8).

## 5.4 Discussion

A large body of literature, including several in-depth review articles, suggests that RSC head impacts over an extended period may cumulatively induce significant structural and functional changes to the brain (Bailes et al., 2013; Koerte et al., 2015; Mainwaring et al., 2018; Moore et al., 2017). Although there has been recent interest in the cumulative effects of subconcussive impacts (Rawlings et al., 2020), limited discovery has been performed to determine the pathophysiological consequences (Bree, Stratton, et al., 2020; Gangolli et al., 2019; Hiles-Murison et al., 2021; Lavender et al., 2020; Long, 2017; Sagarkar et al., 2017; Wilson, 2019). As such, the present study utilized, for the first time, a rat model to investigate

the comparative pathodynamics between a single concussive impact and RSC head impacts with subdivided cumulative energy of the single concussive impact extending over multiple time points.

### 5.4.1 Behavioral Alterations Due to Impact

In order to explore potential behavioral deficits following a single concussive and repeated SC impact, the open field (general locomotor activity and anxiety-like behavior) and rotarod (motor function) tests were utilized.

#### 5.4.1.1 General Locomotor Activity

In general, animals with head trauma will be less active and have lower ambulatory activity (Bree, Stratton, Levy 2020; Beitchman et al., 2020; Budde et al., 2013; Schwerin et al., 2017; L. Y. Yang et al., 2016). This is typically associated with decreased total distance traveled and movement time measurements assessed in the open field test. In the present study, injured rats were no different than shams at 3- and 7-days after injury on measures of locomotive activity in the open field (Figure 5.3). However, we did see a decrease in mobility upon recovery among the $mTBI_3$ animal group compared to baseline (Figure 5.3). This decrease in mobility could an indication of memory loss due to injury whereas group $Sham_3$ showed no signs of change in mobility following recovery. Future analysis exploring this hypothesis would be needed to confirm the previous statement.

In previous studies, deficits in locomotive activity following a single mTBI have been reported in rodent models up to 14-DPI (Bodnar et al., 2019; Bree & Levy, 2018; Fromm et al., 2004; Mychasiuk et al., 2014, 2015, 2016; Sharma et al., 2014). Alternatively, other rodent models of head trauma reported unaffected general locomotor activity utilizing the open field test

(Bodnar et al., 2019; Ritter et al., 2021; Washington et al., 2012; Shultz et al., 2011; Taib et al., 2017; Almeida-Suhett et al., 2014). Additionally, a finite number of studies have been done for repeated subconcussive injury models and their role in locomotor activity deficits (D Bree, Stratton, et al., 2020; Wilson, 2019; Gangolli et al., 2019).

#### 5.4.1.2 Anxiety-Like Behavior

Similarly seen with measurements of locomotive activity, evaluation of anxiety states by using the open field test did not show distinct differences in anxiety-like behavior between sham and injured rats. Interestingly, though, our results did show group $mTBI_3$ spending significantly less time in the center zone following impact compared to baseline measurements (Figure 5.4). Outside of individual variations within the $mTBI_3$ animal group's measurements at baseline, we are unsure of this change in behavior over time. Furthermore, even though the injury groups were not statistically significant from their associated sham groups, our data does indicate injury groups, on average, to be statistically different from each other with respect to time spent in the outer zone of the open field test (Tables 5.3-5.4). Thus, this is the study's first evidence of pathodynamic differences resulting from a single impact of an mTBI and repeated SC impacts with subdivided cumulative kinetic energies (KEs) equal to the single mTBI impact.

Although our results following the single concussive group do not replicate the majority of literature (D Bree, Mackenzie, et al., 2020; Sagarkar et al., 2017; Beitchman et al., 2020; Almeida-Suhett et al., 2014; Namjoshi et al., 2017; Kosari-Nasab et al., 2019; Meyer et al., 2012), they do agree with other reports of insignificant evidence of anxious-like behavior compared to sham observed up to 7-days following a single mTBI (Taib et al., 2017; Beitchman et al., 2020; Nichols et al., 2016). Furthermore, a limited number of studies have investigated evidence of anxious-like behavior due to repeated subconcussive injury models (Sagarkar et al,

2017; Gangolli et al., 2019; Wilson, 2019). Among these, two experiments report no differences in anxiety-related behavior in rats receiving repetitive subconcussive injuries compared to shams (Gangolli et al., 2019; Wilson, 2019). Thus, our results in the RSC group do replicate the majority of those reported in the literature.

#### 5.4.1.3 Motor Coordination

Our study employed the rotarod test as a proxy of motor function and coordination. We observed that neither injury groups led to significant motor deficits. As previously examined in Chapter IV's discussion (see 4.4.1.3), the effects of mild TBI on neuromotor function in rodents are inconsistent in terms of impact intensity (Namjoshi et al., 2017; Sauerbeck et al., 2018). Alternatively, our findings agree with the majority of preclinical models of repeated SC injuries reveal a lack of neuromotor impairment (Hiles-Murison et al., 2021; Wilson, 2019).

Our present and previous (see Chapter IV) models of a mild TBI could be too benign to show deficits in the less-sensitive task used to assess motor coordination which is typically used in mild head injury models. It is also possible that the rotarod test is not a completely effective means of studying motor coordination post-concussion. There are separate motor coordination tasks such as the foot fault test and balance beam task that could be used in future studies to try to better assess motor coordination following a single mild head injury. Overall, this study's investigative model of a single concussion and repeated subconcussive injuries was insufficient to produce short-term behavioral deficits at 3- and 7-DPI.

### 5.4.2 Role of Neuroinflammation

As seen in many cases of an mTBI, the injury may result in damaged neurons, neuronal death, axonal injury, disruption to the blood-brain barrier, and other changes in the extracellular

space, such as ionic fluctuations, that are detected by, and activate, microglia (Eyolfson et al., 2020; Sofroniew & Vinters, 2010; Wofford et al., 2019; Yi & Hazell, 2006). Upon activation, microglia undergo a morphological change, taking on an amoeboid shape, and scavenge the central nervous system producing and releasing pro-inflammatory cytokines, chemokines, and free radicals (Kumar & Brain, 2012; Chiu et al., 2016; Aihara et al., 2009). As activated microglia congregate to the injury sites, clearance of cellular debris (i.e., broken myelin or cellular membranes) and toxic substances become the main role of these cells, known as phagocytosis (Chiu et al., 2016). Similarly, astrocytes are also involved in neuroinflammation, undergoing a morphological change known as reactive astrogliosis that involves cellular hypertrophy, lengthened processes, increased expression of GFAP, and the production/release of pro-inflammatory mediators (Sofroniew & Vinters, 2010; Zhang et al., 2010).

In the present study, we evaluated evidence of neuronal loss and neuroinflammation up to 7-days following a single mTBI and repeated SC impacts. To assess evidence of neuronal loss and neuroinflammation occurring at an early stage following trauma, a marker of mature neurons (NeuN), reactive astrocytes (GFAP), and microglia (Iba-1) was employed. All three immunohistochemical tissue stains (NeuN, GFAP, and Iba-1) were quantitatively assessed through the analysis of the positive cell counts of immunoreactivity within the DG, CA1, and CA3 subregions of the hippocampus.

Results indicated that the number of NeuN positive cells/$mm^2$ for both injury groups, mTBI and RSC, following a 3- and 7-day recovery period, was approximately equal to their associated sham groups for all three investigated brain regions indicating no evidence of neuronal loss (Figure 5.6). Thus, these findings suggest that the investigative impact loads do not lead to neuronal loss within the hippocampus at a subacute timeframe. Moreover, because the

mTBI load magnitude investigated in the present study is within the lower end range found in literature for rat CHI models that employed WDI devices (see Chapter 3's Discussion Section), our discovery of the absence of neuronal loss was somewhat expected. Likewise, previous work from DeFord et al. (2002) showed similarly following a single episode of an mTBI (0.589 J), repeated mild injury (cumulative input energy of 2.35 J) was associated with impairments in spatial learning and cognition (Morris water maze) in mice despite the absence of observed cell death in the cortex and hippocampus.

Our histological results also indicated that the number of GFAP positive cells/$mm^2$ for both injury groups, mTBI and RSC, following a 3- and 7-day recovery, was approximately equal to that of their sham groups for all three brain regions indicating no evidence of astrogliosis (Figure 5.7). This finding is paralleled by the work of Singh et al. (2016), who showed that following a single mTBI (1.1 J) using a WDI device, GFAP+ cells were significantly increased at 3- and 5-days following impact in the cortical gray matter but not in the hippocampus or corpus callosum regions as compared to shams. It is hypothesized that the reason the injury groups do not show a significant difference in GFAP immunoreactivity compared to their associated shams is perhaps that the significant influx of reactive astrocytes, often recruited by microglial cells (Liu et al., 2011; Jha et al., 2019), occurs at an alternative or later recovery time point as similarly seen in Y. C. Chen et al. (2014). Using a controlled cortical impact (CCI) to induce an mTBI on a murine model, a significant increase in GFAP expression occurred 8-days following injury in the hippocampus & cortex brain regions compared to sham (Y. C. Chen et al., 2014). Furthermore, it has been suggested by Eyolfson et al. (2020) that microglial are thought to be the first responders to injury, followed by astrocytes, thereafter.

As with the GFAP analysis results, neither injury group, regardless of recovery day, revealed a significant difference from their associated sham group with respect to Iba-1 immunoreactivity within the DG and CA3 brain regions (Figure 5.8A, C). However, our data indicated that following a 3-day recovery period, both mTBI and RSC injury groups revealed a significant increase in microgliosis in tandem with minimal evidence of astrogliosis. After 7-days of recovery, histological findings showed a significant decrease in microgliosis from the RSC group compared to its 3-day recovery group within CA1 region (Figure 5.8B). It is speculated that following this reducing shift in activated microglia cells, at a recovery time point not investigated in the present study, astrocytes may subsequently become reactive and assemble at the site of injury to aid in neurogenesis, synaptogenesis, and glial scar formation following neurotrauma (Zhou et al., 2020).

## 5.5 Conclusion

We aimed to investigate the pathodynamic differences between a single mTBI and repeated subconcussive impacts with subdivided cumulative KEs equal to the single mTBI impact using a rat model. For this investigation, a weight drop injury platform was employed to model a surgery-free, closed-head injury in rats. We utilized two impact magnitudes for investigation, 1.0 J for the single, mild TBI group and 0.33 J for the repeated subconcussive injury group for a total of 3 impacts with an inter-injury of 24 hrs (3 x 0.33 J ≈ 1.0 J). According to literature, a single head impact around this magnitude (1.0 J) can induce subacute behavior alterations (Bree, Mackenzie, et al., 2020) and neuroinflammation (Fraunberger et al., 2020; Singh et al., 2016) in a rodent model. Thus, we anticipated our mTBI model would result in transient evidence of behavioral dysfunction and neuroinflammation. Alternatively, for the repeated SC injury model, since this is the first report of its kind using a rat model, the

behavioral and histological outcomes were predicted to subtlety echo that of the mTBI pathodynamics.

To this end, although there was no significant difference between injury and sham groups with respect to behavioral disturbances, we identified one significant difference between the injury groups with respect to behavioral outcomes. On average, a significant increase in anxious-like behavior was seen in the RSC animal group compared to the single mTBI group after 7-days of recovery. Thus, directed investigations into the specifics of this unique phenomenon would greatly add to our understanding of functional disturbances resulting from the two injury groups. Alternatively, from an neuroinflammatory perspective, both mTBI and RSC injury groups led to extensive microgliosis in the gray matter following 3-days post-impact.

Overall, the present study revealed important aspects of the cumulative effects of SC injuries. This work does not provide evidence in support of the notion that, upon recovery, repeated subconcussive impacts do result in behavioral disturbances, that do not manifest following a single mTBI of the same energy input. Therefore, as demonstrated, the repetitive occurrence of low-level impacts, with a 0.33 J impact load and an inter-injury interval of 24 hrs for a total of 3 impacts, do not lead to deleterious behavioral deficits following a 3- and 7- day recovery period. However, RSC impacts do lead to neuroinflammation as early as 3-days post-final impact, as similarly seen in the mTBI impact group.

Although a cumulative injury threshold for subconcussive impacts was not evident in the current investigation, there still may be a threshold at which no pathodynamic shift occurs. Future investigations would be necessary to explore evidence of a cumulative threshold. The importance of this cannot be understated. Not only could this data inform low-level injury

mitigation strategies, but it would directly affect treatment targets and the development of therapeutic interventions.

One limitation of this study was the inability to histologically assess the corpus callosum pathology, part of the white matter structure within the cerebral tissue, due to inconsistent hemisphere cutting following extraction of the tissue. This limitation prevented analysis of a white matter damage due to injury and restricted analysis to deeper gray matter parenchymal structures. Because there was limited evidence of inflammatory markers within the gray matter hippocampal regions of the cerebral tissue, it would be beneficial to analyze a commonly explored white matter region, such as the corpus callosum, where tracts of myelinated axons reside.

Another constraint of this study was the limited recovery times explored. Due to financial reasons, only two subacute recovery times were explored to investigate behavioral dysfunction and inflammatory analysis. This may explain why there was no evidence of a significant increase in positive GFAP cells/$mm^2$ within the hippocampal regions. Understanding these limitations will allow researchers to advance basic experimental properties, in an effort to produce findings that have greater clinical relevance.

Future investigations would aim to address the current limitations and improve or expand our current findings. For example, although 3- and 7-days recovery times are typically associated with systematic perturbations following head injury (Bree, Stratton, et al., 2020; Ekmark-Lewén et al., 2013; Fraunberger et al., 2020; Hsieh et al., 2017; Marschner et al., 2019; Singh et al., 2016), we did not see evidence of increased astrogliosis following our injury profiles. One hypothesis is that the significant influx of reactive astrocytes might occur at a recovery time point not currently investigated. Perhaps an increase in astrogliosis for a single mTBI impact,

with a 1.0 J impact load, and repeated SC impacts, with a 0.33 J impact load with an inter-injury interval of 24 hrs for a total of 3 impacts, occurs at an alternative recovery time point, e.g. 0.5-, 1-, 10-, 14-, 21-, or 30-days. Adding acute (0-24 hours), subacute (1-14 days), and long-term (> 14 days) recovery time points would provide further insight into understanding the neuropathological response following concussive and subconcussive injuries of the same cumulative impact magnitude. Alternatively, it could be because the total impact magnitude (~1.0 J) was too benign to cause an increase in reactive astrocytes. Targeted investigations would need to be explored to confirm these hypotheses. Additionally, the inclusion of cytokine and chemokine analysis would also expand our understanding of neuroinflammatory signaling dynamics.

Moreover, including neuronal degeneration analysis would shed light on our current findings. Our histological results showed no evidence of neuronal loss due to injury. However, there was evidence of increased microgliosis within the gray matter, namely the CA1 hippocampal region, following a single mTBI and repeated SC injury. This increased number of Iba-1 cells/$mm^2$ observed in both injury groups may imply disruption of neurons. Thus, it may be interesting to include histological analysis of neuronal degeneration to further complement our inflammatory findings.

Furthermore, the addition of behavioral assays traditionally associated with motor coordination such as the balance beam test and foot fault test would be beneficial in growing our understanding of the current behavioral findings. These would provide additional assays that might be more sensitive to a single mild TBI impact.

REFERENCES


Abd-Elfattah Foda, M. A., & Marmarou, A. (1994). A new model of diffuse brain injury in rats. Part II: Morphological characterization. *Journal of Neurosurgery*, *80*(2), 301–313. https://doi.org/10.3171/jns.1994.80.2.0301

Abdelhak, A., Foschi, M., Abu-Rumeileh, S., Yue, J. K., D'Anna, L., Huss, A., Oeckl, P., Ludolph, A. C., Kuhle, J., Petzold, A., Manley, G. T., Green, A. J., Otto, M., & Tumani, H. (2022). Blood GFAP as an emerging biomarker in brain and spinal cord disorders. *Nature Reviews Neurology 2022*, 1–15. https://doi.org/10.1038/s41582-021-00616-3

Abrahams, P. (2016). *How the brain works.* . Amber Books Ltd. https://books.google.com/books?hl=en&lr=&id=bv_LDwAAQBAJ&oi=fnd&pg=PT13&dq=how+the+brain+works+understainding+brain+function+thought+and+personality+professor+peter+abrahams&ots=ZO8lZGwc7v&sig=q6Zcbh3ZD8z3YJ7l3LLvND4b6Nw#v=onepage&q=how the brain works understainding brain function thought and personality professor peter abrahams&f=false

Aihara, N., Hall, J. J., Pitts, L. H., Fukuda, K., & Noble, L. J. (2009). Altered Immunoexpression of Microglia and Macrophages after Mild Head Injury. *Https://Home.Liebertpub.Com/Neu*, *12*(1), 53–63. https://doi.org/10.1089/NEU.1995.12.53

Albert-Weissenberger, C., & Sirén, A. L. (2010). Experimental traumatic brain injury. *Experimental & Translational Stroke Medicine*, *2*(1), 16. https://doi.org/10.1186/2040-7378-2-16

Alder, J., Fujioka, W., Lifshitz, J., Crockett, D. P., & Thakker-Varia, S. (2011). Lateral Fluid Percussion: Model of Traumatic Brain Injury in Mice. *Journal of Visualized Experiments*, *54*, 3063. https://doi.org/10.3791/3063

Alekseeva, O. S., Kirik, O. V., Gilerovich, E. G., & Korzhevskii, D. E. (2019). Microglia of the Brain: Origin, Structure, Functions. *Journal of Evolutionary Biochemistry and Physiology*, *55*(4), 257–268. https://doi.org/10.1134/s002209301904001x

Almeida-Suhett, C. P., Prager, E. M., Pidoplichko, V., Figueiredo, T. H., Marini, A. M., Li, Z., Eiden, L. E., & Braga, M. F. M. (2014). Reduced GABAergic inhibition in the basolateral amygdala and the development of anxiety-like behaviors after mild traumatic brain injury. *PLoS ONE*, *9*(7). https://doi.org/10.1371/journal.pone.0102627

Anderson, T., Heitger, M., & Macleod, S. (2006). Concussion and mild head injury. *Practical Neurology*, *6*(6), 342–357. https://doi.org/10.1136/jnnp.2006.106583

Argente-Arizón, P., Freire-Regatillo, A., Argente, J., & Chowen, J. A. (2015). Role of non-neuronal cells in body weight and appetite control. In *Frontiers in Endocrinology* (Vol. 6, Issue MAR, p. 42). Frontiers Media S.A. https://doi.org/10.3389/fendo.2015.00042

Armstrong, C. L., & Morrow, L. A. (2019). Handbook of medical neuropsychology: Applications of cognitive neuroscience, second edition. In C. L. Armstrong & L. A. Morrow (Eds.), *Handbook of Medical Neuropsychology: Applications of Cognitive Neuroscience, Second Edition*. Springer International Publishing. https://doi.org/10.1007/978-3-030-14895-9

Azevedo, F. A. C., Carvalho, L. R. B., Grinberg, L. T., Farfel, J. M., Ferretti, R. E. L., Leite, R. E. P., Filho, W. J., Lent, R., & Herculano-Houzel, S. (2009). Equal numbers of neuronal and nonneuronal cells make the human brain an isometrically scaled-up primate brain. *The Journal of Comparative Neurology*, *513*(5), 532–541. https://doi.org/10.1002/cne.21974

Bailes, J. E., Petraglia, A. L., Omalu, B. I., Nauman, E., & Talavage, T. (2013). Role of subconcussion in repetitive mild traumatic brain injury. *Journal of Neurosurgery*, *119*(5), 1235–1245. https://doi.org/10.3171/2013.7.JNS121822

Bao, F., Shultz, S. R., Hepburn, J. D., Omana, V., Weaver, L. C., Cain, D. P., & Brown, A. (2012). A CD11d monoclonal antibody treatment reduces tissue injury and improves neurological outcome after fluid percussion brain injury in rats. *Journal of Neurotrauma*, *29*(14), 2375–2392. https://doi.org/10.1089/NEU.2012.2408

Baugh, C. M., Stamm, J. M., Riley, D. O., Gavett, B. E., Shenton, M. E., Lin, A., Nowinski, C. J., Cantu, R. C., McKee, A. C., & Stern, R. A. (2012). Chronic traumatic encephalopathy: Neurodegeneration following repetitive concussive and subconcussive brain trauma. *Brain Imaging and Behavior*, *6*(2), 244–254. https://doi.org/10.1007/s11682-012-9164-5

Bayly, P. V., Taber, L. A., & Kroenke, C. D. (2014). Mechanical forces in cerebral cortical folding: A review of measurements and models. *Journal of the Mechanical Behavior of Biomedical Materials*, *29*, 568–581. https://doi.org/10.1016/j.jmbbm.2013.02.018

Bazarian, J. J., Zhu, T., Blyth, B., Borrino, A., & Zhong, J. (2012). Subject-specific changes in brain white matter on diffusion tensor imaging after sports-related concussion. *Magnetic Resonance Imaging*, *30*(2), 171–180. https://doi.org/10.1016/j.mri.2011.10.001

Beitchman, J. A., Griffiths, D. R., Hur, Y., Ogle, S. B., Bromberg, C. E., Morrison, H. W., Lifshitz, J., Adelson, P. D., & Thomas, T. C. (2020). Experimental Traumatic Brain Injury Induces Chronic Glutamatergic Dysfunction in Amygdala Circuitry Known to Regulate Anxiety-Like Behavior. *Frontiers in Neuroscience*, *0*, 1434. https://doi.org/10.3389/FNINS.2019.01434

Bell-Temin, H., Culver-Cochran, A. E., Chaput, D., Carlson, C. M., Kuehl, M., Burkhardt, B. R., Bickford, P. C., Liu, B., & Stevens Jr, S. M. (2015). Novel Molecular Insights into Classical and Alternative Activation States of Microglia as Revealed by Stable Isotope Labeling by Amino Acids in Cell Culture (SILAC)-based Proteomics* □ S. *Molecular & Cellular Proteomics*, *14*, 3173–3184. https://doi.org/10.1074/mcp

Bennett, M. R., & Lagopoulos, J. (2014). Stress and trauma: BDNF control of dendritic-spine formation and regression. In *Progress in Neurobiology* (Vol. 112, pp. 80–99). Elsevier Ltd. https://doi.org/10.1016/j.pneurobio.2013.10.005

Blennow, K., Hardy, J., & Zetterberg, H. (2012). The Neuropathology and Neurobiology of Traumatic Brain Injury. *Neuron*, *76*(5), 886–899. https://doi.org/10.1016/J.NEURON.2012.11.021

Block, M., Zecca, L., Hong, J., & Block, M. L. (2007). Microglia-mediated neurotoxicity: uncovering the molecular mechanisms. *Nature Reviews Neuroscience*, *8*(1), 57–69. https://doi.org/10.1038/nrn2038

Blyth, B. J., & Bazarian, J. J. (2010). Traumatic Alterations in Consciousness: Traumatic Brain Injury. In *Emergency Medicine Clinics of North America* (Vol. 28, Issue 3, pp. 571–594). W.B. Saunders. https://doi.org/10.1016/j.emc.2010.03.003

Bodnar, C. N., Roberts, K. N., Higgins, E. K., & Bachstetter, A. D. (2019). A Systematic Review of Closed Head Injury Models of Mild Traumatic Brain Injury in Mice and Rats. In *Journal of Neurotrauma* (Vol. 36, Issue 11, pp. 1683–1706). Mary Ann Liebert Inc. https://doi.org/10.1089/neu.2018.6127

Bogoslovsky, T., Wilson, D., Chen, Y., Hanlon, D., Gill, J., Jeromin, A., Song, L., Moore, C., Gong, Y., Kenney, K., & Diaz-Arrastia, R. (2017). Increases of Plasma Levels of Glial Fibrillary Acidic Protein, Tau, and Amyloid β up to 90 Days after Traumatic Brain Injury. *Https://Home.Liebertpub.Com/Neu*, *34*(1), 66–73. https://doi.org/10.1089/NEU.2015.4333

Bolouri, H., & Zetterberg, H. (2015). Animal Models for Concussion: Molecular and Cognitive Assessments—Relevance to Sport and Military Concussions. In: Kobeissy FH, editor. Brain Neurotrauma: Molecular, Neuropsychological, and Rehabilitation Aspects. In F. Kobeissy (Ed.), *Kobeissy FH, editor. Brain Neurotrauma: Molecular, Neuropsychological, and Rehabilitation Aspects.* CRC Press/Taylor & Francis. https://www.ncbi.nlm.nih.gov/books/NBK299196/

Bolton, A. N., & Saatman, K. E. (2014). Regional neurodegeneration and gliosis are amplified by mild traumatic brain injury repeated at 24-hour intervals. *Journal of Neuropathology and Experimental Neurology*, *73*(10), 933–947. https://doi.org/10.1097/NEN.0000000000000115

Bondi, C. O., Semple, B. D., Noble-Haeusslein, L. J., Osier, N. D., Carlson, S. W., Dixon, C. E., Giza, C. C., & Kline, A. E. (2015). Found in translation: Understanding the biology and behavior of experimental traumatic brain injury. In *Neuroscience and Biobehavioral Reviews* (Vol. 58, pp. 123–146). Elsevier Ltd. https://doi.org/10.1016/j.neubiorev.2014.12.004

Bree, D., & Levy, D. (2018). Development of CGRP-dependent pain and headache related behaviours in a rat model of concussion: Implications for mechanisms of post-traumatic headache. *Cephalalgia*, *38*(2), 246–258. https://doi.org/10.1177/0333102416681571

Bree, Mackenzie, Stratton, & Levy. (2020). Enhanced post-traumatic headache-like behaviors and diminished contribution of peripheral CGRP in female rats following a mild closed head injury. *Cephalalgia*. https://doi.org/10.1177/0333102420907597

Bree, Stratton, & Levy. (2020). Increased severity of closed head injury or repetitive subconcussive head impacts enhances post-traumatic headache-like behaviors in a rat model. *Cephalalgia*. https://doi.org/10.1177/0333102420937664

Breedlove, E. L., Robinson, M., Talavage, T. M., Morigaki, K. E., Yoruk, U., O'Keefe, K., King, J., Leverenz, L. J., Gilger, J. W., & Nauman, E. A. (2012). Biomechanical correlates of symptomatic and asymptomatic neurophysiological impairment in high school football. *Journal of Biomechanics*, *45*(7), 1265–1272. https://doi.org/10.1016/J.JBIOMECH.2012.01.034

Breedlove, K. M., Breedlove, E. L., Robinson, M., Poole, V. N., King, J. R., Rosenberger, P., Rasmussen, M., Talavage, T. M., Leverenz, L. J., & Nauman, E. A. (2014). Detecting Neurocognitive and Neurophysiological Changes as a Result of Subconcussive Blows Among High School Football Athletes. *Athletic Training & Sports Health Care*, *6*(3), 119–127. https://doi.org/10.3928/19425864-20140507-02

Briones, T. L., Woods, J., & Rogozinska, M. (2014). Decreased neuroinflammation and increased brain energy homeostasis following environmental enrichment after mild traumatic brain injury is associated with improvement in cognitive function. *Acta Neuropathologica Communications*, *2*(1), 1–10. https://doi.org/10.1186/2051-5960-1-57/FIGURES/4

Broglio, S. P., Eckner, J. T., Paulson, H. L., & Kutcher, J. S. (2012). Cognitive decline and aging: The role of concussive and subconcussive impacts. *Exercise and Sport Sciences Reviews*, *40*(3), 138–144. https://doi.org/10.1097/JES.0b013e3182524273

Brooks, D. M., Patel, S. A., Wohlgehagen, E. D., Semmens, E. O., Pearce, A., Sorich, E. A., & Rau, T. F. (2017). Multiple mild traumatic brain injury in the rat produces persistent pathological alterations in the brain. *Experimental Neurology*, *297*, 62–72. https://doi.org/10.1016/j.expneurol.2017.07.015

Broussard, J. I., Acion, L., De Jesús-Cortés, H., Yin, T., Britt, J. K., Salas, R., Costa-Mattioli, M., Robertson, C., Pieper, A. A., Arciniegas, D. B., & Jorge, R. (2018). Repeated mild traumatic brain injury produces neuroinflammation, anxiety-like behaviour and impaired spatial memory in mice. *Brain Injury*, *32*(1), 113–122. https://doi.org/10.1080/02699052.2017.1380228

Budde, M. D., Shah, A., McCrea, M., Cullinan, W. E., Pintar, F. A., & Stemper, B. D. (2013). Primary Blast Traumatic Brain Injury in the Rat: Relating Diffusion Tensor Imaging and Behavior. *Frontiers in Neurology*, *4*. https://doi.org/10.3389/FNEUR.2013.00154

Budson Andrew E., McKee Ann C , Cantu Robert C., S. R. A. (2017). *Chronic Traumatic Encephalopathy: Proceedings of the Boston University Alzheimer's Disease Center Conference* (1st ed.). Elsevier.

Burda, J. E., Bernstein, A. M., & Sofroniew, M. V. (2016). Astrocyte roles in traumatic brain injury. In *Experimental Neurology* (Vol. 275, pp. 305–315). Academic Press Inc. https://doi.org/10.1016/j.expneurol.2015.03.020

Centers for Disease Control and Prevention (CDC), N. C. for I. P. and C. (2003). *Report to Congress on Mild Traumatic Brain Injury in the United States: Steps to Prevent a Serious Public Health Problem*. https://stacks.cdc.gov/view/cdc/6544

Chen, H., Desai, A., & Kim, H.-Y. (2017). Repetitive Closed-Head Impact Model of Engineered Rotational Acceleration Induces Long-Term Cognitive Impairments with Persistent Astrogliosis and Microgliosis in Mice. *Journal of Neurotrauma*, *34*(14), 2291–2302. https://doi.org/10.1089/neu.2016.4870

Chen, Y. C., Mao, H., Yang, K. H., Abel, T., & Meaney, D. F. (2014). A modified controlled cortical impact technique to model mild traumatic brain injury mechanics in mice. *Frontiers in Neurology*, *5 JUN*, 100. https://doi.org/10.3389/FNEUR.2014.00100/ABSTRACT

Chitturi, J., Li, Y., Santhakumar, V., & Kannurpatti, S. S. (2019). Consolidated biochemical profile of subacute stage traumatic brain injury in early development. *Frontiers in Neuroscience*, *13*(MAY). https://doi.org/10.3389/fnins.2019.00431

Chiu, C. C., Liao, Y. E., Yang, L. Y., Wang, J. Y., Tweedie, D., Karnati, H. K., Greig, N. H., & Wang, J. Y. (2016). Neuroinflammation in animal models of traumatic brain injury. In *Journal of Neuroscience Methods* (Vol. 272, pp. 38–49). Elsevier B.V. https://doi.org/10.1016/j.jneumeth.2016.06.018

Christie, B. R., Trivino-Paredes, J., Pinar, C., Neale, K. J., Meconi, A., Reid, H., & Hutton, C. P. (2019). A Rapid Neurological Assessment Protocol for Repeated Mild Traumatic Brain Injury in Awake Rats. *Current Protocols in Neuroscience*, *89*(1). https://doi.org/10.1002/cpns.80

Chung, W. S., Allen, N. J., & Eroglu, C. (2015). Astrocytes Control Synapse Formation, Function, and Elimination. *Cold Spring Harbor Perspectives in Biology*, *7*(9), a020370. https://doi.org/10.1101/CSHPERSPECT.A020370

Clark, R. S., Schiding, J. K., Kaczorowski, S. L., Marion, D. W., & Kochanek, P. M. (1994). Neutrophil accumulation after traumatic brain injury in rats: comparison of weight drop and controlled cortical impact models. *Journal of Neurotrauma*, *11*(5), 499–506.

Clark, D. P. Q., Perreau, V. M., Shultz, S. R., Brady, R. D., Lei, E., Dixit, S., Taylor, J. M., Beart, P. M., & Boon, W. C. (2019). Inflammation in Traumatic Brain Injury: Roles for Toxic A1 Astrocytes and Microglial–Astrocytic Crosstalk. *Neurochemical Research*, *44*(6), 1410–1424. https://doi.org/10.1007/S11064-019-02721-8

Cole, J. T., Yarnell, A., Kean, W. S., Gold, E., Lewis, B., Ren, M., McMullen, D. C., Jacobowitz, D. M., Pollard, H. B., O'Neill, J. T., Grunberg, N. E., Dalgard, C. L., Frank, J. A., & Watson, W. D. (2011). Craniotomy: True sham for traumatic brain injury, or a sham of a sham? *Journal of Neurotrauma*, *28*(3), 359–369. https://doi.org/10.1089/neu.2010.1427

Collins-Praino, L. E., Arulsamy, A., Katharesan, V., & Corrigan, F. (2018). The effect of an acute systemic inflammatory insult on the chronic effects of a single mild traumatic brain injury. *Behavioural Brain Research*, *336*(August 2017), 22–31. https://doi.org/10.1016/j.bbr.2017.08.035

Danbolt, N. C. (2001). Glutamate uptake. In *Progress in Neurobiology* (Vol. 65, Issue 1, pp. 1–105). Pergamon. https://doi.org/10.1016/S0301-0082(00)00067-8

Dashnaw, M., Petraglia, A., & Bailes, J. (2012). An overview of the basic science of concussion and subconcussion: where we are and where we are going. *Neurosurg. Focus*, *33*, 1–9. https://doi.org/10.3171/2012.10.FOCUS12284

DeFord, S. M., Wilson, M. S., Rice, A. C., Clausen, T., Rice, L. K., Barabnova, A., Bullock, R., & Hamm, R. J. (2002). Repeated mild brain injuries result in cognitive impairment in B6C3F1 mice. *Journal of Neurotrauma*, *19*(4), 427–438. https://doi.org/10.1089/08977150252932389

Dixon, C., Clifton, G., Lighthall, J., Yaghmai, A., & Hayes, R. (1991). A controlled cortical impact model of traumatic brain injury in the rat. *Journal of Neuroscience Methods*, *39*(3), 253–262. https://doi.org/10.1016/0165-0270(91)90104-8

Ekmark-Lewén, S., Flygt, J., Kiwanuka, O., Meyerson, B. J., Lewén, A., Hillered, L., & Marklund, N. (2013). Traumatic axonal injury in the mouse is accompanied by a dynamic inflammatory response, astroglial reactivity and complex behavioral changes. *Journal of Neuroinflammation*, *10*(1), 1–19. https://doi.org/10.1186/1742-2094-10-44/FIGURES/9

Ellis, H., & Mahadevan, V. (2014). The surgical anatomy of the scalp. In *Surgery (United Kingdom)* (Vol. 32, Issue SUPPL. 1, pp. e1–e5). Elsevier BV. https://doi.org/10.1016/j.mpsur.2013.04.024

Eme, R. (2017). Neurobehavioral Outcomes of Mild Traumatic Brain Injury: A Mini Review. *Brain Sciences 2017, Vol. 7, Page 46*, *7*(5), 46. https://doi.org/10.3390/BRAINSCI7050046

Emery, C. A., Barlow, K. M., Brooks, B. L., Max, J. E., Villavicencio-Requis, A., Gnanakumar, V., Robertson, H. L., Schneider, K., & Yeates, K. O. (2016). A systematic review of psychiatric, psychological, and behavioural outcomes following mild traumatic brain injury in children and adolescents. *Canadian Journal of Psychiatry*, *61*(5), 259–269. https://doi.org/10.1177/0706743716643741

Eyolfson, E., Khan, A., Mychasiuk, R., & Lohman, A. W. (2020). Microglia dynamics in adolescent traumatic brain injury. *Journal of Neuroinflammation 2020 17:1*, *17*(1), 1–19. https://doi.org/10.1186/S12974-020-01994-Z

Faden, A. I., Wu, J., Stoica, B. A., & Loane, D. J. (2016). Progressive inflammation-mediated neurodegeneration after traumatic brain or spinal cord injury. *British Journal of Pharmacology*, *173*(4), 681–691. https://doi.org/10.1111/BPH.13179

Faul, M., Xu, L., Wald, M. M., & Coronado, V. G. (2010). Traumatic brain injury in the United States: emergency department visits, hospitalizations, and deaths. *Centers for Disease Control and Prevention, National Center for Injury Prevention and Control*, 891–904. https://doi.org/10.1016/B978-0-444-52910-7.00011-8

Fehily, B., Bartlett, C. A., Lydiard, S., Archer, M., Milbourn, H., Majimbi, M., Hemmi, J. M., Dunlop, S. A., Yates, N. J., & Fitzgerald, M. (2019). Differential responses to increasing numbers of mild traumatic brain injury in a rodent closed-head injury model. *Journal of Neurochemistry*, *149*(5), 660–678. https://doi.org/10.1111/jnc.14673

Fehily, B., & Fitzgerald, M. (2017). Repeated mild traumatic brain injury: Potential mechanisms of damage. *Cell Transplantation*, *26*(7), 1131–1155. https://doi.org/10.1177/0963689717714092

Flierl, M. A., Stahel, P. F., Beauchamp, K. M., Morgan, S. J., Smith, W. R., & Shohami, E. (2009). Mouse closed head injury model induced by a weight-drop device. *Nature Protocols*, *4*(9), 1328.

Fox, S. I. (2009). The Nervous System: Neurons and Synapses. In *Human Physiology Eleventh Edition* (pp. 160–203).

Fraunberger, E. A., Dejesus, P., Zanier, E. R., Shutt, T. E., & Esser, M. J. (2020). Acute and Persistent Alterations of Cerebellar Inflammatory Networks and Glial Activation in a Rat Model of Pediatric Mild Traumatic Brain Injury. *Journal of Neurotrauma*, *37*(11), 1315–1330. https://doi.org/10.1089/neu.2019.6714

Freire-Regatillo, A., Argente-Arizón, P., Argente, J., García-Segura, L. M., & Chowen, J. A. (2017). Non-neuronal cells in the hypothalamic adaptation to metabolic signals. In *Frontiers in Endocrinology* (Vol. 8, Issue MAR, p. 51). Frontiers Media S.A. https://doi.org/10.3389/fendo.2017.00051

Fromm, L., Heath, D. L., Vink, R., & Nimmo, A. J. (2004). Magnesium attenuates post-traumatic depression/anxiety following diffuse traumatic brain injury in rats. *Journal of the American College of Nutrition*, *23*(5), 529S-533S. https://doi.org/10.1080/07315724.2004.10719396

Fujita, M., Wei, E. P., & Povlishock, J. T. (2012). Intensity-and interval-specific repetitive traumatic brain injury can evoke both axonal and microvascular damage. *Journal of Neurotrauma*, *29*(12), 2172–2180. https://doi.org/10.1089/neu.2012.2357

Furman, J. L., Sompol, P., Kraner, S. D., Pleiss, M. M., Putman, E. J., Dunkerson, J., Abdul, H. M., Roberts, K. N., Scheff, S. W., & Norris, C. M. (2016). Blockade of Astrocytic Calcineurin/NFAT Signaling Helps to Normalize Hippocampal Synaptic Function and Plasticity in a Rat Model of Traumatic Brain Injury. *Journal of Neuroscience*, *36*(5), 1502–1515. https://doi.org/10.1523/JNEUROSCI.1930-15.2016

Galgano, M. A., Cantu, R., & Chin, L. S. (2016). Chronic Traumatic Encephalopathy: The Impact on Athletes. *Cureus*, *8*(3). https://doi.org/10.7759/cureus.532

Gangolli, M., Benetatos, J., Esparza, T. J., Fountain, E. M., Seneviratne, S., & Brody, D. L. (2019). Repetitive Concussive and Subconcussive Injury in a Human Tau Mouse Model Results in Chronic Cognitive Dysfunction and Disruption of White Matter Tracts, But Not Tau Pathology. *Journal of Neurotrauma*, *36*(5), 735–755. https://doi.org/10.1089/neu.2018.5700

Gardner, A. J., & Zafonte, R. (2016). Neuroepidemiology of traumatic brain injury. In *Handbook of Clinical Neurology* (Vol. 138, pp. 207–223). Elsevier B.V. https://doi.org/10.1016/B978-0-12-802973-2.00012-4

Gavett, B. E., Stern, R. A., & McKee, A. C. (2011). Chronic Traumatic Encephalopathy: A Potential Late Effect of Sport-Related Concussive and Subconcussive Head Trauma. In *Clinics in Sports Medicine* (Vol. 30, Issue 1, pp. 179–188). Elsevier. https://doi.org/10.1016/j.csm.2010.09.007

Gennarelli, T. A. (1993). Mechanisms of brain injury. *The Journal of Emergency Medicine*, *11*, 5–11. https://europepmc.org/article/med/8445204

Gould, T. D., Dao, D. T., & Kovacsics, C. E. (2009). The open field test. *Neuromethods*, *42*, 1–20. https://doi.org/10.1007/978-1-60761-303-9_1

Greenwald, R. M., Gwin, J. T., Chu, J. J., & Crisco, J. J. (2008). Head impact severity measures for evaluating mild traumatic brain injury risk exposure. *Neurosurgery*, *62*(4), 789–798. https://doi.org/10.1227/01.neu.0000318162.67472.ad

Greve, M. W., & Zink, B. J. (2009). Pathophysiology of traumatic brain injury. *Mount Sinai Journal of Medicine*, *76*(2), 97–104. https://doi.org/10.1002/MSJ.20104

Gysland, S. M., Mihalik, J. P., Register-Mihalik, J. K., Trulock, S. C., Shields, E. W., & Guskiewicz, K. M. (2012). The relationship between subconcussive impacts and concussion history on clinical measures of neurologic function in collegiate football players. *Annals of Biomedical Engineering*, *40*(1), 14–22. https://doi.org/10.1007/s10439-011-0421-3

Hamm, R. J., Pike, B. R., O'dell, D. M., Lyeth, B. G., & Jenkins, L. W. (1994). The Rotarod Test: An Evaluation of Its Effectiveness in Assessing Motor Deficits Following Traumatic Brain Injury. *Journal of Neurotrauma*, *11*(2), 187–196. https://doi.org/10.1089/neu.1994.11.187

Hanisch, U. K. (2013). Functional diversity of microglia - How heterogeneous are they to begin with? In *Frontiers in Cellular Neuroscience* (Vol. 7, Issue MAY, p. 65). Frontiers Research Foundation. https://doi.org/10.3389/fncel.2013.00065

Harting, M. T., Jimenez, F., Adams, S. D., Mercer, D. W., & Cox, C. S. (2008). Acute, regional inflammatory response after traumatic brain injury: Implications for cellular therapy. *Surgery*, *144*(5), 803–813. https://doi.org/10.1016/J.SURG.2008.05.017

Hartlage, L. C., Durant-Wilson, D., & Patch, P. C. (2001). Persistent neurobehavioral problems following mild traumatic brain injury. *Archives of Clinical Neuropsychology*, *16*(6), 561–570. https://doi.org/10.1016/S0887-6177(00)00067-6

Henninger, N., Sicard, K. M., Li, Z., Kulkarni, P., Dützmann, S., Urbanek, C., Schwab, S., & Fisher, M. (2007). Differential recovery of behavioral status and brain function assessed with functional magnetic resonance imaging after mild traumatic brain injury in the rat. *Critical Care Medicine*, *35*(11), 2607–2614. https://doi.org/10.1097/01.CCM.0000286395.79654.8D

Hiles-Murison, B., Lavender, A. P., Hackett, M. J., Armstrong, J. J., Nesbit, M., Rawlings, S., McGonigle, T., Warnock, A., Lam, V., Mamo, J. C. L., Fitzgerald, M., & Takechi, R. (2021). Blood–brain barrier disruption and ventricular enlargement are the earliest neuropathological changes in rats with repeated sub-concussive impacts over 2 weeks. *Scientific Reports 2021 11:1*, *11*(1), 1–12. https://doi.org/10.1038/s41598-021-88854-9

Hofmann, K., Rodriguez-Rodriguez, R., Gaebler, A., Casals, N., Scheller, A., & Kuerschner, L. (2017). Astrocytes and oligodendrocytes in grey and white matter regions of the brain metabolize fatty acids. *Scientific Reports*, *7*(1), 1–12. https://doi.org/10.1038/s41598-017-11103-5

Holmin, S., Schalling, M., Höjeberg, B., Nordqvist, A. C. S., Skeftruna, A. K., & Mathiesen, T. (1997). Delayed cytokine expression in rat brain following experimental contusion. *Journal of Neurosurgery*, *86*(3), 493–504. https://doi.org/10.3171/JNS.1997.86.3.0493

Honig, M. G., Dorian, C. C., Worthen, J. D., Micetich, A. C., Mulder, I. A., Sanchez, K. B., Pierce, W. F., Del Mar, N. A., & Reiner, A. (2020). Progressive long-term spatial memory loss following repeat concussive and subconcussive brain injury in mice, associated with dorsal hippocampal neuron loss, microglial phenotype shift, and vascular abnormalities. *European Journal of Neuroscience*, ejn.14711. https://doi.org/10.1111/ejn.14711

Hoogenboom, W. S., Branch, C. A., & Lipton, M. L. (2019). Animal models of closed-skull, repetitive mild traumatic brain injury. *Pharmacology and Therapeutics*, *198*, 109–122. https://doi.org/10.1016/j.pharmthera.2019.02.016

Hovda, D., Giza, C., Bergsneider, M., & Vespa, P. (2014). Metabolic Dysfunction Following Traumatic Brain Injury. In *Concussions in Athletics* (pp. 205–215).

Hsieh, T. H., Kang, J. W., Lai, J. H., Huang, Y. Z., Rotenberg, A., Chen, K. Y., Wang, J. Y., Chan, S. Y., Chen, S. C., Chiang, Y. H., & Peng, C. W. (2017). Relationship of mechanical impact magnitude to neurologic dysfunction severity in a rat traumatic brain injury model. *PLoS ONE*, *12*(5). https://doi.org/10.1371/journal.pone.0178186

Igarashi, T., Potts, M. B., & Noble-Haeusslein, L. J. (2007). Injury severity determines Purkinje cell loss and microglial activation in the cerebellum after cortical contusion injury. *Experimental Neurology*, *203*(1), 258–268.

Iverson, G. L., & Lange, R. T. (2011). Post-Concussion Syndrome. *The Little Black Book of Neuropsychology*, 745–763. https://doi.org/10.1007/978-0-387-76978-3_24

Jamnia, N., Urban, J. H., Stutzmann, G. E., Chiren, S. G., Reisenbigler, E., Marr, R., Peterson, D. A., & Kozlowski, D. A. (2017). A Clinically Relevant Closed-Head Model of Single and Repeat Concussive Injury in the Adult Rat Using a Controlled Cortical Impact Device. *Journal of Neurotrauma*, *34*(7), 1351–1363. https://doi.org/10.1089/neu.2016.4517

Janzer, R. C., & Raff, M. C. (1987). Astrocytes induce blood-brain barrier properties in endothelial cells. *Nature*, *325*(6101), 253–257. https://doi.org/10.1038/325253a0

Jenkins, L., Moszynski, K., Lyeth, B., Lewelt, W., DeWitt, D., Allen, A., Dixon, C., Povlishshock, J., Majewski, T., Clifton, G., Young, H., Becker, D., & Hayes, R. (1989). Increased vulnerability of the midly traumatized rat brain to cerebral ischemia: the use of controlled secondary ischemia as a research tool to identify common or. *Brain Research*, *477*(1–2), 211–224. https://www.sciencedirect.com/science/article/pii/0006899389914091

Jha, M. K., Jo, M., Kim, J. H., & Suk, K. (2019). Microglia-astrocyte crosstalk: an intimate molecular conversation. *The Neuroscientist* , *25*(3), 227–240. https://journals.sagepub.com/doi/pdf/10.1177/1073858418783959

Johnson, V. E., Meaney, D. F., cullen, D. K., & Smith, D. H. (2015). Animal models of traumatic brain injury. *Handbook of Clinical Neurology*, *127*, 115. https://doi.org/10.1016/B978-0-444-52892-6.00008-8

Kabadi, S. V., Hilton, G. D., Stoica, B. A., Zapple, D. N., & Faden, A. I. (2010). Fluid-percussion-induced traumatic brain injury model in rats. In *Nature Protocols* (Vol. 5, Issue 9, pp. 1552–1563). https://doi.org/10.1038/nprot.2010.112

Kamm, K., VanderKolk, W., Lawrence, C., Jonker, M., & Davis, A. T. (2006). The effect of traumatic brain injury upon the concentration and expression of interleukin-1β and interleukin-10 in the rat. *Journal of Trauma and Acute Care Surgery*, *60*(1), 152–157. https://journals.lww.com/jtrauma/Fulltext/2006/01000/Production_of_Tumor_Necrosis_Factor_alpha_and.00021.aspx

Karve, I. P., Taylor, J. M., & Crack, P. J. (2016). The contribution of astrocytes and microglia to traumatic brain injury. *British Journal of Pharmacology*, *173*(4), 692–702. https://doi.org/10.1111/bph.13125

Kegel, D. De. (2018). *Tissue-Level Tolerance Criteria for Crash-Related Head Injuries: A Combined Experimental and Numerical Approach*. https://lirias.kuleuven.be/2302462?limo=0

Killam, C., Cautin, R. L., & Santucci, A. C. (2005). Assessing the enduring residual neuropsychological effects of head trauma in college athletes who participate in contact sports. *Archives of Clinical Neuropsychology*, *20*(5), 599–611. https://doi.org/10.1016/J.ACN.2005.02.001

Kim, H. J., & Han, S. J. (2017). A simple rat model of mild traumatic brain injury: A device to reproduce anatomical and neurological changes of mild traumatic brain injury. *PeerJ*, *2017*(1). https://doi.org/10.7717/peerj.2818

King, D., Hume, P., Gissane, C., Brughelli, M., & Clark, T. (2015). The Influence of Head Impact Threshold for Reporting Data in Contact and Collision Sports: Systematic Review and Original Data Analysis. *Sports Medicine 2015 46:2*, *46*(2), 151–169. https://doi.org/10.1007/S40279-015-0423-7

Koerte, I. K., Lin, A. P., Willems, A., Muehlmann, M., Hufschmidt, J., Coleman, M. J., Green, I., Liao, H., Tate, D. F., Wilde, E. A., Pasternak, O., Bouix, S., Rathi, Y., Bigler, E. D., Stern, R. A., & Shenton, M. E. (2015). A Review of Neuroimaging Findings in Repetitive Brain Trauma. *Brain Pathology*, *25*(3), 318–349. https://doi.org/10.1111/BPA.12249

Koliatsos, V. E., Rao, V., & Hopkins, J. (2020). The behavioral neuroscience of traumatic brain injury. *Psychiatric Clinics of North America*, *43*(2), 305–330.

Kortbeek, J. B., Al Turki, S. A., Ali, J., Antoine, J. A., Bouillon, B., Brasel, K., Brenneman, F., Brink, P. R., Brohi, K., Burris, D., Burton, R. A., Chapleau, W., Cioffi, W., Collet e Silva, F. D. S., Cooper, A., Cortes, J. A., Eskesen, V., Fildes, J., Gautam, S., … Winter, R. (2008). Advanced Trauma Life Support, 8th Edition, The Evidence for Change. *The Journal of Trauma: Injury, Infection, and Critical Care*, *64*(6), 1638–1650. https://doi.org/10.1097/TA.0b013e3181744b03

Kosari-Nasab, M., Shokouhi, G., Ghorbanihaghjo, A., Mesgari-Abbasi, M., & Salari, A. A. (2019). Quercetin mitigates anxiety-like behavior and normalizes hypothalamus-pituitary-adrenal axis function in a mouse model of mild traumatic brain injury. *Behavioural Pharmacology*, *30*(2and3-SpecialIssue), 282–289. https://doi.org/10.1097/FBP.0000000000000480

Kreutzberg GW. (1996). Microglia: a sensor for pathological events in the CNS. *Trends in Neurosciences*, *19*(8), 312–318. https://www.sciencedirect.com/science/article/pii/0166223696100497

Kumar, A., & Brain, D. L. (2012). Neuroinflammation after traumatic brain injury: opportunities for therapeutic intervention. *Brain, Behavior, and Immunity*, *26*(8), 1191–1201. https://www.sciencedirect.com/science/article/pii/S088915911200150X

Lafrenaye, A. D., Mondello, S., Wang, K. K., Yang, Z., Povlishock, J. T., Gorse, K., Walker, S., Hayes, R. L., & Kochanek, P. M. (2020). Circulating GFAP and Iba-1 levels are associated with pathophysiological sequelae in the thalamus in a pig model of mild TBI. *Scientific Reports*, *10*(1), 13369. https://doi.org/10.1038/s41598-020-70266-w

Lagraoui, M., Latoche, J. R., Cartwright, N. G., Sukumar, G., Dalgard, C. L., & Schaefer, B. C. (2012). Controlled cortical impact and craniotomy induce strikingly similar profiles of inflammatory gene expression, but with distinct kinetics. *Frontiers in Neurology*, *OCT*. https://doi.org/10.3389/fneur.2012.00155

Langlois, J. A., Rutland-Brown, W., & Wald, M. M. (2006). The Epidemiology and Impact of Traumatic Brain Injury A Brief Overview. In *J Head Trauma Rehabil* (Vol. 21, Issue 5). www.headtraumarehab.com

LaPlaca, M. C., Simon, C. M., Prado, G. R., & Cullen, D. K. (2007). CNS injury biomechanics and experimental models. *Progress in Brain Research*, *161*, 13–26. https://doi.org/10.1016/S0079-6123(06)61002-9

Lavender, A. P., Rawlings, S., Warnock, A., McGonigle, T., Hiles-Murison, B., Nesbit, M., Lam, V., Hackett, M. J., Fitzgerald, M., & Takechi, R. (2020). Repeated Long-Term Sub-concussion Impacts Induce Motor Dysfunction in Rats: A Potential Rodent Model. *Frontiers in Neurology*, *11*, 491. https://doi.org/10.3389/fneur.2020.00491

Lee, H., Lee, T., & YR Kou. (2012). Anti-inflammatory and neuroprotective effects of triptolide on traumatic brain injury in rats. *Respiratory Physiology & Neurobiology*, *182*(1), 1–8. https://www.sciencedirect.com/science/article/pii/S1569904812000407

Leo, P., & McCrea, M. (2016). Frontiers in Neuroscience\Epidemiology. In D. Laskowitz & G. Grant (Eds.), *Translational Research in Traumatic Brain Injury* (pp. 1-25 (Chapter 1)). CRC Press/Taylor and Francis Group. https://www.ncbi.nlm.nih.gov/books/NBK326730/

Li, B., Mahmood, A., Lu, D., Wu, H., Xiong, Y., Qu, C., & Chopp, M. (2009). SIMVASTATIN ATTENUATES MICROGLIAL CELLS AND ASTROCYTE ACTIVATION AND DECREASES INTERLEUKIN1 LEVEL AFTER TRAUMATIC BRAIN INJURY. *NEUROSURGERY*, *65*(1), 179–186. https://doi.org/10.1227/01.NEU.0000346272.76537.DC

Li, Y., Zhang, L., Kallakuri, S., Cohen, A., & Cavanaugh, J. M. (2015). Correlation of mechanical impact responses and biomarker levels: A new model for biomarker evaluation in TBI. *Journal of the Neurological Sciences*, *359*(1–2), 280–286. https://doi.org/10.1016/j.jns.2015.08.035

Liddelow, S. A., Guttenplan, K. A., Clarke, L. E., Bennett, F. C., Bohlen, C. J., Schirmer, L., Bennett, M. L., Münch, A. E., Chung, W. S., Peterson, T. C., Wilton, D. K., Frouin, A., Napier, B. A., Panicker, N., Kumar, M., Buckwalter, M. S., Rowitch, D. H., Dawson, V. L., Dawson, T. M., … Barres, B. A. (2017). Neurotoxic reactive astrocytes are induced by activated microglia. *Nature*, *541*(7638), 481. https://doi.org/10.1038/NATURE21029

Linninger, A. A., Tangen, K., Hsu, C.-Y., & Frim, D. (2016). Cerebrospinal Fluid Mechanics and Its Coupling to Cerebrovascular Dynamics. *Annual Review of Fluid Mechanics*, *48*(1), 219–257. https://doi.org/10.1146/annurev-fluid-122414-034321

Liu, W., Tang, Y., & Feng, J. (2011). Cross talk between activation of microglia and astrocytes in pathological conditions in the central nervous system. *Life Sciences*, *89*(5–6), 141–146. https://doi.org/10.1016/J.LFS.2011.05.011

Loane, D. J., & Kumar, A. (2016). Microglia in the TBI brain: the good, the bad, and the dysregulated. *Experimental Neurology*, *275*, 316–327. https://www.sciencedirect.com/science/article/pii/S0014488615300790

Long, T. (2017). Modeling subconcussive and cumulative subconcussive impacts using a lateral fluid percusion injury device. *Dissertations*. https://digitalcommons.njit.edu/dissertations/53

Ma, X., Aravind, A., Pfister, B. J., Chandra, N., & Haorah, J. (2019). Animal Models of Traumatic Brain Injury and Assessment of Injury Severity. In *Molecular Neurobiology* (Vol. 56, Issue 8, pp. 5332–5345). Humana Press Inc. https://doi.org/10.1007/s12035-018-1454-5

Macvicar, B. A., & Newman, E. A. (2015). Astrocyte regulation of blood flow in the brain. *Cold Spring Harbor Perspectives in Biology*, *7*(5), 1–15. https://doi.org/10.1101/cshperspect.a020388

Madathil, S. K., Wilfred, B. S., Urankar, S. E., Yang, W., Leung, L. Y., Gilsdorf, J. S., & Shear, D. A. (2018). Early Microglial Activation Following Closed-Head Concussive Injury Is Dominated by Pro-Inflammatory M-1 Type. *Frontiers in Neurology*, *9*(NOV). https://doi.org/10.3389/fneur.2018.00964

Mainwaring, L., Ferdinand Pennock, K. M., Mylabathula, S., & Alavie, B. Z. (2018). Subconcussive head impacts in sport: A systematic review of the evidence. *International Journal of Psychophysiology*, *132*, 39–54. https://doi.org/10.1016/J.IJPSYCHO.2018.01.007

Maldonado, K. A., & Alsayouri, K. (2020). Physiology, Brain. In *StatPearls*. StatPearls Publishing. http://www.ncbi.nlm.nih.gov/pubmed/31869182

Malkesman, O., Tucker, L. B., Ozl, J., & McCabe, J. T. (2013). Traumatic brain injury - modeling neuropsychiatric symptoms in rodents. *Frontiers in Neurology*, *4 OCT*(October), 1–14. https://doi.org/10.3389/fneur.2013.00157

Marklund, N. (2016). Rodent Models of Traumatic Brain Injury: Methods and Challenges. *Methods in Molecular Biology (Clifton, N.J.)*, *1462*, 29–46. https://doi.org/10.1007/978-1-4939-3816-2_3

Marmarou, A., Abd-Elfattah Foda, M. A., Van den Brink, W., Campbell, J., Kita, H., & Demetriadou, K. (1994). A new model of diffuse brain injury in rats. Part I: Pathophysiology and biomechanics. *Journal of Neurosurgery*, *80*(2), 291–300. https://doi.org/10.3171/jns.1994.80.2.0291

Marschner, L., Schreurs, A., Lechat, B., Mogensen, J., Roebroek, A., Ahmed, T., & Balschun, D. (2019). Single mild traumatic brain injury results in transiently impaired spatial long-term memory and altered search strategies. *Behavioural Brain Research*, *365*, 222–230. https://doi.org/10.1016/J.BBR.2018.02.040

McAllister, T. W., Flashman, L. A., Maerlender, A., Greenwald, R. M., Beckwith, J. G., Tosteson, T. D., Crisco, J. J., Brolinson, P. G., Duma, S. M., Duhaime, A. C., Grove, M. R., & Turco, J. H. (2012). Cognitive effects of one season of head impacts in a cohort of collegiate contact sport athletes. *Neurology*, *78*(22), 1777–1784. https://doi.org/10.1212/WNL.0B013E3182582FE7

McAteer, K. M., Corrigan, F., Thornton, E., Turner, R. J., & Vink, R. (2016). Short and long term behavioral and pathological changes in a novel rodent model of repetitive mild traumatic brain injury. *PLoS ONE*, *11*(8), 1–18. https://doi.org/10.1371/journal.pone.0160220

McKee, A. C., Cantu, R. C., Nowinski, C. J., Hedley-Whyte, E. T., Gavett, B. E., Budson, A. E., Santini, V. E., Lee, H.-S., Kubilus, C. A., & Stern, R. A. (2009). Chronic Traumatic Encephalopathy in Athletes: Progressive Tauopathy After Repetitive Head Injury. *Journal of Neuropathology & Experimental Neurology*, *68*(7), 709–735. https://doi.org/10.1097/NEN.0B013E3181A9D503

McNamara, E. H., Grillakis, A. A., Tucker, L. B., & McCabe, J. T. (2020). The closed-head impact model of engineered rotational acceleration (CHIMERA) as an application for traumatic brain injury pre-clinical research: A status report. *Experimental Neurology*, *333*, 113409. https://doi.org/10.1016/J.EXPNEUROL.2020.113409

Meaney, D. F., Morrison, B., & Bass, C. D. (2014). The Mechanics of Traumatic Brain Injury: A Review of What We Know and What We Need to Know for Reducing Its Societal Burden. *Journal of Biomechanical Engineering*, *136*(2), 0210081. https://doi.org/10.1115/1.4026364

Mederos, S., González-Arias, C., & Perea, G. (2018). Astrocyte–Neuron Networks: A Multilane Highway of Signaling for Homeostatic Brain Function. *Frontiers in Synaptic Neuroscience*, *10*, 45. https://doi.org/10.3389/fnsyn.2018.00045

Medical gallery of Blausen Medical 2014. (2014). *WikiJournal of Medicine*, *1*(2). https://doi.org/10.15347/wjm/2014.010

Meehan III, W. P., Zhang, J., Mannix, R., & Whalen, M. J. (2012). Increasing recovery time between injuries improves cognitive outcome after repetitive mild concussive brain injuries in mice. *Neurosurgery*, *71*(4), 885–891. https://doi.org/10.1227/NEU.0b013e318265a439

Mena, J. H., Sanchez, A. I., Rubiano, A. M., Peitzman, A. B., Sperry, J. L., Gutierrez, M. I., & Puyana, J. C. (2011). Effect of the modified glasgow coma scale score criteria for mild traumatic brain injury on mortality prediction: Comparing classic and modified glasgow coma scale score model scores of 13. *Journal of Trauma - Injury, Infection and Critical Care*, *71*(5), 1185–1193. https://doi.org/10.1097/TA.0b013e31823321f8

Meyer, D. L., Davies, D. R., Barr, J. L., Manzerra, P., & Forster, G. L. (2012). Mild traumatic brain injury in the rat alters neuronal number in the limbic system and increases conditioned fear and anxiety-like behaviors. *Experimental Neurology*, *235*(2), 574–587. https://doi.org/10.1016/J.EXPNEUROL.2012.03.012

Meythaler, J. M., Peduzzi, J. D., Eleftheriou, E., & Novack, T. A. (2001). Current concepts: Diffuse axonal injury–associated traumatic brain injury. *Archives of Physical Medicine and Rehabilitation*, *82*(10), 1461–1471. https://doi.org/10.1053/APMR.2001.25137

Miller, J. R., Adamson, G. J., Md, ‡, Pink, M. M., Sweet, J. C., & Ma, §. (2007). *Comparison of Preseason, Midseason, and Postseason Neurocognitive Scores in Uninjured Collegiate Football Players*. https://doi.org/10.1177/0363546507300261

Moore, R. D., Lepine, J., & Ellemberg, D. (2017). The independent influence of concussive and sub-concussive impacts on soccer players' neurophysiological and neuropsychological function. *International Journal of Psychophysiology*, *112*, 22–30. https://doi.org/10.1016/J.IJPSYCHO.2016.11.011

Morales, D. M., Marklund, N., Lebold, D., Thompson, H. J., Pitkanen, A., Maxwell, W. L., Longhi, L., Laurer, H., Maegele, M., Neugebauer, E., Graham, D. I., Stocchetti, N., & McIntosh, T. K. (2005). Experimental models of traumatic brain injury: Do we really need to build a better mousetrap? *Neuroscience*, *136*(4), 971–989. https://doi.org/10.1016/J.NEUROSCIENCE.2005.08.030

Mouzon, B., Chaytow, H., Crynen, G., Bachmeier, C., Stewart, J., Mullan, M., Stewart, W., & Crawford, F. (2012). Repetitive mild traumatic brain injury in a mouse model produces learning and memory deficits accompanied by histological changes. *Journal of Neurotrauma*, *29*(18), 2761–2773. https://doi.org/10.1089/neu.2012.2498

Mukherjee, S., Katki, K., Arisi, G. M., Foresti, M. L., & Shapiro, L. A. (2011). Early TBI-Induced Cytokine Alterations are Similarly Detected by Two Distinct Methods of Multiplex Assay. *Frontiers in Molecular Neuroscience*, *0*, 21. https://doi.org/10.3389/FNMOL.2011.00021

Mustafa, A. G., & Al-Shboul, O. A. (2013). Pathophysiology of traumatic brain injury. *Neurosciences*, *18*(3), 222–234. www.neurosciencesjournal.org

Mychasiuk, R., Farran, A., & Esser, M. J. (2014). Assessment of an experimental rodent model of pediatric mild traumatic brain injury. *Journal of Neurotrauma*, *31*(8), 749–757. https://doi.org/10.1089/NEU.2013.3132

Mychasiuk, R., Hehar, H., Candy, S., Ma, I., & Esser, M. J. (2016). The direction of the acceleration and rotational forces associated with mild traumatic brain injury in rodents effect behavioural and molecular outcomes. *Journal of Neuroscience Methods*, *257*, 168–178. https://doi.org/10.1016/J.JNEUMETH.2015.10.002

Mychasiuk, R., Hehar, H., Ma, I., & Esser, M. J. (2015). Dietary intake alters behavioral recovery and gene expression profiles in the brain of juvenile rats that have experienced a concussion. *Frontiers in Behavioral Neuroscience*, *9*(FEB). https://doi.org/10.3389/FNBEH.2015.00017

Namjoshi, D. R., Cheng, W. H. an., McInnes, K. A., Martens, K. M., Carr, M., Wilkinson, A., Fan, J., Robert, J., Hayat, A., Cripton, P. A., & Wellington, C. L. (2014). Merging pathology with biomechanics using CHIMERA (Closed-Head Impact Model of Engineered Rotational Acceleration): a novel, surgery-free model of traumatic brain injury. *Molecular Neurodegeneration*, *9*, 55. https://doi.org/10.1186/1750-1326-9-55

Namjoshi, D. R., Cheng, W. H., Bashir, A., Wilkinson, A., Stukas, S., Martens, K. M., Whyte, T., Abebe, Z. A., McInnes, K. A., Cripton, P. A., & Wellington, C. L. (2017). Defining the biomechanical and biological threshold of murine mild traumatic brain injury using CHIMERA (Closed Head Impact Model of Engineered Rotational Acceleration). *Experimental Neurology*, *292*, 80–91. https://doi.org/10.1016/j.expneurol.2017.03.003

Natale, J. E., Ahmed, F., Cernak, I., Stoica, B., & Faden, A. I. (2003). Gene Expression Profile Changes are Commonly Modulated across Models and Species after Traumatic Brain Injury. *Journal of Neurotrauma*, *20*(10), 907–927. https://doi.org/10.1089/089771503770195777

Nauman, E. A., Talavage, T. M., & Auerbach, P. S. (2020). Mitigating the Consequences of Subconcussive Head Injuries. In *Annual Review of Biomedical Engineering* (Vol. 22, Issue 1, pp. 387–407). Annual Reviews Inc. https://doi.org/10.1146/annurev-bioeng-091219-053447

Nelson, A. D., & Jenkins, P. M. (2017). Axonal membranes and their domains: Assembly and function of the axon initial segment and node of Ranvier. In *Frontiers in Cellular Neuroscience* (Vol. 11, p. 136). Frontiers Research Foundation. https://doi.org/10.3389/fncel.2017.00136

Neri, M., Frati, A., Turillazzi, E., Cantatore, S., Cipolloni, L., Di Paolo, M., Frati, P., La Russa, R., Maiese, A., Scopetti, M., Santurro, A., Sessa, F., Zamparese, R., & Fineschi, V. (2018). Immunohistochemical Evaluation of Aquaporin-4 and its Correlation with CD68, IBA-1, HIF-1α, GFAP, and CD15 Expressions in Fatal Traumatic Brain Injury. *International Journal of Molecular Sciences 2018, Vol. 19, Page 3544*, *19*(11), 3544. https://doi.org/10.3390/IJMS19113544

Ng, S. Y., & Lee, A. Y. W. (2019). Traumatic Brain Injuries: Pathophysiology and Potential Therapeutic Targets. *Frontiers in Cellular Neuroscience*, *13*, 528. https://doi.org/10.3389/FNCEL.2019.00528/BIBTEX

Nichols, J. N., Deshane, A. S., Niedzielko, T. L., Smith, C. D., & Floyd, C. L. (2016). Greater neurobehavioral deficits occur in adult mice after repeated, as compared to single, mild traumatic brain injury (mTBI). *Behavioural Brain Research*, *298*, 111–124. https://doi.org/10.1016/J.BBR.2015.10.052

Onyszchuk, G, Al-Hafez, B., He, Y.-Y., Bilgen, M., Berman, N. E. J., & Brooks, W. M. (2007). A mouse model of sensorimotor controlled cortical impact: Characterization using longitudinal magnetic resonance imaging, behavioral assessments and histology. *Journal of Neuroscience Methods*, *160*(2), 187–196. https://doi.org/10.1016/j.jneumeth.2006.09.007

Onyszchuk, Gregory, Al-Hafez, B., He, Y. Y., Bilgen, M., Berman, N. E. J., & Brooks, W. M. (2007). A mouse model of sensorimotor controlled cortical impact: Characterization using longitudinal magnetic resonance imaging, behavioral assessments and histology. *Journal of Neuroscience Methods*, *160*(2), 187–196. https://doi.org/10.1016/J.JNEUMETH.2006.09.007

Osier, N. D., & Dixon, C. E. (2016). The controlled cortical impact model: Applications, considerations for researchers, and future directions. In *Frontiers in Neurology* (Vol. 7, Issue AUG). Frontiers Media S.A. https://doi.org/10.3389/fneur.2016.00134

Pavlova, V., Filipova, E., Uzunova, K., Kalinov, K., & Vekov, T. (2018). Recent Advances in Pathophysiology of Traumatic Brain Injury. *Current Neuropharmacology*, *16*(8), 1224. https://doi.org/10.2174/1871530318666180423121833

Perez, E. J., Tapanes, S. A., Loris, Z. B., Balu, D. T., Sick, T. J., Coyle, J. T., & Liebl, D. J. (2017). Enhanced astrocytic d-serine underlies synaptic damage after traumatic brain injury. *The Journal of Clinical Investigation*, *127*(8), 3114–3125. https://doi.org/10.1172/JCI92300

Peterson, A. B., Xu, L., Daugherty, J., & Breiding, M. J. (2019). *Surveillance report of traumatic brain injury-related emergency department visits, hospitalizations, and deaths, United States, 2014.* www.cdc.gov/TraumaticBrainInjury

Petraglia, A. L., Plog, B. A., Dayawansa, S., Chen, M., Dashnaw, M. L., Czerniecka, K., Walker, C. T., Viterise, T., Hyrien, O., Iliff, J. J., Deane, R., Nedergaard, M., & Huang, J. H. (2014). The spectrum of neurobehavioral sequelae after repetitive mild traumatic brain injury: A novel mouse model of chronic traumatic encephalopathy. *Journal of Neurotrauma*, *31*(13), 1211–1224. https://doi.org/10.1089/neu.2013.3255

Petraglia, A., Plog, B., Dayawansa, S., Dashnaw, M., Czerniecka, K., Walker, C., Chen, M., Hyrien, O., Iliff, J., Deane, R., Huang, J., & Nedergaard, M. (2014). The pathophysiology underlying repetitive mild traumatic brain injury in a novel mouse model of chronic traumatic encephalopathy. *Surgical Neurology International*, *5*(1). https://doi.org/10.4103/2152-7806.147566

Pleasant, J. M., Carlson, S. W., Mao, H., Scheff, S. W., Yang, K. H., & Saatman, K. E. (2011). Rate of neurodegeneration in the mouse controlled cortical impact model is influenced by impactor tip shape: Implications for mechanistic and therapeutic studies. *Journal of Neurotrauma*, *28*(11), 2245–2262. https://doi.org/10.1089/neu.2010.1499

Popovich, P. G., Jakeman, L. B., & McTigue, D. M. (2009). Glial responses to injury. In *Encyclopedia of Neuroscience* (pp. 853–859). Elsevier Ltd. https://doi.org/10.1016/B978-008045046-9.00018-8

Prins, M. L., Alexander, D., Giza, C. C., & Hovda, D. A. (2013). Repeated mild traumatic brain injury: Mechanisms of cerebral vulnerability. *Journal of Neurotrauma*, *30*(1), 30–38. https://doi.org/10.1089/neu.2012.2399

Prins, M. L., Hales, A., Reger, M., Giza, C. C., & Hovda, D. A. (2010). Repeat Traumatic Brain Injury in the Juvenile Rat Is Associated with Increased Axonal Injury and Cognitive Impairments. *Developmental Neuroscience*. https://doi.org/10.1159/000316800

Prut, L., & Belzung, C. (2003). The open field as a paradigm to measure the effects of drugs on anxiety-like behaviors: a review. *European Journal of Pharmacology2*, *463*(1–3), 3–33.

Purves, D., Augustine, G. J., Fitzpatrick, D., Katz, L. C., LaMantia, A.-S., McNamara, J. O., & Williams, S. M. (2001). *Neuroglial Cells*. https://www.ncbi.nlm.nih.gov/books/NBK10869/

Rawlings, S., Takechi, R., & Lavender, A. P. (2020). Effects of sub-concussion on neuropsychological performance and its potential mechanisms: A narrative review. In *Brain Research Bulletin* (Vol. 165, pp. 56–62). Elsevier Inc. https://doi.org/10.1016/j.brainresbull.2020.09.021

Ritter, K., Jung, K., Dolderer, C., Appel, D., Oswald, C. C., Ritz, U., & Schäfer, M. K. E. (2021). Early Reciprocal Effects in a Murine Model of Traumatic Brain Injury and Femoral Fracture. *Mediators of Inflammation*, *2021*. https://doi.org/10.1155/2021/8835730

Robinson, S., Berglass, J. B., Denson, J. L., Berkner, J., Anstine, C. V, Winer, J. L., Maxwell, J. R., Qiu, J., Yang, Y., Sillerud, L. O., Meehan III, W. P., Mannix, R., & Jantzie, L. L. (2017). Microstructural and microglial changes after repetitive mild traumatic brain injury in mice. *Journal of Neuroscience Research*, *95*(4), 1025–1035. https://doi.org/10.1002/jnr.23848

Ryan, L. M., & Warden, D. L. (2003). Post concussion syndrome. In *International Review of Psychiatry* (Vol. 15, Issue 4, pp. 310–316). https://doi.org/10.1080/09540260310001606692

Safinia, C., Bershad, E. M., Clark, H. B., SantaCruz, K., Alakbarova, N., Suarez, J. I., & Divani, A. A. (2016). Chronic Traumatic Encephalopathy in Athletes Involved with High-impact Sports. *Journal of Vascular and Interventional Neurology*, *9*(2), 34–48. http://www.ncbi.nlm.nih.gov/pubmed/27829969

Sagarkar, S., Bhamburkar, T., Shelkar, G., Choudhary, A., Kokare, D. M., & Sakharkar, A. J. (2017). Minimal traumatic brain injury causes persistent changes in DNA methylation at BDNF gene promoters in rat amygdala: A possible role in anxiety-like behaviors. *Neurobiology of Disease*, *106*, 101–109. https://doi.org/10.1016/j.nbd.2017.06.016

Sandhir, R., Onyszchuk, G., & Berman, N. E. J. (2008). Exacerbated glial response in the aged mouse hippocampus following controlled cortical impact injury. *Experimental Neurology*, *213*(2), 372–380. https://doi.org/10.1016/J.EXPNEUROL.2008.06.013

Sarkaki, A. R., Haddad, M. K., Soltani, Z., Shahrokhi, N., & Mahmoodi, M. (2013). Time-and Dose-Dependent Neuroprotective Effects of Sex Steroid Hormones on Inflammatory Cytokines after a Traumatic Brain Injury. *Journal of Neurotrauma*, *30*(1), 47–54. https://doi.org/10.1089/neu.2010.1686

Sauerbeck, A. D., Fanizzi, C., Kim, J. H., Gangolli, M., Bayly, P. V., Wellington, C. L., Brody, D. L., & Kummer, T. T. (2018). ModCHIMERA: A novel murine closed-head model of moderate traumatic brain injury. *Scientific Reports*, *8*(1). https://doi.org/10.1038/s41598-018-25737-6

Schmidt, O., Infanger, M., Heyde, C., … W. E.-E. J. of, & 2004, U. (2004). The role of neuroinflammation in traumatic brain injury. *European Journal of Trauma*, *30*(3), 135–149. https://doi.org/10.1007/s00068-004-1394-9

Schousboe, A., & Waagepetersen, H. S. (2005). Role of astrocytes in glutamate homeostasis: Implications for excitotoxicity. *Neurotoxicity Research*, *8*(3–4), 221–225. https://doi.org/10.1007/BF03033975

Schwerin, S. C., Hutchinson, E. B., Radomski, K. L., Ngalula, K. P., Pierpaoli, C. M., & Juliano, S. L. (2017). Establishing the ferret as a gyrencephalic animal model of traumatic brain injury: Optimization of controlled cortical impact procedures. *Journal of Neuroscience Methods*, *285*, 82–96. https://doi.org/10.1016/J.JNEUMETH.2017.05.010

Seibenhener, M. L., & Wooten, M. C. (2015). Use of the Open Field Maze to Measure Locomotor and Anxiety-like Behavior in Mice. *Journal of Visualized Experiments: JoVE*, *96*, 52434. https://doi.org/10.3791/52434

Selwyn, R. G., Cooney, S. J., Khayrullina, G., Hockenbury, N., Wilson, C. M., Jaiswal, S., Bermudez, S., Armstrong, R. C., & Byrnes, K. R. (2016). Outcome after repetitive mild traumatic brain injury is temporally related to glucose uptake profile at time of second injury. *Journal of Neurotrauma*, *33*(16), 1479–1491. https://doi.org/10.1089/neu.2015.4129

Shapira, Y., Shohami, E., Sidi, A., Soffer, D., Freeman, S., & Cotev, S. (1988). Experimental closed head injury in rats: Mechanical, pathophysiologic, and neurologic properties. In *Critical Care Medicine* (Vol. 16, Issue 3, pp. 258–265). https://doi.org/10.1097/00003246-198803000-00010

Shapiro, L., Perez, Z., Foresti, M., Arisi, G., & Ribak, C. (2009). Morphological and ultrastructural features of Iba1-immunolabeled microglial cells in the hippocampal dentate gyrus. *Brain Research*, *1266*, 29–36. https://www.sciencedirect.com/science/article/pii/S0006899309003084

Sharma, A., Chandran, R., Barry, E. S., Bhomia, M., Hutchison, M. A., Balakathiresan, N. S., Grunberg, N. E., & Maheshwari, R. K. (2014). Identification of serum microRNA signatures for diagnosis of mild traumatic brain injury in a closed head injury model. *PloS One*, *9*(11). https://doi.org/10.1371/JOURNAL.PONE.0112019

Sheng, W. S., Hu, S., Feng, A., & Rock, R. B. (2013). Reactive oxygen species from human astrocytes induced functional impairment and oxidative damage. *Neurochemical Research*, *38*(10), 2148–2159. https://doi.org/10.1007/S11064-013-1123-Z

Shitaka, Y., Tran, H. T., Bennett, R. E., Sanchez, L., Levy, M. A., Dikranian, K., & Brody, D. L. (2011a). Repetitive closed-skull traumatic brain injury in mice causes persistent multifocal axonal injury and microglial reactivity. *Journal of Neuropathology and Experimental Neurology*, *70*(7), 551–567. https://doi.org/10.1097/NEN.0b013e31821f891f

Shitaka, Y., Tran, H. T., Bennett, R. E., Sanchez, L., Levy, M. A., Dikranian, K., & Brody, D. L. (2011b). Repetitive closed-skull traumatic brain injury in mice causes persistent multifocal axonal injury and microglial reactivity. *Journal of Neuropathology and Experimental Neurology*, *70*(7), 551–567. https://doi.org/10.1097/NEN.0b013e31821f891f

Shultz, S. R., Bao, F., Weaver, L. C., Cain, D. P., & Brown, A. (2013). Treatment with an anti-CD11d integrin antibody reduces neuroinflammation and improves outcome in a rat model of repeated concussion. *Journal of Neuroinflammation*, *10*. https://doi.org/10.1186/1742-2094-10-26

Shultz, S. R., MacFabe, D. F., Foley, K. A., Taylor, R., & Cain, D. P. (2011). A single mild fluid percussion injury induces short-term behavioral and neuropathological changes in the Long-Evans rat: Support for an animal model of concussion. *Behavioural Brain Research*, *224*(2), 326–335. https://doi.org/10.1016/j.bbr.2011.06.012

Shultz, S. R., MacFabe, D. F., Foley, K. A., Taylor, R., & Cain, D. P. (2012). Sub-concussive brain injury in the Long-Evans rat induces acute neuroinflammation in the absence of behavioral impairments. *Behavioural Brain Research*, *229*(1), 145–152. https://doi.org/10.1016/j.bbr.2011.12.015

Shultz, S. R., McDonald, S. J., Vonder Haar, C., Meconi, A., Vink, R., van Donkelaar, P., Taneja, C., Iverson, G. L., & Christie, B. R. (2017). The potential for animal models to provide insight into mild traumatic brain injury: Translational challenges and strategies. *Neuroscience & Biobehavioral Reviews*, *76*, 396–414. https://doi.org/10.1016/J.NEUBIOREV.2016.09.014

Shurley, J. P., & Todd, J. S. (2016). Boxing Lessons: An Historical Review of Chronic Head Trauma in Boxing and Football. *Kinesiology Review*, *1*(3), 170–184. https://doi.org/10.1123/krj.1.3.170

Simon, D. W., McGeachy, M. J., Baylr, H., Clark, R. S. B., Loane, D. J., & Kochanek, P. M. (2017). The far-reaching scope of neuroinflammation after traumatic brain injury. *Nature Reviews Neurology 2017 13:3*, *13*(3), 171–191. https://doi.org/10.1038/nrneurol.2017.13

Singh, K., Trivedi, R., Devi, M. M., Tripathi, R. P., & Khushu, S. (2016). Longitudinal changes in the DTI measures, anti-GFAP expression and levels of serum inflammatory cytokines following mild traumatic brain injury. *Experimental Neurology*, *275*, 427–435. https://doi.org/10.1016/j.expneurol.2015.07.016

Skandsen, T., Kvistad, K., Solheim, O., … I. S.-J. of, & 2010, U. (2010). Prevalence and impact of diffuse axonal injury in patients with moderate and severe head injury: a cohort study of early magnetic resonance imaging findings and 1. *Journal of Neurosurgery*, *113*(3), 556–563. https://doi.org/10.3171/2009.9.jns09626

Smith, D. H., Johnson, V. E., & Stewart, W. (2013). Chronic neuropathologies of single and repetitive TBI: Substrates of dementia? *Nature Reviews Neurology*, *9*(4), 211–221. https://doi.org/10.1038/nrneurol.2013.29

Smits, M., Dippel, D. W. J., De Haan, G. G., Dekker, H. M., Vos, P. E., Kool, D. R., Nederkoorn, P. J., Hofman, P. A. M., Twijnstra, A., Tanghe, H. L. J., & Hunink, M. G. M. (2005). External validation of the Canadian CT head rule and the New Orleans criteria for CT scanning in patients with minor head injury. *Journal of the American Medical Association*, *294*(12), 1519–1525. https://doi.org/10.1001/jama.294.12.1519

Sofroniew, M. V, & Vinters, H. V. (2010). Astrocytes: Biology and pathology. *Acta Neuropathologica*, *119*(1), 7–35. https://doi.org/10.1007/s00401-009-0619-8

Sominsky, L., De Luca, S., & Spencer, S. J. (2018). Microglia: Key players in neurodevelopment and neuronal plasticity. In *International Journal of Biochemistry and Cell Biology* (Vol. 94, pp. 56–60). Elsevier Ltd. https://doi.org/10.1016/j.biocel.2017.11.012

Spiotta, A. M., Bartsch, A. J., & Benzel, E. C. (2012). Heading in soccer: Dangerous play? In *Neurosurgery* (Vol. 70, Issue 1, pp. 1–11). https://doi.org/10.1227/NEU.0b013e31823021b2

Stein, T. D., Alvarez, V. E., & McKee, A. C. (2014). Chronic traumatic encephalopathy: A spectrum of neuropathological changes following repetitive brain trauma in athletes and military personnel. In *Alzheimer's Research and Therapy* (Vol. 6, Issue 1, pp. 1–11). BioMed Central. https://doi.org/10.1186/alzrt234

Stern, R. A., Riley, D. O., Daneshvar, D. H., Nowinski, C. J., Cantu, R. C., & McKee, A. C. (2011). Long-term Consequences of Repetitive Brain Trauma: Chronic Traumatic Encephalopathy. In *PM and R* (Vol. 3, Issue 10 SUPPL. 2). https://doi.org/10.1016/j.pmrj.2011.08.008

Stiell, I. G., Clement, C. M., Rowe, B. H., Schull, M. J., Brison, R., Cass, D., Eisenhauer, M. A., McKnight, R. D., Bandiera, G., Holroyd, B., Lee, J. S., Dreyer, J., Worthington, J. R., Reardon, M., Greenberg, G., Lesiuk, H., MacPhail, I., & Wells, G. A. (2005). Comparison of the Canadian CT head rule and the New Orleans criteria in patients with minor head injury. *Journal of the American Medical Association*, *294*(12), 1511–1518. https://doi.org/10.1001/jama.294.12.1511

Su, E., & Bell, M. (2016). Diffuse Axonal Injury. *Encyclopedia of the Neurological Sciences*, 998–999. https://doi.org/10.1016/B978-0-12-385157-4.00326-2

Taib, T., Leconte, C., Steenwinckel, J. Van, Cho, A. H., Palmier, B., Torsello, E., Kuen, R. L., Onyeomah, S., Ecomard, K., Benedetto, C., Coqueran, B., Novak, A.-C., Deou, E., Plotkine, M., Gressens, P., Marchand-Leroux, C., & Besson, V. C. (2017). Neuroinflammation, myelin and behavior: Temporal patterns following mild traumatic brain injury in mice. *PLOS ONE*, *12*(9), e0184811. https://doi.org/10.1371/JOURNAL.PONE.0184811

Talavage, T. M., Nauman, E. A., Breedlove, E. L., Yoruk, U., Dye, A. E., Morigaki, K. E., Feuer, H., & Leverenz, L. J. (2014). Functionally-detected cognitive impairment in high school football players without clinically-diagnosed concussion. *Journal of Neurotrauma*, *31*(4), 327–338. https://doi.org/10.1089/neu.2010.1512

Teasdale, G., Maas, A., Lecky, F., Manley, G., Stocchetti, N., & Murray, G. (2014). The Glasgow Coma Scale at 40 years: Standing the test of time. In *The Lancet Neurology* (Vol. 13, Issue 8, pp. 844–854). Lancet Publishing Group. https://doi.org/10.1016/S1474-4422(14)70120-6

The principles of nerve cell communication. (1997). In *Alcohol health and research world* (Vol. 21, Issue 2, pp. 107–108). National Institute on Alcohol Abuse and Alcoholism. /pmc/articles/PMC6826821/

Thomsen, G. M., Ko, A., Harada, M. Y., Ma, A., Wyss, L., Haro, P., Vit, J.-P., Avalos, P., Dhillon, N. K., Cho, N., Shelest, O., & Ley, E. J. (2017). Clinical correlates to assist with chronic traumatic encephalopathy diagnosis: Insights from a novel rodent repeat concussion model. In *Journal of Trauma and Acute Care Surgery* (Vol. 82, Issue 6). https://doi.org/10.1097/TA.0000000000001443

Tucker, L. B., Burke, J. F., Fu, A. H., & McCabe, J. T. (2017). Neuropsychiatric Symptom Modeling in Male and Female C57BL/6J Mice after Experimental Traumatic Brain Injury. *Journal of Neurotrauma*, *34*(4), 890–905. https://doi.org/10.1089/neu.2016.4508

Tweedie, D., Fukui, K., Li, Y., Yu, Q. S., Barak, S., Tamargo, I. A., Rubovitch, V., Holloway, H. W., Lehrmann, E., Wood, W. H., Zhang, Y., Becker, K. G., Perez, E., Van Praag, H., Luo, Y., Hoffer, B. J., Becker, R. E., Pick, C. G., & Greig, N. H. (2016). Cognitive impairments induced by concussive mild traumatic brain injury in mouse are ameliorated by treatment with phenserine via multiple non-cholinergic and cholinergic mechanisms. *PLoS ONE*, *11*(6). https://doi.org/10.1371/journal.pone.0156493

van Dijck, J. T. J. M., Dijkman, M. D., Ophuis, R. H., de Ruiter, G. C. W., Peul, W. C., & Polinder, S. (2019). In-hospital costs after severe traumatic brain injury: A systematic review and quality assessment. In *PLoS ONE* (Vol. 14, Issue 5). Public Library of Science. https://doi.org/10.1371/journal.pone.0216743

VanItallie, T. B. (2019). Traumatic brain injury (TBI) in collision sports: Possible mechanisms of transformation into chronic traumatic encephalopathy (CTE). *Metabolism: Clinical and Experimental*, *100*. https://doi.org/10.1016/j.metabol.2019.07.007

Velayudhan, P. S., Schwab, N., Hazrati, L. N., & Wheeler, A. L. (2021). Temporal patterns of microglial activation in white matter following experimental mild traumatic brain injury: a systematic literature review. *Acta Neuropathologica Communications*, *9*(1), 1–22. https://doi.org/10.1186/S40478-021-01297-1/FIGURES/4

Wang, G. H., Jiang, Z. L., Li, Y. C., Li, X., Shi, H., Gao, Y. Q., Vosler, P. S., & Chen, J. (2011). Free-Radical Scavenger Edaravone Treatment Confers Neuroprotection Against Traumatic Brain Injury in Rats. *Https://Home.Liebertpub.Com/Neu*, *28*(10), 2123–2134. https://doi.org/10.1089/NEU.2011.1939

Wang, G., Zhang, J., Hu, X., Zhang, L., Mao, L., Jiang, X., Liou, A. K. F., Leak, R. K., Gao, Y., & Chen, J. (2013). Microglia/macrophage polarization dynamics in white matter after traumatic brain injury. *Journal of Cerebral Blood Flow and Metabolism*, *33*(12), 1864–1874. https://doi.org/10.1038/jcbfm.2013.146

Washington, P. M., Forcelli, P. A., Wilkins, T., Zapple, D. N., Parsadanian, M., & Burns, M. P. (2012). The effect of injury severity on behavior: a phenotypic study of cognitive and emotional deficits after mild, moderate, and severe controlled cortical impact injury in mice. *Journal of Neurotrauma*, *29*(13), 2283–2296. https://doi.org/10.1089/NEU.2012.2456

Webster, K. M., Wright, D. K., Sun, M., Semple, B. D., Ozturk, E., Stein, D. G., O'Brien, T. J., & Shultz, S. R. (2015). Progesterone treatment reduces neuroinflammation, oxidative stress and brain damage and improves long-term outcomes in a rat model of repeated mild traumatic brain injury. *Journal of Neuroinflammation*, *12*(1), 1–13. https://doi.org/10.1186/S12974-015-0457-7

Weller, R. O. (2005). Microscopic morphology and histology of the human meninges. *Morphologie : Bulletin de l'Association Des Anatomistes*, *89*(284), 22–34. https://doi.org/10.1016/S1286-0115(05)83235-7

Wilson, R. (2019). Sex Differences in Behavioral Responses to Repeat Subconcussive Events. *College of Science and Health Theses and Dissertations*. https://via.library.depaul.edu/csh_etd/324

Wirth, P., Yu, W., Kimball, A. L., Liao, J., Berkner, P., & Glenn, M. J. (2017). New method to induce mild traumatic brain injury in rodents produces differential outcomes in female and male Sprague Dawley rats. *Journal of Neuroscience Methods*, *290*, 133. https://doi.org/10.1016/J.JNEUMETH.2017.07.030

Witcher, K. G., Eiferman, D. S., & Godbout, J. P. (2015). Priming the inflammatory pump of the CNS after TBI. *Trends in Neuroscience*, *38*(10), 609–620. https://doi.org/10.1002/aur.1474.Replication

Wofford, K., Loane, D., Research, D. C.-N. regeneration, & 2019, U. (2019). Acute drivers of neuroinflammation in traumatic brain injury. *Neural Regeneration Research*, *14*(9), 1481. https://www.ncbi.nlm.nih.gov/pmc/articles/pmc6557091/

Wood, R. L., Ohagan, G., Williams, C., McCabe, M., & Chadwick, N. (2014). Anxiety sensitivity and alexithymia as mediators of postconcussion syndrome following mild traumatic brain injury. *Journal of Head Trauma Rehabilitation*, *29*(1). https://doi.org/10.1097/HTR.0B013E31827EABBA

Wright, D. K., Brady, R. D., Kamnaksh, A., Trezise, J., Sun, M., McDonald, S. J., Mychasiuk, R., Kolbe, S. C., Law, M., Johnston, L. A., O'Brien, T. J., Agoston, D. V, & Shultz, S. R. (2019). Repeated mild traumatic brain injuries induce persistent changes in plasma protein and magnetic resonance imaging biomarkers in the rat. *Scientific Reports*, *9*(1). https://doi.org/10.1038/s41598-019-51267-w

Xia, L., Jiang, Z.-L., Wang, G.-H., Hu, B.-Y., & Ke, K.-F. (2012). Treatment With Ginseng Total Saponins Reduces the Secondary Brain Injury in Rat After Cortical Impact. *Journal of Neuroscience Research*, *90*(7), 1424–1436. https://doi.org/10.1002/jnr.22811

Xiong, Y., Mahmood, A., & Chopp, M. (2014). Animal models of traumatic brain injury. *Nature Reviews Neuroscience*, *14*(2), 128–142. https://doi.org/10.1038/nrn3407.Animal

Yang, L. Y., Greig, N. H., Huang, Y. N., Hsieh, T. H., Tweedie, D., Yu, Q. S., Hoffer, B. J., Luo, Y., Kao, Y. C., & Wang, J. Y. (2016). Post-traumatic administration of the p53 inactivator pifithrin-α oxygen analogue reduces hippocampal neuronal loss and improves cognitive deficits after experimental traumatic brain injury. *Neurobiology of Disease*, *96*, 216–226. https://doi.org/10.1016/J.NBD.2016.08.012

Yang, S. H., Gustafson, J., Gangidine, M., Stepien, D., Schuster, R., Pritts, T. A., Goodman, M. D., Remick, D. G., & Lentsch, A. B. (2013). A murine model of mild traumatic brain injury exhibiting cognitive and motor deficits. *Journal of Surgical Research*, *184*(2), 981–988. https://doi.org/10.1016/J.JSS.2013.03.075

Yang, Z., & Wang, K. K. W. (2015). Glial fibrillary acidic protein: From intermediate filament assembly and gliosis to neurobiomarker. In *Trends in Neurosciences* (Vol. 38, Issue 6, pp. 364–374). Elsevier Ltd. https://doi.org/10.1016/j.tins.2015.04.003

Yates, N. J., Lydiard, S., Fehily, B., Weir, G., Chin, A., Bartlett, C. A., Alderson, J., & Fitzgerald, M. (2017). Repeated mild traumatic brain injury in female rats increases lipid peroxidation in neurons. *Experimental Brain Research*, *235*(7), 2133–2149. https://doi.org/10.1007/s00221-017-4958-8

Yi, J., & Hazell, A. (2006). Excitotoxic mechanisms and the role of astrocytic glutamate transporters in traumatic brain injury. *Neurochemistry International*, *48*(5), 394–403. https://www.sciencedirect.com/science/article/pii/S0197018605002895

Yoshino, A., Hovda, D., Kawamata, T., Katayama, Y., & Becker, D. (1991). Dynamic changes in local cerebral glucose utilization following cerebral concussion in rats: evidence of a hyper-and subsequent hypometabolic state. *Brain Research*, *561*(1), 106–119. https://www.sciencedirect.com/science/article/pii/000689939190755K

Yuan, M., & Wu, H. (2022). Astrocytes in the Traumatic Brain Injury: the Good and the Bad. *Experimental Neurology*, *348*, 113943. https://doi.org/10.1016/J.EXPNEUROL.2021.113943

Zacko, J. C., Hawryluk, G. W. J., & Bullock, M. R. (2011). Neurochemical Pathomechanisms in Traumatic Brain Injury. In *Youmans Neurological Surgery* (pp. 3305–3324). Elsevier. https://doi.org/10.1016/B978-1-4160-5316-3.00331-2

Zhang, D., Hu, X., Qian, L., O'Callaghan, J. P., & Hong, J. S. (2010). Astrogliosis in CNS pathologies: Is there a role for microglia? *Molecular Neurobiology*, *41*(2–3), 232–241. https://doi.org/10.1007/S12035-010-8098-4/FIGURES/2

Zhang, F., Wu, H., Jin, Y., & Zhang, X. (2018). Proton Magnetic Resonance Spectroscopy (H1-MRS) Study of the Ketogenic Diet on Repetitive Mild Traumatic Brain Injury in Adolescent Rats and Its Effect on Neurodegeneration. *World Neurosurgery*, *120*, e1193–e1202. https://doi.org/10.1016/j.wneu.2018.09.037

Zhao, G. W., Wang, Y., Li, Y. C., Jiang, Z. L., Sun, L., Xi, X., He, P., Wang, G. H., Xu, S. H., Ma, D. M., & Ke, K. F. (2014). The neuroprotective effect of modified "Shengyu" decoction is mediated through an anti-inflammatory mechanism in the rat after traumatic brain injury. *Journal of Ethnopharmacology*, *151*(1), 694–703. https://doi.org/10.1016/J.JEP.2013.11.041

Zhou, Y., Shao, A., Yao, Y., Tu, S., Deng, Y., & Zhang, J. (2020). Dual roles of astrocytes in plasticity and reconstruction after traumatic brain injury. *Cell Communication and Signaling 2020 18:1*, *18*(1), 1–16. https://doi.org/10.1186/S12964-020-00549-2

Ziebell, J., & Morganti-Kossmann, M. (2010). Involvement of pro-and anti-inflammatory cytokines and chemokines in the pathophysiology of traumatic brain injury. *Neurotherapeutics*, *7*(1), 22–30. https://www.sciencedirect.com/science/article/pii/S1933721309002177

Zonta, M., Angulo, M. C., Gobbo, S., Rosengarten, B., Hossmann, K. A., Pozzan, T., & Carmignoto, G. (2003). Neuron-to-astrocyte signaling is central to the dynamic control of brain microcirculation. *Nature Neuroscience*, *6*(1), 43–50. https://doi.org/10.1038/nn980

# APPENDIX A

# IACUC APPROVAL LETTER

MISSISSIPPI STATE UNIVERSITY

**Office of Research Compliance**
Institutional Animal Care and Use Committee

P.O. Box 6223
53 Morgan Avenue
Mississippi State, MS 39762
P. 662.325.3294

**www.orc.msstate.edu**

January 22, 2021

Suminto To

Ag & Bio Engineering

Re: Protocol # **IACUC-20-456**

Dear Suminto:

The Mississippi State Institutional Animal Care and Use Committee (IACUC) has completed it's review of your protocol titled Rodent Model Study for Single mTBI v. Repeated Subconcussive Blunt Impacts. In light of federal policies on the care and use of animals in research and requirements established specifically for the Institute, the committee has chosen to grant approval of this protocol on January 19, 2021. The expiration date for this project will be January 20, 2024 and the approval number is IACUC-20-456.

If you would like to involve additional members in this protocol or change aspects of the protocol in the future, please submit a Protocol Amendment Form for review.

Concurrent with this approval, please be advised the MSU-IACUC holds the principal investigator(s) named in this protocol responsible in ensuring that each procedure described in the protocol will be followed exactly (unless amended and such amendment is approved by the IACUC before implementation).

If the animal care and use aspects of this study change, approval of a new protocol or of an amendment is necessary. The project must be reviewed by the IACUC annually with the number of animals used during the year reported to the IACUC on the annual update form. When the project is complete, please notify the IACUC Administrator, Trina Smith, at 325-0994.

The committee appreciates your cooperation and wish you continued good luck in your research endeavors.

Sincerely,

Brian Rude

Chair, IACUC

brude@ads.msstate.edu

Figure A.1 IACUC approval letter for experimental studies.

# APPENDIX B

# PILOT STUDY: IRREGULAR STAINING OF GFAP AND IBA-1 SLIDES

## B.1 Methods

Each GFAP and Iba-1 immunostained tissue section on a slide was scanned using a PathScan Enabler 5 (Meyer Instruments, Houston, TX, USA) whole slide scanner and then processed in HistoView software, (Pacific Image Electronics Inc., CA USA). Representative images for GFAP and Iba-1 immunostained tissue sections were selected based on tissue sections with uneven staining across the tissue. The scans were not used for analytical purposes but allowed spatial context for visualization of unevenness in staining.

## B.2 Results

Figures B.1 and B.2 show representative GFAP and Iba-1 immunostained tissue images from each experimental group of the pilot study. As seen in each representative image (Figure B.1 and B.2), there is noticeable unevenness in staining. Visually, the proportion of GFAP+ (brown colored stain) often varied between cerebral hemispheres (Figure B.1a, b, and f), while other sections showed disproportion of staining at an angle (Figure B.1c, d, and e). Similarly, the proportion of Iba-1+ also showed inconsistencies at an angle (Figure B.2).

As a result, a criterion was set to determine the appropriate tissue section and hemisphere of the cerebral tissue for properly stained regions of interest (DG, CA1, and CA3). The criteria for selecting the appropriate section and hemisphere of the cingulum were based on the stained areas that had evidence of correctly stained internal control (cells around blood vessels). Whichever section and hemisphere met this criterion, was marked for moving forward with cell count image analysis.

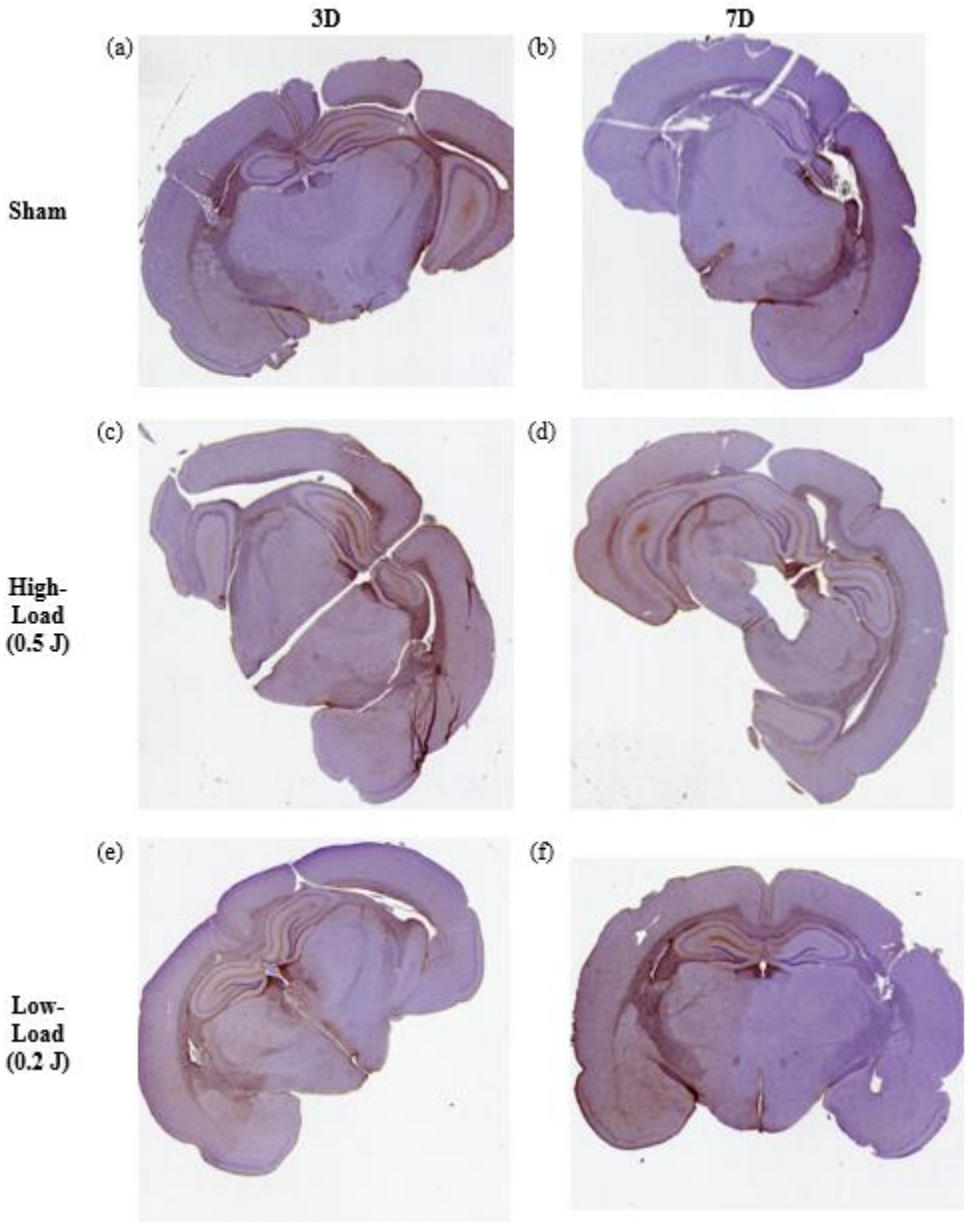


Figure B.1 Representative GFAP micrographs (4x) of each group according to recovery days that show disproportion in GFAP+ staining.

Micrographs (4x) of GFAP expression at 3- (a, c, and e) and 7-DPI (b, d, and f) for sham, high (0.5J), and low (0.2J) impact recovery groups.

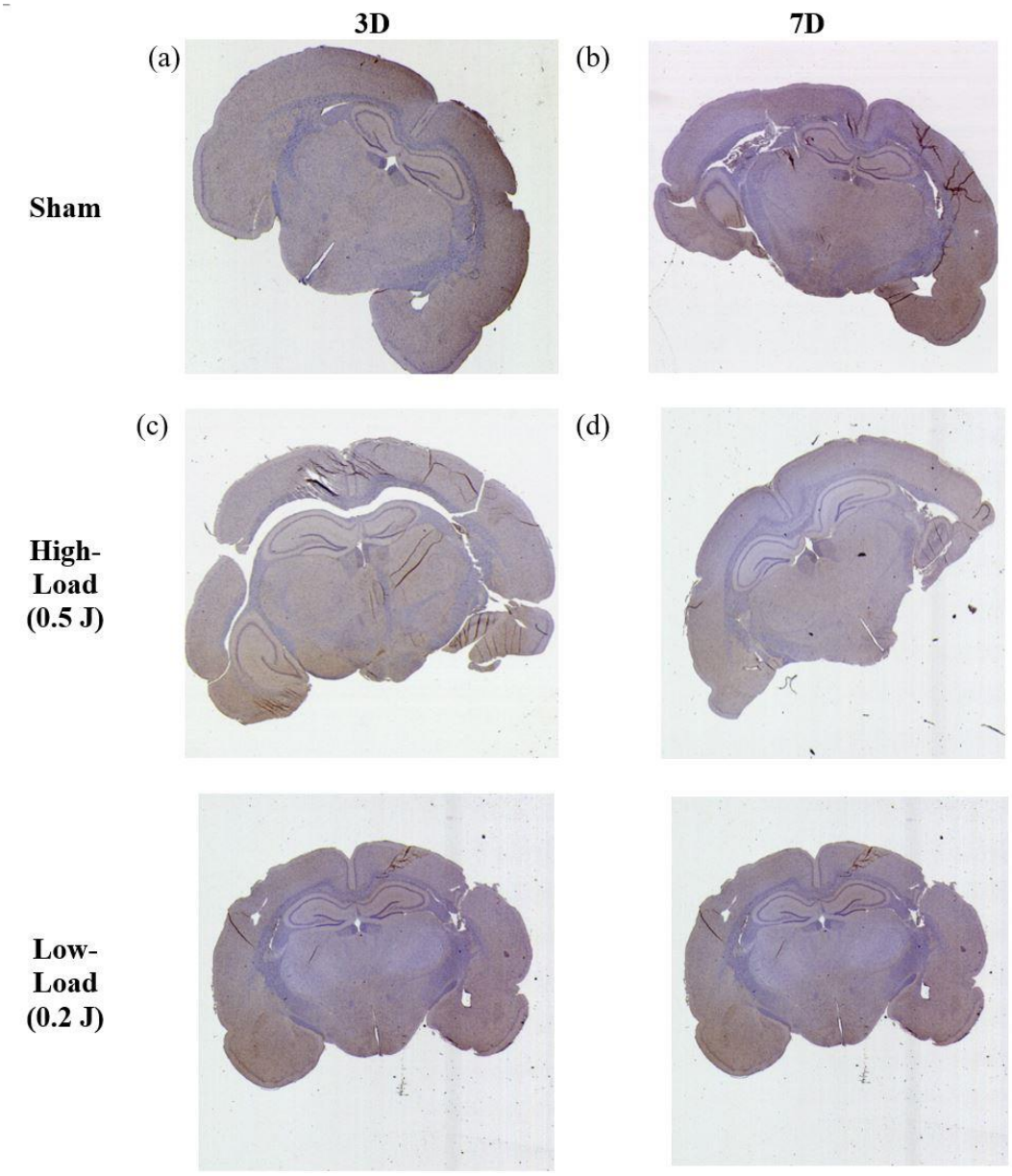


Figure B.2 Representative Iba-1 micrographs (4x) of each group according to recovery days depicting the irregularity of Iba-1+ staining.

Micrographs (4x) of Iba-1 expression at 3- (a, c, and e) and 7-DPI (b, d, and f) for sham, high (0.5J), and low (0.2J) impact recovery groups.

# APPENDIX C

## PILOT STUDY: REPRESENTATIVE MICROGRAPHS FOR GFAP AND IBA-1

## C.1 Methods

Representative micrographs (20x magnification) for GFAP and Iba-1 immunostained tissue sections were selected based on tissue sections with a positive cell count measurement most representative of the mean positive cell count for each group. Selected representative 20x magnification micrographs are presented for injury (High3, Low3, High7, and Low7) and sham groups (Sham3 and Sham7) for each hippocampal region of interest (DG, CA1, and CA3) for both Iba-1 and GFAP in conjunction with a representative 4x magnification image for reference. For this section, animal groups are labeled as follows: High-load impact groups (0.5 J mTBI), Low-load impact groups (0.2 J mTBI), and Sham recovery groups (Sham). Lastly, the 4x magnification micrograph was not used for analytical purposes but allows spatial context for higher magnification micrographs.

## C.2 Results

### C.2.1 GFAP Micrographs

Representative GFAP micrographs at 4x magnification are presented for DG (Figure C.1a), CA1 (Figure C.2a), and CA3 (Figure C.3a) with a representative imaging location for each indicated with a black box. The average number of positive GFAP cells for all sample images of the hippocampal regions of interest were referred to in selecting representative 20x magnification micrographs. For each representative GFAP 20x magnification micrograph, a representative astrocyte expressing positive GFAP immunoreactivity is indicated by a black arrow.

Despite the unevenness in staining (Appendix B), the representative GFAP micrographs (20x magnification) of each region of interest illustrate that the sections were able to undergo

image analysis of immunoreactivity of astrocytes via cell count. As seen in the number of positive cells plot for DG (Figure 4.10a), the representative micrographs (20x magnification) shown in Figure E.1b-g do not show observable differences between groups by or between recovery days. Furthermore, this is confirmed visually, as the proportion of GFAP+ (brown colored stain) is not different between recovery groups (Figure C.1d-g) or sham (Figure C.1b-c), regardless of recovery day.

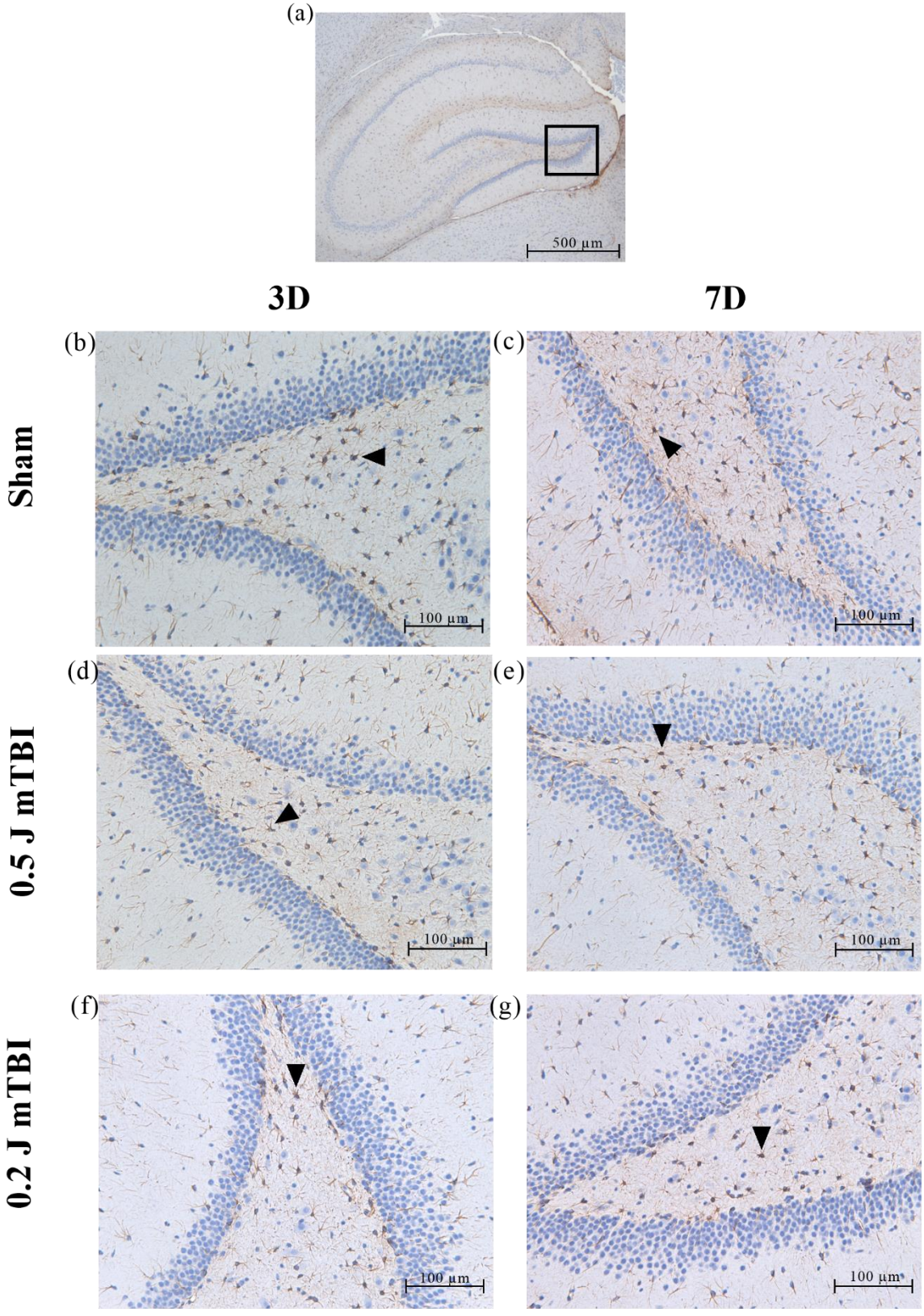
(a)
500 µm
3D
7D
Sham
0.5 J mTBI
0.2 J mTBI
(b)
(c)
(d)
(e)
(f)
(g)
100 µm

Figure C.1 Representative GFAP micrographs of DG.

Rats were subjected to sham or closed-head mTBI impact (either 0.5 or 0.2 J) and euthanized at 3- or 7-DPI. The (a) location of the DG representative images is presented using 4x magnification with a 500μm scale bar. Micrographs (20x) of GFAP expression in dentate gyrus region at 3- (b, d, and f) and 7-DPI (c, e, and g) for sham, high (0.5J), and low (0.2J) impact recovery groups with a 100μm scale bar. A representative astrocyte expressing positive GFAP immunoreactivity is indicated for each 20x magnification micrograph by a black arrowhead.

Figure C.2 shows a representative GFAP micrograph of the hippocampus at 4x magnification with a representative CA1 imaging location indicated by a black box. While the representative 20x magnification micrographs of CA1 visually reflect significant variations of the intensity/darkness of the DAB stain in injury groups (see Figures C.2e,f), the reader must understand that the measurements were based off positive cell counts of GFAP rather than staining intensity. As such, data indicated no significant variations of GFAP positive cell count analysis within the CA1 region between all experimental groups, regardless of recovery day.

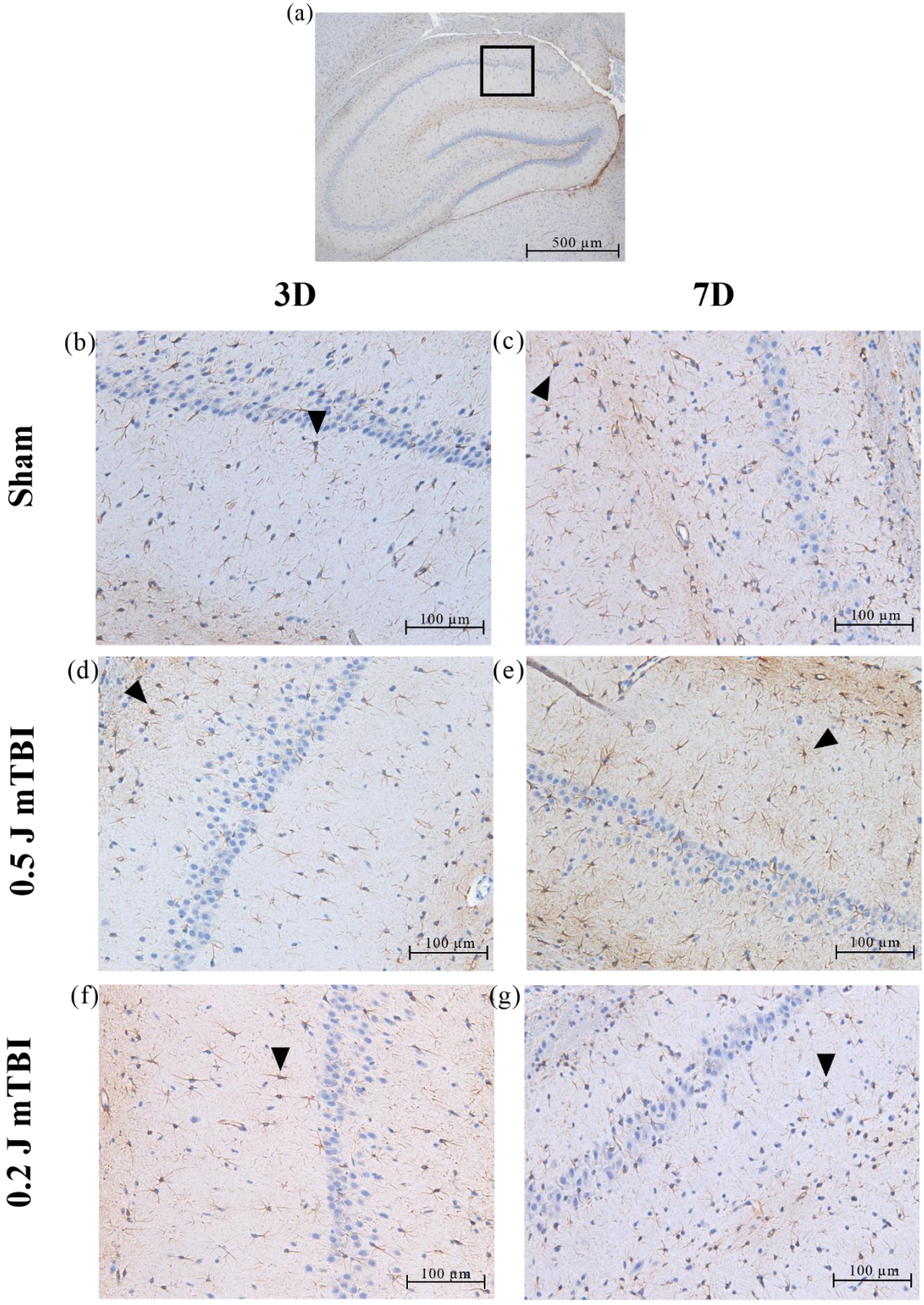
(a)
500 µm
3D
7D
Sham
0.5 J mTBI
0.2 J mTBI
(b)
(c)
(d)
(e)
(f)
(g)
100 µm

Figure C.2 Representative GFAP micrographs of CA1.

Rats were subjected to sham or closed-head mTBI impact (either 0.5 or 0.2 J) and euthanized at 3- or 7-DPI. The (a) location of the representative images is presented using 4x magnification with a 500μm scale bar. Micrographs (20x) of GFAP expression in CA1 region at 3- (b, d, and f) and 7-DPI (c, e, and g) for sham, high (0.5J), and low (0.2J) impact recovery groups with a 100μm scale bar. A representative astrocyte expressing positive GFAP immunoreactivity is indicated for each 20x magnification micrograph by a black arrowhead.

Figure C.3 shows a representative GFAP micrograph of the hippocampus at 4x magnification with a representative CA3 imaging location indicated by a black box. Again, the representative 20x magnification micrographs of CA3 visually reflect the insignificant variations seen in the GFAP positive cell count analysis of CA3 (Figure 4.10c) when comparing injury (Figure C.3d-g) and sham (Figure C.3b-c) groups, regardless of recovery day.

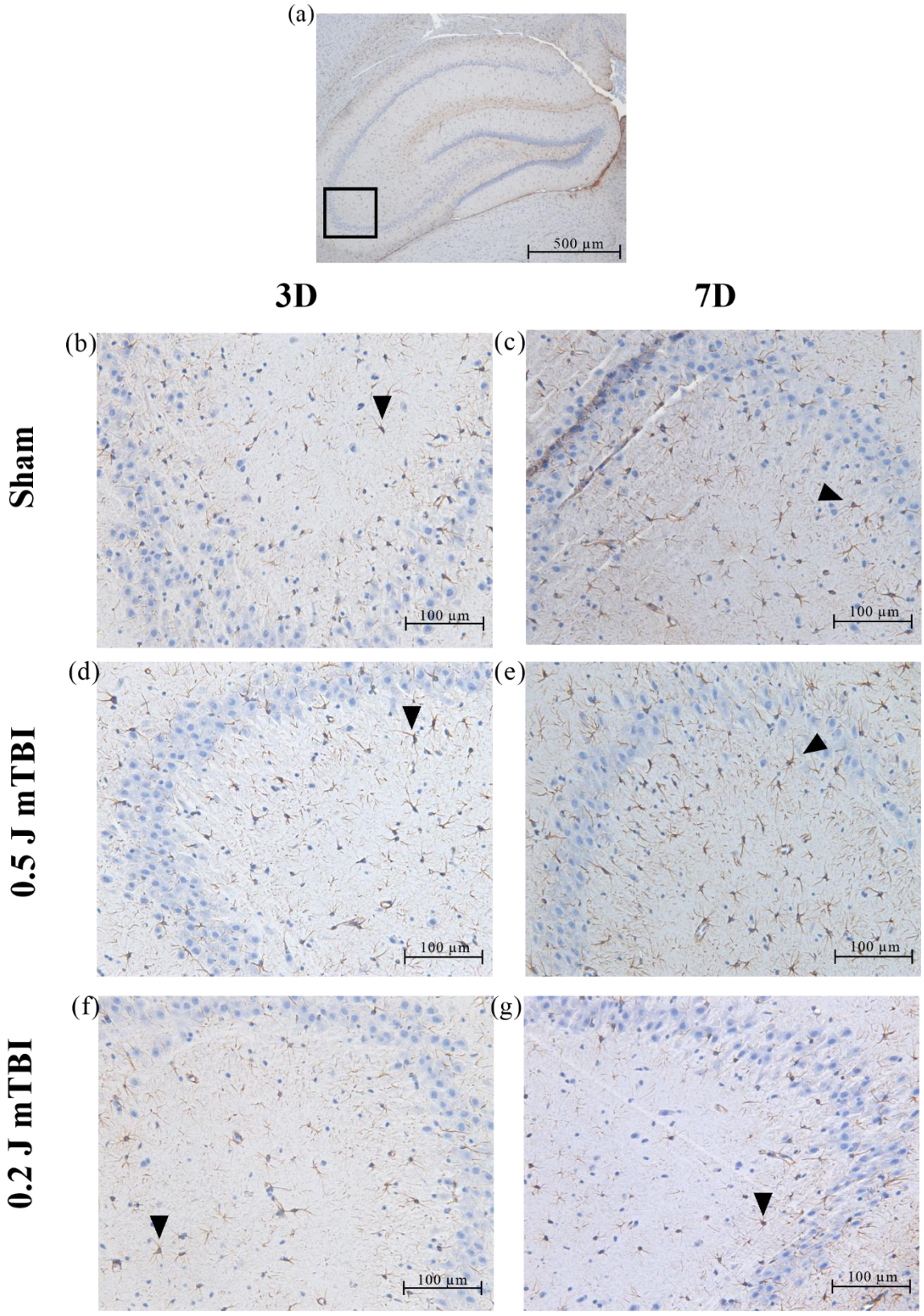
(a)
500 µm
3D
7D
Sham
0.5 J mTBI
0.2 J mTBI
(b)
(c)
(d)
(e)
(f)
(g)
100 µm

Figure C.3 Representative GFAP micrographs of CA3

Rats were subjected to sham or closed-head mTBI impact (either 0.5 or 0.2 J) and euthanized at 3- or 7-DPI. The (a) location of the representative images is presented using 4x magnification with a 500μm scale bar. Micrographs (20x) of GFAP expression in CA3 region at 3- (b, d, and f) and 7-DPI (c, e, and g) for sham, high (0.5J), and low (0.2J) impact recovery groups with a 100μm scale bar. A representative astrocyte expressing positive GFAP immunoreactivity is indicated for each 20x magnification micrograph by a black arrowhead.

### C.2.2 Iba-1 Micrographs

Similarly seen in GFAP immunostained tissue images immunostained tissue images(Figure B.1), Iba-1 immunostained tissue images also showed evidence of disproportional staining (Figure B.2). Still, representative Iba-1 micrographs (20x magnification) of the three regions of interest illustrated that the sections were able to undergo image analysis of immunoreactivity of microglia via positive cell count. Representative Iba-1 micrographs at 4x magnification are presented for DG (Figure C.4a), CA1 (Figure C.5a), and CA3 (Figure C.6a) with a representative imaging location for each indicated with a black box. A representative astrocyte expressing positive Iba-1 immunoreactivity is indicated for each 20x magnification micrograph by a black arrow.

The proportion of positive Iba-1 immunoreactivity (brown color) within the DG tissue section did not show significant differences between groups within recovery groups as well as

between recovery day groups (Figure 4.11a).

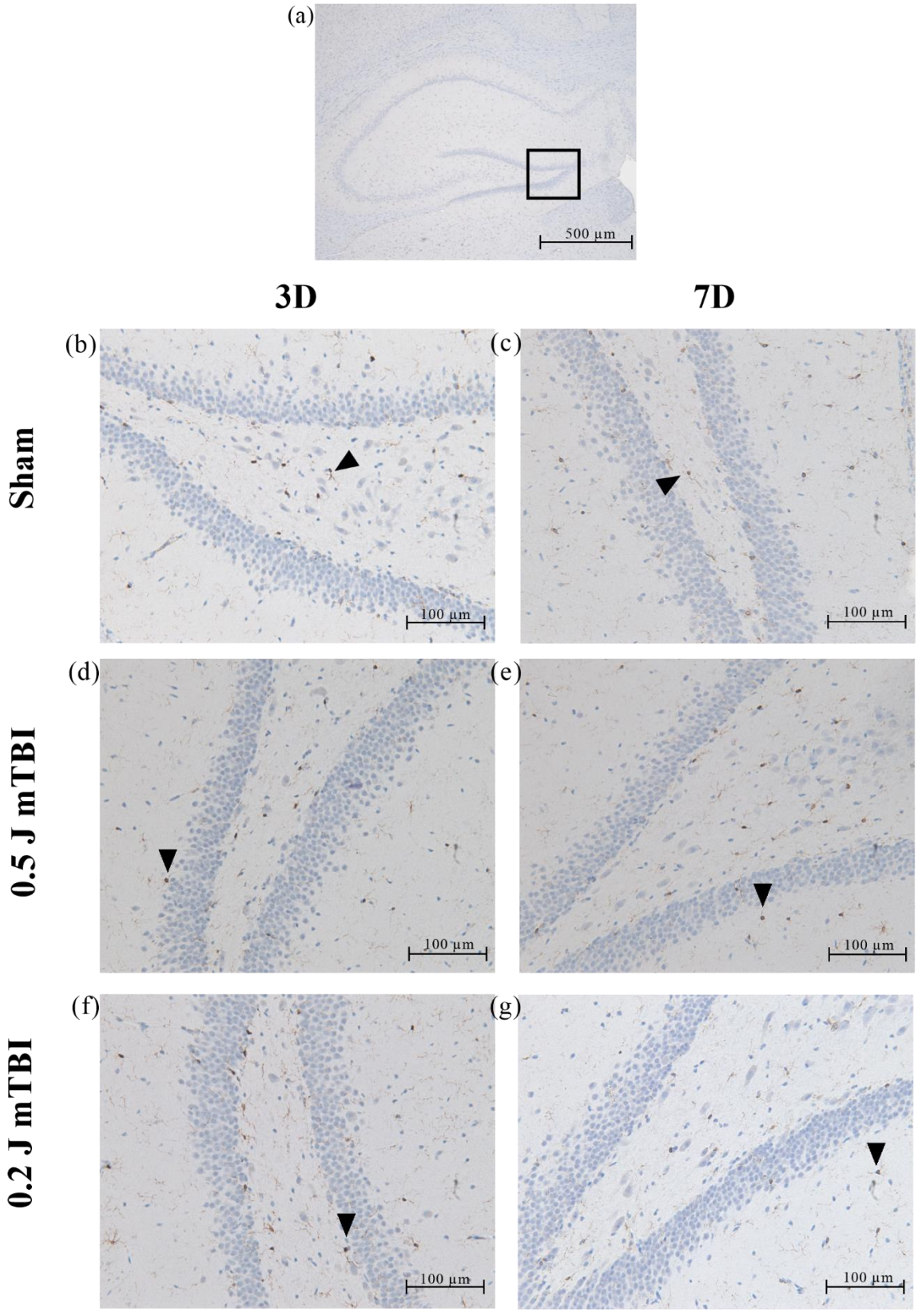
(a)
500 μm
3D
7D
Sham
(b)
(c)
100 μm
100 μm
0.5 J mTBI
(d)
(e)
100 μm
100 μm
0.2 J mTBI
(f)
(g)
100 μm
100 μm

Figure C.4 Representative Iba-1 micrographs of DG.

Rats were subjected to sham or closed-head mTBI impact (either 0.5 or 0.2 J) and euthanized at 3- or 7-DPI. The (a) location of the representative images is presented using 4x magnification with a 500μm scale bar. Micrographs (20x) of Iba-1 expression in dentate dyrus region at 3- (b, d, and f) and 7-DPI (c, e, and g) for sham, high (0.5J), and low (0.2J) impact recovery groups with a 100μm scale bar. A representative microglial cell expressing positive Iba-1 immunoreactivity is indicated for each 20x magnification micrograph by a black arrowhead.

Figure C.5 shows a representative Iba-1 micrograph of the hippocampus at 4x magnification with a representative CA1 imaging location indicated by a black box. As seen in the number of positive cells plot for CA1 (Figure 4.11b), the representative micrographs (20x magnification) shown in Figure C.5b-g do not show observable differences between groups by or between recovery days. Furthermore, this is confirmed visually, as the proportion of Iba-1+ cells (brown colored stain) are not different between recovery groups (Figure C.5d-g) or sham (Figure C.5b-c), regardless of recovery day.

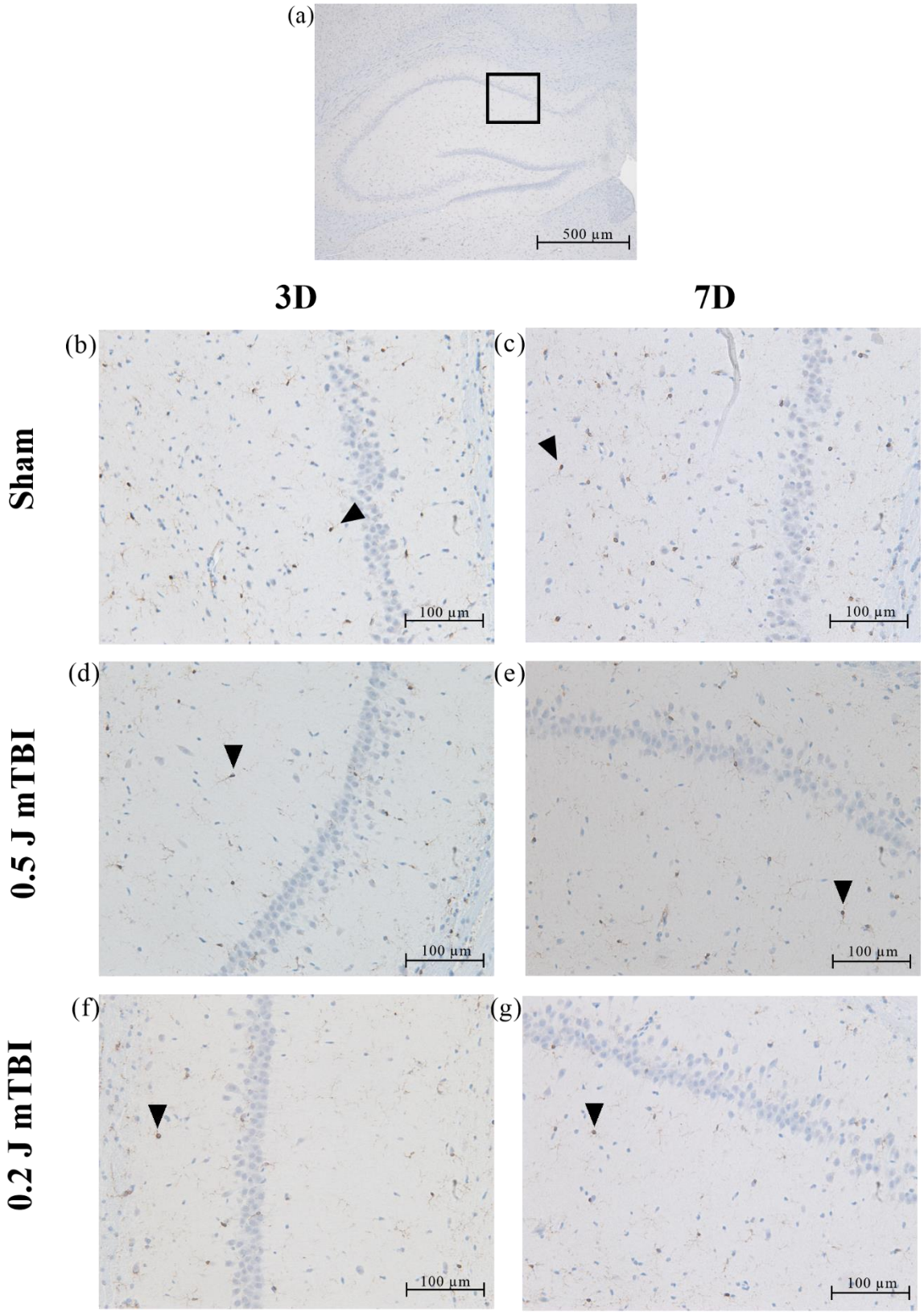
(a)
500 µm
3D
7D
Sham
(b)
(c)
100 µm
0.5 J mTBI
(d)
(e)
100 µm
0.2 J mTBI
(f)
(g)
100 µm

Figure C.5 Representative Iba-1 micrographs of CA1.

Rats were subjected to sham or closed-head mTBI impact (either 0.5 or 0.2 J) and euthanized at 3- or 7-DPI. The (a) location of the representative images is presented using 4x magnification with a 500μm scale bar. Micrographs (20x) of Iba-1 expression in CA1 region at 3- (b, d, and f) and 7-DPI (c, e, and g) for sham, high (0.5J), and low (0.2J) impact recovery groups with a 100μm scale bar. A representative microglial cell expressing positive Iba-1 immunoreactivity is indicated for each 20x magnification micrograph by a black arrowhead.

Although not easily appreciated by the representative Iba-1 micrographs (20x magnification) for CA3, on average the proportion of positive Iba-1 immunoreactivity for the 7-day recovery high impact group (Figure C.6e) was notably greater than the 3-day recovery high impact group (Figure C.6d). Notably, with respect to the proportion of Iba-1 immunoreactivity (brown colored stain, not intensity/darkness of stain), the representative CA1 micrographs of the high-load impact recovery groups are not easily reflected visually. This difficulty in visual observation might be due to the low intensity/staining of positive cells for Iba-1 immunoreactivity, and thus does not adequately reflect the results obtained for cell count analysis of CA3 (Figure 4.11c).

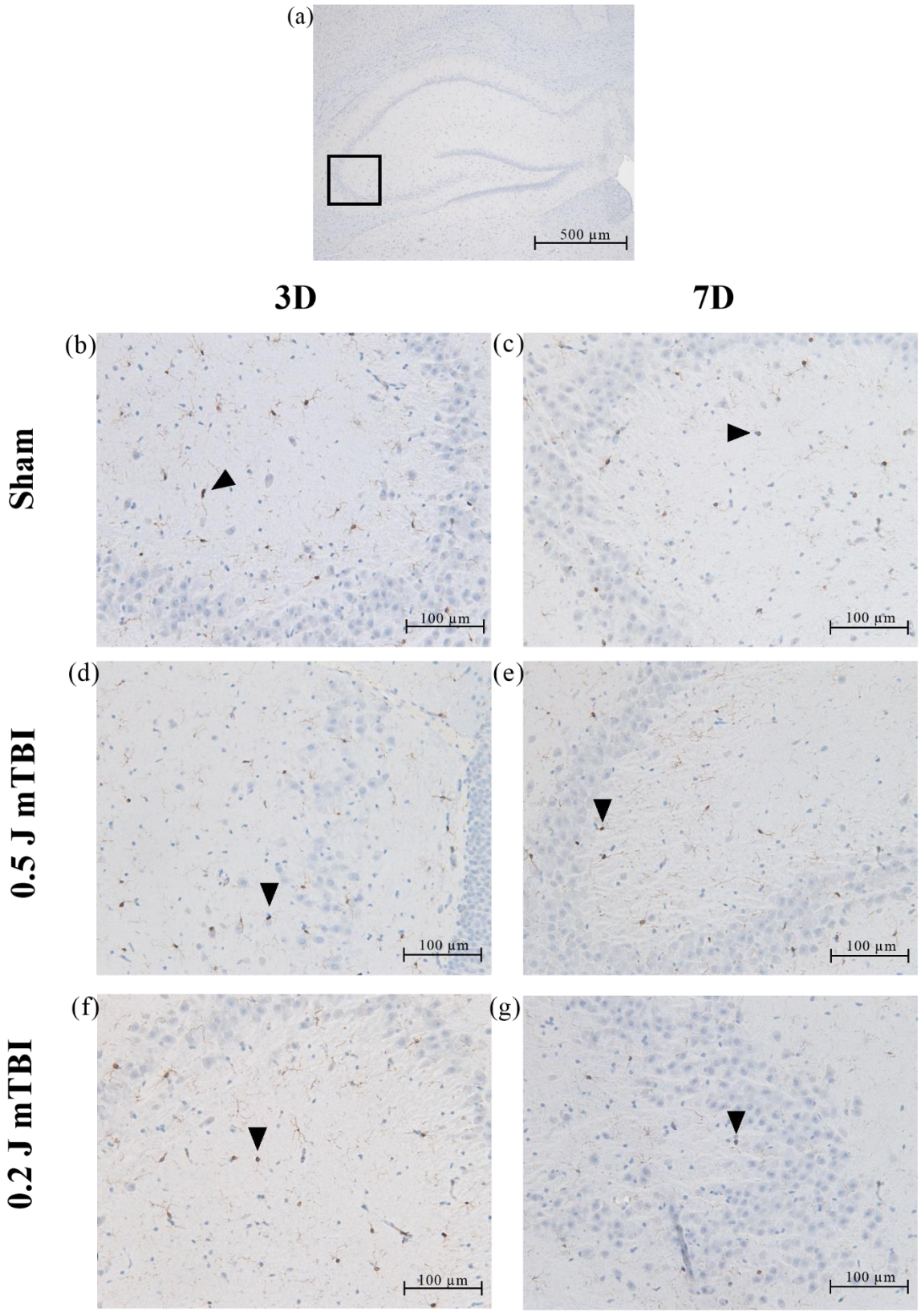
(a)
500 µm
3D
7D
Sham
0.5 J mTBI
0.2 J mTBI
(b)
(c)
(d)
(e)
(f)
(g)
100 µm

Figure C.6 Representative Iba-1 micrographs of CA3.

Rats were subjected to sham or closed-head mTBI impact (either 0.5 or 0.2 J) and euthanized at 3- or 7-DPI. The (a) location of the representative images is presented using 4x magnification with a 500μm scale bar. Micrographs (20x) of Iba-1 expression in CA3 region at 3- (b, d, and f) and 7-DPI (c, e, and g) for sham, high (0.5J), and low (0.2J) impact recovery groups with a 100μm scale bar. A representative microglial cell expressing positive Iba-1 immunoreactivity is indicated for each 20x magnification micrograph by a black arrowhead.

# APPENDIX D

# PILOT STUDY: MULTIPLEX ASSAY PLATE SET UP AND RESULTS

## D.1 Methods

Table D.1 Procartaplex Plate Setup.

| | 1 | 2 | 3 | 4 | 5 | 6 | 7 | 8 | 9 |
|---|---|---|---|---|---|---|---|---|---|
| A | Std1 | Std1 | H3_1 HPC | H3_3 MC | L3_3 HPC | S3_3 HPC | H7_2 MC | L7_2 HPC | S7_2 HPC |
| B | Std2 | Std2 | H3_1 HPC | L3_1 HPC | L3_3 MC | S3_3 HPC | H7_3 HPC | L7_2 MC | S7_2 MC |
| C | Std3 | Std3 | H3_1 MC | L3_1 HPC | S3_1 HPC | S3_3 MC | H7_3 HPC | L7_3 HPC | S7_3 HPC |
| D | Std4 | Std4 | H3_2 HPC | L3_1 MC | S3_1 MC | H7_1 HPC | H7_3 MC | L7_3 HPC | S7_3 HPC |
| E | Std5 | Std5 | H3_2 HPC | L3_2 HPC | S3_1 MC | H7_1 HPC | H7_3 MC | L7_3 MC | S7_3 MC |
| F | Std6 | Std6 | H3_2 MC | L3_2 HPC | S3_2 HPC | H7_1 MC | L7_1 HPC | S7_1 HPC | |
| G | Std7 | Std7 | H3_3 HPC | L3_2 MC | S3_2 HPC | H7_2 HPC | L7_1 HPC | S7_1 HPC | |
| H | Std8 | Std8 | H3_3 HPC | L3_3 HPC | S3_2 MC | H7_2 MC | L7_1 MC | S7_2 HPC | |

Note, H3, L3, S3, H7, L7, and S7 represents High3, Low3, Sham3, High7, Low7, and Sham7 group animals, respectively. Furthermore, HPC and MC represent tissue from the hippocampus and motor cortex regions, respectively.

## D.2 Results

Table D.2 Level of detection for analytes, IL-6, TNF-α, and IL-10 from pilot study.

| **Plate Location** | **Well/Animal Information** | **IL-6 (pg/ml)** | **TNFα (pg/ml)** | **IL-10 (pg/ml)** |
|---|---|---|---|---|
| A1 & A2 | Avg Standard 1 | NA | NA | Invalid curve fit |
| B1 & B2 | Avg Standard 2 | NA | NA | Invalid curve fit |
| C1 & C2 | Avg Standard 3 | 513.989 | 2899.686 | Invalid curve fit |
| D1 & D2 | Avg Standard 4 | 173.958 | 291.984 | Invalid curve fit |
| E1 & E2 | Avg Standard 5 | NA | 68.025 | Invalid curve fit |
| F1 & F2 | Avg Standard 6 | 14.917 | 13.503 | Invalid curve fit |
| G1 & G2z | Avg Standard 7 | 64.266 | 5.288 | Invalid curve fit |
| A3 | H3_1 HPC | <0 | <0 | NA |
| B3 | H3_1 HPC | 12.681 | <0 | NA |
| C3 | H3_1 MC | <0 | NaN | NaN |
| D3 | H3_2 HPC | <0 | NaN | NaN |
| E3 | H3_2 HPC | NaN | 0.852 | NA |
| F3 | H3_2 MC | <0 | <0 | NA |
| G3 | H3_3 HPC | <0 | 0.727 | NA |
| H3 | H3_3 HPC | <0 | <0 | NA |
| A4 | H3_3 MC | <0 | 0.52 | NA |
| B4 | L3_1 HPC | 3.035 | <0 | NA |
| C4 | L3_1 HPC | 8.405 | NaN | NaN |

Table E.2 (continued)

| | | | | |
|---|---|---|---|---|
| D4 | L3_1 MC | <0 | <0 | NA |
| E4 | L3_2 HPC | <0 | NaN | NaN |
| F4 | L3_2 HPC | NaN | NaN | NaN |
| G4 | L3_2 MC | <0 | 1.743 | NA |
| H4 | L3_3 HPC | <0 | <0 | NA |
| A5 | L3_3 HPC | <0 | <0 | NA |
| B5 | L3_3 MC | 55.287 | 0.267 | NA |
| C5 | S3_1 HPC | NaN | 1.402 | NaN |
| D5 | S3_1 MC | <0 | <0 | NaN |
| E5 | S3_1 MC | 0.63 | <0 | NaN |
| F5 | S3_2 HPC | 32.516 | <0 | NA |
| G5 | S3_2 HPC | 32.516 | <0 | NA |
| H5 | S3_2 MC | <0 | <0 | NA |
| A6 | S3_3 HPC | <0 | <0 | NA |
| B6 | S3_3 HPC | 201.899 | <0 | NA |
| C6 | S3_3 MC | NaN | <0 | NA |
| D6 | H7_1 HPC | NaN | NaN | NaN |
| E6 | H7_1 HPC | <0 | <0 | NA |
| F6 | H7_1 MC | <0 | <0 | NaN |
| G6 | H7_2 HPC | <0 | <0 | NA |
| H6 | H7_2 MC | <0 | <0 | NA |
| A7 | H7_2 MC | <0 | <0 | NA |
| B7 | H7_3 HPC | 1.792 | 1.193 | NaN |
| C7 | H7_3 HPC | <0 | <0 | NA |
| D7 | H7_3 MC | <0 | <0 | NA |
| E7 | H7_3 MC | 11.238 | <0 | NA |
| F7 | L7_1 HPC | <0 | <0 | NA |
| G7 | L7_1 HPC | <0 | <0 | NA |
| H7 | L7_1 MC | 14.14 | 0.157 | NA |
| A8 | L7_2 HPC | <0 | NaN | NaN |
| B8 | L7_2 MC | <0 | <0 | NA |
| C8 | L7_3 HPC | <0 | NaN | NA |
| D8 | L7_3 HPC | NaN | NaN | NaN |
| E8 | L7_3 MC | NaN | NaN | NaN |
| F8 | S7_1 HPC | 56.952 | <0 | NA |
| G8 | S7_1 HPC | <0 | <0 | NA |
| H8 | S7_2 HPC | <0 | <0 | NA |
| A9 | S7_2 HPC | 27.799 | <0 | NaN |
| B9 | S7_2 MC | <0 | <0 | NA |
| C9 | S7_3 HPC | <0 | <0 | NA |
| D9 | S7_3 HPC | 8.405 | <0 | NA |
| E9 | S7_3 MC | 53.625 | <0 | NA |

Under “Well/Animal Information,” H3, L3, S3, H7, L7, and S7 represents High3, Low3, Sham3, High7, Low7, and Sham7 group animals, respectively. Furthermore, HPC and MC represent tissue from the hippocampus and motor cortex regions, respectively.

All IL-1, IL-10, and Tumour necrosis factor alpha values for injury and sham groups were below threshold for detection for each recovery time in the study.

# APPENDIX E

## FULL STUDY: REPRESENTATIVE MICROGRAPHS FOR NEUN, GFAP, AND IBA-1

## E.1 Methods

Representative micrographs (20x magnification) for NeuN, GFAP and Iba-1 immunostained tissue sections were selected based on tissue sections with a positive cell count measurement most representative of the mean positive cell count for each group. Selected representative 20x magnification micrographs are presented for injury ($mTBI_3$, $RSC_3$, $mTBI_7$, and $RSC_7$) and sham groups ($Sham_3$, $RSham_3$, $Sham_7$, and $RSham_7$) for each hippocampal region of interest (DG, CA1, and CA3) for all three stains in conjunction with a representative 4x magnification image for reference. The 4x magnification micrograph was not used for analytical purposes but allows spatial context for higher magnification micrographs.

## E.2 Results

### E.2.1 NeuN Micrographs

Representative NeuN micrographs at 4x magnification are presented for DG (Figure E.1a), CA1 (Figure E.2a), and CA3 (Figure E.3a) with a representative imaging location for each indicated with a black box. The average number of positive NeuN cells for all sample images of the hippocampal regions of interest were referred to in selecting representative 20x magnification micrographs. For each representative NeuN 20x magnification micrograph, a representative neuron expressing positive NeuN immunoreactivity is indicated by a black arrow.

As seen in the number of positive cells plot for the DG, CA1, and CA3 regions (Figure 5.6A-C), the representative micrographs (20x magnification) shown in Figures E.1-3b-i do not show observable differences between groups by or between recovery days. Furthermore, this is confirmed visually, as the proportion of NeuN+ (brown colored stain) is not different between injury (Figure E.1-3f-i) or sham (Figure E.1-3b-e) groups, regardless of recovery day.

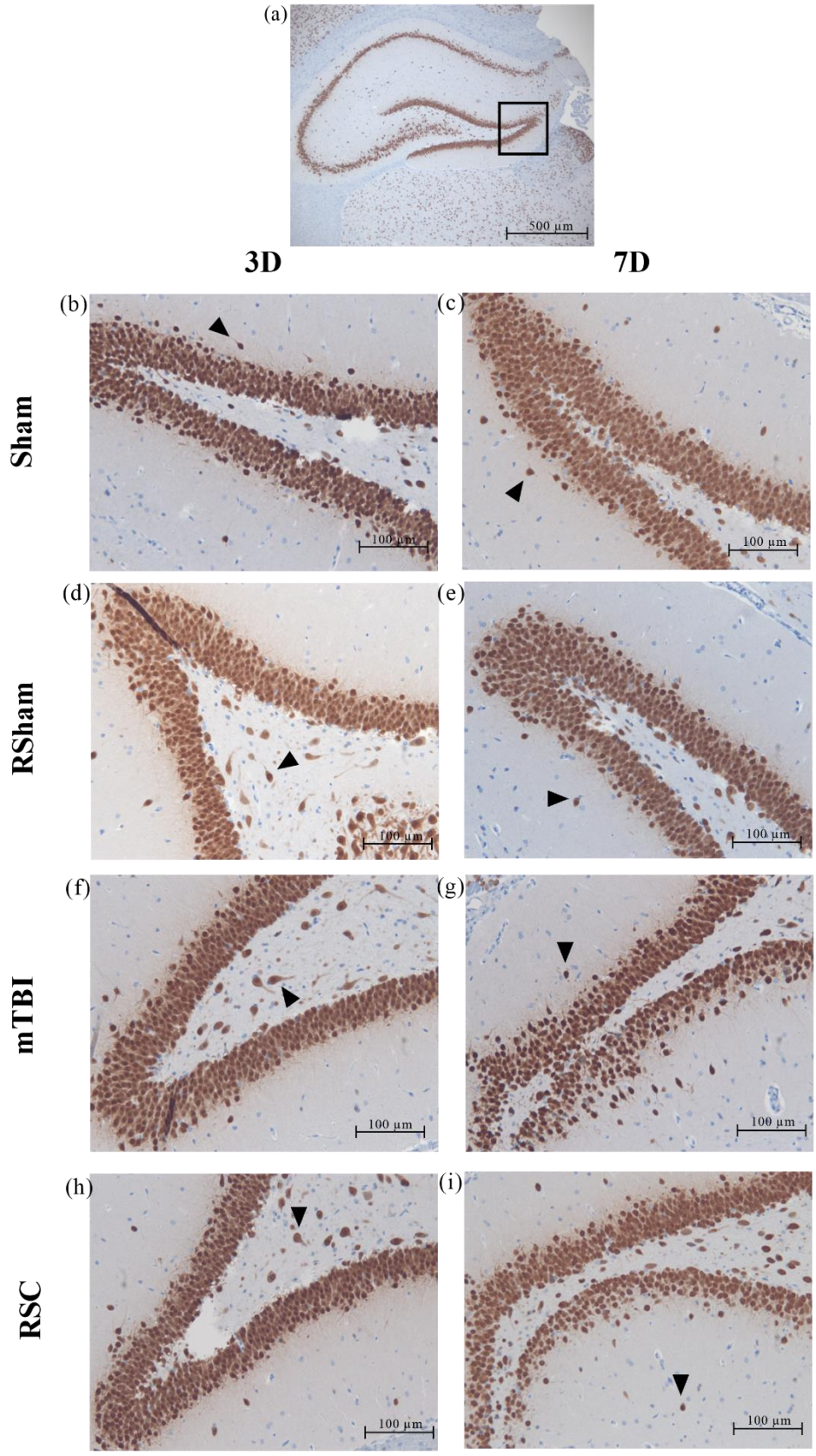
(a)
500 µm
3D
7D
Sham
RSham
mTBI
RSC
(b)
(c)
(d)
(e)
(f)
(g)
(h)
(i)
100 µm

Figure E.1 Representative NeuN micrographs of DG.

Rats were subjected to sham or closed-head impact(s) and euthanized at either 3- or 7-DPI. The (a) location of the DG representative images is presented using 4x magnification with a 500μm scale bar. Micrographs (20x) of NeuN expression in dentate gyrus region at 3- (b, d, f, and h) and 7-DPI (c, e, g, and i) for Sham, RSham, mTBI, and RSC impact recovery groups with a 100μm scale bar. A representative neuron expressing positive NeuN immunoreactivity is indicated for each 20x magnification micrograph by a black arrowhead.

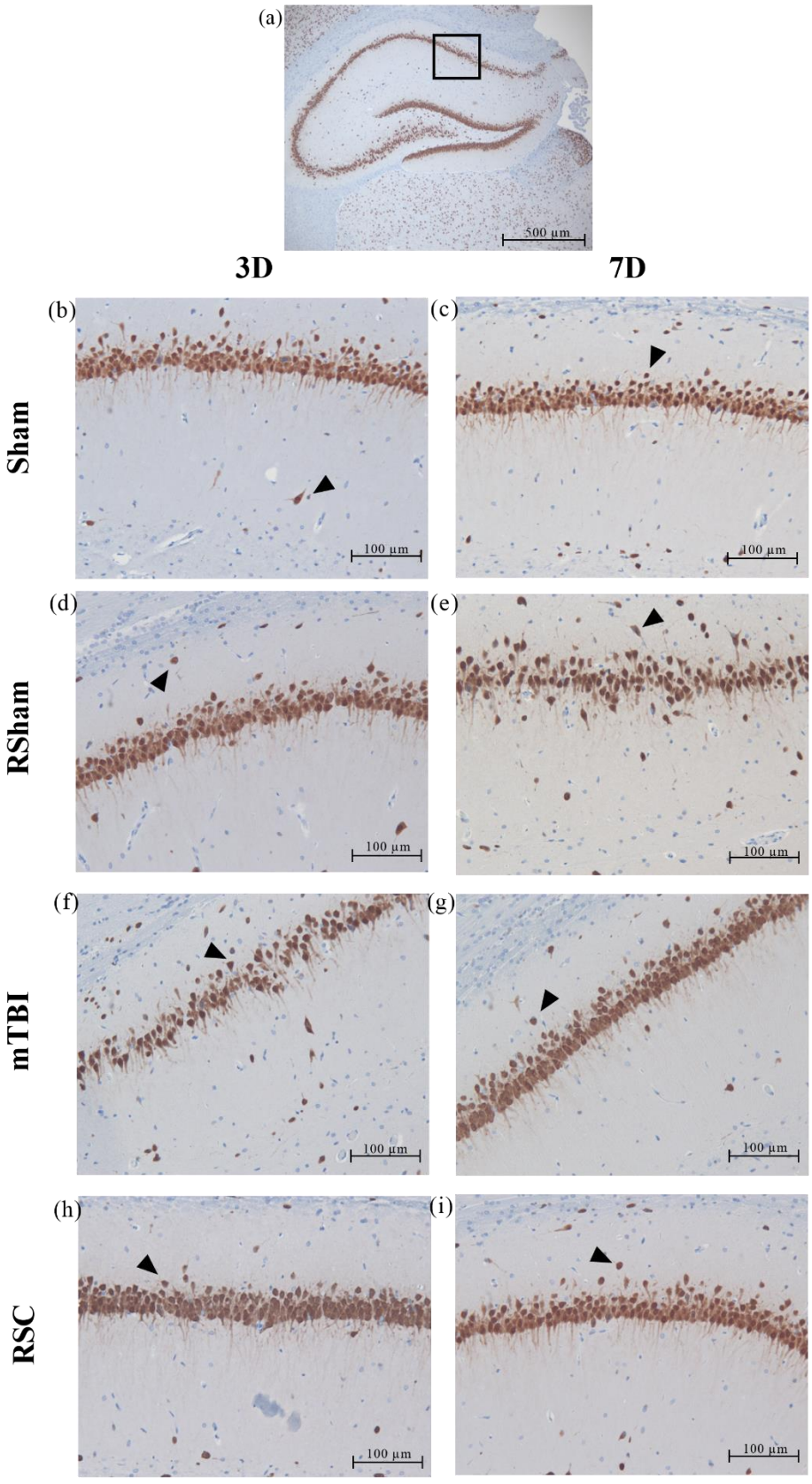
(a)
500 μm
3D
7D
(b)
(c)
Sham
100 μm
100 μm
(d)
(e)
RSham
100 μm
100 μm
(f)
(g)
mTBI
100 μm
100 μm
(h)
(i)
RSC
100 μm
100 μm

Figure E.2 Representative NeuN micrographs of CA1.

Rats were subjected to sham or closed-head impact(s) and euthanized at either 3- or 7-DPI. The (a) location of the CA1 representative images is presented using 4x magnification with a 500μm scale bar. Micrographs (20x) of NeuN expression in CA1 region at 3- (b, d, f, and h) and 7-DPI (c, e, g, and i) for Sham, RSham, mTBI, and RSC impact recovery groups with a 100μm scale bar. A representative neuron expressing positive NeuN immunoreactivity is indicated for each 20x magnification micrograph by a black arrowhead.

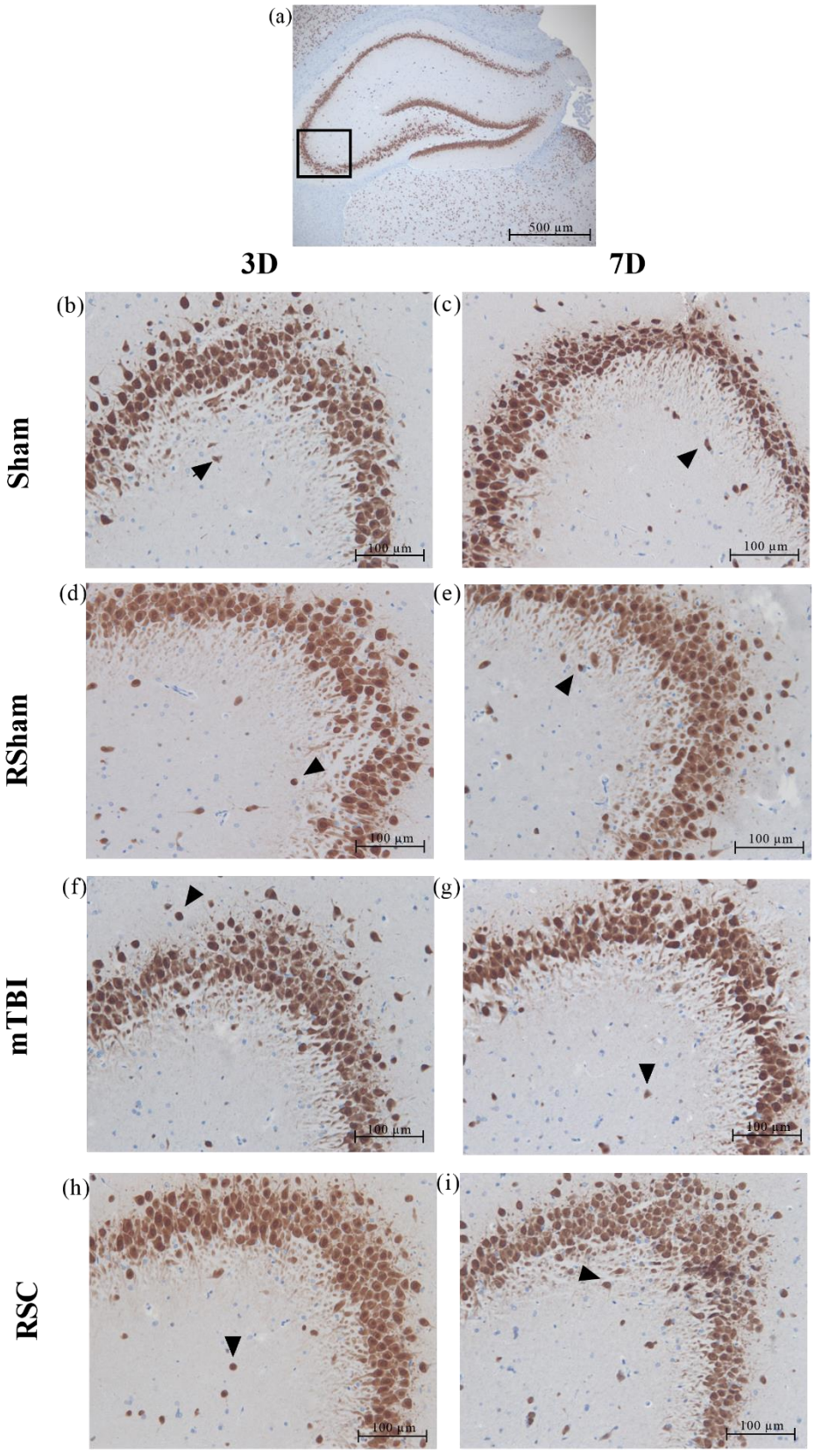
(a)
500 μm
3D
7D
(b)
(c)
Sham
100 μm
100 μm
(d)
(e)
RSham
100 μm
100 μm
(f)
(g)
mTBI
100 μm
100 μm
(h)
(i)
RSC
100 μm
100 μm

Figure E.3 Representative NeuN micrographs of CA3.

Rats were subjected to sham or closed-head impact(s) and euthanized at either 3- or 7-days post-injury. The (a) location of the CA3 representative images is presented using 4x magnification with a 500μm scale bar. Micrographs (20x) of NeuN expression in CA3 region at 3- (b, d, f, and h) and 7-days (c, e, g, and i) post-injury for Sham, RSham, mTBI, and RSC impact recovery groups with a 100μm scale bar. A representative neuron expressing positive NeuN immunoreactivity is indicated for each 20x magnification micrograph by a black arrowhead.

### E.2.2 GFAP Micrographs

Representative GFAP micrographs at 4x magnification are presented for DG (Figure E.4a), CA1 (Figure E.5a), and CA3 (Figure E.6a) with a representative imaging location for each indicated with a black box. The average number of positive GFAP cells for all sample images of the hippocampal regions of interest were referred to in selecting representative 20x magnification micrographs. For each representative GFAP 20x magnification micrograph, a representative neuron expressing positive GFAP immunoreactivity is indicated by a black arrow.

As seen in the number of positive cells plot for the DG, CA1, and CA3 regions (Figure 5.7A-C), the representative micrographs (20x magnification) shown in Figures E.4-6b-i do not show observable differences between groups by or between recovery days. Furthermore, this is confirmed visually, as the proportion of GFAP + (brown colored stain) is not different between injury (Figure E.4-6f-i) or sham (Figure E.4-6b-e) groups, regardless of recovery day.

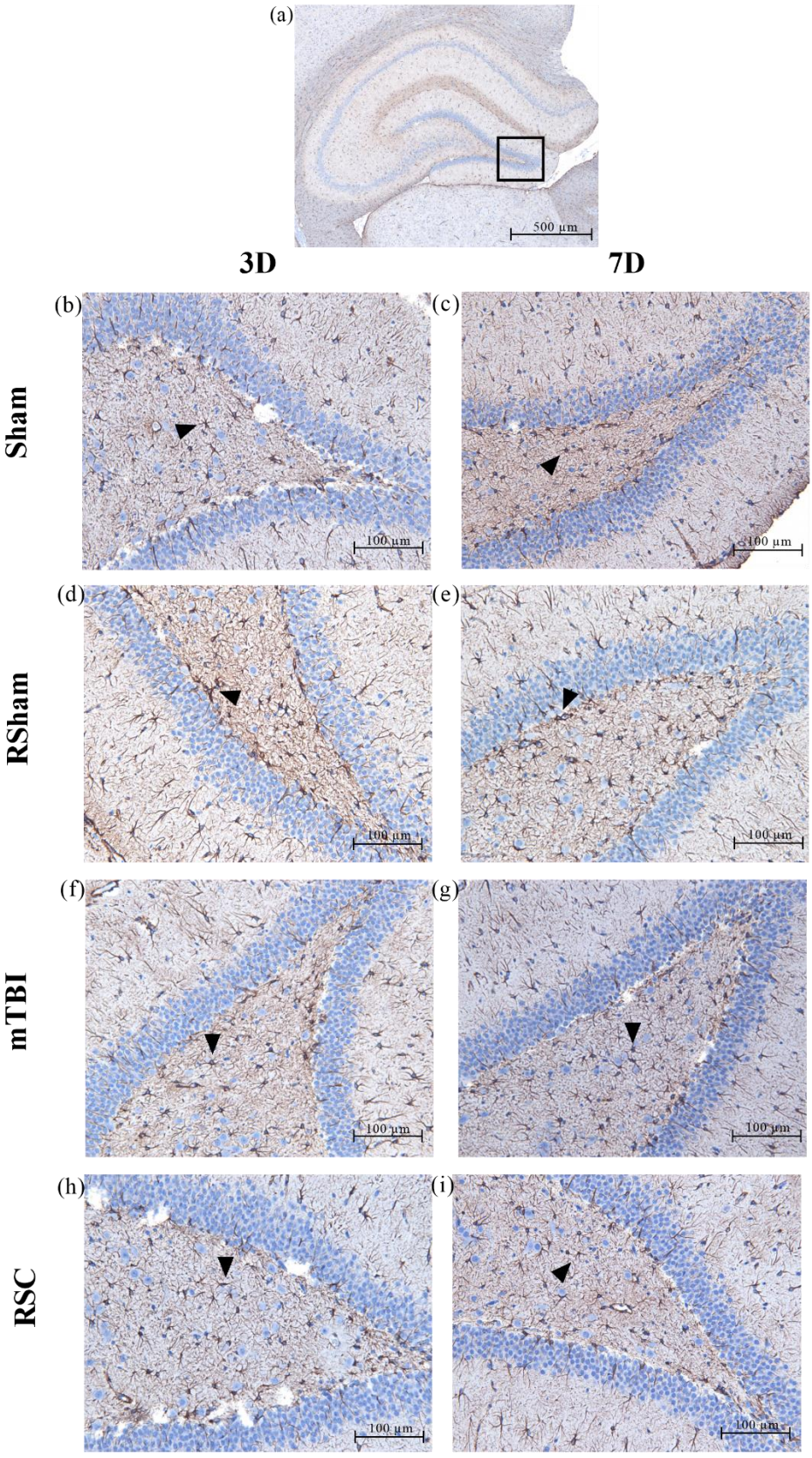
(a)
500 μm
3D
7D
Sham
RSham
mTBI
RSC
(b)
(c)
(d)
(e)
(f)
(g)
(h)
(i)
100 μm

Figure E.4 Representative GFAP micrographs of DG.

Rats were subjected to sham or closed-head impact(s) and euthanized at either 3- or 7-days post-injury. The (a) location of the DG representative images is presented using 4x magnification with a 500μm scale bar. Micrographs (20x) of GFAP expression in dentate gyrus region at 3- (b, d, f, and h) and 7-days (c, e, g, and i) post-injury for Sham, RSham, mTBI, and RSC impact recovery groups with a 100μm scale bar. A representative neuron expressing positive GFAP immunoreactivity is indicated for each 20x magnification micrograph by a black arrowhead.

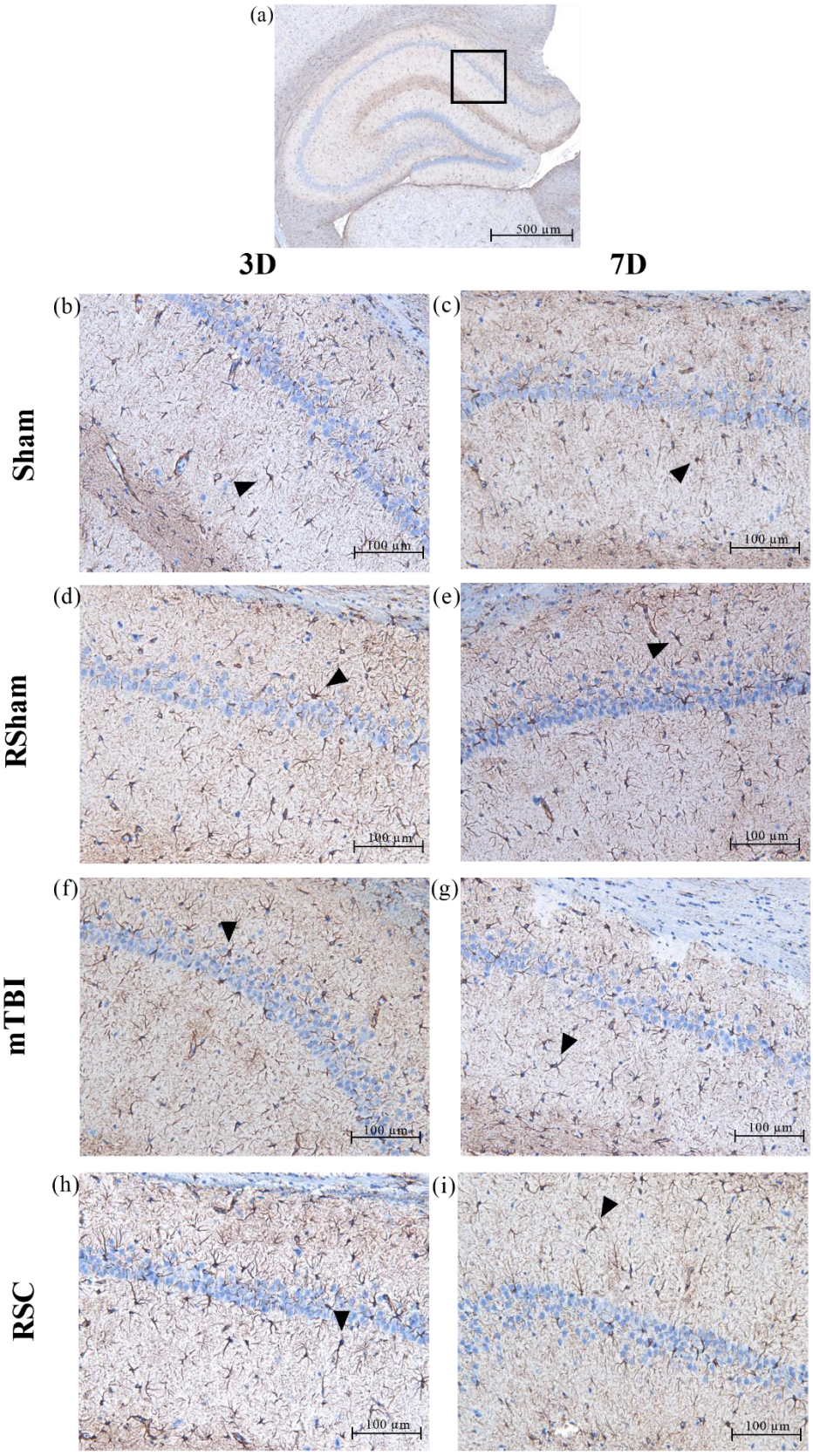
(a)
500 µm
3D
7D
(b)
(c)
Sham
100 µm
100 µm
(d)
(e)
RSham
100 µm
100 µm
(f)
(g)
mTBI
100 µm
100 µm
(h)
(i)
RSC
100 µm
100 µm

Figure E.5 Representative GFAP micrographs of CA1.

Rats were subjected to sham or closed-head impact(s) and euthanized at either 3- or 7-days post-injury. The (a) location of the CA1 representative images is presented using 4x magnification with a 500μm scale bar. Micrographs (20x) of GFAP expression in CA1 region at 3- (b, d, f, and h) and 7-days (c, e, g, and i) post-injury for Sham, RSham, mTBI, and RSC impact recovery groups with a 100μm scale bar. A representative neuron expressing positive GFAP immunoreactivity is indicated for each 20x magnification micrograph by a black arrowhead.

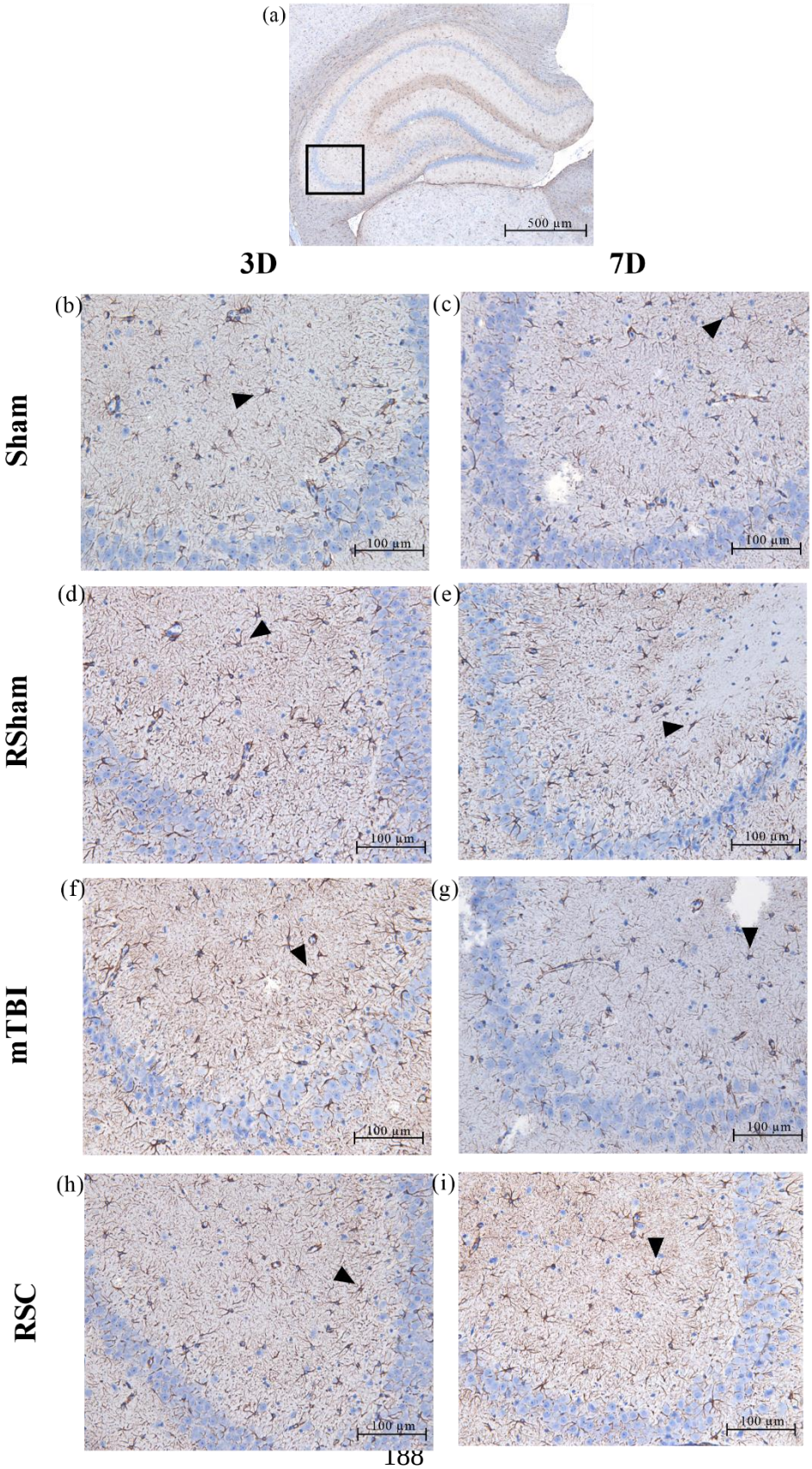
(a)
500 μm
3D
7D
Sham
RSham
mTBI
RSC
(b)
(c)
(d)
(e)
(f)
(g)
(h)
(i)
100 μm

Figure E.6 Representative GFAP micrographs of CA3.

Rats were subjected to sham or closed-head impact(s) and euthanized at either 3- or 7-days post-injury. The (a) location of the CA3 representative images is presented using 4x magnification with a 500μm scale bar. Micrographs (20x) of GFAP expression in CA3 region at 3- (b, d, f, and h) and 7-days (c, e, g, and i) post-injury for Sham, RSham, mTBI, and RSC impact recovery groups with a 100μm scale bar. A representative neuron expressing positive GFAP immunoreactivity is indicated for each 20x magnification micrograph by a black arrowhead.

### E.2.3 Iba-1 Micrographs

Representative Iba-1 micrographs at 4x magnification are presented for DG (Figure E.7a), CA1 (Figure E.8a), and CA3 (Figure E.9a) with a representative imaging location for each indicated with a black box. The average number of positive Iba-1 cells for all sample images of the hippocampal regions of interest were referred to in selecting representative 20x magnification micrographs. For each representative Iba-1 20x magnification micrograph, a representative neuron expressing positive Iba-1 immunoreactivity is indicated by a black arrow.

Figure E.7a shows a representative Iba-1 micrograph of the hippocampus at 4x magnification with a representative DG imaging location indicated by a black box. Figure E.8a shows a representative Iba-1 micrograph of the hippocampus at 4x magnification with a representative CA1 imaging location indicated by a black box. Histological results shown previously in Figure 5.8A reveal that the proportion of positive Iba-1 immunoreactivity (brown color) within the DG tissue section showed significant differences between RSC injury groups with respect to recovery. This is visually seen as the positively stained microglia evident in the representative micrograph for the $RSC_3$ (Figure E.7h) injury group is slightly more than that of the $RSC_7$ (Figure E.7i) injury group. Notably, although the representative micrographs for groups $mTBI_3$ and $RSham_3$ look visibly weaker in positive Iba-1 immunoreactivity, this

irregularity in staining intensity does not hinder the positive cell count analysis, as seen in Figure E.8A.

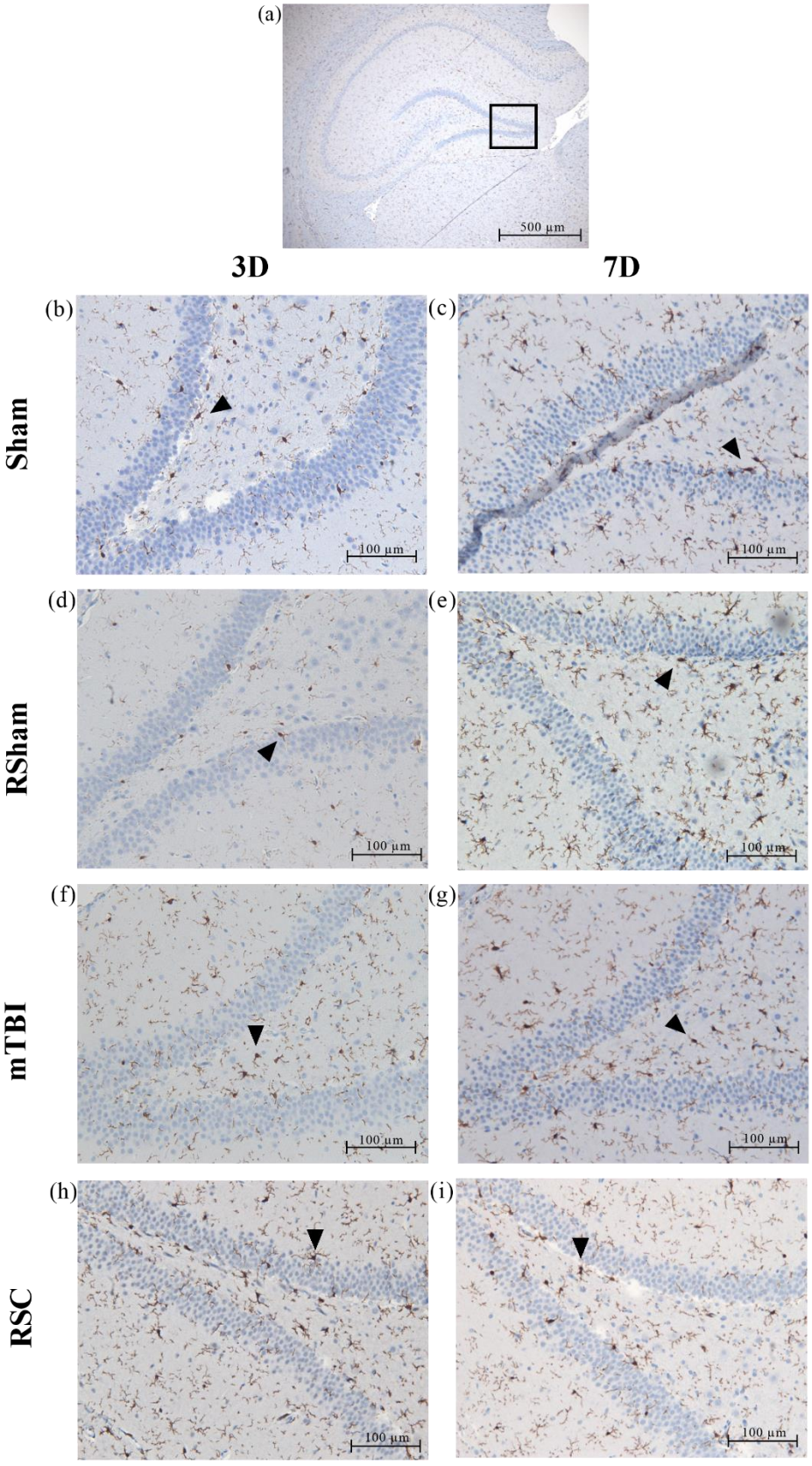
(a)
500 μm
3D
7D
(b)
(c)
Sham
100 μm
100 μm
(d)
(e)
RSham
100 μm
100 μm
(f)
(g)
mTBI
100 μm
100 μm
(h)
(i)
RSC
100 μm
100 μm

Figure E.7 Representative Iba-1 micrographs of DG.

Rats were subjected to sham or closed-head impact(s) and euthanized at either 3- or 7-days post-injury. The (a) location of the DG representative images is presented using 4x magnification with a 500μm scale bar. Micrographs (20x) of Iba-1 expression in dentate gyrus region at 3- (b, d, f, and h) and 7-days (c, e, g, and i) post-injury for Sham, RSham, mTBI, and RSC impact recovery groups with a 100μm scale bar. A representative neuron expressing positive Iba-1 immunoreactivity is indicated for each 20x magnification micrograph by a black arrowhead.

Figure E.8a shows a representative Iba-1 micrograph of the hippocampus at 4x magnification with a representative CA1 imaging location indicated by a black box. According to the histological analysis of the positive cell counts for Iba-1, data revealed statistical differences between injury and sham groups following 3-days of recovery (Figure 5.8B). However, the represented micrographs for the Iba-1 stain do not visually demonstrate this trend; the number of positively stained microglia evident in the representative micrographs for injury groups $mTBI_3$ and $RSham_3$ (Figure E.8f,h, respectively) are not greater than their associated sham (Sham and RSham, respectively) groups (Figure E.8b,d). Furthermore, again, although not easily seen visibly from the representative micrographs, according to the histological analysis, the repeated SC injury group showed a greater number of positive Iba-1 cells after 3-days of recovery compared to 7-days of recovery (Figure E.8h-i).

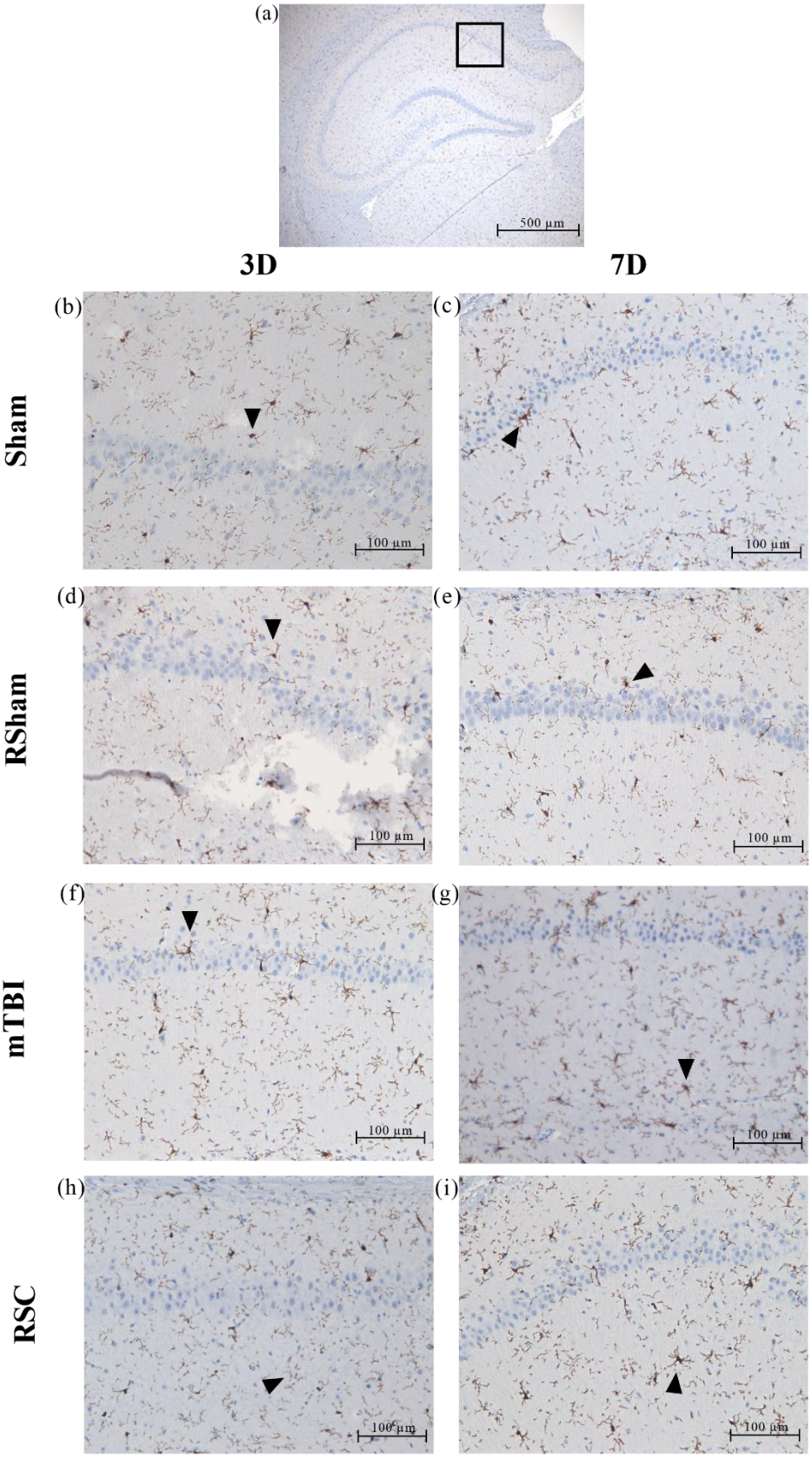
(a)
500 µm
3D
7D
(b)
(c)
Sham
100 µm
100 µm
(d)
(e)
RSham
100 µm
100 µm
(f)
(g)
mTBI
100 µm
100 µm
(h)
(i)
RSC
100 µm
100 µm

Figure E.8 Representative Iba-1 micrographs of CA1.

Rats were subjected to sham or closed-head impact(s) and euthanized at either 3- or 7-days post-injury. The (a) location of the CA1 representative images is presented using 4x magnification with a 500μm scale bar. Micrographs (20x) of Iba-1 expression in CA1 region at 3- (b, d, f, and h) and 7-days (c, e, g, and i) post-injury for Sham, RSham, mTBI, and RSC impact recovery groups with a 100μm scale bar. A representative neuron expressing positive Iba-1 immunoreactivity is indicated for each 20x magnification micrograph by a black arrowhead.

Similarly seen within the CA3 regions of the NeuN and GFAP positive cell count analysis, the number of positive cells plot for the CA3 region (Figure 5.8B) does not show differences between groups by or between recovery days. This is confirmed visually, as the proportion of Iba-1+ (brown colored stain) is not different between injury (Figure E.9f-i) or sham (Figure E.9b-e) groups, regardless of recovery day.

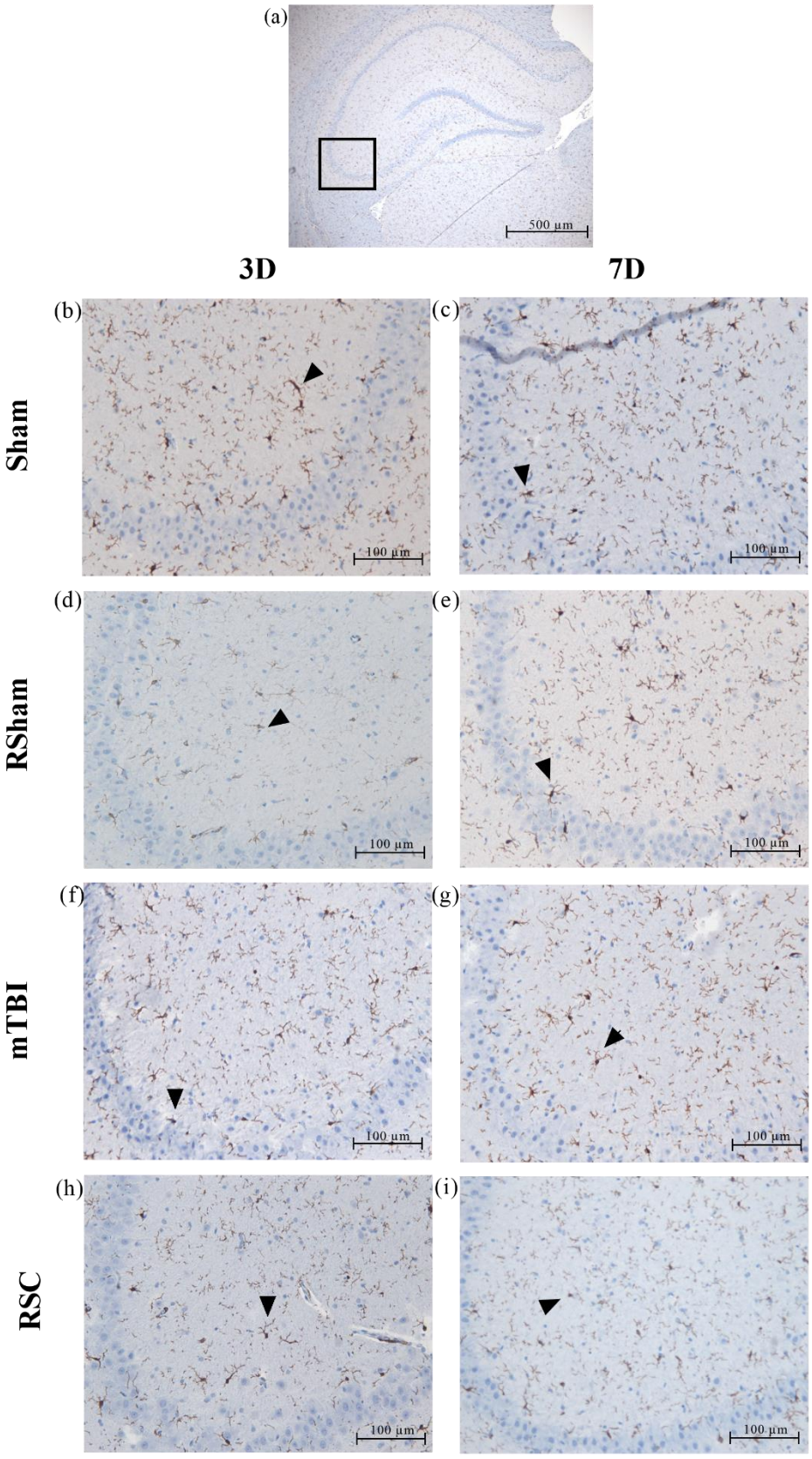
(a)
500 µm
3D
7D
(b)
(c)
Sham
100 µm
100 µm
(d)
(e)
RSham
100 µm
100 µm
(f)
(g)
mTBI
100 µm
100 µm
(h)
(i)
RSC
100 µm
100 µm

Figure E.9 Representative Iba-1 micrographs of CA3.

Rats were subjected to sham or closed-head impact(s) and euthanized at either 3- or 7-days post-injury. The (a) location of the CA3 representative images is presented using 4x magnification with a 500μm scale bar. Micrographs (20x) of Iba-1 expression in CA3 region at 3- (b, d, f, and h) and 7-days (c, e, g, and i) post-injury for Sham, RSham, mTBI, and RSC impact recovery groups with a 100μm scale bar. A representative neuron expressing positive Iba-1 immunoreactivity is indicated for each 20x magnification micrograph by a black arrowhead.